

**Developing a fluorescent, tumour-
specific, molecular imaging
platform for laparoscopic colorectal
cancer surgery.**

James Patrick Tiernan

200606350

*Submitted in accordance with the requirements for the degree of
Doctor of Philosophy*

The University of Leeds

School of Medicine and Health

Leeds Institute of Clinical and Biomedical Sciences

Submitted for examination May 2014

Publications and presentations

I confirm that the work submitted is my own, except where work which has formed part of jointly authored publications has been included. My contribution and that of the other authors to this work has been explicitly indicated below. I confirm that appropriate credit has been given within the thesis where reference has been made to the work of others.

Permission has been granted by the publishers of all manuscripts below allowing use of text and figures in this thesis.

Chapter 1

JP Tiernan, I Ansari, NA Hirst, PA Millner, TA Hughes, DG Jayne. Intra-operative tumour detection and staging in colorectal cancer surgery.

Colorectal Disease 2012;14(9):e510-20

My involvement: conception, literature search, analysis, manuscript

Involvement of others: guidance, manuscript corrections

Chapter 3

JP Tiernan, SL Perry, ET Verghese, NP West, S Yeluri, DG Jayne, TA Hughes. Carcinoembryonic antigen (CEA) is the preferred biomarker for *in vivo* colorectal cancer targeting.

British Journal of Cancer 2013; 108(3):662-7

My involvement: conception, design, all experimental work, all analysis, manuscript

Involvement of others: design, supervision, guidance, manuscript corrections

Presentations:

European Society of Coloproctology 2012

Society of Academic Research Surgery 2013

Chapter 5

Presentation:

Society of Academic Research Surgeons 2015

Chapter 6

JP Tiernan, N Ingram, G Marston, SL Perry, JV Rushworth, PL Coletta, PA Millner, DG Jayne, TA Hughes. CEA-targeted nanoparticles allow specific *in vivo* fluorescent imaging of colorectal cancer models.

Nanomedicine 2015; 10(8):1223-31

My involvement: conception, design, all experimental work, all analysis, manuscript

Involvement of others: design, supervision, guidance, manuscript corrections

Presentations:

Patey Prize finalist, Society of Academic Research Surgeons 2014

John of Arderne Medal finalist, Royal Society of Medicine 2014

Faculty of Medicine & Health Postgraduate Researcher of the Year 2013

Runner-up, University of Leeds Postgraduate Researcher of the Year 2013

The Phil Robinson Prize for Best Oral Research Presentation 2013

Yorkshire & Humber Deanery Academic Prize Session: Best Oral Presentation 2013

This copy has been supplied on the understanding that it is copyright material and that no quotation from the thesis may be published without proper acknowledgement.

© 2015 The University of Leeds and James Tiernan.

The right of James Tiernan to be identified as Author of this work has been asserted by him in accordance with the Copyright, Designs and Patents Act 1988.

Acknowledgements

I would like to thank the following people for their support, advice, time and patience whilst I undertook this work:

Asif Ahmed

Louise Coletta

Thomas Hughes

Nicola Ingram

David Jayne

Baek Kim

Paul Millner

Amit Nair

Sarah Perry

Eldo Verghese

I would also like to thank Cancer Research UK for funding this project.

Finally, I would like to thank my wife for her unwavering and continued support.

Abstract

Background

Fluorescent laparoscopic imaging of primary colorectal tumours and lymph node metastases would improve localisation of early tumours and allow intra-operative staging, potentially facilitating intra-operative stratification of the extent of surgical resections thereby improving patient outcomes. I aimed to develop and test a fluorescent molecular probe capable of allowing localisation of tumours *in vivo*.

Methods

Immunohistochemistry was used to identify the most appropriate colorectal cancer target from a panel of seven biomarkers in prospectively collected, matched normal and tumour tissue from 280 colorectal cancer patients. The availability of targets for antibody binding was assessed in live cells, fresh frozen tumour samples and *ex vivo* cancer specimens. Indocyanine green was conjugated to anti-CEA and control IgG antibodies, and CEA-specific fluorescence was quantified in live cancer cells. Dye-doped silica nanoparticles loaded with NIR664 dye were synthesised using a water-in-oil microemulsion technique. Anti-CEA IgGs or control IgGs were conjugated to nanoparticles using a variety of different chemical conjugation strategies and binding to cells was quantified *in vitro*. A murine xenograft model and live IVIS imaging were used to assess PAMAM-linked nanoparticles *in vivo*.

Results

Of the biomarkers tested, CEA showed the greatest differential expression between normal and tumour samples ($p < 0.001$) and the best sensitivity (93.7%) and specificity (96.1%) for colorectal cancer detection. ICG-anti-CEA exhibited CEA-specific fluorescence in all three cell lines tested ($p < 0.01$) with fluorescence peaking at 24-36

hours. CEA-targeted, PAMAM dendrimer-conjugated nanoparticles allowed strong tumour-specific targeting, demonstrating up to 12.3-fold greater fluorescence than control nanoparticles when incubated with colorectal cancer cell lines ($p < 0.002$). In LS174T xenografts, CEA-targeted nanoparticles demonstrated clear tumour-specific fluorescence from 6 to 72h after injection, as compared to only background fluorescence for control IgG-targeted nanoparticles at all time points ($p < 0.0001$).

Conclusions

CEA has the greatest potential to allow highly specific tumour imaging. ICG-conjugated anti-CEA antibodies allow CEA-specific imaging of colorectal cancer cells *in vitro*. Dye-doped silica nanoparticles conjugated to anti-CEA antibodies via PAMAM dendrimers have potential to allow intra-operative fluorescent visualisation of tumour cells. These findings are the first to demonstrate live tumour-specific fluorescent colorectal cancer imaging using an antibody-targeted nanoparticle *in vivo*.

Table of contents

1	INTRODUCTION	20
1.1	The clinical problem.....	20
1.1.1	Current limitations in pre-operative staging	21
1.1.2	Laparoscopic surgery and the National Bowel Cancer Screening Programme.....	23
1.1.3	Radical resections.....	24
1.1.4	Under-staging of stage II tumours	26
1.2	<i>In vivo</i> colorectal cancer detection: current technologies	29
1.2.1	Radioimmunoguided surgery	29
1.2.2	Radioimmunotherapy and targeted chemotherapy.....	30
1.2.3	Targeted non-invasive imaging	30
1.2.4	Sentinel lymph node mapping	31
1.3	A potential solution: intra-operative fluorescent imaging	34
1.3.1	Tumour-specific localisation component.....	35
1.3.2	Fluorescent visualisation component	37
1.3.3	Nanoparticle scaffold.....	41
1.4	HYPOTHESIS AND AIMS	47
2	METHODS.....	49
2.1	Immunohistochemistry.....	49
2.1.1	Immunohistochemistry methods.....	49
2.1.2	Antibodies	51
2.1.3	Optimisation	52
2.1.4	Tissue micro-arrays	52

2.1.5	Scoring	53
2.2	Tissue culture	54
2.2.1	Cell line authentication	55
2.3	Immunofluorescence	56
2.3.1	Cell lines	56
2.3.2	Fresh frozen tissue	57
2.4	Ex vivo model	57
2.4.1	In vitro proof of concept.....	57
2.4.2	Human study.....	58
2.5	Antibody-fluorophore conjugates	58
2.5.1	Antibody-fluorescein	58
2.5.2	Antibody-indocyanine green.....	60
2.6	Western Blot.....	66
2.6.1	Protein lysate production and protein standardisation	67
2.6.2	Gel electrophoresis	67
2.7	Nanoparticles	69
2.7.1	Dendrimer-linked nanoparticle-IgG conjugates.....	69
2.7.2	SMCC-linked nanoparticle-IgG conjugates.....	72
2.7.3	Polyethylene glycol (PEG)-linked nanoparticle-IgG conjugates	74
2.7.4	EDC-linked nanoparticle-IgG conjugates.....	74
2.7.5	Nanoparticle in vitro assay	75
2.7.6	Nanoparticle Characterisation	79
2.8	Animal model.....	79
3	CARCINOEMBRYONIC ANTIGEN IS THE PREFERRED BIOMARKER FOR IN VIVO COLORECTAL CANCER TARGETING	82

3.1	Abstract	82
3.2	Introduction	84
3.3	Results	86
3.3.1	Selection of potential colorectal cancer-specific biomarkers and optimisation of antibodies for their analysis.....	86
3.3.2	Expression of selected biomarkers in 280 matched normal and tumour tissue samples.....	92
3.3.3	Specificity and sensitivity of selected biomarkers for tumour detection..	99
3.3.4	Expression of selected biomarkers in 18 matched normal and metastatic mesenteric lymph nodes.....	102
3.4	Discussion.....	107
4	CEA AND TAG-72 ARE AVAILABLE FOR ANTIBODY BINDING IN LIVE CELLS.....	113
4.1	Abstract	113
4.2	Introduction	115
4.3	Results	116
4.3.1	CEA, but not TAG-72, is available for antibody binding in fixed cells...	116
4.3.2	CEA and TAG-72 are available for antibody binding in live cells	119
4.3.3	Assessment of the accessibility of CEA and TAG-72 for imaging in the context of tumour architecture	125
4.3.4	Assessment of biomarker localisation in an <i>ex vivo</i> model of systemic antibody delivery.....	128
4.4	Discussion.....	132
5	INDOCYANINE GREEN CONJUGATED ANTI-CEA ANTIBODIES ALLOW FLUORESCENT IMAGING OF COLORECTAL CANCER CELLS	137
5.1	Abstract	137

5.2	Introduction	139
5.3	Results	142
5.3.1	Qualitative assessment of ICG-anti-CEA fluorescence in LS174T cells.....	142
5.3.2	Quantitative assessment of ICG-anti-CEA vs ICG-anti-digoxin fluorescence in colorectal cell lines	146
5.4	Discussion.....	153
6	CEA-TARGETED, DYE-DOPED SILICA NANOPARTICLES ALLOW SPECIFIC <i>IN VIVO</i> FLUORESCENT IMAGING OF COLORECTAL CANCER MODELS	158
6.1	Abstract	158
6.2	Introduction	160
6.2.1	Aims.....	160
6.3	Results	164
6.3.1	Dye-doped silica nanoparticles: manufacture and characterisation	164
6.3.2	Chemical linkage strategies for antibody conjugation	170
6.3.3	<i>In vitro</i> analysis of binding of colorectal cancer cells by targeted nanoparticles	181
6.3.4	<i>In vivo</i> analysis of binding of colorectal cancer cells by targeted NPs ..	187
6.4	Discussion.....	195
6.4.1	Manufacture and optimisation of dye-doped silica nanoparticles.....	196
6.4.2	<i>In vitro</i> assays for specific antibody-directed binding.....	201
6.4.3	The relative merits of the chemical linkage strategies tested.....	204
6.4.4	<i>In vivo</i> potential for PAMAM-linked antibody-directed nanoparticles....	206
7	SUMMARY	212
7.1	Future perspectives	212

7.1.1	Biomarker targeting.....	212
7.1.2	Targeted indocyanine green.....	214
7.1.3	Targeted fluorescent nanoparticles	214
7.2	Limitations	216
7.3	Potential impact.....	217
8	REFERENCES	219

List of tables

Table 1.1. Colon and rectum cancer staging (American Joint Committee on Cancer 5 th Edition).	27
Table 2.1. Antibodies selected for the chosen panel of antigens.....	51
Table 2.2. Cell lines used for in vitro experiments.	55
Table 3.1. Antibody optimisation.	89
Table 3.2. Clinico-pathological details of patient cohort.....	93
Table 3.3. CEA, TAG-72 and FR α are significantly more highly expressed in colorectal tumour tissue than matched normal tissue.....	96
Table 3.4. Peak sensitivity and specificity for each biomarker.....	101
Table 4.1. Summary of immunostaining patterns.	124
Table 6.1 Summary of in vitro fluorescence quantification analysis.....	185

List of illustrative figures

Figure 2.1. Cell selection for fluorescence quantification.....	63
Figure 2.2. Whole cell fluorescence quantification.	65
Figure 2.3. Membrane fluorescence quantification.....	77
Figure 3.1. Anti-CEA antibody comparison.	90
Figure 3.2. CD105 staining.	91
Figure 3.3. CEA, TAG-72, EGFR and FR α expression in tumour and normal tissue.	94
Figure 3.4. Allred versus modified Histoscore scoring results.	95
Figure 3.5. Biomarker expression in matched tumour and normal tissue.	96
Figure 3.6. Differential expression for each biomarker..	98
Figure 3.7. Receiver operating characteristic curve for CEA, TAG-72, EGFR and FR α	100
Figure 3.8. Optimum cut-off scores.....	102
Figure 3.9. Biomaker expression in lymph nodes.....	104
Figure 3.10. Non-specific staining in normal lymph nodes.	105
Figure 3.11. Tumour specific expression in lymph nodes.....	106
Figure 4.1. Immunostaining in fixed cells.	118
Figure 4.2. Anti-CD105 antibodies as a negative control.....	120
Figure 4.3. HUVECs as a negative control cell line.	121
Figure 4.4. Immunostaining in live cells.	123
Figure 4.5. CEA immunostaining in fresh frozen tissue.....	126
Figure 4.6. TAG-72 immunostaining in fresh frozen tissue.....	127
Figure 4.7. Immunostaining in fresh frozen tissue is not tumour-specific.....	128
Figure 4.8. Formalin fixation did not prevent CEA immunostaining.	130
Figure 4.9. <i>Ex vivo</i> model mmunohistochemical staining.	131
Figure 5.1. ICG-labelled IgG antibodies.	141

Figure 5.2. ICG-anti-CEA antibodies allow cytoplasmic fluorescence.	144
Figure 5.3. ICG-anti-CEA cytoplasmic fluorescence is dose-dependent.	145
Figure 5.4. Anti-digoxin antibodies are a suitable negative control for colorectal cancer cell targeting experiments.	147
Figure 5.5. Expression of CEA by colorectal cancer cells was confirmed by Western Blot analysis.	148
Figure 5.6. ICG-anti-CEA fluorescence in LS174T, LoVo and HCT116 cells.....	150
Figure 5.7. Pulse and chase incubation.	152
Figure 6.1. The availability of amine groups on the surface of the bare nanoparticle quantified using Fmoc-Cl.	166
Figure 6.2. Fluorescence spectra of RupBy-doped and NIR664-doped silica nanoparticles.	168
Figure 6.3. The relationship between RupBy-doped nanoparticle concentration and emission fluorescence.	169
Figure 6.4. Size distribution of dye-doped silica nanoparticles.	170
Figure 6.5. Nanoparticle-antibody conjugation.	171
Figure 6.6. IgG antibody reduction.	172
Figure 6.7. SMCC conjugation.	174
Figure 6.8. Bifunctional PEG conjugation.....	175
Figure 6.9. EDC conjugation.	176
Figure 6.10. Absorbance assay to determine effectiveness of particle washing.	177
Figure 6.11. PAMAM dendrimer conjugation.....	180
Figure 6.12. Bare particle versus targeted particle size.....	180
Figure 6.13. Fluorescence analysis: SMCC, PEG and EDC.	182
Figure 6.14. Fluorescence analysis: PAMAM dendrimers.	184
Figure 6.15. Three dimensional reconstruction of nanoparticle-coated cells.	186
Figure 6.16. Fluorescent nanoparticles are detectable using an IVIS imaging system.	188

Figure 6.17. Systemically delivered nanoparticles are detectable <i>in vivo</i>	189
Figure 6.18. Hepatic fluorescence is similar for control and CEA-targeted nanoparticles.	191
Figure 6.19. Systemic administration of CEA-targeted nanoparticles leads to tumour-specific fluorescence in a xenograft murine model of colorectal cancer.	194
Figure 6.20. CEA-targeted nanoparticles allow fluorescent tumour detection in vivo.	194
Figure 6.21. 'Bare' NIR664 doped silica nanoparticles.	200
Figure 6.22. Dissection of xenograft tumour with the greatest tumour-specific signal.	209

Abbreviations

ACBGBI	Association of Coloproctology of Great Britain and Ireland
AJCC	American Joint Committee on Cancer
APTES	3-aminopropyl)triethoxysilane
ASTM	American Society for Testing and Materials
AUC	Area under the curve
BSA	Bovine serum albumin
CEA	Carcinoembryonic antigen
CLASICC	Conventional versus laparoscopic-assisted surgery in patients with colorectal cancer (trial)
CRC	Colorectal cancer
CRUK	Cancer Research UK
CT	Computed tomography
Cy	Cyanine
DAPI	4',6-Diamidino-2-phenylindole
DEATA	Diethylenetriamine
DMF	Dimethylformamide
DMSO	Dimethyl sulfoxide
EDC	N-(3-dimethylaminopropyl)-N'-ethylcarbodiimide
EGFR	Epidermal growth factor receptor
ETV	Eldo Thomas Vergehese (pathologist)
FCS	Fetal calf serum
FDA	Food and Drug Administration
FEG-SEM	Field emission gun scanning electron microscopy
FFPE	Formalin fixed paraffin embedded
FITC	Fluorescein isothiocyanate
Fmoc-Cl	Fluorenylmethyloxycarbonyl chloride

Fra	Folate receptor a
H&E	Haematoxylin and eosin
HER2	Human epidermal growth factor receptor 2
HUVEC	Human umbilical vein endothelial cell
ICG	Indocyanine green
IgG	Immunoglobulin G
ISO	International Organisation for Standardisation
MEA	Mercaptoethylamine
MES	2-(N-morpholino)ethanesulfonic acid
MHRA	Medicines and Healthcare Products Regulatory Agency
MPTES	3-mercaptopropyl) triethoxysilane
MRI	Magnetic resonance imaging
NBCSP	National Bowel Cancer Screening Programme
NCIN	National Cancer Intelligence Network
NHS	N-hydroxysulfosuccinimide
NIR664	N-succinimidyl ester
NOTES	Natural orifice endoluminal surgery
OCT	Optical coherence tomography
PAMAM	Polyamidoamine
PBS	Phosphate buffered saline
PEG	Polyethylene glycol
RES	Reticuloendothelial system
RIGS	Radioimmunoguided surgery
Robo1	Roundabout protein 1
ROC	Receiver operating characteristic
RT-PCR	Reverse transcriptase polymerase chain reaction
Rubpy	Tris(bipyridine)ruthenium(II) chloride
SDS	Sodium dodecyl sulphate

SMCC	Succinimidyl 4-N-maleimidomethylcyclohexane
TAG-72	Tumour associated glycoprotein 72
TBS	Tris buffered saline
TEMS	Transanal endoscopic microsurgery
TEOS	Tetraethyl orthosilicate
TMA	Tissue micro-array
TNBSA	2,4,6-Trinitrobenzene sulfonic acid

Chapter One

Introduction

Some parts of the text in this chapter have been published in the manuscript “Intra-operative tumour detection and staging in colorectal cancer surgery” (*Colorectal Disease* 2012;14(9):e510-20) and reproduced here with permission.

1 INTRODUCTION

My project has focussed on developing an intra-operative, fluorescent imaging system for laparoscopic colorectal cancer surgery. Here, I describe the various clinical factors that such a system would address and current, relevant *in vivo* tumour targeting technologies. I then describe the three principle components of my proposed solution: tumour-specific localisation, fluorescent visualisation and nanoparticle linkage.

1.1 The clinical problem

Colorectal cancer (CRC) is the fourth most common cancer in the UK, accounting for 13% of all new cancer cases. In 2010 there were 22834 new cases diagnosed in men (56%) and 17861 in women (CRUK, 2010). Although five year survival from colorectal cancer has doubled in the last 30 years, from 25% for those diagnosed in 1971-75 to over 50% for those diagnosed in 2001-06 (Office for National Statistics, 2010), overall incidence rates have been increasing since the mid-1970s (CRUK, 2010). The mainstay of treatment is surgical resection, although this is aided by neo-adjuvant and adjuvant therapies, which can improve disease-free survival, downstage tumours and render initially unresectable tumours resectable. Surgical resection is a one-size-fits-all approach, with the tumour, the supplying blood vessels and the draining lymphatics resected in an *en bloc* fashion.

A number of different clinical factors, some long-standing and others due to more recent developments have highlighted the limitations of current treatment paradigms

and the potential benefit of intra-operative tumour detection. Factors are listed here, with further detailed discussion below.

- Current limitations in pre-operative staging;
- The widespread use of laparoscopic resection;
- The effect of the National Bowel Cancer Screening Programme on case mix;
- Evidence that more radical resections improve survival;
- The under-staging of stage II tumours.

1.1.1 Current limitations in pre-operative staging

There are explicit guidelines that dictate a common patient pathway from diagnosis of a colorectal cancer through to various treatment modalities depending on the patient's physiological reserve, the anatomical location of the tumour and the stage of their disease (ACPGBI, 2007). Colorectal cancer has been shown to metastasise via the portal venous and lymphatic systems (Jamieson and Dobson, 1909). The large Wessex (George et al., 2006) and Trent/Wales (Mella et al., 1997) audits of the 1990s and early 2000s showed that over 20% of patients have distant metastases at initial presentation. Patients therefore undergo detailed pre-operative staging to assess tumour extent, location, and both local and distant metastases. The Association of Coloproctologists of Great Britain and Ireland dictate that, ideally, all patients undergo a colonoscopy with tissue taken for histology, a staging thoracic and abdominal computed tomography (CT) scan, and in the case of rectal tumours a magnetic resonance imaging (MRI) scan with endoanal ultrasound if necessary (ACPGBI, 2007). In patients with distant metastases (most commonly hepatic or thoracic), the appropriateness and timing of surgery for the primary and secondary tumours must be decided, and additionally whether neo-adjuvant chemotherapy is

required. If the metastases are resectable, surgery is planned to resect both the primary and the secondary tumours and chemotherapy is indicated due to the presence of metastases. For resectable metastases, a 'staged approach' has traditionally been used, with initial resection of the primary, followed by chemotherapy and then by hepatectomy or pneumonectomy (de Haas et al., 2010, Feng et al., 2014), on the basis that locoregional control is the priority. For hepatic metastases, there has been a recent trend towards simultaneous resection of both the primary and secondary tumours during the same procedure, particularly with advances in peri- and post-operative care, and minimally invasive techniques (Adam et al., 2004, Siriwardena et al., 2014). In the case of rectal tumours, neo-adjuvant radiotherapy with or without chemotherapy is indicated where there is local lymph node metastasis or the circumferential resection margin is threatened.

It is clear that the accuracy of the information gathered from histopathological examination and radiological investigations has a huge bearing on the treatment pathway and chance of recurrence. Despite this extensive pre-operative work-up, small metastases are often missed; a meta-analysis showed CT to have a sensitivity of 70% (95% confidence interval: 65-73%) and specificity of 78% (95% confidence interval: 73-82%) in detecting nodal disease in colonic cancer (Dighe et al., 2010) whilst MRI has a sensitivity of 66-85% and specificity of 41-97% in nodal staging for rectal cancer (Kim et al., 2000, Bipat et al., 2004, Brown et al., 2003). Positron emission tomography (PET) scanning combined with CT colonography has been shown to be significantly more accurate in detecting lymph node metastases than CT alone (Veit-Haibach et al., 2006, Sun et al., 2008), but is still not sensitive enough to detect micro-metastases (tumour deposits of 0.2 to 2mm (Hermanek et al., 1999)). Potentially, intra-operative tumour visualisation would allow more accurate tumour staging by sensitive detection of lymph node deposits.

1.1.2 Laparoscopic surgery and the National Bowel Cancer Screening Programme

Laparoscopic or 'keyhole' resection for CRC has slowly gained popularity in the UK since its introduction in 1991 (Jacobs et al., 1991, Taylor et al., 2013) and short-term advantages have been demonstrated. This minimally invasive approach results in several small scars instead of the traditional midline laparotomy wound that is associated with post-operative pain and compromises respiratory function (Schwenk et al., 1999). As a result, randomised controlled trials have demonstrated a shorter hospital stay, earlier mobilisation and quicker functional recovery (Stead et al., 2000, van der Pas et al., 2013, COLOR Study Group, 2005, Weeks et al., 2002, Guillou et al., 2005, Abraham et al., 2004) following laparoscopic resection, without compromising oncological clearance. One important disadvantage is the loss of haptic feedback that is present at open surgery: the surgeon's fingertips are an important and sensitive tool used to locate primary tumour margins, metastatic deposits and both embryological and oncological resection planes. Early tumours tend to be small and can be impossible to locate accurately with laparoscopic instruments. Colonic tattooing, where a tumour is injected with a permanent dye at endoscopy prior to surgery, is often used to help locate small tumours. This then appears as an ink stain on the colonic wall but the technique can be variable and unreliable (Conaghan et al., 2010).

This problem has been compounded by an increasing proportion of tumours detected early in their natural history by the National Bowel Cancer Screening Programme (NBCSP), introduced in 2006. The incidence of Dukes A tumours (confined to the mucosa (Dukes, 1932)) in the NBCSP is 32% (Logan et al., 2011) compared to 8.7% in symptomatic patients (National Cancer Intelligence Network (NCIN), 2009). This

shift towards earlier disease means that surgeons will be required to resect a higher proportion of small tumours that are difficult to locate intra-operatively. A sensitive intra-operative tumour visualisation system would allow small tumours to be located with ease and aid laparoscopic resection. It could also be used to exclude lymph node metastasis in patients who might otherwise be suitable for endoscopic resection of a tumour.

1.1.3 Radical resections

1.1.3.1 Current practice and rationale

When resecting a colorectal tumour, the aim is to remove the tumour with clear margins and remove the surrounding lymph nodes that drain it ((Jamieson and Dobson, 1909)). The intra-abdominal lymph nodes lie in close proximity to the blood vessels that supply the colorectum; the typical lymphovascular route of colorectal cancer metastasis requires that the entire anatomical territory of the artery supplying the tumour is resected *en bloc* along with the tumour. The exact location of the tumour therefore dictates the operation.

1.1.3.2 Complete mesocolic resection and central vascular ligation.

There is emerging evidence that survival outcomes following colon cancer surgery might be improved by increasing the radicality of lymphadenectomy and meticulously adhering to oncological planes of resection. The technique of complete mesocolic excision with extended lymphadenectomy (central vascular ligation), as described by Hohenberger (Hohenberger et al., 2009), has reported local recurrence rates of 3.6% and 5-year disease free survival of 89.1%. This has been attributed to the removal of more tissue and lymph nodes in the correct surgical planes. These figures compare

favourably to local recurrence rates of 8-10% reported elsewhere (Jayne et al., 2010). Further, West *et al* showed a survival advantage from mesocolic plane surgery in patients with lymph node involvement (West et al., 2008), an observation that has been corroborated in the Medical Research Council (MRC) CLASICC trial that compared laparoscopic to open resection. There is, however, a reluctance to adopt this approach for all patients due to a lack of robust survival data, with papers focussing on pathological specimen quality only (West et al., 2010, Bertelsen et al., 2011). A study of 914 patients undergoing potentially curative surgery for T2-T4 colonic tumours by Hashiguchi *et al* (Hashiguchi et al., 2011) found no staging benefit and minimal survival benefit in removing nodes greater than five centimetres from the tumour.

It could therefore be argued that as only some 30% of colorectal cancers have evidence of nodal disease (CRUK, 2007), subjecting all patients to a radical segmental resection is over-treatment for the majority (Cahill et al., 2009). Whether this translates into unnecessary morbidity is a point of debate; experience would suggest that the close dissection of the delicate structures around the root of the mesentery, the increase in length of colon mobilised and excised, and an increase in operative time all add up to a longer and potentially more problematic peri-operative period. Hohenberger reported no difference in complication rates pre- and post-introduction of the complete mesocolic resection and central vascular ligation technique, but there are a number of potentially confounding issues such as the experience of the surgeon and the ancillary staff, a 24 year study period, and the limitations of extrapolating results from a single institution experience (Hogan and Winter, 2009). If patients with lymph node metastases could be identified accurately either pre- or intra-operatively, those most likely to benefit from a more radical resection could be selected.

This 'personalised' approach, where the operation is tailored to the individual biology of the tumour, offers a number of advantages. The aim is to ensure that an adequate oncological resection is performed whilst minimising the impact of surgical trauma on postoperative function. It is probably best exemplified in rectal cancer where the benefits of transanal endoscopic microsurgery (TEMS), with or without radiotherapy, for early stage disease (T1-2, N0) are beginning to be recognised, particularly in terms of organ preservation, restoration of normal bowel function and quality of life (Doornebosch et al., 2007, Doornebosch et al., 2008, Suppiah et al., 2008). The concept of tailored cancer surgery also fits comfortably with recent developments in minimally invasive surgery, including single incision laparoscopic surgery (SILS) and natural orifice transluminal endoscopic surgery (NOTES) (Cahill, 2010). These techniques aim to facilitate patient recovery by minimising surgical access trauma, and if they can be combined with a reduction in surgical site trauma then the outcomes might be appreciably better.

1.1.4 Under-staging of stage II tumours

Following surgical resection and post-operative histopathological examination of the specimen, patients diagnosed as having stage II disease (no evidence of lymph node metastasis, Table 1.1) and no evidence of 'high risk' features (lymphovascular invasion, poor differentiation) are considered to have had a curative resection and adjuvant chemotherapy is not offered, on the grounds that no benefit has been shown (Andre et al., 2009). However, some 25% of stage II patients subsequently develop metastatic disease (Chen and Bilchik, 2006, Weitz et al., 2005), implying that a proportion of these patients might have had occult lymph node metastases that were not detected during routine histopathological examination.

Stage	T	N	M	Dukes
0	Tis	N0	M0	-
I	T1	N0	M0	A
	T2	N0	M0	
II	T3	N0	M0	B
	T4	N0	M0	
III	Any T	N1	M0	C
	Any T	N2	M0	
IV	Any T	Any N	M1	

Definitions	
Primary tumour (T)	
TX	Primary tumour cannot be assessed
T0	No evidence of primary
Tis	Carcinoma in-situ or invasion of lamina propria
T1	Invades submucosa
T2	Invades muscularis propria
T3	Invades through muscularis propria
T4	Tumour directly invades other organs or structures, and/or perforates visceral peritoneum (including colorectum)
Regional lymph nodes (N)	
NX	Regional lymph nodes cannot be assessed
N0	No regional lymph node metastasis
N1	Metastasis in 1-3 regional nodes
N2	Metastasis in ≥ 4 regional nodes
Distant metastases (M)	
MX	Distant metastasis cannot be assessed
M0	No distant metastasis
M1	Distant metastasis

Table 1.1. Colon and rectum cancer staging (American Joint Committee on Cancer 5th Edition).

1.1.4.1 The clinical significance of micrometastases

There has been significant debate over the last two decades about whether histologically detected 'micro-metastases' (lymph node deposits 0.2 – 2 mm (AJCC, 2002)) actually impact overall survival. A meta-analysis by Iddings et al (Iddings et al., 2006) reported no difference in 3-year survival when step-sectioning and immunohistochemistry were performed to identify micrometastases, but when

reverse-transcription polymerase chain reaction (RT-PCR) was used the presence of micro-metastases was associated with a significantly worse outcome. Bilchik *et al* (Bilchik et al., 2007) published their interim results of a prospective, multi-centre trial that suggested a possible survival benefit in patients with no micro-metastases in the sentinel lymph node. However a detailed meta-analysis by Rahbari *et al* (Rahbari et al., 2012) has shown them to be clinically significant, suggesting these patients would benefit from adjuvant therapy if they could be identified.

This has led some to argue that histological 'ultra-staging', where each lymph node is evaluated using a combination of exhaustive step-sectioning, immunohistochemical staining for cytokeratins and/or polymerase chain reaction (Bilchik et al., 2002, Bembenek et al., 2005), would lead to higher rates of micrometastasis detection. This would mean a proportion of stage II patients would be 'up-staged' to stage III and therefore benefit from adjuvant chemotherapy (Bilchik et al., 2010). Currently only nodes that are positive either on macroscopic examination or on single section examination undergo further examination; ultra-staging every node would have significant cost and time implications (Wiese et al., 2010) that, in a resource-limited healthcare system such as the NHS, are difficult to justify. Sentinel lymph node mapping, which targets those nodes most likely to contain metastases, has been proposed as a compromise (discussed in section 1.2.4).

1.2 *In vivo* colorectal cancer detection: current technologies

1.2.1 Radioimmunoguided surgery

Radioimmunoguided surgery (RIGS) is an intra-operative tumour detection system pioneered in the 1990s that is effectively a precursor to this project. This system has three components: an antibody to an antigen expressed by the tumour in question; a radionuclide that can be used to radiolabel the antibody; and a hand-held gamma detector that can be used intra-operatively to detect the antibody/radionuclide complex bound to the tumour cells. It was first described by Aitken et al in 1984 (Aitken et al., 1984). This initial report has been followed by 29 clinical trials for colorectal cancer, using either carcinoembryonic antigen (CEA) or tumour-associated glycoprotein 72 (TAG-72) as the target antigen. Overall the sensitivity of RIGS in detecting colorectal cancer ranged from 20% (Hamy et al., 1995) to 100% (Kim et al., 2005) for primary disease and 63% (Cohen et al., 1991) to 97% (Arnold et al., 1992) for recurrent disease, although in the vast majority it was over 75% and tended to be higher in cases of recurrence. There have been no systematic reviews or meta-analyses due to significant heterogeneity between studies.

Despite showing promise in both detection and an ability to improve outcomes (Sun et al., 2007), the difficulties in handling and disposing of radiolabelled material combined with ever-improving imaging modalities for pre-operative staging and management planning have meant that RIGS has become relatively redundant in the last decade.

1.2.2 Radioimmunotherapy and targeted chemotherapy

Radioimmunotherapy uses antibodies to cancer-specific antigens to deliver cytotoxic radiation directly to tumour cells and minimise collateral damage to normal cells (Meyer et al., 2009, Meredith et al., 1996, de Jong et al., 2011). The majority of work has targeted CEA or TAG-72 and it has shown to be effective in small-volume disease (Koppe et al., 2005, Barbet et al., 2012) but has only had limited translational success. Similarly, targeted cytotoxic drug delivery has the potential to deliver high dose chemotherapy to cancer cells whilst limiting damage to normal cells, and has utilised a variety of biomarkers, including FR α (Zhang et al., 2012, Elias et al., 2011), EGFR (Kopansky et al., 2011) and CEA (Conaghan et al., 2008).

1.2.3 Targeted non-invasive imaging

Pre- and post-operative imaging is essential in the planning and follow-up of colorectal cancer patients. Recently Iodine-124-labelled antibodies to CEA have been administered to patients systemically and detected using positron emission tomography (PET) scanning (Carrasquillo et al., 2011, Schoffelen et al., 2012, O'Donoghue et al., 2011, Meller et al., 2011, Schoffelen et al., 2010, Boerman and Oyen, 2011); a high target-to-background ratio has the potential to add specificity when evaluating undetermined masses, a common clinical scenario during the follow-up of colorectal cancer patients. Other experimental work has used antibodies to CEA or EGFR to deliver MRI contrast agents to cancer-specific antigens (Cherukuri and Curley, 2010, Kamphuis et al., 2010, Vigor et al., 2010) to improve sensitivity and specificity.

1.2.4 Sentinel lymph node mapping

In colorectal cancer surgery, sentinel lymph node mapping (using a dye injected subserosally around the tumour) can be used to allow focussed ultra-staging of one or more nodes most likely to contain metastases. It is used routinely in the management of breast cancer (Association of Breast Surgery at BASO, 2009) and melanoma (Marsden et al., 2010) and relies on the assumption that if a sentinel lymph node is tumour free, then there will be no lymphatic metastases in any remaining nodes (Bembenek et al., 2005, Wiese et al., 2010). This provides a practical means for avoiding the resource implications of ultra-staging every resected lymph node. Since its introduction in 1999 (Joosten et al., 1999), hundreds of studies have been published, including a number of systematic reviews and meta-analyses (Mulsow et al., 2003, Bembenek et al., 2008, Des Guetz et al., 2007, van der Pas et al., 2011). These have highlighted various limitations, including false negatives, variable sensitivity in detecting the sentinel node, technical difficulties (particularly with rectal tumours) and aberrant drainage patterns. However, in the most recent and in-depth meta-analysis, Van der Pas *et al* (van der Pas et al., 2011) suggest that a sentinel lymph node procedure should be considered in all colon cancer patients without clinical evidence of lymph node metastases.

Although this is basically a method for intra-operatively delineating normal anatomy rather than tumour-specific detection, when combined with pathological ultra-staging it has the potential to alter post-operative management and has attracted further technological development. These developments have led to the emphasis of sentinel lymph node mapping shifting from a post-operative staging tool to a potential role in selective lymphadenectomy, by combining it with more cutting edge technologies such as near-infrared laparoscopy, optical coherence tomography or real time elastography.

1.2.4.1 Near-infrared laparoscopy

Indocyanine green (ICG) is a photosensitive tricarbo-cyanine dye with a peak spectral absorbance at approximately 780 nm (Landsman et al., 1976, Haritoglou et al., 2003), in the near-infrared region. Several feasibility studies have used indocyanine green as a substitute for patent blue V dye in sentinel lymph node mapping in colorectal cancer (Nagata et al., 2006, Kusano et al., 2008, Hutteman et al., 2011, Cahill et al., 2012). It can be injected subserosally (either lumenally via a colonoscope or laparoscopically) and a modified laparoscope used to detect the fluorescent signal. Compared to conventional blue dye mapping, it penetrates more deeply through living tissue and does not distort the view of the surgical field. The technique is not tumour-specific, but if combined with intra-operative, morphological sentinel node assessment, it has the potential to allow intra-operative staging and surgical stratification.

Cahill *et al* recently combined the technique with intra-operative ultrasound assessment of the sentinel node in patients with early-stage cancer (Cahill et al., 2012). The sensitivity of a 12 MHz probe is currently not high enough to detect micro-metastases but it is foreseeable that the resolution will increase with further development of high frequency ultrasound. Optical coherence tomography and elastography (see sections 1.2.4.2 and 1.2.4.3) may offer a better chance of accurately assessing the sentinel node for small deposits and micrometastases via a 'virtual biopsy'.

1.2.4.2 Optical coherence tomography

Optical coherence tomography (OCT) works in a similar way to conventional ultrasound but uses light instead of sound waves (Huang et al., 1991, Osiac et al.,

2011). Near-infrared light is used to penetrate a 'scattering media' (in this case human tissue) and back-scattering is detected to construct a three-dimensional, cross-sectional image. The properties of certain biological tissues enable OCT to act as a real-time, high resolution, microscopic imaging technique (Boppart et al., 1998, Boppart et al., 1999, Boppart et al., 2004). OCT has been used in a variety of clinical applications, including ophthalmology, evaluating coronary artery disease and, of note here, lymph node imaging (Zysk et al., 2007). When compared to conventional histopathology there is a strong correlation between images of lymph nodes (McLaughlin et al., 2010) but penetration tends to be limited to a few millimetres. The technique has since been applied to colorectal cancer surgery (Cahill et al., 2010) by passing a fibred OCT probe down the working channel of an endoscope in order to perform a real-time, *in vivo*, 'virtual biopsy' of peritoneal lymph nodes via a transgastric NOTES approach in a porcine model. OCT therefore has the potential to provide an intra-operative, real-time assessment of a sentinel node following near-infrared laparoscopic mapping.

1.2.4.3 Real-time elastography

Real time elastography is a method of assessing the elasticity of tissues and exploits the fact that most tumours are harder or stiffer than surrounding normal tissue. When an external compression force is applied to the tissue, high frequency ultrasound is used to measure the strain in the tissue and construct elastography images. It was used initially to image breast (Itoh et al., 2006), thyroid (Lyshchik et al., 2005) and prostate tumours (Konig et al., 2005). Development of intra-operative staging applications is at an early stage with work focussing on liver and pancreatic tumours (Kato et al., 2008, Inoue et al., 2010, Elias et al., 2011) but it has also been applied to the detection of malignant lymph node deposits (Săftoiu et al., 2007, McCormack et

al., 2009). This is another technology that could be combined with sentinel lymph node mapping to provide a real-time virtual biopsy of the sentinel node.

Intra-operative sentinel lymph node mapping with real-time virtual biopsy retains the limitations of conventional lymph node mapping. The assessed stage of a colorectal tumour would be entirely dependent on the assumption that the sentinel node is reflective of the true nodal status. Tan *et al* (Tan et al., 2010b) conducted a study to determine the distribution of the first metastatic lymph node in colorectal cancer by examining the mesentery of 93 patients who had only one involved lymph node found on histology. This node was not located directly below the tumour in 48% of cases and was found to have skipped the pericolic nodes or to be 5 cm beyond the longitudinal tumour margin in 18% of cases. Similarly, Park *et al* (Park et al., 2009) reported that in 6% of caecal cancers, metastasis occurred to lymph nodes along the right branch of the middle colic artery rather than the expected location of the sentinel node alongside the ileocolic artery. This suggests that however accurate the *in vivo* biopsy technology is at assessing the sentinel node, the results may not reflect the true disease stage.

1.3 A potential solution: intra-operative fluorescent imaging

My proposed solution to the limitations of current treatment paradigms is a tumour-specific fluorescent probe, capable of binding to colorectal cancer tissue at a molecular level, which could be administered to a patient prior to undergoing laparoscopic surgery. A modified laparoscopic system could then be used to identify the fluorescent probe bound to cancer cells, enabling delineation of the primary

tumour margins and detection of metastatic disease. This would then allow an intra-operative assessment of the stage of the tumour and the appropriate resection to take place. Such an application requires at least two components: a tumour-specific localisation component and a fluorescent visualisation component. A third component - a scaffold to chemically attach and arrange the two - could be used to optimise the fluorescent signal.

1.3.1 Tumour-specific localisation component

There is much interest in developing strategies for tumour-specific delivery of agents to increase our diagnostic capability or enhance the selectivity and effectiveness of therapeutics. These strategies rely on the ability to target tumour cells accurately using biomarkers that are differentially expressed between tumour and normal tissue. Antibodies to various tumour-associated antigens provide an ideal mechanism for this (Chester et al., 2004, Brennan et al., 2010). In colorectal cancer, the most commonly used biomarkers include carcinoembryonic antigen (CEA) (Muguruma et al., 1999, Heine et al., 2011, Sharkey et al., 2005, Yazaki et al., 2008, Kaushal et al., 2008), tumour-associated glycoprotein 72 (TAG-72) (Tang et al., 2007, Zou et al., 2009, Chen et al., 2008, Chen et al., 2011b), endothelial growth factor receptor (EGFR) (Qi et al., 2012, Goetz et al., 2010, Jeong et al., 2012), and folate receptor alpha (FR α) (Reddy and Low, 1998, Chen et al., 2005, Yang et al., 2010a).

Carcinoembryonic antigen (CEA):

CEA is a membrane-bound glycoprotein that is over-expressed in approximately 90% of colorectal cancers and is minimally expressed in normal colonic cells (Jantscheff et al., 2003). It is expressed less strongly in gastric, pancreatic, breast, lung and medullary thyroid cancer (Hammarström, 1999). CEA actually represents a family of

proteins encoded by 29 genes (Hammarström, 1999), meaning the actual epitope is not always clear.

Tumour-associated glycoprotein 72 (TAG-72):

TAG-72 is a mucin-like molecule with a similar expression to CEA in colorectal cancer and normal tissue. It is also over-expressed on the surface of a variety of adenocarcinomas including gastric, pancreatic, breast, prostate, endometrial and ovarian tumours (Colcher et al., 1989, Johnson et al., 1986). Like CEA, TAG-72 is not encoded by a single gene.

Folate receptor α (FR α):

FR α is a membrane-bound protein that binds and transports folic acid and is over-expressed in epithelial-derived cancers, including those of the colorectum (Shia et al., 2008). It appears to be expressed relatively infrequently in colorectal tumours but is absent in the vast majority of normal tissues, hinting at a potentially high specificity (Shia et al., 2008).

Epidermal growth factor receptor (EGFR):

EGFR is a well-known target for anti-cancer therapies but the literature concerning the degree and frequency of EGFR over-expression in colorectal cancer is contradictory, with reported expression varying from 33% to 97% of cases (Koretz et al., 1990, Lee et al., 2002, Spano et al., 2005, Bhargava et al., 2006). It is also reported to be expressed in up to 48% of normal colorectal samples (Koretz et al., 1990), which could compromise its specificity for cancer tissue.

These four biomarkers have been targeted in the majority of diagnostic and therapeutic applications in colorectal cancer. A surprising feature of all the examples of in vivo tumour targeting described in section 0 is that the choice of biomarker used

is rarely justified in terms of its tumour sensitivity and specificity. The characteristics of suitable cancer biomarkers are that they must be highly expressed in a large majority of tumours and have low or no expression in normal tissue, encompassing the normal tissue from which the tumour is derived and – ideally – most or all normal adult tissues accessible to systemic delivery. Suitable molecules must also be located on the external facing surfaces of cancer cells so as to be accessible to systemically-delivered recognition molecules. To my knowledge, expression of the most commonly used markers for colorectal cancer has never been rigorously evaluated in a well-defined cohort of cancer and normal tissue. I will need to choose the most appropriate biomarker-specific antibody to use for my application

1.3.2 Fluorescent visualisation component

Once bound specifically to a cancer cell, the antibody must be visible to the operating surgeon but must not distort views of the surrounding anatomy. Fluorescence is ideal for this purpose as it can effectively be turned on or off on the screen of a modified laparoscope using selective filters of different wavelengths. Fluorescence occurs when a substance (a fluorophore) absorbs electromagnetic radiation, exciting electrons to a higher quantum state before returning to their ground state and emitting a photon (light) at a different wavelength to that which was absorbed. Normal biological tissues naturally emit non-specific auto-fluorescence when excited by light with wavelengths commonly used in fluorescent imaging (e.g. from mitochondria and lysosomes) which can potentially interfere with an imaging system (Monici, 2005). I require a fluorophore that absorbs electromagnetic radiation at a wavelength that penetrates tissues deeply without damaging them, emits light at a wavelength different to that of auto-fluorescing tissues, and is suitably bright. Near infra-red light (wavelength approximately 700 - 3000 nm) is ideal because

haemoglobin, lipids and water tend to absorb the least amount of light at wavelengths in the near-infrared range, allowing deeper tissue penetration than other wavelengths (Weissleder and Ntziachristos, 2003, Hilderbrand and Weissleder, 2010). Non-specific tissue auto-fluorescence is also significantly lower at longer wavelengths, improving the target to background ratio (Muller et al., 2001). A fluorophore with a longer wavelength is therefore desirable in an *in vivo* imaging system. The near-infrared cyanine (Cy) dyes (absorption wavelength 650-900 nm) have been used in clinical trials for anatomical delineation of lymph channels and nodes, bile ducts, mesenteric and anastomotic perfusion, and ureters (Ashitate et al., 2012, Soltesz et al., 2006, Kusano et al., 2008, Hutteman et al., 2010, Cahill et al., 2011, Matsui et al., 2011, Cahill et al., 2012), frequently combined with modified laparoscopes. However, none of these applications use fluorophores targeted to specific tissues or cells - instead they are simply inserted into the anatomical compartment of interest.

Several groups have published small studies evaluating fluorophores conjugated to targeting antibodies in murine models of colorectal (Kaushal et al., 2008, Zou et al., 2009), pancreatic (Kaushal et al., 2008), breast (van Scheltinga et al., 2011, Wu et al., 2013) and head and neck cancers (Heath et al., 2012, van Scheltinga et al., 2011) using near infrared dyes including Oregon Green Thermo (Thermo-Fisher, Massachusetts, USA), Cy7, IRDye 800CW (Li-Cor, Nebraska, USA) and rhodamine as the fluorophore. All studies demonstrated fluorescent labelling of the tumours but when the tumour-to-background ratio and non-specific fluorescence were taken into account the results were potentially less impressive, as detailed below. For such systems to be effective in laparoscopic colorectal cancer surgery, three important criteria must be fulfilled: the fluorescent signal must be of adequate magnitude to pass through the muscular bowel wall and the fatty mesentery; the tumour-to-background ratio must be large enough to allow sensitive and specific detection; and the fluorophore must be relatively resistant to photobleaching, a particular issue due

to the sometimes extended duration of operations for colorectal cancers. The results of the published studies suggest that the systems used were unlikely to fulfil these criteria. For example, Heath *et al* used a IRDye800CW-conjugated anti-EGFR antibody in mice with head and neck xenograft tumours combined with a fluorescent intra-operative imaging system (Heath et al., 2012). The authors found the signal-to-background ratio to be only 2.9 for the test particle and 1.4 for their control antibody, meaning the fluorescence achieved was not dramatically above background and exhibited only slight antibody directed targeting. Similarly, van Scheltinga et al achieved a tumour-to-background ratio of 2.8 using the same dye in a murine breast cancer model (van Scheltinga et al., 2011). It is notable that despite initial studies suggesting potential for translation to the operating theatre in 2008, there has been no progress beyond mouse models.

1.3.2.1 Indocyanine green

Unlike the dyes used in the examples above, indocyanine green (ICG) is insoluble in water at physiological pHs and is not easily conjugated to protein molecules (Landsman et al., 1976). Ito et al developed ICG-Sulfo-OSu, which has a succinimidyl ester available for binding to a free amine group on an IgG molecule (Ito et al., 1995). Following this there were limited attempts to use ICG-labelled antibodies for fluorescent immunohistochemistry of fixed tissues (Muguruma et al., 1998, Muguruma et al., 1999) that received no further attention. This might be explained by the data published by Ogawa et al (Ogawa et al., 2009): the authors showed that when ICG-Sulfo-OSu was conjugated to IgG antibody the fluorescence intensity was low and this remained the case when alternative antibodies were used. Furthermore, when the antibody to ICG molar ratio was increased, this 'quenching' effect also increased; at 1:1 conjugation the observed quenching capacity was 6-fold,

whereas at 1:8 it was 58-fold. When the authors added 2% sodium dodecyl sulphate (SDS) and 2-mercaptoethanol (2-MEA), the fluorescence dramatically increased. The authors hypothesised that this was due to the covalent bond between the two being cleaved although this mechanism is not fully understood. They found that following cell membrane binding, ICG-antibody conjugates were gradually internalised into the cell cytoplasm and gradually became 'activated' over eight hours, producing detectable cytoplasmic fluorescence. Presumably this occurs during lysosomal metabolism. The authors exploited this phenomenon by conjugating ICG-Sulfo-OSu to anti-human epidermal growth factor receptor 2 (HER2) monoclonal antibodies and successfully using them for *in vivo* imaging in a murine xenograft model of breast cancer. The same group also published further similar work using a murine xenograft of prostate cancer (Nakajima et al., 2011). This property implies that the non-specific background signal in an *in vivo* system would be reduced, as only internalised ICG will be fluorescent and all other ICG-antibody conjugates that have not bound to the target antigen will remain quenched. In addition, the ICG appears to remain fluorescent within the cytoplasm for up to 10 days (Nakajima et al., 2011). The logistics involved in administering the drug and scheduling surgery would therefore be more flexible and multiple doses could be administered to increase the number of ICG molecules in the cell. These factors may allow improved fluorescent detection compared to simple surface-bound fluorescent antibody systems.

Importantly, ICG is a U.S. Food and Drug Standards Agency (FDA) and UK Medicines and Healthcare Products Regulatory Agency (MHRA) approved dye, so translation from *in vitro* studies to clinical trials could be rapid. Its potential as a medical dye was first described in 1957 (Fox et al., 1957) and it has been used in clinical studies for ophthalmic angiography (Holz et al., 1998), hepatosplanchnic blood flow estimation (Uusaro et al., 1995), intra-operative small bowel angiography (Matsui et al., 2011), biliary cholangiography (Ishizawa et al., 2009), anastomotic

perfusion estimation (Ris et al., 2014) and sentinel lymph node mapping (Cahill et al., 2012, Kusano et al., 2008, Soltesz et al., 2006). It has been used in the majority of the anatomical delineation clinical trials mentioned in section 1.2.4.1 with no reported side effects. It also has an emission spectrum in the near-infrared range (810 nm in water and 830 nm in blood (Fox et al., 1957)), potentially reducing background autofluorescence (Vahrmeijer et al., 2013, Alander et al., 2012).

1.3.3 Nanoparticle scaffold

A nanoparticle is generally considered to be a particle with lengths in two or three dimensions of between one and 100 nm (ISO, 2008, ASTM, 2012). They can be synthesised in a vast number of shapes, sizes and materials, with a similarly variable chemical composition and surface chemistry. There has been great interest in their potential for biomedical applications ever since the field of nanotechnology was established and throughout its subsequent rapid expansion.

A fluorescent, tumour-specific molecular probe for live *in vivo* colorectal cancer imaging must fulfil the following criteria:

- The molecule must have pharmacokinetic properties that enable it to be delivered efficiently to a tumour following systemic vasculature delivery;
- The fluorescent signal must be of adequate magnitude to pass through the muscular bowel wall and the mesentery;
- The tumour-to-background ratio must be large enough to allow sensitive and specific detection;
- The fluorophore must be relatively resistant to photobleaching;
- It must have a favourable toxicity profile.

Nanotechnology may provide a potential solution to the limitations seen with simple fluorophore-antibody conjugates and improve the above criteria. If a chemical nanoparticle scaffold could be used to link the two components, the fluorescent signal could be concentrated by providing many more fluorophore molecules per antibody molecule. Multiple antibodies targeting different tumour-specific antigens could theoretically be attached to maximise sensitivity.

For systemic delivery, the fluorophore-nanoparticle-antibody complex would have to be small enough to pass through the small capillaries in tumour tissue to reach the target antigen and be non-toxic. Although dependent upon many factors including particle shape, surface chemistry and charge, it is generally accepted that for this to occur, nanoparticles must have a diameter of less than 200 nm (Matsumura and Maeda, 1986, Moghimi et al., 2012, Perrault et al., 2009). Solid tumours display an inherent 'leaky' vasculature and deficient lymphatic drainage that allows intravenously delivered nanoparticles to passively accumulate, known as the enhanced permeation and retention effect (Peer et al., 2007, Matsumura and Maeda, 1986). The combination of small particle size and relatively permeable tumour-associated vasculature enables deep tumour penetration (Brannon-Peppas and Blanchette, 2004). They are usually rapidly sequestered by the liver, spleen and other parts of the reticuloendothelial system (RES) depending on their surface characteristics (Gabizon et al., 2003). The surface of a nanoparticle can be functionalised to carry a variety of chemical groups, enabling specific molecules (such as antibodies or fluorophores) to bind to them. By controlling these surface functional groups, a particle can be made to have a hydrophilic surface, reducing uptake and prolonging circulation time and hence affording greater targeting potential (Gaur et al., 2000). Incorporation of polyethylene glycol (PEG), a hydrophilic copolymer, to nanoparticle surfaces has been shown to effectively increase the

circulating half-life by preventing opsonisation by the RES (Owens Iii and Peppas, 2006).

1.3.3.1 Toxicity

Research into the potential toxicity of nanoparticles for biomedical applications appears to have taken a backseat during the field's rapid expansion (Lewinski et al., 2008) but concerns have been raised regarding the toxic effects of exposure and accumulation (Li et al., 2010, Marquis et al., 2009, Soenen and De Cuyper, 2010, Yang et al., 2010b). This tends to affect the route of administration and the organ(s) responsible for their clearance - if the nanoparticle is non-biodegradable, accumulation in these organs can lead to toxicity (Ilium et al., 1986, Peracchia et al., 1999) with unknown long term effects. In addition, the unique kinetic properties of nanoparticles in solution have led to errors when extrapolating toxicity data obtained *in vitro* experiments (Teeguarden et al., 2007). This is because nanoparticles usually exist as a suspension in a fluid as opposed to a true solution, therefore predicting their behaviour based on *in vitro* results can be difficult.

1.3.3.2 Liposomes, polymeric and silica nanoparticles

The variable shape, size, material and surface chemistry all impact the fate of a nanoparticle in a complex biological system (Alexis et al., 2008). These factors and the potential for toxicity has led to the majority of work concentrating on liposomes and polymeric nanoparticles (Petros and DeSimone, 2010), which have shown the greatest potential *in vivo*.

Liposomes are vesicles consisting of spherical phospholipid bilayers. They provide a non-toxic system for delivering drugs to target tissue and controlling their release, via endocytosis at the cell membrane. They have been successfully employed in delaying the release of local anaesthetic agents (Davidson et al., 2010) and in delivering chemotherapy agents (Kaasgaard and Andresen, 2010, Andresen et al., 2010), vaccines, anti-fungals, anti-virals and gene therapeutics (Lian and Ho, 2001). Whilst ideal for delivery of a payload, they are less suitable for *in vivo* fluorescent imaging because of rapid endocytosis and poor specificity (Miller et al., 1998).

Polymeric microspheres, synthesised using an emulsion polymerisation process, have tended to be the most common type of particle used in biological applications (Soppimath et al., 2001). Their size can be readily controlled and their surface can be functionalised with a variety of groups for conjugation. Mesoporous silica, containing multiple micropores, has been the preferred choice of material due to its relative non-toxicity, ease of manufacture and optical transparency (allowing fluorophores to be incorporated) (Burns et al., 2006, Li et al., 2012, Slowing et al., 2008, Tang et al., 2012).

1.3.3.3 Dye-doped silica nanoparticles

Dye-doped silica nanoparticles fulfil many of the criteria required for a targeted intra-operative imaging platform and are my preferred choice. They comprise a fluorescent core with thousands of dye molecules embedded in silica. A silica shell that can be functionalised with various chemical groups for conjugation surrounds this. They were first described in 2001 (Qhobosheane et al., 2001) and since then a limited number of studies have been published in which these particles have been investigated as agents to allow fluorescent labelling of cancer cells *in vitro* (Huang et

al., 2009, Santra et al., 2001, Tivnan et al., 2012). They have been shown to be relatively non-toxic compared to many nanoparticles, with excretion via the faeces and urine following intravenous administration (Fu et al., 2013).

There are two important limitations to the data presented: firstly, the methodology for manufacturing this type of particle is highly variable, with large variations between techniques and several different chemical conjugation strategies for linking a targeting antibody to the nanoparticle; secondly, in the limited number of papers that describe cell targeting experiments, the methodology is poor with a lack of robust controls or fluorescence quantification. A key concern is the high level of non-specific binding potentially exhibited by these particles when using some conjugations to antibodies, meaning that use of appropriate non-tumour targeted controls is critical. The vast majority of published work in this field has used either 'bare' nanoparticles as a control, with no targeting antibody attached, or no control particle at all. There are no reports of successful live *in vivo* tumour targeting in colorectal cancer.

1.3.3.4 Quantum dots

Quantum dots are fluorescent semiconductor nanocrystals that have a number of characteristics differentiating them from organic fluore (Michalet et al., 2005). Their size determines the absorption and emission spectra and can be closely controlled or 'tuned' during their manufacture. Their extinction coefficients - the amount of light that can be absorbed - are also claimed to be longer and they are more stable than conventional dyes, with a high resistance to photobleaching, where the the fluore is damaged by the exciting light (Watson et al., 2003, Ballou et al., 2003). These properties make quantum dots potentially ideal fluorophores for imaging purposes but their toxicity remains a concern (Pelley et al., 2009), particularly as they are

commonly constructed from cadmium and either tellurium or selenium, all of which are toxic to humans. Efforts have been made to coat quantum dots with a chemical shell, such as zinc sulphide, to reduce toxicity without compromising their optical properties (Cho et al., 2010, Darbandi et al., 2010). It is also possible to conjugate antibodies to their surface (Gao et al., 2004, Wu et al., 2003, Ballou et al., 2003, Yang et al., 2009), allowing antigen-specific fluorescence. Despite early claims of huge advantages over traditional fluorophores for biomedical imaging, supporting robust and conclusive data have not been forthcoming.

1.4 HYPOTHESIS AND AIMS

My hypothesis is that a tumour-specific, intra-operative fluorescent imaging system for detecting colorectal cancer would allow more accurate identification of primary tumour margins and more sensitive detection of metastatic disease, leading to more effective tumour treatment and improvement in patient outcomes.

My aims are:

- i) To identify sensitive and specific antibodies for colorectal cancer cell antigens and examine their expression in a large cohort of tumour and normal colon samples;
- ii) To produce a fluorescent nanoparticle and conjugate it to the best performing antibody;
- iii) To examine the sensitivity and specificity of these fluorescent nanoparticles for colorectal cancer cells using model systems including cell lines and xenograft mouse models.

Use of this intra-operative imaging system could potentially be examined in future clinical trials and if successful could improve outcomes for colorectal cancer treatment.

Chapter Two

Methods

The tissue micro-arrays described in this chapter were prepared by S Yeluri.

2 METHODS

2.1 Immunohistochemistry

2.1.1 Immunohistochemistry methods

Blocks were sectioned (5 µm) onto SuperFrost Plus microscope slides (Menzel-Glaser, Braunschweig, Germany), dewaxed with xylene and rehydrated through graded ethanol before rinsing in water for 5 minutes. Antibody-binding epitopes were retrieved either by heating the slides in pre-warmed 10mM citric acid buffer (pH 6.0), using a microwave (buffer pre-heated at 900W for 2 minutes, slides heated at 900W for 10 minutes), using a pressure cooker (pre-heated for 10 minutes, slides heated for eight minutes, 125°C, 103.4 kilopascals), or by incubating with 100 µl of proteinase K in 50 ml of phosphate buffered saline (PBS) at 37°C for 25 minutes. Endogenous peroxidase activity was blocked with 10% hydrogen peroxide (H₂O₂) for 10 minutes before re-rinsing in water for 5 minutes. If non-specific stromal staining was present, an extra block step was then performed using casein (1:10 dilution in Tris-buffered saline, TBS; 60 ml 2.5 M NaCl mixed with 20 ml Tris-HCl pH 7.4 and 920 ml distilled water) for 20 minutes. Each slide was mounted in a sequenza (Thermo Scientific, Massachusetts, USA) and rinsed with TBS followed by antibody diluent reagent solution (Invitrogen, Carlsbad, USA) to prevent non-specific binding. 100µl of primary antibody diluted in diluent was added at a range of concentrations and incubated at room temperature for 1 hour or overnight at 4°C. Slides were washed twice with TBS-tween (TBS-T, TBS plus 10% [v/v] Tween-20) and once with TBS, for five minutes each before incubating with an appropriate horseradish peroxidase (HRP)-conjugated polymer secondary antibody (Invitrogen) for 30 minutes

at room temperature. The slides were re-washed, twice with TBS-T and once with TBS for 5 minutes. 100µl of 3,3'-diaminobenzidine DAB (Invitrogen) solution was added to each slide for 10 minutes before a 5 minute wash in water. Slides were then stained with haematoxylin for 1 minute, washed in water for 1 minute, washed in Scott's tap water for 1 minute and re-washed in water for 1 minute. They were then dehydrated with graded ethanol and xylene before being mounted with DPX Histology mountant (Sigma Aldrich, St Louis, USA).

2.1.2 Antibodies

Antibodies to the eight chosen antigens were selected as detailed below:

Antibody	Type	Clone	Code & Manufacturer	Publications
Anti-CEA	IgG1 monoclonal mouse anti-human	II-7	M7072, Dako, Denmark	(Zoubir et al., 1990)
Anti-CEA	IgG1 monoclonal mouse anti-human	-	A5B7, Biotherapeutics Development Unit, Cancer Research UK, Clare Hall Laboratories, Potters Bar, UK	(Meyer et al., 2009) (Dawson et al., 1991) (Lane et al., 1994)
Anti-TAG-72	IgG1 monoclonal mouse anti-human	-	sc-20043, Santa Cruz, Texas, USA	(Povoski et al., 2012) (Sun et al., 2007)
Anti-EGFR	IgG1 monoclonal mouse anti-human	31G7	Invitrogen, Carlsbad, USA	(Buckley and Kakar, 2007)
Anti-VEGFR2	IgG1 monoclonal mouse anti-human	KDR/EIC	ab9530, Abcam, Cambridge, UK	(Duff et al., 2006) (Schimanski et al., 2010b)
Anti-folate receptor α	IgG1 monoclonal mouse anti-human	BN3.2	Leica Biosystems, Newcastle, UK	(Smith et al., 2007)
Anti-robot1	IgG1 polyclonal goat anti-human	I-20	sc-16612, Santa Cruz, USA	(Grone et al., 2006) (Wang et al., 2003)
Anti-CD105	IgG1 polyclonal mouse anti-human	SN6h	M3527, Dako, Denmark	(Bellone et al., 2010) (Burrows et al., 1995)

Table 2.1. Antibodies selected for the chosen panel of antigens.

2.1.3 Optimisation

Thirteen specimens of formalin-fixed, paraffin-embedded colorectal cancer of various grades and one sample of normal colonic tissue were used to optimise antibody concentrations and experimental protocols. For each primary antibody, a range of concentrations was tested according to the manufacturers' guidelines and relevant published papers. Control slides with no primary antibody were included. Duplicate slides were tested using different methods of antigen retrieval: no retrieval; heat retrieval; and proteinase K retrieval. Slides were examined by a pathologist (ETV) and the quality of staining assessed, specifically comparing tumour samples to the normal sample and looking for positive cancer cell staining with negative stromal fibroblasts and leukocytes. If staining was non-specific, with stromal and cancer cell staining present, fresh slides were incubated with 100µl of 10% casein for 20 minutes and reassessed by a pathologist. If staining was absent, slides were incubated with the primary antibody overnight at 4°C and reassessed.

2.1.4 Tissue micro-arrays

2.1.4.1 Ethics and patient cohort

Ethical approval was obtained from the National Research Ethics Service (London-Dulwich Committee), reference 12/LO/1327. Formalin-fixed paraffin-embedded (FFPE) tissue blocks containing primary colorectal carcinoma and matched normal colorectal mucosa, collected prospectively for the MRC CLASICC trial (Guillou et al., 2005), were available from 280 patients. FFPE blocks containing mesenteric lymph nodes (both tumour-cell positive and negative) were available for 18 of the patients.

2.1.4.2 Procedure

Tissue microarrays (TMAs) were constructed from formalin-fixed samples of colorectal cancer and normal colonic mucosa using 0.6mm cores embedded in paraffin blocks by SY. For each patient, three cores selected from the most representative tumour area (as determined by haematoxylin and eosin (H&E) staining) and three cores from normal colon were included. The 280 colorectal tumours and matched normal tissues were sampled in seven TMAs, with three cores for each tumour and three cores for each matched normal tissue sample. Immunohistochemistry was performed on each TMA with anti-CEA (A5B7), anti-TAG-72, anti-EGFR and anti-FR α at concentrations of 1:150000, 1:100, 1:50 and 1:25 respectively. Microwave antigen retrieval was used for anti-CEA and anti-TAG-72, proteinase K retrieval was used for anti-EGFR and pressure cooker retrieval was used for anti-FR α .

2.1.5 Scoring

Slides were digitally scanned using Scanscope XT (Aperio, Vista, USA) at 20x magnification and were observed for scoring using ImageScope v11 (Aperio, Vista, USA). Staining was assessed semi-quantitatively using a bespoke scoring system developed in consultation with two pathologists (ETV and NPW). Cores were scored for intensity of epithelial cell staining (0, no staining; 1, mild; 2, moderate; 3, strong) and an estimate of the percentage of epithelial cells staining positively (0, <5%; 1, 5-20%; 2, 21-40%; 3, 41-60%; 4, 61-80%; 5, 81-100%). These scores were multiplied to give final scores of 0 to 15, as has been done previously (Lombardi et al., 1999, Soslow et al., 2000, Lyall et al., 2006, Leeman et al., 2002). A mean score was calculated from the core scores for each tumour and each matched normal sample. Tumour cores with no tumour cells and normal cores with no epithelial cells

visible were discounted. Carcinoembryonic antigen and TAG-72 were scored for apical membranous staining only. Folate receptor α showed mild cytoplasmic staining only, and was scored solely for this. EGFR showed membranous, and - more rarely - cytoplasmic and nuclear staining. However, following established literature (Buckley and Kakar, 2007, Scartozzi et al., 2004) EGFR was scored for membranous expression only. Two independent observers were involved in the scoring: I scored all cores and a pathologist (ETV) blinded to the antibodies scored a sample representing 15% of the cases. Scoring reproducibility was determined for each antibody using the intra-class correlation coefficient; the process of calculating the mean score for each patient led to 61 possible outcomes and therefore the data were treated as continuous rather than categorical. Scores for each case of tumour or normal tissue were means of scores allocated by me for each core from that tissue. If only one core score was available, for example due to lack of appropriate cell types or core loss (where the core is stripped from the slide during the staining process) this single score was used; a method that has been validated previously (Camp et al., 2000, Torhorst et al., 2001)). Means for normal and tumour tissue were compared using Wilcoxon signed-rank tests for paired non-parametric data. Sensitivities and specificities were calculated from the mean scores for tumour and normal tissue expression for each case using two different cut-off points: the 95th percentile of the normal tissue score distribution and optimal cut-offs identified by receiver operating characteristic curves (Maraqa et al., 2008).

2.2 Tissue culture

Six cell lines were used in this work, as detailed in Table 2.2. All cell lines tested negative for mycoplasma. Cells were grown in T75 flasks at 37°C and 5% CO₂.

Cell line	Description	Supplier	Media
HT-29	Human colorectal adenocarcinoma	ATCC	RPMI 1640 + 10% fetal calf serum (Life Technologies)
HRT-18	Human colorectal adenocarcinoma	ATCC	RPMI 1640 + 10% fetal calf serum (Life Technologies)
CACO2	Human colorectal adenocarcinoma	ATCC	RPMI 1640 + 10% fetal calf serum (Life Technologies)
LS174T	Dukes' B human colorectal adenocarcinoma	ATCC	Advanced MEM + 10% fetal calf serum (ATCC)
LoVo	Dukes' C human colorectal adenocarcinoma	ATCC	F12 Nutmix (Life Technologies)
HCT116	Human colorectal adenocarcinoma	ATCC	RPMI 1640 + 10% fetal calf serum (Life Technologies)

Table 2.2. Cell lines used for *in vitro* experiments.

2.2.1 Cell line authentication

The cell lines used most extensively in this work, LS174T, LoVo and HCT116, were authenticated using deoxyribonucleic acid (DNA) profiling. Genomic DNA was extracted using a Qiagen DNA extraction kit (Qiagen, Venio, Netherlands). This was then sent to Dr Claire Taylor of the Leeds Genomic Centre who used a PowerPlex 16 HS system (Promega, Wisconsin, USA) to profile the cellular DNA and compared the results to reference material for each cell line. All three were considered authentic.

2.3 Immunofluorescence

2.3.1 Cell lines

HT-29, HRT-18 and CACO2 colorectal cancer cells were cultured on plastic in RPMI 1640 with L-glutamine media supplemented with 10% heat-treated foetal calf serum (FCS) (GIBCO, 21875, Invitrogen, UK). Human umbilical vein endothelial cells (HUVEC) were cultured on plastic in large vessel endothelial growth media (ZHM 2961, TSC Cellworks, UK). All cell lines were incubated at 37°C and 5% CO₂. For immunofluorescence, cells were seeded on to glass cover slips in six well plates at least 24 hours before use.

2.3.1.1 Fixed cells

The media was removed and the coverslips were washed in PBS before being incubated in 4% paraformaldehyde for 10 minutes at room temperature. The paraformaldehyde was removed and the cells were washed twice in PBS. The coverslips were washed in diluent reagent solution to prevent non-specific binding and incubated with each primary antibody, diluted to the appropriate concentration with diluent, for one hour at room temperature. Control slides with no primary antibody were included. They were washed twice with TBS-T and once with TBS for five minutes each and incubated with a fluorescent secondary antibody (Alexa Fluor 594 or 488 goat anti-mouse, Life Technologies, Carlsbad, USA) for 30 minutes at room temperature in the dark. Five minute washes with TBS-T and TBS were repeated. The coverslips were then mounted onto SuperFrost Plus microscope slides (Menzel-Glaser) using Prolong Gold Anti-fade DAPI Reagent (Invitrogen) and left overnight in the dark to cure. Slides were viewed using a Zeiss Axiovision fluorescent microscope (Carl Zeiss, Oberkochen, Germany) with the appropriate filter for the

secondary antibody. Phase and fluorescent (DAPI and FITC or Texas Red) images were captured at 63X magnification.

2.3.1.2 Live cells

As above, except coverslips were not incubated in chilled methanol.

2.3.2 Fresh frozen tissue

Ethical approval from the National Research Ethics Service (Leeds East), reference 15/YH/0080, was already in place for the Leeds Multidisciplinary Research Tissue Bank. Archived samples of freshly frozen colorectal cancer tissue and matched normal controls from five patients were cryosectioned (Leica LM3050, Leica Biosystems, Newcastle, UK) into 5 μm thick sections using and mounted directly onto SuperFrost Plus slides. They were left to dry at room temperature for 60 minutes and rehydrated with TBS. They were then incubated with each antibody, mounted, viewed and captured as per the live cells.

2.4 Ex vivo model

2.4.1 In vitro proof of concept

LS174T cells were grown and seeded onto glass coverslips in a six-well plate as in 2.2. The media was removed, the cells were washed with PBS and anti-CEA was then added and incubated for one hour at room temperature. The cells were washed twice with TBS and once with TBS-T and then fixed in formalin (one hour at room

temperature). They were then washed, incubated with a fluorescent secondary antibody and mounted as per section 2.3. The slides were analysed using a Zeiss Axiovision fluorescent microscope with the appropriate filter for the secondary antibody. The results were compared to immunofluorescence carried out on fixed cells where the primary antibody was added following fixation in formalin.

2.4.2 Human study

Ethical approval for this work was obtained from the National Research Ethics Service (Leeds), reference 12/YH/0002. Three patients undergoing elective resection of colorectal cancer were recruited. Immediately following resection of the specimen, a 21G cannula was inserted into the inferior mesenteric artery (descending/sigmoid colon tumour), ileocolic artery (caecal tumour) or right colic artery (ascending colon tumour) and secured with a vicryl ligature. Three ml of 0.48 mg/ml A5B7 anti-CEA in PBS was injected and the artery ligated. The specimen was fixed in formalin and underwent routine histopathological examination. Paraffin-embedded blocks of tumour tissue were then cut and mounted onto glass slides. The slides were subjected to routine immunohistochemistry but only a secondary antibody was used.

2.5 Antibody-fluorophore conjugates

2.5.1 Antibody-fluorescein

A 15-fold molar excess of NHS-fluorescein dye (Thermo Scientific) to IgG antibody was used. One mg of NHS-fluorescein was dissolved in 100 μ l of DMSO. Five μ l of

the NHS-fluorescein solution was added to 500 μ l of 2 mg/ml IgG dissolved in borate buffer (0.05 M, pH 8.5) and mixed thoroughly. It was incubated for 1 hour at room temperature. It was then transferred to a 10 kDa cut-off spin filter (Amicon) and centrifuged for 2.5 minutes at 16100 g. The eluent was discarded and the chamber was topped up with borate buffer (0.05 M, pH 8.5) and the spin repeated. This was repeated a further six times but PBS was added between spins. The flow-through was tested for fluorescence using a fluorometer to ensure no further unbound fluorescein was present. The filtrate was then collected in a fresh collection tube by inverting the filter chamber and centrifuging at 100 g for 30 seconds. The total volume was made up to 500 μ l with PBS and used as a stock solution. It was stored at 4°C in the dark. The degree of fluorescein labelling was calculated using the following formulae:

$$\text{Correction factor, } CF = \frac{A_{280}}{A_{\text{max of fluorescein}}}$$

- A_{280} = absorbance of the labelled antibody at 280 nm
- A_{max} = maximum absorbance

$$\text{Antibody concentration (moles)} = \frac{A_{280} - (A_{\text{max}} \times CF)}{\epsilon_{\text{antibody}}} \times \text{dilution factor}$$

- $\epsilon_{\text{antibody}}$ = molar extinction coefficient of IgG

$$\text{Moles fluorescein per mole antibody} = \frac{A_{\text{max of labelled antibody}}}{\epsilon_{\text{fluorescein}} \times \text{antibody concentration}}$$

LS174T colorectal cancer cells were cultured on plastic in Advanced MEM (ATCC, Virginia, USA) media supplemented with 10% FCS and L-glutamine (1%). They were incubated at 37°C and 5% CO₂ and grown in T75 flasks (Corning, New York, USA) until confluent. They were seeded onto glass coverslips and left for 48 hours for the cells to become confluent. 200 µg of Fluorescein-anti-CEA was added to one well and 200 µg of fluorescein anti-digoxin was added to another. After one hour incubation at 37°C, the media was removed, the cells washed and the coverslips mounted as in section 2.3. A Nikon A1R-A1 confocal microscope (Nikon, Tokyo, Japan) with NHS Elements software (version 4.0) was used for imaging. For each slide, the cells were focussed in phase mode and fluorescent images were captured with the appropriate wavelength filter selected. The settings (such as laser power and gain) remained constant for each slide.

2.5.2 Antibody-indocyanine green

ICG-Sulfo-OSu was purchased from Dojindo, USA. The conjugation method was adapted from Ogawa and Nakajima (Ogawa et al., 2009, Nakajima et al., 2011). An approximate 8-fold molar excess of ICG-Sulfo-OSu to IgG antibody was used for labelling. 1.1 µl of a 10 mM stock solution of ICG-sulfo-OSu in dimethylsulfoxide (DMSO, 10.9 nM) was added to 200 µg (1.34 nM) of IgG suspended in carbonate-bicarbonate buffer (0.1 M, pH 9.1) and mixed thoroughly. It was left to react in the dark for two hours with gentle stirring. Excess dye was removed using the same spin filter protocol as in 2.5.1, washing first with carbonate-bicarbonate buffer and then PBS. The flow-through was tested for fluorescence using a fluorometer to ensure no further unbound ICG was present. The total volume was made up to 500 µl with PBS.

2.5.2.1 Pilot incubation and qualitative analysis

LS174T colorectal cancer cells were cultured as above (section 2.5.1). Cells were seeded onto 35 mm glass-bottomed wells (Iwaki, Japan, two per cell line) with 2 ml of the appropriate media. After 24 hours the media was replaced and at 48 hours 200 μ l, 20 μ l or 2 μ l of 1 μ g/ μ l ICG-anti-CEA was added to wells. As a control, I incubated one well of cells with free, unbound anti-CEA antibody at 480 μ g/ml for one hour, discarded the media/antibody solution, washed the cells, and replaced the media. I then incubated the cells with the ICG-anti-CEA conjugates at as above. The wells were then imaged at 1, 4, 8, 12, 16, 30 and 80 hours after the start of incubation using confocal microscopy and the images saved.

2.5.2.2 Continuous incubation

LS174T cells were grown as above. LoVo and HCT116 cells were grown in F12K Nutmix (Life Technologies) and RPMI1640 (Life Technologies) media respectively, supplemented with fetal calf serum (FCS, 10%) and L-glutamine (1%) at 37°C and 5% CO₂, in T75 flasks (Corning, New York, USA) until confluent. Cells were seeded onto 35 mm glass-bottomed wells (Iwaki, Japan, two per cell line) with 2 ml of the appropriate media. After 24 hours the media was replaced and at 48 hours, for each cell line, 200 μ l of 1 μ g/ μ l ICG-anti-CEA was added to one well and 200 μ l 1 μ g/ μ l ICG-anti-digoxin added to the other. The wells were then imaged individually at 1, 6, 12, 24, 36 and 48 hours using confocal microscopy (maintaining 37°C and 5% CO₂).

For each slide, the cells were focussed in phase mode in the centre of one quadrant of the coverslip (Figure 2.1). The operator did not view the fluorescent image prior to cell selection. The Cy7 and phase filters were then selected and automatically calibrated for the first image capture only; the settings (such as laser power and gain) were then saved and used for all subsequent image capture. A phase/Cy7 z-stack

image (distance between stacks: 0.5 μm , 0.2 μm and 0.4 μm for LS174T, LoVo and HCT116 cells respectively, chosen to produce a similar number of z-stack images) was captured for the first quadrant. The upper and lower limits of the z-stack were set to ensure that the whole depth of at least one cell was included. The microscope stage was then moved to the next quadrant, the white light image focussed, and a z-stack captured without the operator viewing the fluorescent image. This was repeated so that for each coverslip, five z-stack files were captured: an image from approximately the centre of each quadrant and one from the centre of the entire coverslip. By not examining the fluorescent image during image location selection, potential selection bias was removed.

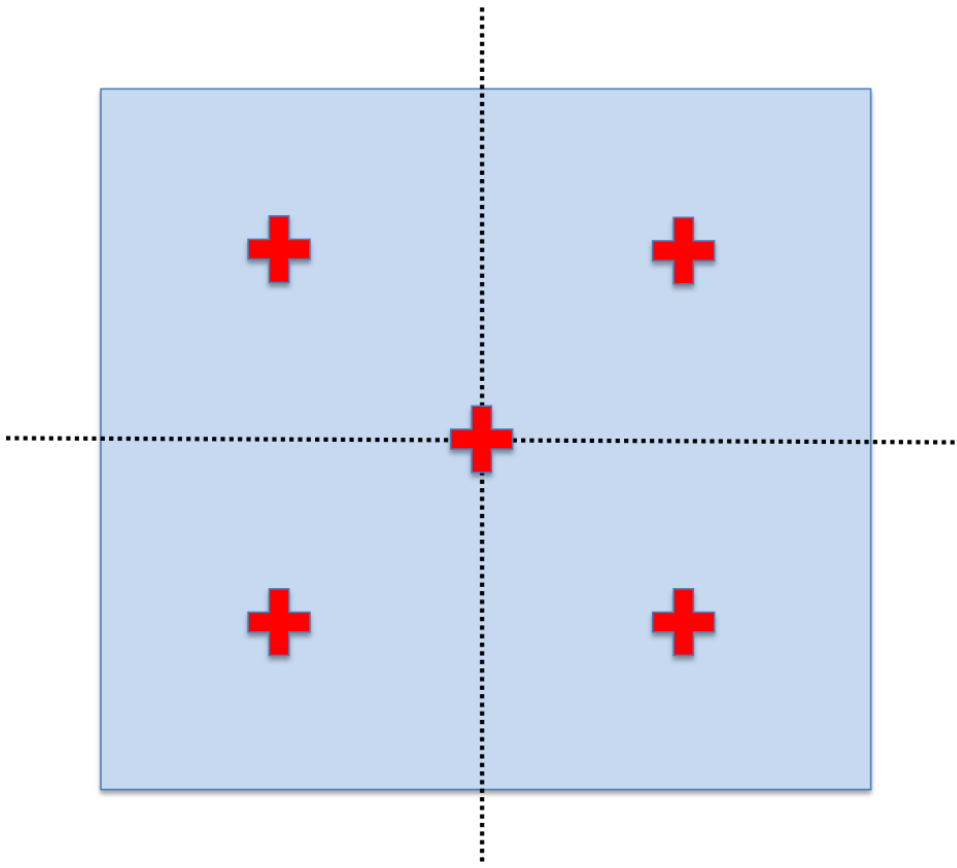


Figure 2.1. Cell selection for fluorescence quantification.

For each coverslip, confocal cellular images were captured from five points as shown. Cells were selected using white light (phase) imaging only to prevent selection bias.

2.5.2.2.1 Image analysis

A single slice from each z-stack was selected. This was chosen by identifying a distance from the base of the cells for each cell line such that the slice would always be approximately half way between the base and top of the cell. These distances were 5 μm , 1.4 μm and 4.8 μm for LS174T, LoVo and HCT116 cells respectively. These slices were saved as fluorescent, phase and combined '.tiff' images for each cell analysed. LS174T cells grow as clusters so small clusters of a similar size were selected (mean 6 cells). Fluorescence was quantified using ImageJ software version

1.42q (NIH Freeware, Maryland, USA). The phases were 'stacked' and, using the phase image only (to prevent operator bias), the outer boundaries of cell membranes were traced using the freehand tool (Figure 2.2A). This trace was then applied to the fluorescent only image and the raw integrated density (RawIntDen, the sum of the pixel values in the selected area) and the area of the selection were recorded (Figure 2.2 B). A background area was then selected (ie. an area with no cell fluorescence) and the same measurements taken (Figure 2.2 C-D). This process was repeated for each coverslip, for both ICG-anti-CEA and ICG-anti-digoxin, at each time point.

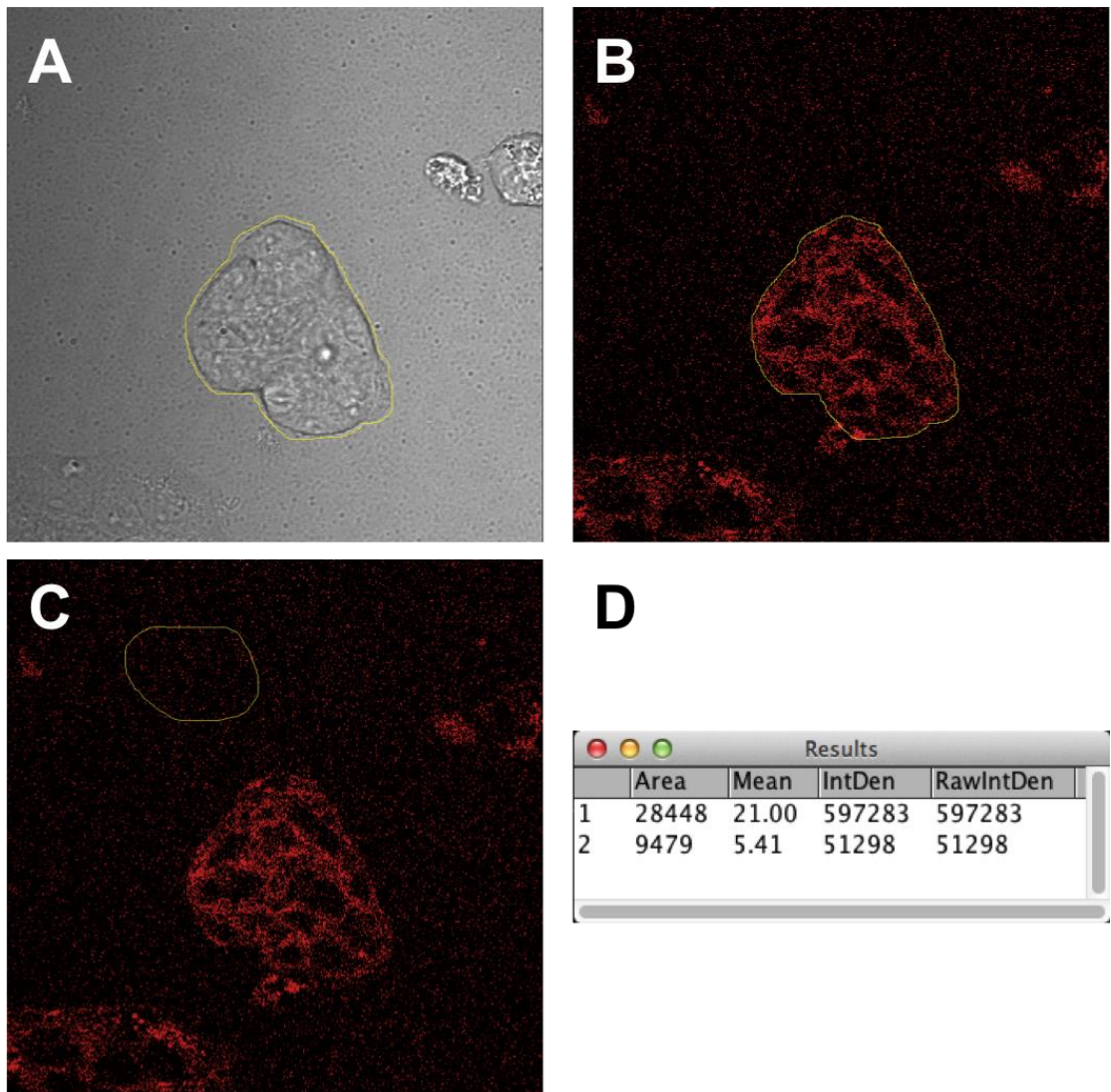


Figure 2.2. Whole cell fluorescence quantification.

Image J was used to quantify the fluorescence seen on confocal microscopy. Phase and fluorescent images were stacked. The cell membrane was traced on the phase image (A) and measurements taken for the fluorescent image (B). A mean background measurement was taken (C) and subtracted from the cell measurement (D).

If the fluorescence of every cell on any given coverslip were to be measured, the data would most likely follow a Gaussian distribution. However, for completeness I treated the data as both parametric and non-parametric. The mean fluorescence was compared for CEA-targeted ICG and control IgG-targeted ICG in all three cell lines at all time points using the unpaired t-test (if the data are considered to be parametric) and the median fluorescence was compared using the Mann-Whitney test (if the data are considered to be non-parametric).

2.5.2.3 LS174T pulse and chase incubation

LS174T cells were grown and seeded onto two 35 mm glass-bottomed wells. The media was changed at 24 hours and at 48 hours 80 μ l of 1 μ g/ μ l anti-CEA-ICG was added to the first well and incubated for two hours. The media/antibody-ICG mixture was then removed and the media from the second well was added in its place. The well was imaged at 6, 12, 24, 36, 48 and 72 hours using the same confocal microscopy protocol. The same analysis as in 2.5.2.2.1 was used.

2.6 Western Blot

The three cell lines used in 2.5.2.2 have all been shown to express CEA: LS174T (intermediate/high expression (Fahlgren et al., 2003), LoVo (high expression (Ashraf et al., 2009)) and HCT116 (low expression (Wang et al., 1999)).

2.6.1 Protein lysate production and protein standardisation

Protein lysate buffer was made by mixing 12.5 ml of a solution containing 5 ml of 1 M Tris-HCl (pH 7.4), 6 ml of 2.5 M NaCl, 1 ml of 10% NP40 (Sigma, USA) and 38 ml of distilled water with 12.5 ml of Complete Tabs solution (1 tablet dissolved in 12.5 ml of distilled water; Roche, Penzberg, Germany). LS174T, LoVo and HCT116 cells were grown in Advanced MEM (ATCC, Virginia, USA), F12K Nutmix (Life Technologies) and RPMI1640 (Life Technologies) media respectively, supplemented with FCS (10%) and L-glutamine (1%) at 37°C and 5% CO₂ were grown in T75 flasks (Corning, New York, USA) until confluent. The media was removed and the cells were washed three times with fresh media (with no FCS added) and 2 ml of ice cold protein lysis buffer was added to each flask and incubated at 4°C for 10 minutes. The cells were then gently scraped from the plastic and each lysis buffer/cell mix was removed and placed in a 1.5 ml microfuge tube. These were centrifuged at 14000 rpm for 10 minutes at 4°C. The supernatant was then removed and stored at -80°C.

The protein concentration in each supernatant was measured using the Bio-Rad DC protein assay (Biorad Laboratories, Hercules, USA) which is adapted from the Lowry assay (Lowry et al., 1951). A standard curve for bovine serum albumin (BSA) was prepared using concentrations of 0.1, 0.5, 1 and 2 mg/ml and 18 µl of each cell lysate containing equal amounts of protein was prepared for the running gel.

2.6.2 Gel electrophoresis

The LS174T, LoVo and HCT116 lysates were mixed with 6 µl of a mixture containing 60 µl of NuPAGE LDS Sample Buffer (Invitrogen) and 12 µl of 2-mercaptoethanol. The samples were heated at 100°C for five minutes and then cooled on ice prior to electrophoresis. A NuPage 10% Bis-Tris precast gel (1 mm, 10 lanes) was loaded

into a NuPage gel tank and filled with running buffer (25 ml of NuPage MOPS SDS running buffer + 475 ml distilled water). The gel was loaded with 20 μ l of each cell line sample and 5 μ l of SeeBlue Plus 2 molecular marker (Invitrogen). Spare lanes were filled with a distilled water/buffer mix. Electrophoresis was performed at 180 V for 90 minutes. Proteins were transferred onto a nitrocellulose membrane (Hybond P, G.E. Helathcare, Little Chalfont, UK). Transfer buffer was prepared by mixing 25 ml of NuPage 20X Transfer Buffer with 425 ml of distilled water and 50 ml of 100% methanol. The membrane and two pieces of 3MM filter paper (Whatman International, Maidstone, UK) were soaked in 100% methanol for 30 seconds, rinsed in running water for five minutes and soaked in transfer buffer. Sponges were soaked in water and then transfer buffer. The membrane was then loaded into the transfer module between the two pieces of filter paper with sponges placed on either side. Transfer buffer was added to the module so that the sponges were immersed and distilled water was added to the outer tank. A constant voltage of 30 V was applied for 1 hour. The membrane was removed and incubated with blocking buffer (5% [w/v] skimmed milk in TBS-T) overnight at 4°C on a rocker. This was replaced with 1% [w/v] skimmed milk in TBS-T containing 1:100000 A5B7 anti-CEA antibody and incubated at room temperature for one hour on a rocker. The membrane was washed with TBS-T (3 x 10 minutes) and then incubated in 1% [w/v] skimmed milk in TBS-T containing 1:1000 horseradish peroxidase-conjugated goat anti-mouse secondary antibody (sc-2005, Santa Cruz) at room temperature for 1 hour on a rocker. Following further TBS-T washes (3 x 10 minutes), the membrane was covered with 3 ml of a solution containing SuperSignal West Pico and SuperSignal West Femto (Thermo Scientific, Waltham, USA) mixed in a 5:1 ratio for 2 minutes. Excess fluid was drained from the membrane and it was then exposed to Hyperfilm (GE Healthcar, UK) for 1 minute. The film was developed with a Compact X2 X-Ograph automatic film processor (Compact, Malmesbury, UK).

2.7 Nanoparticles

Dye-doped silica nanoparticles were manufactured using methods adapted from Santra et al (Santra et al., 2001), Huang et al (Huang et al., 2009) and Gubala et al (Gubala et al., 2010). IgG antibodies were then conjugated to the surface of the particles using both novel and published experimental techniques. The effectiveness of the linking methods was evaluated and compared in vitro by quantifying specific tumour cell binding using confocal microscopy. Unless otherwise stated, all chemicals were purchased from Sigma (Sigma Aldrich, St Louis, USA). 'Wash' steps refer to the nanoparticles being pelleted via centrifugation, resuspended in the wash solution using ultrasound sonication, re-pelleted with centrifugation and the supernatant discarded.

2.7.1 Dendrimer-linked nanoparticle-IgG conjugates

2.7.1.1 NIR664-doped silica nanoparticle manufacture

Two batches of particles were made; one was dried overnight to calculate the yield for calculations in the conjugation steps. For each batch, five mg of NIR 664-iodoacetamide dye was dissolved in 6.25 ml of 1-hexanol and 3.25 μ l of (3-mercaptopropyl) triethoxysilane, (MPTES) to give a dye:MPTES molar ratio of 1:2. The mixture was stirred under nitrogen gas for four hours at room temperature to ensure conjugation of the dye and organosilane.

3.78 g (4.045 ml) of the non-ionic surfactant Triton X-100 was added to 15 ml of cyclohexane, 1.6 ml of 1-hexanol, 2 ml of the conjugated dye and 960 μ l of distilled water in a plastic tube covered in aluminium foil. The mixture was stirred for five

minutes until a microemulsion had formed. 200 μ l of tetraethyl orthosilicate (TEOS) was then added and the tube was stirred for 30 minutes at room temperature. 120 μ l of ammonia hydroxide (28% [w/w]) was added as a catalyst and the mixture was stirred for 24 hours at room temperature. 150 μ l of TEOS was then added and the tube contents stirred for a further 30 minutes at room temperature.

The microemulsion was then broken by adding excess ethanol (20 ml) and the contents were divided into two equal volumes and added to 30 ml Corex centrifuge tubes (Corning). These underwent centrifugation at 11 000g for 25 minutes at room temperature. The liquid was discarded and the particles were resuspended in ethanol using sonication. The particles were washed four times in this way with ethanol. One of the tubes was stored at 4°C and the other left to dry out overnight so that the particles could be weighed and the yield calculated.

2.7.1.2 Amination

4 ml of 2 mg/ml nanoparticles suspended in ethanol plus 4% (3-aminopropyl)triethoxysilane (APTES) was reacted for three hours at room temperature with stirring in a 15 ml Falcon tube. The contents were then transferred to a Corex centrifuge tube and washed twice with ethanol at 11000g for 25 minutes. The particles were then washed once in 2-(*N*-morpholino)ethanesulfonic acid (MES) buffer, pH 7.0 before being re-suspended in MES buffer pH 7.0 at 2 mg/ml.

2.7.1.3 Amine quantification

The number of free amine groups on the surface of the nanoparticles was determined using Fluorenylmethyloxycarbonyl chloride (Fmoc-Cl) in a method adapted from Chen et al (Chen and Zhang, 2011). This assay involves binding the fluorescent Fmoc-Cl molecule (a protecting reagent for amino groups, used in peptide synthesis (King et al., 1990)) to free amine groups on the silica nanoparticle

outer shell, cleaving them with piperidine and calculating how many amino groups were bound. The fluorescent core of dye-doped silica nanoparticles precludes common amine quantification assays (eg. 2,4,6-Trinitrobenzene sulfonic acid, TNBSA (Goodwin and Choi, 1970)) because it confounds the result. The quantification step of the Fmoc-Cl fluorescent assay takes place independently of the nanoparticles and therefore is ideal for particles with inherent fluorescent properties. A standard calibration curve of Fmoc fluorescence was created by measuring the fluorescence of various concentrations of Fmoc-Cl in a borate buffer (0.1 M, pH 8.0) containing 10% piperidine. The relationship between Fmoc-Cl and fluorescence is linear at concentrations below 1×10^{-6} mol L⁻¹ (Chen and Zhang, 2011). The nanoparticles were suspended in borate buffer (0.1 M, pH 8.0) at a concentration of 60 mg/ml. 435 μ l of the particle suspension was mixed with 15 μ l of Fmoc-Cl solution (0.01 M in acetonitrile) and incubated at room temperature for 40 minutes with mixing. The particles were then washed twice with 10 ml of 0.5% Tween-20 and four times with distilled water, until the fluorescence of the unconjugated Fmoc-Cl in the supernatant was approximately zero when measured on a fluorometer at an excitation wavelength of 267 nm. The particles were then resuspended in 450 μ l of borate buffer and 50 μ l of piperidine was added (giving a 10% piperidine solution) to release the Fmoc bound to the amine groups. The reaction was allowed to proceed for 10 minutes and then the mixture was centrifuged at 10000g for 15 minutes. The supernatant was removed and its fluorescence recorded at an excitation wavelength of 267 nm.

2.7.1.4 Dendrimer conjugation

41.7 mg of sulfo-NHS and 71.6 mg of N-(3-dimethylaminopropyl)-N'-ethylcarbodiimide (EDC) were added to 1 μ mol of PAMAM dendrimer generation 4.5 (Dentritech, Midland, USA) dissolved in distilled water. The total reaction volume was

made up to 1 ml using MES buffer, pH 6.0. The reaction mixture was stirred at room temperature for 25 minutes and then added to 1 ml of 2 mg/ml nanoparticles suspended in MES pH 7.0. The reaction mixture was stirred at room temperature for 25 minutes. Unbound dendrimer was removed in the supernatant after centrifugation (16 000g for 8 minutes) and the particles were washed twice with MES buffer pH 7.0.

2.7.1.5 Antibody conjugation

The reaction mixture was split into two and 10 µg of anti-CEA IgG antibody were added to one sample and 10 µg of anti-digoxin IgG antibody to the other. These were then incubated at room temperature for four hours with gentle stirring. The reaction was halted by the addition of 100 µl of sodium hydroxide pH 9.0. The functionalised nanoparticles were washed in 0.1M sodium phosphate, 0.15 M sodium chloride, pH 7.2 (referred to hereon in as 0.1M PBS) twice (11 000g x 25 minutes) to remove unbound IgG antibody before being resuspended in 0.1M PBS at 2 mg/ml. 2% [w/v] bovine serum albumin (BSA) was added and the particles were stored at 4°C in the dark.

2.7.2 SMCC-linked nanoparticle-IgG conjugates

2.7.2.1 Antibody reduction

500 µl of 4.8 mg/ml anti-CEA IgG antibody was added to 500 µl of 9.6 mg/ml 2-mercaptoethylamine (2-MEA). The mixture was incubated at 37°C for 90 minutes and then cooled rapidly on ice. 2-MEA was then removed using a 100 kDa spin centrifuge filter (Millipore, Billerica, USA); the mixture was centrifuged in 0.1M PBS (14000g for 2.5 minutes) and the eluent discarded. This was repeated seven times. The concentrated antibody solution was then retrieved by gentle centrifugation with the

tube inverted (1000g x 30 seconds) and 0.1M PBS was added to make the total volume up to 500 μ l. A Dionex Ultimate 300 high pressure liquid chromatography system (Thermo Scientific) was used to confirm that this product contained both half and whole IgG molecules. The solution was reacted with the nanoparticles immediately.

2.7.2.2 Nanoparticle manufacture

Two batches of particles were made; one was dried overnight to calculate the yield. For each batch, 1.77 ml of triton X-100, 7.5 ml cyclohexane and 1.8 ml n-hexanol were added to a 50 ml Falcon tube to form a microemulsion. This was shaken until it was transparent. 400 μ l of deionised water, 80 μ l of 43 mM aqueous $\text{Ru}(\text{bpy})_3^{2+}$ solution and 60 μ l ammonium hydroxide (28-30%) was added to the tube and it was stirred for 15 minutes at room temperature. 50 μ l of TEOS was added and the reaction was stirred for a further 24 hours. Another 50 μ l of TEOS was added and the reaction stirred for 30 minutes. 10 μ l of APTES was then added and the reaction stirred for a further 24 hours. 10 ml of acetone was added to break the microemulsion. The contents were transferred to a Corex centrifugation tube and centrifuged at 10000g for 15 minutes. They were then resuspended in ethanol and washed twice with ethanol and twice with water. Finally, they were resuspended in 0.1M PBS at a concentration of 1 mg/ml.

2.7.2.3 SMCC reaction

6 mg of fresh sulfo-SMCC was added to 4 ml of 1mg/ml nanoparticles and stirred at room temperature for 1 hour. The maleimide-activated particles were then washed twice in PBS (10000g x 15 minutes) to remove unbound sulfo-SMCC and resuspended at 2 mg/ml. The sample was split into two and 30 μ g of reduced anti-CEA or anti-digoxin was added to each tube. The reaction mixture was gently stirred

at room temperature for 2 hours and then washed twice with PBS (6000g x 15 minutes). Finally, the particles were resuspended at 2 mg/ml and 0.1% [w/v] BSA added. The finished nanoparticles were stored in the dark at 4°C.

2.7.3 Polyethylene glycol (PEG)-linked nanoparticle-IgG conjugates

Antibodies were reduced as per section 2.7.2.1 and particles manufactured as per section 2.7.2.2. A stock solution of 250 mM NHS-PEG-Maleimide (SM(PEG))₄ was made by dissolving 100 mg in 680 µl of dimethyl sulfoxide (DMSO). 8 µl of 250 mM SM(PEG)₄ solution was added to 5 ml of 2 mg/ml nanoparticles and reacted for 30 minutes at room temperature with gentle mixing. Unreacted linker was removed by washing the particles twice with PBS (pH 7.2, 10000g x 15 minutes) and resuspending them in PBS at 2mg/ml. The sample was divided into two. 30 µl of either anti-CEA or anti-digoxin IgG was added for each mg of nanoparticles. The reaction mixture was incubated at room temperature for 2 hours with gentle mixing. The particles were then washed twice with PBS and resuspended at 2 mg/ml. 0.1% [w/v] BSA was added and they were stored in the dark at 4°C.

2.7.4 EDC-linked nanoparticle-IgG conjugates

Nanoparticles were manufactured as per section 2.7.2.2.

2.7.4.1 Carboxylation

The nanoparticles were washed twice in DMF (10000g x 15 minutes). They were then resuspended at 1 mg/ml in 15 ml of 10% succinic anhydride dissolved in DMF.

They were reacted under argon gas at room temperature for 4 hours with gentle stirring. The carboxylated particles were then washed three times with distilled water.

2.7.4.2 EDC conjugation

10mg of carboxylated nanoparticles were suspended in 5 ml of 0.1M MES, 0.5M NaCl, pH 6.0 and 1.92 mg of EDC and 5.43 mg of sulfo-NHS were added. They were reacted for 15 minutes at room temperature with gentle mixing, after which the reaction was quenched by the addition of 20mM 2-MEA. Excess reactants were removed by washing the particles twice with PBS (6000g x 10 minutes) and resuspended at 2 mg/ml in 0.1M PBS. 10 µg of either anti-CEA or anti-digoxin IgG was added for each mg of nanoparticles. The reaction mixture was incubated at room temperature for 2 hours with gentle mixing. The particles were then washed twice with PBS and resuspended at 2 mg/ml. 0.1% [w/v] BSA was added and they were stored in the dark at 4°C.

2.7.5 Nanoparticle in vitro assay

2.7.5.1 Cell lines

LS174T, LoVo and HCT116 cells were grown as described previously. Each cell line was seeded onto three sterile glass coverslips (Cellpath, Newtown Powys, UK) in a six-well plate (Corning) and grown for 24 hours. The media was then removed and the cells washed twice with PBS. They were fixed by adding paraformaldehyde (4%) and incubated at room temperature for 30 minutes. The paraformaldehyde was removed and they were washed thrice with PBS. Bovine serum albumin (BSA, 0.1% [w/v], (EMD chemicals, San Diego, USA)) was added to each well for 30 minutes at room temperature to block non-specific binding. The BSA was removed and the cells

were washed three times with PBS. Anti-CEA conjugated nanoparticles and control IgG nanoparticles (suspended in PBS at 1 mg/ml) were added to the wells and incubated at room temperature in the dark. After one hour the particle suspension was removed and the cells washed three times with PBS. The coverslips were then mounted onto glass slides using Depex (Waltham, Massachusetts, USA) and left overnight to cure before being stored at 4°C in the dark.

2.7.5.2 Confocal microscopy

A Nikon A1R-A1 confocal microscope (Nikon, Tokyo, Japan) with NHS Elements software (version 4.0) was used for all imaging. For each slide, the cells were focussed in phase mode in the centre of one quadrant of the coverslip. The Cy7 and phase filters were selected and automatically calibrated for the first image capture only; the settings (such as laser power and gain) were then saved and used for all subsequent image capture. A phase/Cy7 z-stack image (distance between stacks: 0.5 µm, 0.2 µm and 0.4 µm for LS174T, LoVo and HCT116 cells respectively, chosen to produce a similar number of z-stack images) was captured for the first quadrant. The upper and lower limits of the z-stack were set to ensure that the whole depth of at least one cell was included. The microscope stage was then moved to the next quadrant, the white light image focussed, and a z-stack captured. This was repeated so that for each coverslip, five z-stack files were captured: an image from approximately the centre of each quadrant and one from the centre of the entire coverslip. By not examining the fluorescent image during image location selection, potential selection bias was removed.

2.7.5.3 Nanoparticle image analysis: single z-stack slice

Two analyses were employed to measure the fluorescence of the cells. Firstly, a single slice from each z-stack was selected. This was chosen by identifying a

distance from the base of the cells for each cell line such that the slice would always be approximately half way between the base and top of the cell. These distances were 5 μm , 1.4 μm and 4.8 μm for LS174T, LoVo and HCT116 cells respectively. These slices were saved as fluorescent, phase and combined '.tiff' images for each cell analysed. LS174T cells grow as clusters so small clusters of a similar size were selected (mean 6 cells). Fluorescence was quantified using ImageJ software version 1.42q (NIH Freeware, Maryland, USA). The distance per pixel was measured using the scale bar on the image to allow fluorescence measurements to be calibrated to the cell size. Using the phase image, the inner and outer boundaries of the cell membrane were traced using the freehand tool. This trace was then applied to the fluorescent only image and the raw integrated density (RawIntDen, the sum of the pixel values in the selected area) and the area of the selection were recorded (). A background area was then selected (ie. an area with no cell fluorescence) and the same measurements taken.

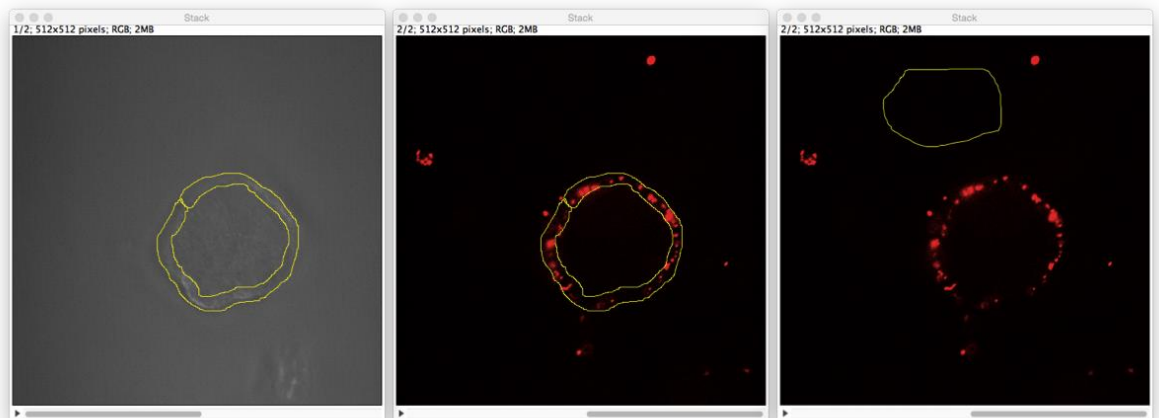


Figure 2.3. Membrane fluorescence quantification.

To quantify the fluorescence on confocal microscope images, I traced around the cell membrane (left) of the phase image, applied the trace to the fluorescent image only (middle) and took a measurement. I then subtracted the mean background fluorescence (right).

Finally, the circumference of the cell in question was measured. A fluorescence value per μm of membrane for the image was calculated as follows:

$$\begin{aligned} & \textit{Membrane fluorescence per } \mu\text{m} \\ & = \left\{ \frac{\text{RawIntDen}_{\text{membrane}} - \left[\left(\frac{\text{RawIntDen}_{\text{background}}}{\text{Area}_{\text{background}}} \right) \times \text{Area}_{\text{membrane}} \right]}{\text{Circumference}} \right\} \end{aligned}$$

This procedure was followed for five z-stacks per cell line, in all three cell lines and for test and control particles in each case, yielding 30 measurements per conjugation method.

2.7.5.4 Nanoparticle image analysis: maximum image projection

The second image analysis utilised the maximum image projection (MIP) function in NHS Elements software. This function analyses all of the z-stack images and constructs a new single image by taking the brightest pixel from all of the z-stacks. It should be noted that this is not a true cumulative image as a saturated bright pixel cannot be made any brighter. It therefore dampens down the overall fluorescence but can be used to verify the results of the single z-stack slice analysis. To analyse the MIP images, the entire cell or cell cluster was traced, including the cell cytoplasm, and the RawIntDen and area were measured. A background measurement was taken as above and the following formula used to calculate the fluorescence:

$$\textit{Mean cell fluorescence} = \left(\frac{\text{RawIntDen}_{\text{cell}}}{\text{Area}_{\text{cell}}} \right) - \left(\frac{\text{RawIntDen}_{\text{background}}}{\text{Area}_{\text{background}}} \right)$$

2.7.5.5 Image analysis: statistical methods

The mean fluorescence and standard error was compared for CEA-targeted nanoparticles and control IgG-targeted nanoparticles for each conjugation method in all three cell lines using the both unpaired t-test (if the data are considered to be parametric) and the Mann-Whitney test (if the data are considered to be non-parametric).

2.7.6 Nanoparticle Characterisation

The size of the nanoparticles was measured using a Zetasizer (Malvern Instruments, Malver, UK), Nanosight (Nanosight, Amesbury, UK) and field emission gun scanning electron microscopy (FEG-SEM, LEO 1530 Gemini FEGSEM fitted with an Oxford Instruments 80 mm X-Max SDD detector, Carl Zeiss).

2.8 Animal model

All procedures were approved and licensed by the Home Office and carried out in accordance with the local ethical review committee. All reasonable efforts were made to minimise any likely suffering and the animals were inspected daily by a qualified technician. The animals were weighed and the tumour dimensions measured twice per week. Nine 4 to 6 week old BALB/c nu/nu female mice were injected subcutaneously with 1.5×10^6 LS174T cells to the right flank. When the tumours reached approximately 8-10 mm in diameter (approximately 12 days), the mice were imaged using an IVIS small animal molecular imaging system (Perkin Elmer, Waltham, USA) with excitation and emission filters set at 672 and 694 nm

respectively). As a pilot experiment, three mice were injected with CEA-targeted nanoparticles via the tail vein and images taken at various time points, comparing them to a control mouse that had not undergone injection. Mice were sacrificed under anaesthesia and sample organs were imaged *ex vivo*. In a second experiment, four mice were injected with CEA-targeted nanoparticle and three were injected with digoxin-targeted nanoparticles via the tail vein (suspended in 100 μ l of PBS, dose 50 mg/kg). The mice were imaged at 1 minute, 1 hour, 6 hours, 24 hours, 36 hours, 48 hours and 72 hours post injection. The animals were then sacrificed under anaesthesia. Fluorescence measurements were taken using Living Image (version 4.3.1, Caliper Life Sciences, Massachusetts, USA). The tumour was traced as a 'region of interest' and a mean quantum efficiency measurement taken. A second region of interest was drawn on the opposite flank and another mean quantum efficiency measurement taken (background fluorescence) and subtracted from the tumour measurement.

Chapter Three

Carcinoembryonic antigen is the preferred biomarker for *in vivo* colorectal cancer targeting

Some of the text and figures in this chapter have been published in the manuscript “Carcinoembryonic antigen (CEA) is the preferred biomarker for *in vivo* colorectal cancer targeting” (British Journal of Cancer 2013; 108(3):662-7) and reproduced here with permission.

3 CARCINOEMBRYONIC ANTIGEN IS THE PREFERRED BIOMARKER FOR IN VIVO COLORECTAL CANCER TARGETING

3.1 Abstract

Background

Colorectal cancer-specific biomarkers have been used as molecular targets for fluorescent intra-operative imaging, targeted PET/MRI, and selective cytotoxic drug delivery, yet the selection of the biomarkers used is rarely evidence-based. We aimed to assess which of the four most commonly used potential biomarkers is most suitable.

Methods

Expression of carcinoembryonic antigen (CEA), tumour-associated glycoprotein-72 (TAG-72), folate receptor alpha (FR α) and endothelial growth factor receptor (EGFR).was evaluated semi-quantitatively in matched mucosal and colorectal cancer tissues from 280 patients using immunohistochemistry (scores of 0-15). Matched positive and negative lymph nodes from 18 patients were also examined. Sensitivities and specificities in terms of colorectal cancer detection over normal tissue were determined for each marker.

Results

Markers were more highly expressed in tumour tissue than in matched normal tissue in 98.8%, 79.0%, 37.1% and 32.8% of cases for CEA, TAG-72, FR α and EGFR respectively. CEA showed the greatest differential expression, with tumours scoring a mean of 10.8 points higher than normal tissues (95% CI 10.31-11.21, $p < 0.001$). Similarly, CEA showed the greatest differential expression between positive and negative lymph nodes. Receiver operating characteristic analyses showed CEA to have the best sensitivity (93.7%) and specificity (96.1%) for colorectal cancer detection.

Conclusion

CEA has the greatest potential to allow highly specific tumour imaging and drug delivery; future translational research should aim to exploit this.

3.2 Introduction

Intra-operative tumour visualisation would allow localisation of small tumours and the nodal status of a colorectal cancer to be determined in real-time, allowing stratification of resection type (as discussed in detail in section 1.1).

One way of achieving intra-operative tumour detection and staging is to target a tumour-specific biomarker using antibodies. This biomarker target must have a number of specific characteristics: it must be located on the tumour cell membrane to allow systemic delivery; it must be highly expressed in a large majority of tumours; and it must have low or no expression in normal tissue, encompassing the normal tissue from which the tumour is derived and – ideally – most or all normal adult tissues accessible by systemic delivery. Experimental work to date has relied mainly on antibodies directed at the cell membrane proteins carcinoembryonic antigen (CEA), tumour-associated glycoprotein 72 (TAG-72), folate receptor α (FR α) or epithelial growth receptor (EGFR): Muguruma et al conjugated anti-CEA antibodies to a near-infrared dye and used it to label colonic cancer cells in paraffin sections with the aim of developing an endoscopic visualisation system (Muguruma et al., 1999); Zou et al conjugated anti-TAG-72 antibodies to a near-infrared dye and injected them into tumour-bearing mice (Zou et al., 2009); Goetz et al and Chen et al used fluorescently labelled anti-EGFR and anti-folate receptor antibodies respectively for endoscopic adenoma detection in mouse models (Goetz et al., 2010, Chen et al., 2005). Surprisingly, given the dependency on accurate biomarker localisation, the selection of the markers used for tumour-targeting is rarely justified based on their sensitivity or specificity. One would not contemplate using a marker giving poor specificity and sensitivity in routine laboratory analysis, and the same stringent criteria should therefore apply to *in vivo* tumour identification. In order to determine

the suitability of each of my potential antigens for use as tumour-specific markers I first aimed to determine the expression frequency and levels of each antigen in a large set of colorectal tumours and matched normal tissues. Only antigens expressed in a relatively large proportion of tumours, and expressed infrequently or at low levels in normal tissues would be suitable.

3.3 Results

3.3.1 Selection of potential colorectal cancer-specific biomarkers and optimisation of antibodies for their analysis

Initially I performed a detailed literature search to identify potential suitable biomarkers with the characteristic outlined above. I established a panel of seven potential target antigens: carcinoembryonic antigen (CEA), tumour-associated glycoprotein 72 (TAG-72), folate receptor alpha ($FR\alpha$), epidermal growth factor receptor (EGFR), VEGFR-2, roundabout protein 1 (ROBO1) and endoglin (CD105). CEA, TAG-72, $FR\alpha$ and EGFR were all described in Chapter 1. VEGFR-2 is a tyrosine kinase receptor for VEGF-A, C, D and E, which are signalling proteins produced in response to hypoxia and that stimulate angiogenesis. Some 40-100% of colorectal cancers are thought to express VEGFR-2 (Duff et al., 2006, Hanrahan et al., 2003, Schimanski et al., 2010a, Amaya et al., 1997). Roundabout protein 1 (ROBO1) is a transmembrane receptor involved in tumour angiogenesis (Wang et al., 2003) that is upregulated in colorectal tumour cells and endothelial cells of tumour vessels compared with normal cells (Grone et al., 2006). Endoglin (CD105) is a protein expressed by angiogenic endothelial cells and is up-regulated in response to hypoxia (Sánchez-Elsner et al., 2002). It is also up-regulated in a range of tumour endothelial cells including those of the colon (Burrows et al., 1995, Bellone et al., 2010).

Antibodies to each antigen were selected by ensuring that they had been used in peer-reviewed publications for colorectal cancer cell recognition. I had access to an

anti-CEA antibody produced in-house by a Cancer Research UK-funded research group in London that had been used in clinical trials for CEA targeting. To check its performance I also used a commercially available anti-CEA antibody.

I used 13 specimens of formalin-fixed, paraffin-embedded colorectal cancer of various grades and one sample of normal colonic tissue to optimise antibody concentrations and experimental conditions for definitive immunohistochemical analysis. I varied antibody concentration, antigen retrieval method and primary antibody incubation conditions for each biomarker target to give a broad range of epithelial staining intensities with minimal background staining (Table 3.1). A5B7 anti-CEA performed equally well as a commercially available, validated anti-CEA antibody (Figure 3.1) and I therefore chose to use this for future work because it is humanised and has been successfully used in both animal models and clinical trials (Dearling et al., 2009, Meyer et al., 2009, Rajkumar et al., 2012). Antibodies to VEGFR2 and robo1 produced no tumour-specific staining on colorectal cancer specimens despite employing extensive optimisation techniques and were therefore not evaluated further. Antibodies to CEA, TAG-72, EGFR and FR α produced tumour-specific staining with little or no stromal or non-cancerous epithelial cell staining. Anti-CD105 strongly stained vessels adjacent to tumour samples with some mild tumour staining. However, the vascular density in the tumour specimens and the epithelial cell staining were markedly variable between specimens (Figure 3.2). Although a nanoparticle delivered systemically would potentially bind to the endothelium of neo-vascularised regions of a tumour, this wide variability limits the potential of CD105 as the sole target of a tumour-specific imaging system. Furthermore, to ascertain the true endothelial and epithelial expression profile of CD105 in colorectal cancer, I would require whole tumour blocks and dual staining for endothelial cells. I intended to use tissue micro-arrays of colorectal cancer and matched normal samples, which would not be suitable for this.

I concluded that the biomarker targets most likely to allow differentiation of tumour from normal tissue were CEA, TAG-72, EGFR and FR α , and selected these for evaluation using a large cohort of matched tumour and normal tissue samples.

Antibody	Concentrations tested	Optimised concentration	Antigen retrieval methods	Chosen antigen retrieval method	Antibody incubation
Anti-CEA (Dako)	1:50, 1:100, 1:200	1:100	Heat retrieval No retrieval	No retrieval	1 hour room temp
Anti-CEA (A5B7)	1:1, 1:100, 1:200, 1:400, 1:800, 1:1200, 1:1600, 1:2000, 1:5000, 1:20000, 1:100000, 1:150000, 1:200000	1:150 000	Heat retrieval No retrieval	No retrieval	1 hour room temp
Anti-TAG-72	1:100, 1:125, 1:150, 1:200, 1:400	1:100	Heat retrieval No retrieval	No retrieval	1 hour room temp
Anti-VEGR2	1:50, 1:150, 1:300	N/A	Heat retrieval No retrieval Proteinase K Casein block	N/A	N/A
Anti-folate receptor α	1:25, 1:50, 1:75	1:50	Heat retrieval No retrieval	Proteinase K	1 hour room temp
Anti-robo1	1:50, 1:250, 1:500	N/A	Heat retrieval No retrieval Proteinase K Casein block	N/A	N/A
Anti-CD105	1:20, 1:50, 1:100	1:20	Heat retrieval No retrieval Proteinase K	Proteinase K	Overnight 4°C

Table 3.1. Antibody optimisation.

Antibodies to each antigen were optimised for immunohistochemistry using specimens of formalin-fixed, paraffin-embedded colorectal cancer and normal tissue. Concentration, retrieval method and antibody incubation conditions were independently varied for each.

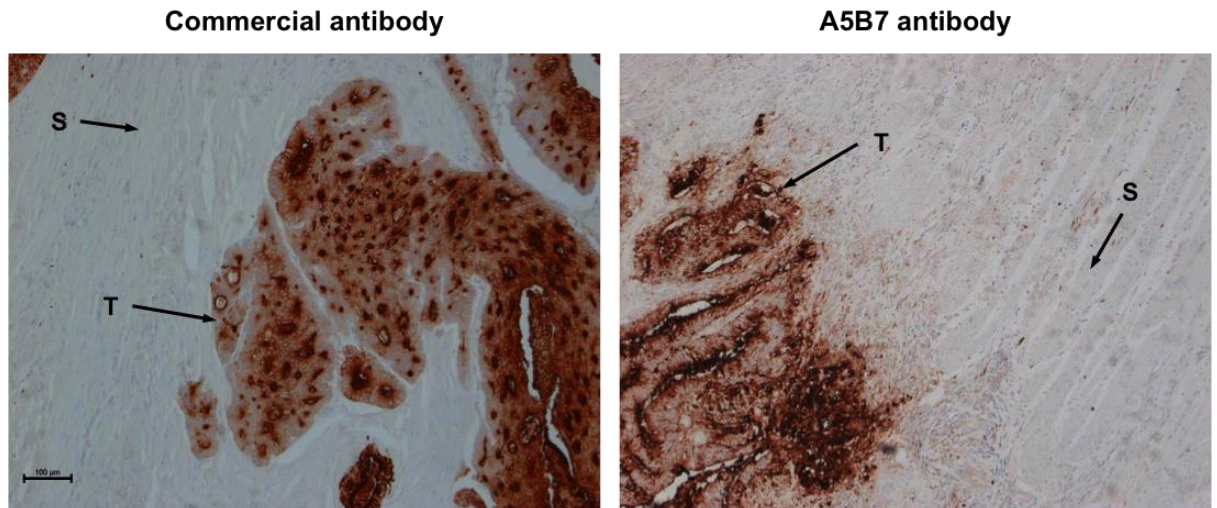


Figure 3.1. Anti-CEA antibody comparison.

A5B7 anti-CEA produced immunostaining of a similar intensity and distribution to that of a commercially available, validated anti-CEA antibody (Dako, USA). Formalin-fixed, paraffin-embedded colorectal cancer were stained for CEA using each antibody under optimised immunohistochemistry conditions. The staining observed was diffuse with marked luminal accentuation in both. T = tumour, S = stroma. Concentrations 1:100 (Dako) and 1:200000 (A5B7), magnification X20. Scale bar = 100 µm.

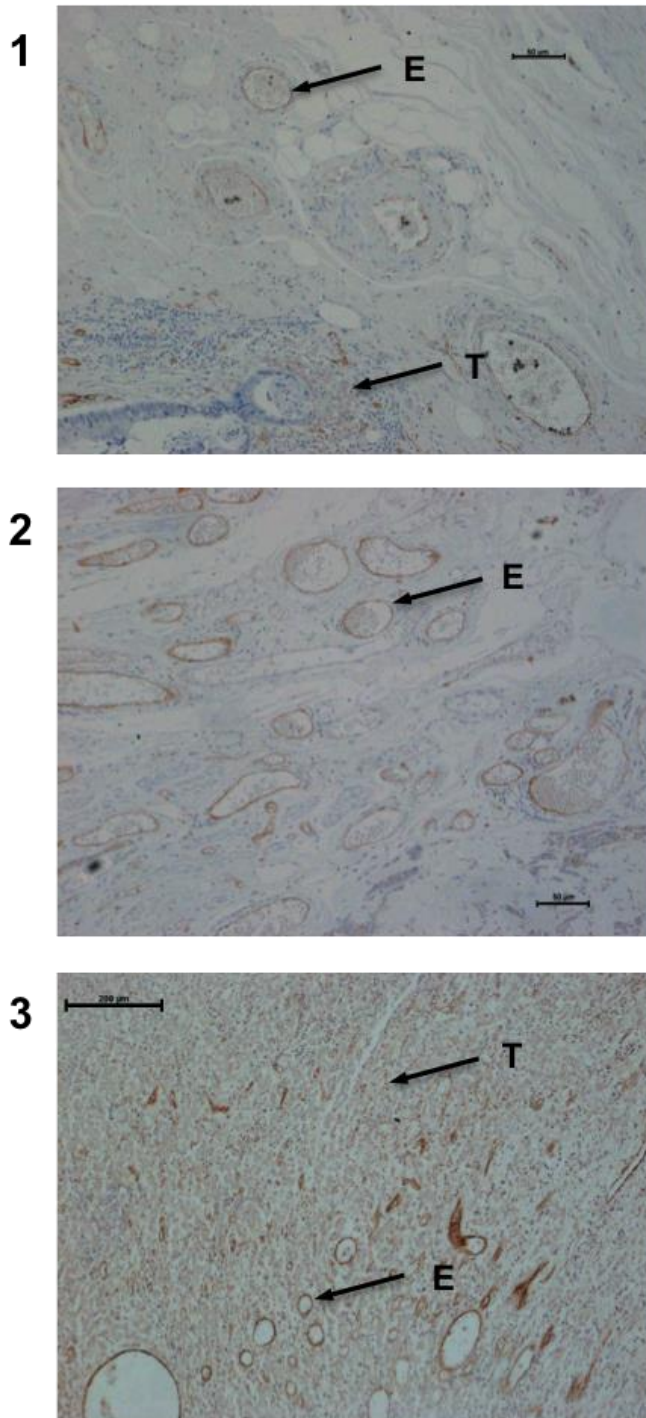


Figure 3.2. CD105 staining.

CD105 endothelial cell and malignant epithelial cell immunostaining varies between specimens. Slides were stained for CD105 expression using immunohistochemistry.

1: mild endothelial (E) and tumour cell (T) staining. 2: Moderate endothelial cell (E) and mild tumour cell (T) staining. 3: Strong endothelial cell (E) and tumour cell (T) staining. Concentration 1:25, magnification X10 (1&2) and x40 (3).

3.3.2 Expression of selected biomarkers in 280 matched normal and tumour tissue samples

Having selected four biomarker targets with the potential to allow tumour-specific targeting, I aimed to use a large cohort of matched normal and tumour tissue samples to examine the expression of each. To do this I used the optimised immunohistochemistry protocols from 3.3.1 and pre-existing tissue micro-arrays containing three tumour samples and three matched normal colonic mucosa samples from 280 patients with colorectal cancer. Clinicopathological data for this cohort are shown in Table 3.2. Carcinoembryonic antigen, TAG-72 and EGFR showed predominantly membranous staining with mild cytoplasmic staining while FR α showed cytoplasmic staining only. Representative images of staining for each antigen in both normal and tumour tissues are shown in Figure 3.3.

Carcinoembryonic antigen and TAG-72 were scored for apical membranous staining only. Folate receptor α showed mild cytoplasmic staining only, and was scored solely for this. EGFR showed membranous, and – more rarely - cytoplasmic and nuclear staining. However, following established literature (Buckley and Kakar, 2007, Scartozzi et al., 2004) EGFR was scored for membranous expression only.

Immunostaining was assessed semi-quantitatively using a bespoke scoring system that assessed both the intensity of staining and the number of cells stained. I initially tested two scoring systems using TMAs stained for CEA: a system based on that described by Allred et al (Allred et al., 1993), where scores for staining intensity and number of cells stained are added, and one based on the Histoscore system (McCarty et al., 1986), where they are multiplied (Figure 3.4). No staining for any marker was noted in blood cells within the sections, suggesting that expression in this compartment is negligible. A pathologist scored a sample representing 15% of cases. The intraclass correlation coefficient was 0.89, demonstrating good agreement between scorers.

Characteristic	Number of cases (%) n=280
Age range: 33-93 years Mean age: 68.9 years	
Male	144 (51.4)
Female	136 (48.6)
pT stage 1	10 (3.6)
2	54 (19.3)
3	161 (57.5)
4	52 (18.6)
Unknown	3 (1.1)

Table 3.2. Clinico-pathological details of patient cohort.

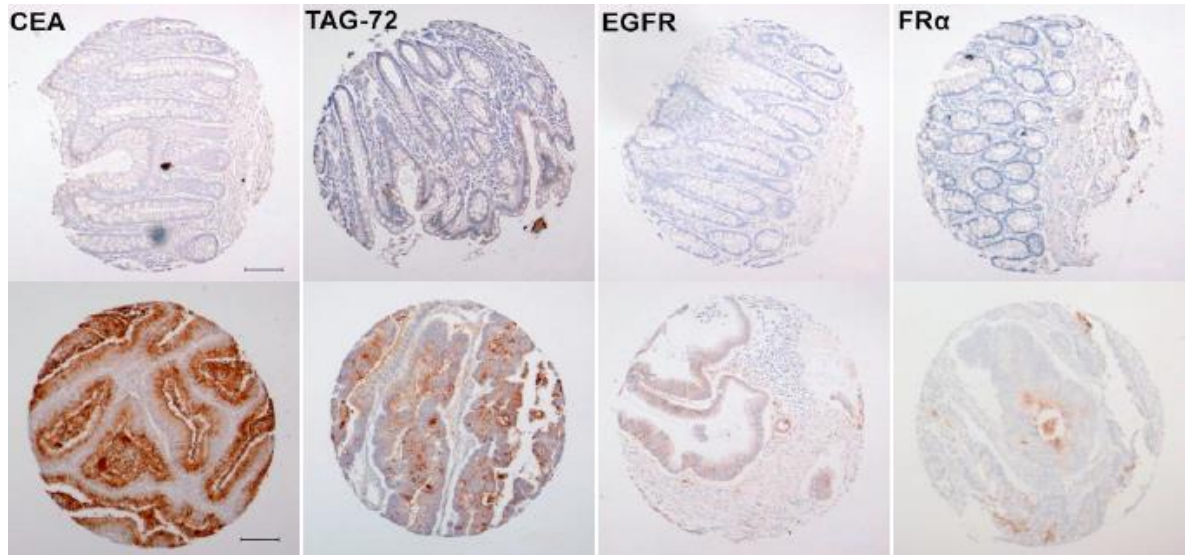


Figure 3.3. CEA, TAG-72, EGFR and FR α expression in tumour and normal tissue.

Representative tumour tissue microarray (TMA) cores of normal colorectal tissue (top row) or colorectal tumours (bottom row) showing immunoreactivity as labelled. Tissue microarrays containing tumour and matched normal tissue from 280 colorectal cancer patients were stained using immunohistochemistry for CEA, TAG-72, EGFR and FR α . The normal tissue cores shown demonstrate the median score for that antigen in normal colorectal tissues (CEA = 1; TAG-72: = 2; EGFR: = 0; FR α : = 0). The tumour cores shown demonstrate the median positive score for that antigen in colorectal tumours (CEA = 15; TAG-72 = 10; EGFR = 2; FR α = 1). Nikon Eclipse E1000, Japan, 20X magnification. Scale bar = 100 μ m.

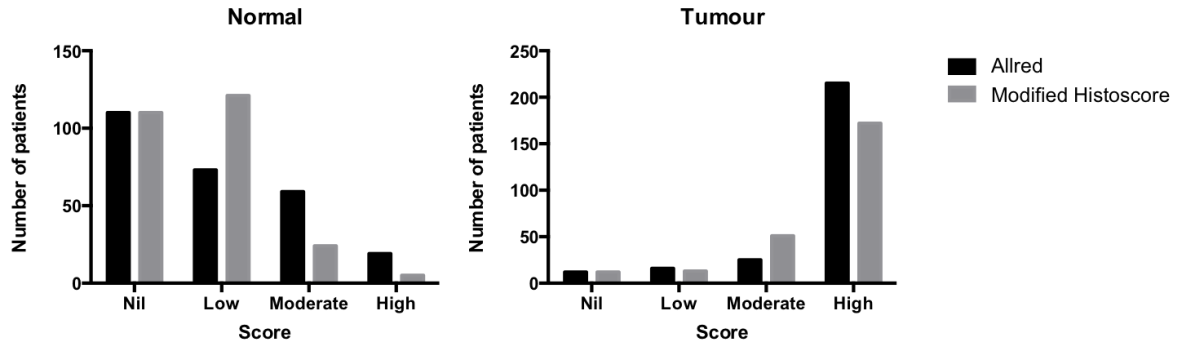


Figure 3.4. Allred versus modified Histoscore scoring results.

Comparison of two semi-quantitative scoring systems for assessing CEA expression in matched normal and colorectal tumour tissue. The Allred method produces a higher proportion of 'high' scoring tumours. 'Low' = lower third of scoring range, 'moderate' = middle third and 'high' = upper third.

Both the proportion of epithelial cells staining positively and the intensity of staining varied widely throughout the cohort in normal and tumour tissues (Figure 3.5).

Strongly positive staining in normal tissues was relatively uncommon for all antigens, especially for FR α (negative in over 99% at the concentrations used). In the tumours, by contrast, strongly positive staining was prevalent for CEA and TAG-72, and was more common for FR α than in normal tissue although tumours were also mostly negative (61%). EGFR staining in tumours showed a similar range of scores to those in normal tissues. CEA, TAG-72 and FR α , but not EGFR, were significantly more highly expressed in colorectal tumour tissues than in the normal tissues ($p < 0.001$; Table 3.3).

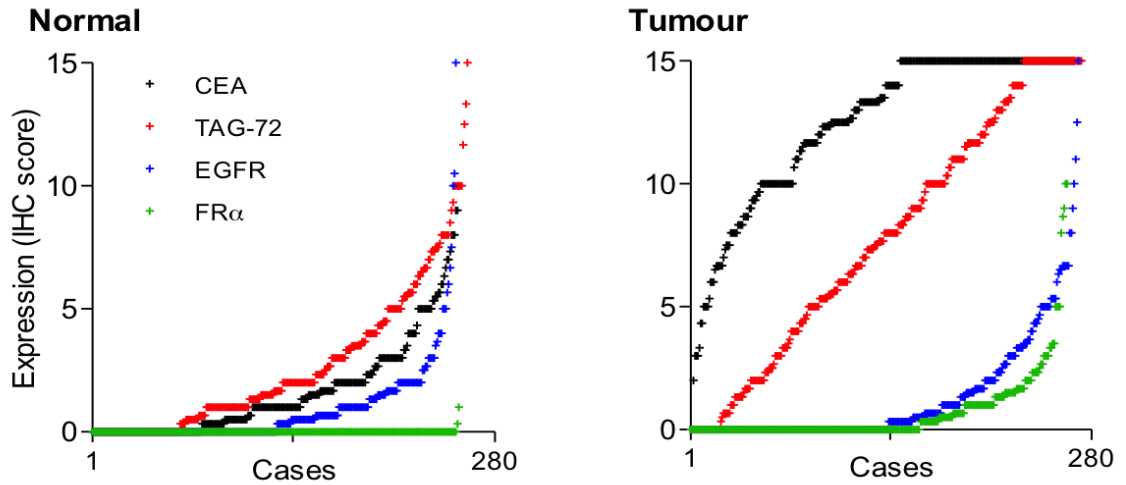


Figure 3.5. Biomarker expression in matched tumour and normal tissue.

Expression levels of CEA TAG-72, EGFR and FR α in normal colorectal tissue (left) and in colorectal tumours (right). Expression levels were determined by immunohistochemistry using a score of 0 to 15 in 280 matched normal and tumour tissues. The scores for each marker are arranged independently in ascending order to demonstrate the distributions across the cohort.

Antigen	Mean normal score	Mean tumour score	p value
CEA	1.7	12.4	<0.001
TAG-72	2.7	7.8	<0.001
FR α	0.0	0.7	<0.001
EGFR	0.9	1.3	0.08

Table 3.3. CEA, TAG-72 and FR α are significantly more highly expressed in colorectal tumour tissue than matched normal tissue.

3.3.2.1 Differential expression between matched normal and tumour tissue

If markers are to be used for tumour-specific imaging, the frequency and the magnitude of increased expression in tumours are key parameters. The frequency of increased expression compared to normal tissue dictates the sensitivity of a biomarker-dependent, tumour-specific imaging system. Expression scores were higher in tumours as compared to matched normal tissues in 98.8%, 79.0%, 37.1% and 32.8% of cases for CEA, TAG-72, FR α and EGFR respectively. Although this percentage is relatively low for FR α it should be noted that expression was higher in tumours as compared to matched normal tissue in almost all cases where positive staining was detected in either tissue. However in the case of EGFR, expression was higher in normal tissue (34% of cases) more frequently than in tumours (33% of cases) indicating little or no bias for tumour-specific expression. I have estimated the magnitude of the differences in expression between matched tumour and normal tissues as the tumour expression score minus the normal expression score (Figure 3.6). CEA demonstrated the greatest difference in expression, with tumours scoring on average 10.8 (95% confidence interval 10.31-11.21) points higher than normal tissues. This difference was more than twice that of the next best marker, TAG-72, which showed tumour expression to be 5.1 (95% CI 4.35-5.77) points higher than normal tissue. Epithelial growth factor receptor and FR α showed a much smaller difference of 0.4 (95% CI 0.09-0.79) and 0.7 points (95% CI 0.49-.086) respectively.

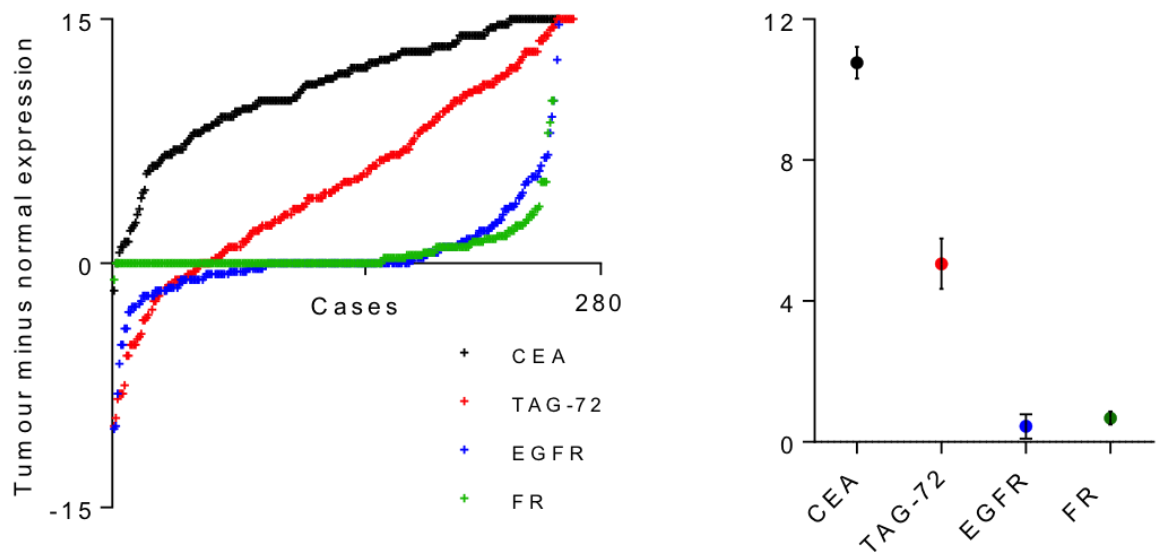


Figure 3.6. Differential expression for each biomarker..

CEA shows the most consistent over-expression in tumour tissues and the greatest differential expression between matched normal and tumour tissues. Expression scores for normal tissues were subtracted from those for matched tumour tissues to quantify the degree of tumour over-expression for each case. Over-expression scores for each marker are arranged in ascending order to demonstrate the distributions across the cohort (left). Minus scores reflect cases where tumour expression was lower than expression in the matched normal tissue. Mean over-expression scores (central marker) with 95% confidence intervals (error bars) are also shown (right).

3.3.3 Specificity and sensitivity of selected biomarkers for tumour detection

Accurate imaging of tumours based on the expression of any marker is heavily influenced by the limit of detection of the imaging system for marker expression. In a fluorescent imaging system, I foresee the gain being adjusted to calibrate the lowest limit of detection and prevent normal tissues producing a signal. I modelled this influence for each marker by examining what proportion of tumours would be successfully visualised when different expression scores were defined as the limit of detection; this is the sensitivity. I also tested what proportion of normal tissues would be “invisible”, as required for tumour-specific imaging, using the same limits; this is the specificity. First, I arbitrarily set this cut-off point as the 95th percentile of the normal score distribution, thereby tolerating a 5% chance of incorrectly detecting normal tissue as positive (a specificity of 95%). This cut-off gave sensitivities of 93.7%, 45.4%, 39.3% and 11.8% for CEA, TAG-72, FR α and EGFR respectively. An alternative approach is to use statistical techniques to identify a cut-off for each marker that allows the maximum sensitivity and specificity. A receiver operating characteristics (ROC) graph allows a visual and numerical assessment of the performance of a classifier (Fawcett, 2006, Zweig and Campbell, 1993), in my case the ability of a biomarker expression score to discriminate between tumour and normal tissue. I produced ROC curves for each biomarker and calculated the ‘area under the curve’ for each (Figure 3.7 and Table 3.4). CEA performed particularly well, with the AUC approaching 1, whereas EGFR was little better than chance alone, with an AUC approaching 0.5. The second best performing biomarker was TAG-72 with an AUC of 0.795 followed by FR α with 0.695.

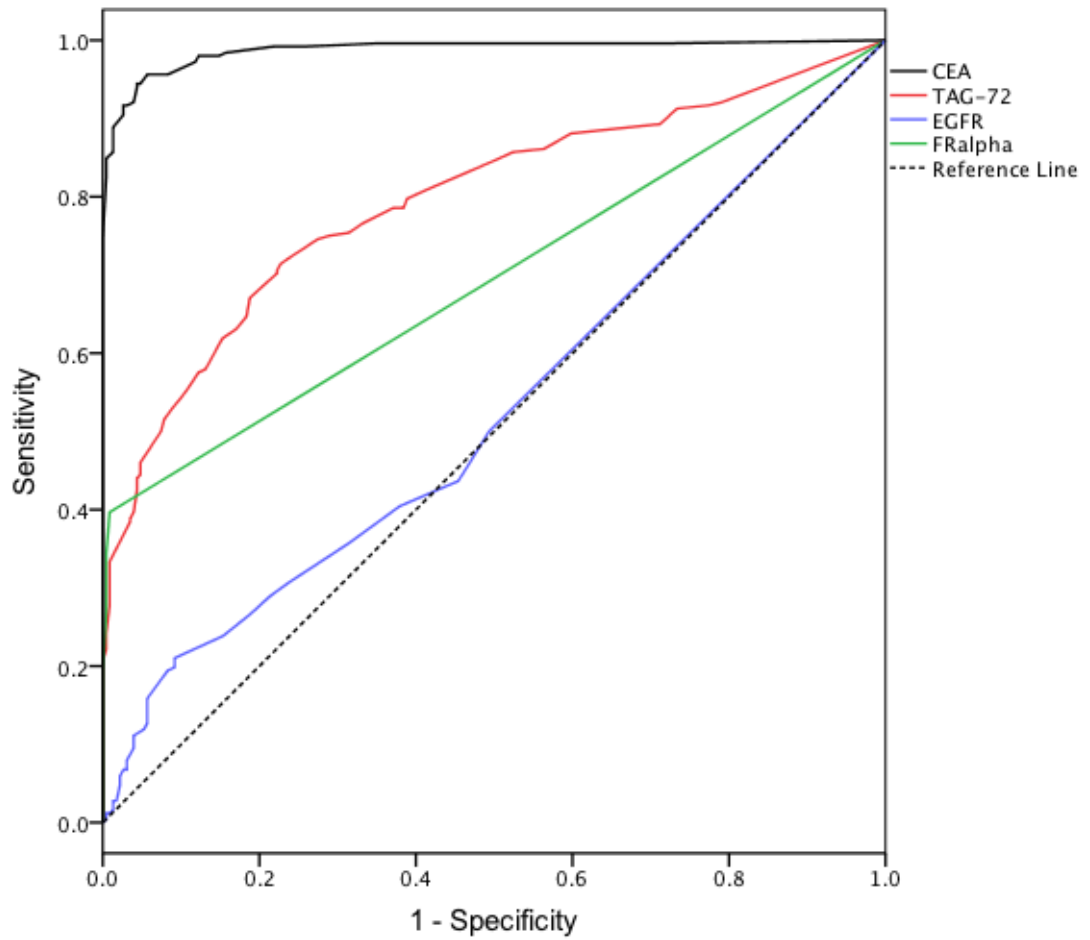


Figure 3.7. Receiver operating characteristic curve for CEA, TAG-72, EGFR and FR α .

CEA performs well in discriminating between tumour and normal tissue (greatest area under the curve, AUC); EGFR performs poorly.

Biomarker	Area under the curve	Sensitivity	Specificity
CEA	0.988	93.7	96.1
TAG-72	0.795	70.3	78.5
EGFR	0.527	39.3	99.2
FRα	0.695	21.7	90.5

Table 3.4. Peak sensitivity and specificity for each biomarker.

CEA out-performed other markers, with a superior area under the curve on receiver operator characteristic analysis, sensitivity and specificity.

In addition to AUC values, I was interested in the sensitivity and specificity of each biomarker. Using the data outputs of the ROC analysis, I added the sensitivity and specificity for each cut-off point and plotted the results (Figure 3.8). The calculated optimal cut-off values were: CEA, 6.42; TAG-72, 4.42; EGFR, 2.17; and FR α , 0. These cut-offs gave sensitivities and specificities of 93.7% and 96.1% for CEA, 70.3% and 78.5% for TAG-72, 39.3% and 99.2% for FR α , and 21.7% and 90.5% for EGFR.

I concluded that, of the biomarkers tested, CEA is the best performing for tumour discrimination in formalin-fixed, paraffin-embedded tissue: it shows the most consistent over-expression in colorectal cancer; it shows the greatest differential expression between normal and matched tumour tissue; and it has the greatest AUC and sensitivity and specificity on ROC analysis.

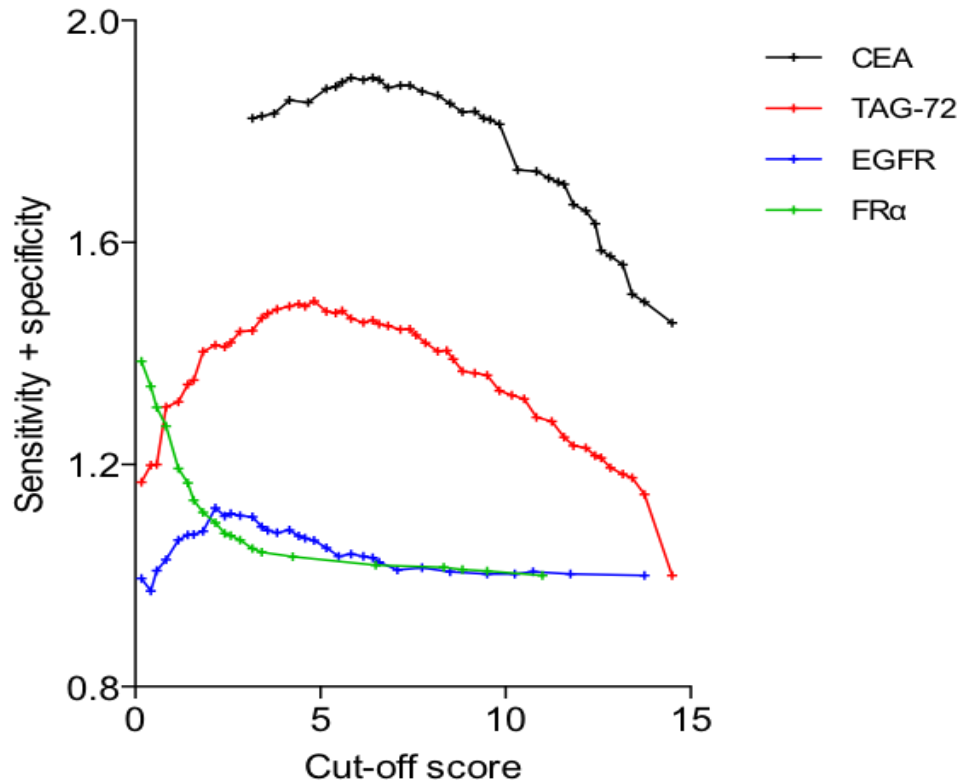


Figure 3.8. Optimum cut-off scores.

Optimum cut-off values were calculated for each marker by testing multiple cut-off points and selecting the value with the greatest combined sensitivity and specificity.

Calculated optimal cut-off values: CEA, 6.42; TAG-72, 4.42; EGFR, 2.17; FR α , 0.

3.3.4 Expression of selected biomarkers in 18 matched normal and metastatic mesenteric lymph nodes.

For intra-operative staging of colorectal cancer to be possible, the status of mesenteric lymph nodes adjacent to primary tumours must be determined. Therefore biomarker expression of both tumour cells in positive lymph nodes and of normal lymph node cells are critical. I aimed to evaluate whether the biomarker expression patterns I observed in primary tumours is similar in lymph node metastases. To do

this I examined the expression of each biomarker in lymph nodes taken during resection from patients from my cohort, using the same immunohistochemistry protocols as above. I had access to the tissue from 18 patients. In each case, I examined a node found to contain metastatic tumour cells (“positive”) and a node that was clear of metastatic deposits (“negative”) (Figure 3.9). Expression of all markers followed the same pattern as in primary tumours, and was uncommon in negative nodes; TAG-72 showed the most staining in negative nodes, being expressed at low levels by cells in the germinal centres in 5 out of 18 cases (Figure 3.10), a feature previously described (Marianicostantini et al., 1991).

Carcinoembryonic antigen also showed very slight germinal centre expression in two of 18 cases, also previously described (Potomski et al., 1979). Carcinoembryonic antigen was expressed in all positive nodes, with high scores in the majority (Figure 3.11). The distributions of expression in positive nodes were similar to the patterns seen in primary tumours, with prevalent and strong expression of CEA and TAG-72 and less frequent and weaker expression of FR α and EGFR.

I concluded that, in this small cohort of samples, the expression of all four biomarkers in metastatic and normal lymph nodes appears similar to the patterns seen in primary tumours and normal colorectal mucosa.

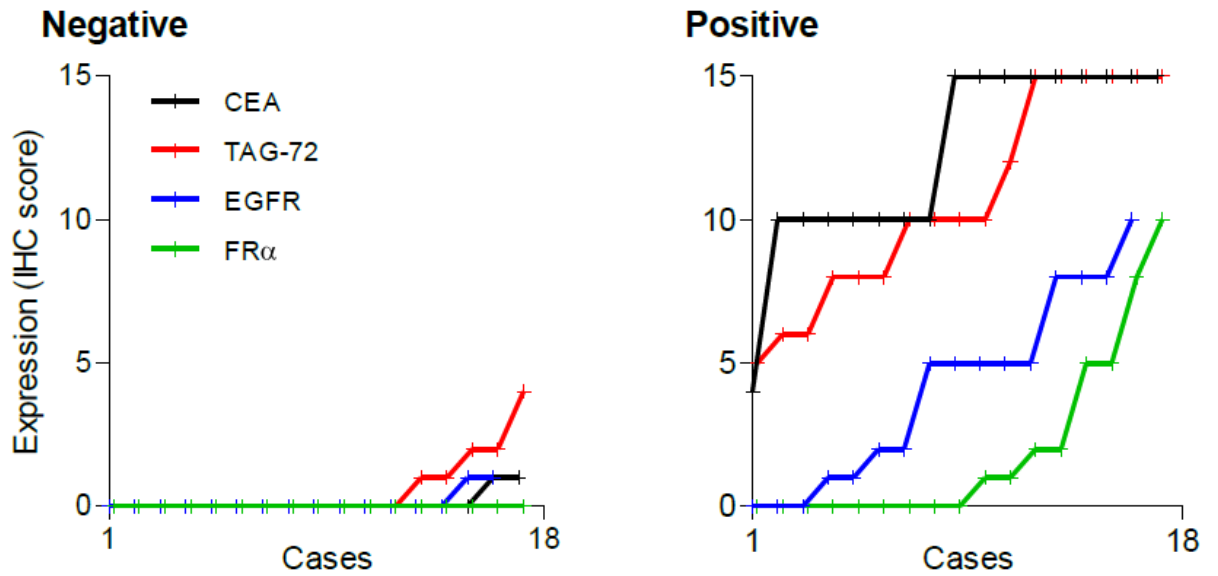


Figure 3.9. Biomarker expression in lymph nodes.

Biomarker expression is similar in lymph nodes to primary tumours. Expression levels of CEA, TAG-72, EGFR or FR α in lymph nodes containing colorectal tumour deposits ("positive"; right) and in matched lymph nodes lacking tumour cells ("negative"; left). Expression levels were determined by immunohistochemistry using scores of 0 to 15 in 18 cases. The scores for each marker are arranged independently in ascending order to demonstrate the distributions across the cohort (note: data points are linked by lines to aid interpretation of the distributions not to imply adjacent data points are directly related).

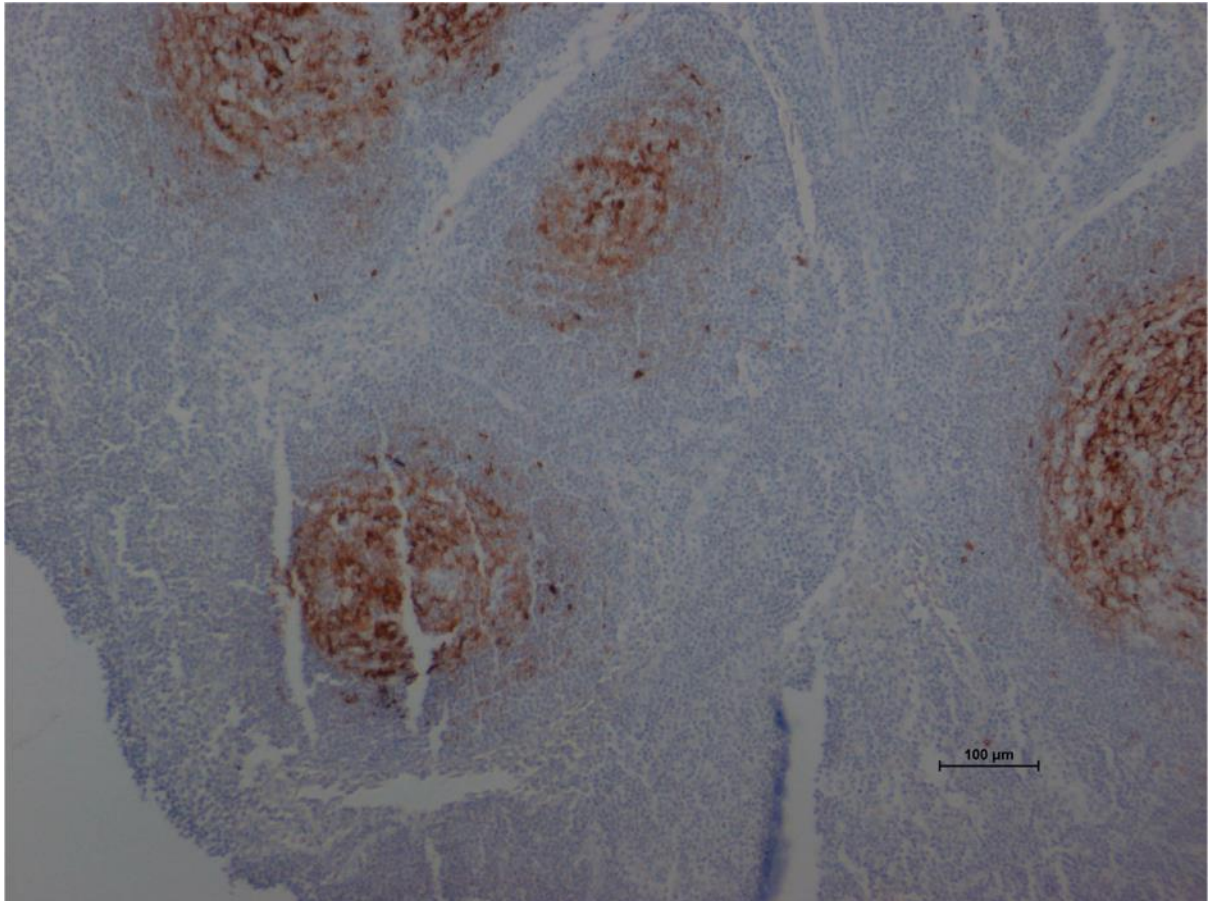


Figure 3.10. Non-specific staining in normal lymph nodes.

Lymph nodes containing no metastases showed moderate positive staining in the germinal centres when incubated with anti-TAG-72 antibodies. Concentration 1:100, magnification X20.

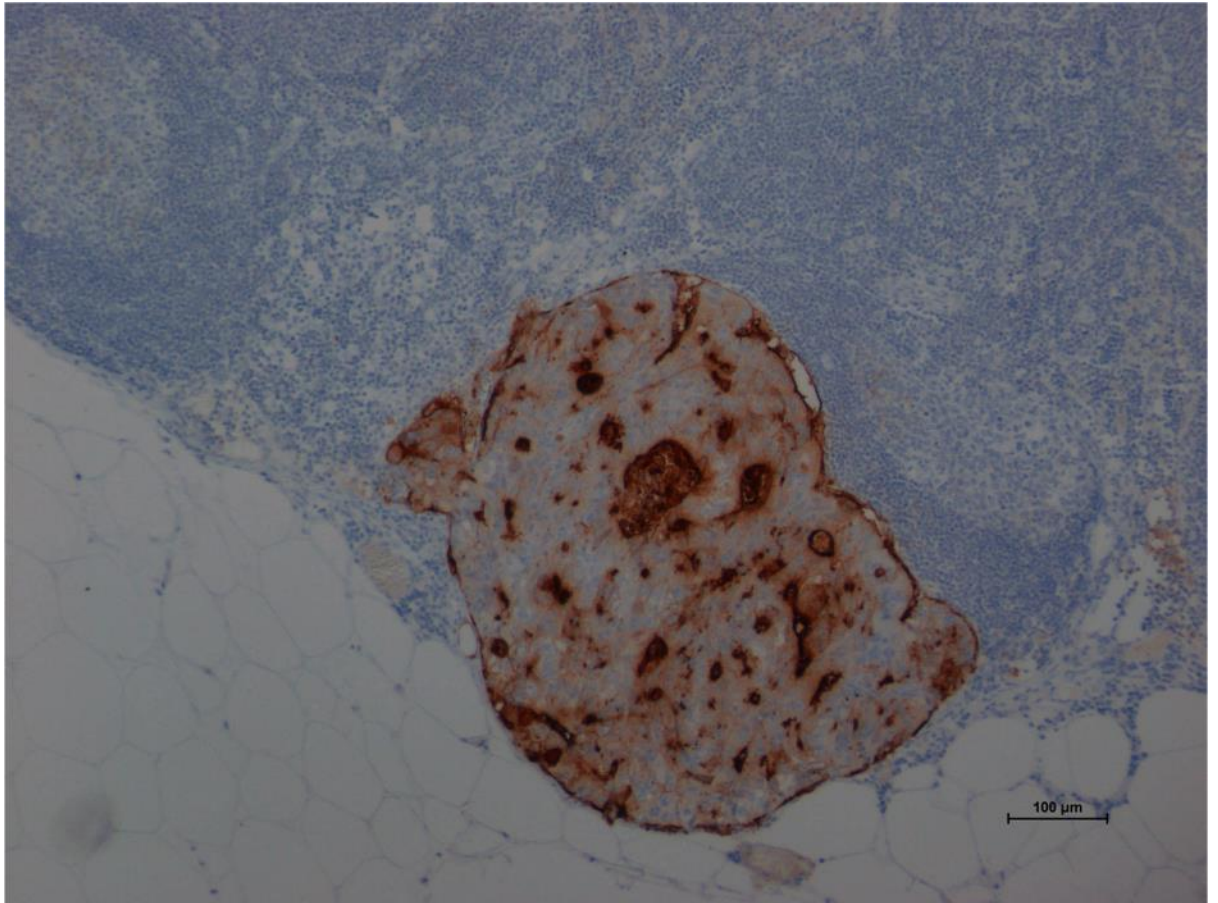


Figure 3.11. Tumour specific expression in lymph nodes.

Metastatic deposits in lymph nodes stained heavily when incubated with anti-CEA antibodies. Tumour-specific staining was present in all 18 positive lymph nodes examined and showed a similar pattern of luminal accentuation to that seen in corresponding primary tumours. Concentration 1:200000, magnification X20.

3.4 Discussion

I have shown that CEA is the best performing biomarker for colorectal cancer-specific targeting, with consistent over-expression in tumour tissue, a high differential expression between normal and matched tumour tissue, and very high sensitivity and specificity values on ROC analysis.

I sought to examine the expression of a panel of membrane-bound colorectal cancer biomarkers in a large cohort of matched normal and tumour tissue using immunohistochemistry to determine their potential for use in my project. My first step was to use a small sample of formalin-fixed, paraffin-embedded colorectal cancer samples and one normal colonic sample to test for tumour-specific immunostaining and to optimise immunohistochemistry experimental conditions. CEA, TAG-72, EGFR and FR α have all been used in experimental colorectal cancer targeting studies (section 3.2) and were therefore obvious choices for inclusion in this work. Antibodies to these biomarkers all showed tumour-specific immunostaining and were selected for evaluation using TMAs. I also included three further biomarkers in this initial phase: VEGFR-2, robo1 and CD105. VEGFR- 2 is an established therapeutic target for metastatic colorectal cancer (Winder and Lenz, 2010, Duff et al., 2006, Tonra et al., 2006, Giantonio et al., 2007) and has been used for *in vivo* imaging of gastrointestinal tract tumours in murine models (Foersch et al., 2010). Most work has concentrated on its expression by endothelial cells but there is some evidence that it is also expressed by colorectal cancer cells (Hanrahan et al., 2003). Despite varying the antibody concentration, incubation conditions and antigen retrieval methods, I failed to demonstrate any tumour cell specific staining during my optimisation process. The evidence for epithelial cell expression is limited to a few studies with small sample sizes that have focussed on endothelial cell expression (Amaya et al.,

1997, Duff et al., 2006, Hanrahan et al., 2003). Similarly, robo1 is thought to be upregulated in both colorectal tumour cells and endothelial cells of tumour vessels compared with normal cells (Wang et al., 2003, Grone et al., 2006), potentially allowing specific binding in two compartments. The evidence for expression in either compartment is limited and, as with VEGFR-2, I failed to demonstrate any tumour-specific staining. Endoglin, also known as CD105, is up regulated in colon cancer endothelial cells and one study has also reported upregulation in colorectal cancer nodal metastases (Clasper et al., 2008). It showed marked variability in expression in both malignant epithelial cells and endothelial cells. I considered this unsuitable as the sole targeting component of a nanoparticle-based imaging system but it holds promise as a secondary targeting antibody; it is conceivable that it could improve the cancer-recognition performance of a nanoparticle with a more appropriate principle targeting antibody such as anti-CEA. Although my antibody optimisation experiments utilised just 14 colorectal cancer samples, the other four biomarkers all showed far greater potential and I therefore decided to concentrate on them for the TMA work.

Immunohistochemistry is a relatively simple, established technique for examining the expression of various antigens in human tissue. However, measuring and comparing this expression is challenging due to the subjective assessment of the staining it produces. Investigators have used a variety of subtly different scoring systems when assessing protein expression in TMAs. These range from simple descriptive measurements such as 'weak', 'moderate' and 'strong' (Adams et al., 1999), to fully automated scoring using software packages (Rizzardi et al., 2012). Consensus reports have been published (van Diest et al., 1997) advising that the staining pattern and area of lesion of interest should first be defined, before scoring taking into account intensity and number of cells. The staining observed in three of my four biomarkers was predominantly membranous with varying degrees of mild cytoplasmic staining. My project requires a membrane-bound target, and it was this

expression that was of most interest. I therefore did not explore an automated scoring method as the results would have potentially been skewed by co-existing mild cytoplasmic staining. I tested two semi-quantitative scoring systems, based on the two most common methods in similar published studies: the Allred method (Allred et al., 1993) and a variation on the Histoscore method (McCarty et al., 1986). The Allred method tended to produce a higher proportion of 'high' scores (defined as being in the top third of the score range for each method) in tumour tissue, potentially reducing the potential for discriminating between two high scoring biomarker targets. Although the modified Histoscore tended to produce a higher proportion of 'low' scores in normal tissue, it allowed greater discrimination of high scores and I therefore elected to use this system for my analysis so that I could compare biomarker performance. The scoring system also appears to be reproducible, with good agreement between observers (intraclass correlation 0.89).

Using this scoring system, I was able to investigate three key criteria: i) the proportion of the cohort in which tumours stained positively for markers; ii) the proportion of the cohort in which tumours stained more strongly for markers than the matched normal tissues; and iii) the magnitude of over-expression in tumours. CEA out-performed other markers dramatically in all three measures, showing the most frequent tumour expression, and the most frequent and greatest tumour over-expression. In particular, differential CEA expression within normal/tumour pairs was notably greater as compared to other markers, providing evidence that CEA is the most reliable marker for differentiating between normal and tumour tissue.

When I repeated the experiments using positive and matched normal lymph nodes, CEA was again the superior target, with high levels and frequency of expression within positive nodes. Although the sample of nodes used was small, the expression pattern was identical to that seen in primary tumour epithelial cells and of a similar

level. There was some low level staining seen in matched normal lymph node tissue for CEA and TAG-72, but this occurred at the germinal centres and has been described previously for both markers (Marianicostantini et al., 1991, Potomski et al., 1979). In the context of my overall project, intra-operative staging relies on the accurate assessment of the mesenteric lymph nodes; these findings suggest an anti-CEA antibody would be suitable as the tumour-recognition component of my imaging probe.

In practical imaging situations, the threshold, or cut-off, used to differentiate between normal and tumour would be determined by the user, by adjusting the signal gain. This could be altered to favour either sensitivity (lowering the cut-off to detect tumours more easily at the risk of detecting normal tissue erroneously) or specificity (raising the cut-off to avoid detection of normal tissue at the risk of missing tumour cells). I quantified the abilities of the markers to be used in tumour cell detection using their optimal cut-offs, as determined using ROC analyses, in terms of sensitivity (proportion of tumours correctly detected) and specificity (proportion of normal tissues correctly not detected). CEA was the most sensitive marker by a considerable margin (93.7%, as compared to the nearest alternative TAG-72 at 70.3%), and was also highly specific (96.1%). FR α was the most specific marker (99.2%), however its utility is limited by the fact that it was not detectable in the majority of tumours, as previously reported (Shia et al., 2008), resulting in a poor sensitivity (39.3%). In addition, the magnitude of differential expression between normal and tumour was relatively narrow, providing less security in determining tumour or normal identities. Most notably, EGFR was a surprisingly poor marker, being detected in less than half the tumours and being commonly more highly expressed in normal tissues than in tumours. Cetuximab, a monoclonal antibody directed against EGFR, has been used in patients with tumours that show immunohistochemical expression of this antigen (Jonker et al., 2007, Van Cutsem et

al., 2009). My findings have no direct relevance to this therapy but the prevalence of EGFR expression I have shown is lower than most published studies, some of which claim up to 97% (Koretz et al., 1990, Lee et al., 2002, Spano et al., 2005, Bhargava et al., 2006). There are a number of different antibodies available and this may be due to differences between them. There is also controversy regarding the relationship between EGFR expression (as assessed by immunohistochemistry) and response to monoclonal antibody therapy (Cunningham et al., 2004) with EGFR-negative patients responding to treatment (Chung et al., 2005).

I therefore concluded that of the four biomarkers tested, and on the basis of immunohistochemical expression, CEA is the most suitable for intra-operative tumour targeting with a fluorescent nanoparticle. However, these results apply to formalin-fixed, paraffin-embedded tissue only; as part of a systemically delivered imaging probe, the antibody will be required to perform in a far more complex biological system. In the next chapter I describe experiments designed to model these conditions.

This is the first immunohistochemistry study to compare commonly used biomarker targets for *in vivo* targeting of colorectal cancer and these results are also relevant to investigators in the fields of non-invasive targeted imaging and targeted therapeutics.

Chapter Four

**CEA and TAG-72 are available for
antibody binding in live cells**

4 CEA AND TAG-72 ARE AVAILABLE FOR ANTIBODY BINDING IN LIVE CELLS

4.1 Abstract

Background

Expression studies of CEA and TAG-72 using immunohistochemistry on formalin fixed paraffin embedded tissue have demonstrated that these markers have potential for use *in vivo* colorectal cancer targeting. I now aimed to ascertain whether these antigens are available for antibody binding in live cancer cells and fresh frozen tumour samples, as would be required in an *in vivo* setting. I also aimed to test whether systemically delivered antibodies were able to reach tumour cells in an *ex vivo* model.

Methods

I used three colorectal cancer cell lines and suitable controls for immunofluorescent evaluation of anti-CEA and anti-TAG-72 antibody binding in both fixed cells and live cells. I also examined binding in fresh frozen tumour tissue. Finally, I injected anti-CEA antibodies into the supplying artery of three freshly resected CEA-expressing human colorectal cancer specimens prior to fixation, and evaluated the tumour cells for evidence of antibody binding using immunohistochemistry.

Results

Incubation with both anti-CEA and anti-TAG-72 antibodies produced staining in live cells, but only anti-CEA produced staining in fixed cells. The staining tended to be stronger and more diffuse with anti-CEA. Only non-specific staining was evident with

both antibodies in fresh frozen tissue. No tumour-bound anti-CEA antibodies were detected following arterial injection in *ex vivo* tumours.

Conclusion

CEA and TAG-72 are available for binding in live colorectal cancer cells but delivery to a tumour *in vivo* may represent a challenge.

4.2 Introduction

The key criteria for markers that are suitable for targeting colorectal cancer cells with fluorescent particles have been described previously (see section 1.3). I have already determined which of a range of candidates display suitable differential expression in Chapter 3. The two best performing biomarkers from these experiments were TAG-72 and CEA, both of which showed high levels of expression in the majority of tumours, relatively low expression in matched normal tissue and a large differential in expression levels between tumour and normal tissues. In this chapter, my aim was to determine which of these antigens was available for antibody-binding in live cells. Previously published work from other laboratories has demonstrated that some antigens from these molecules are apparently available for binding following systemic delivery; iodine¹²⁵-labelled anti-TAG-72 antibodies were used to locate occult tumour cells intra-operatively in radio-immunoguided surgery (Povoski et al., 2012) and iodine¹³¹-labelled anti-CEA antibodies have been used for targeted cytotoxic delivery in radioimmunotherapy applications (Meyer et al., 2009). However in some cases, controls were relatively poor with no non-targeted antibody control to prove that the apparent tumour specificity was due to antibody binding rather than an alternative mechanism such as the EPR phenomenon (Matsumura and Maeda, 1986). Formally, it remains unclear whether these antigens are truly available in a live biological system and to what degree. I used three colorectal cancer cell lines for this work: HT-29 cells, derived from grade II human colonic adenocarcinoma (Fogh J, 1975); CACO2 cells, derived from a human colonic adenocarcinoma (Koivisto and Salaspuro, 1997); and HRT-18 cells, derived from a human rectal adenocarcinoma (Tompkins et al., 1974).

4.3 Results

I aimed to assess the availability of CEA and TAG-72 in various cellular systems in order to assess whether they are available for binding in a live biological system. I used three system models to assess antigen availability: fixed and live cell lines; freshly frozen human colorectal cancer tissue samples; and freshly resected, *ex vivo* colorectal cancer specimens *in situ* within the resected colon. To evaluate antigen availability and antigen binding in cell lines and in fresh frozen tissue I used immunofluorescence or, for *ex vivo* samples, immunohistochemistry.

4.3.1 CEA, but not TAG-72, is available for antibody binding in fixed cells

First, I aimed to assess whether CEA and TAG-72 antigens were available in fixed colorectal cancer cell lines – this was to validate these lines as suitable CEA- and TAG-72-expressing models to use subsequently as live cell models. I used three widely available colorectal cancer cell lines for this: HT-29, CACO2 and HRT18 cells. Having demonstrated antigen availability in FFPE treated colorectal tissue, I hypothesised that fixed colorectal tissue culture cells would show similar antigen availability. I therefore fixed cells from each cell line with paraformaldehyde prior to incubating them with the primary anti-CEA or anti-TAG-72 antibody followed by an appropriate fluorescent secondary antibody. Control conditions involved incubating cells with the fluorescent secondary antibody only, omitting the primary antibodies. Staining was assessed subjectively in terms of whether the membranous staining was present (mild, moderate or strong) or absent, and whether it was diffuse across all cells or focal.

Whilst staining was present in fixed cells in all three cell lines when incubated with anti-CEA antibodies, staining was not present in fixed cells with anti-TAG-72 antibodies (Figure 4.1). When no primary antibody was used, no staining was apparent in any cell line. The lack of staining with anti-TAG-72 antibodies was surprising given the results obtained with FFPE tissue. I concluded that, in this fixed cell *in vitro* model of colorectal cancer, CEA is available for immunostaining but TAG-72 is not.

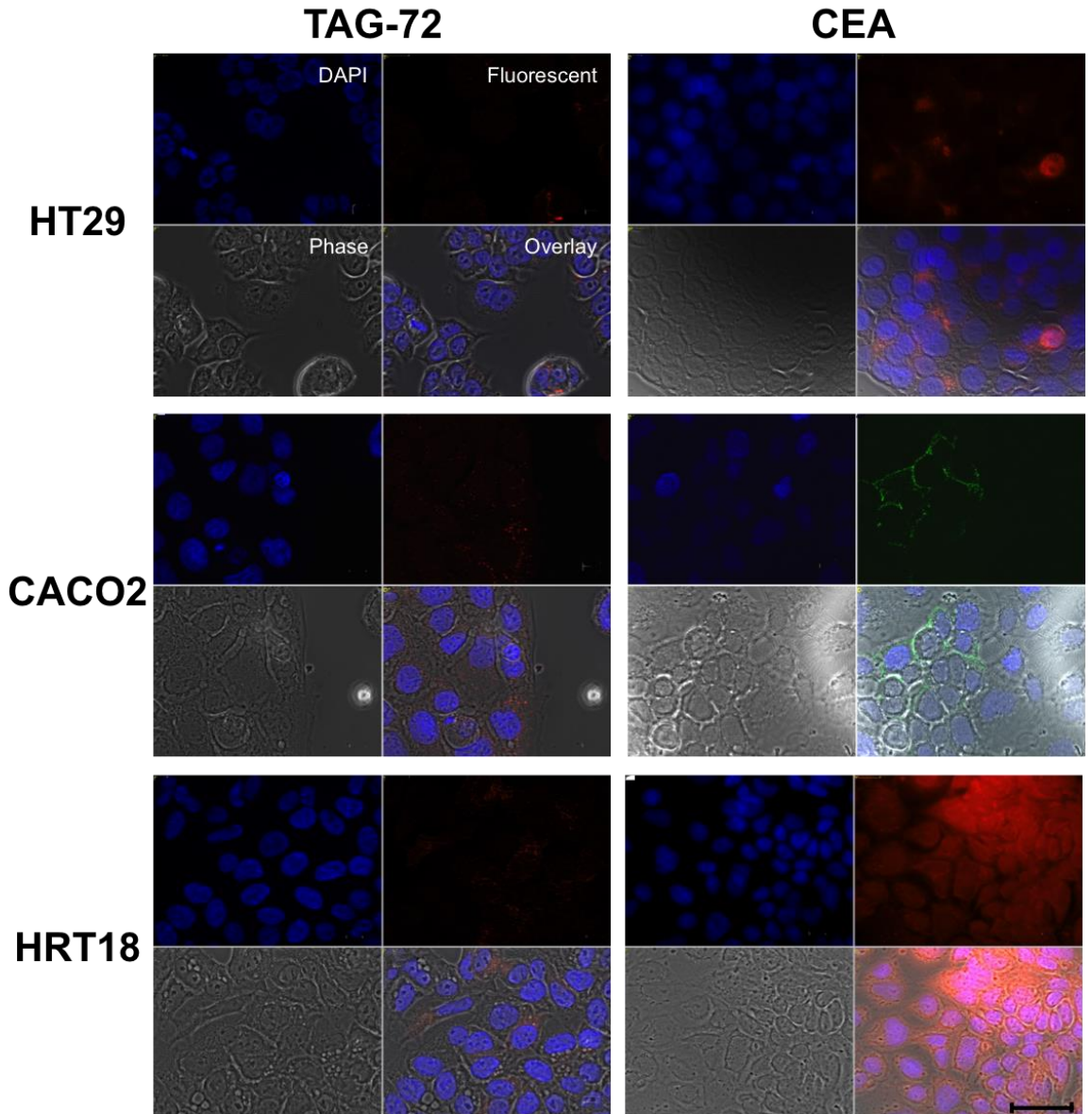


Figure 4.1. Immunostaining in fixed cells.

Fixed HT29, CACO2 and HRT18 cells show colorectal cancer cell specific immunostaining when incubated with anti-CEA but not anti-TAG-72 antibodies and a suitable fluorescent antibody. Four images are shown for each: DAPI staining (top left), CEA/TAG-72 staining (top right), phase contrast (bottom left) and merged image (bottom right), X63 magnification. Although different fluorescent secondary antibodies were used due to availability, gain and exposure settings were consistent. Scale bar = 40 μm .

4.3.2 CEA and TAG-72 are available for antibody binding in live cells

Next, I aimed to assess whether CEA and TAG-72 antigens were available in live cells from the same three colorectal cancer cell lines. I used the same test and control conditions (but with paraformaldehyde fixation omitted). In addition, human endothelial cells (HUVECs) were used as a negative control cell line, since the colorectal markers CEA and TAG-72 would not be expressed in these cells. In order to demonstrate the specificity of any binding further, I used anti-CD105 antibodies as negative control antibodies; CD105 is an endothelial cell marker that should not be detectable on colorectal epithelial cells but should be detected on HUVEC cells (Li et al., 2000).

4.3.2.1 Unfixed (live) cell immunofluorescence allows appropriate imaging of cell surface markers

When live HUVEC cells were incubated with anti-CD105 antibodies, strong fluorescent staining was observed (Figure 4.2). When anti-CD105 antibodies were incubated with live colorectal cancer cell lines there was no evidence of any staining, validating its use as a negative control. When live HUVEC cells were incubated with anti-CEA and anti-TAG-72 antibodies, no fluorescent staining was observed (Figure 4.3). I concluded that live cell immunofluorescence allows appropriate imaging of cell surface markers and that HUVEC cells and anti-CD105 antibodies are appropriate controls for this work.

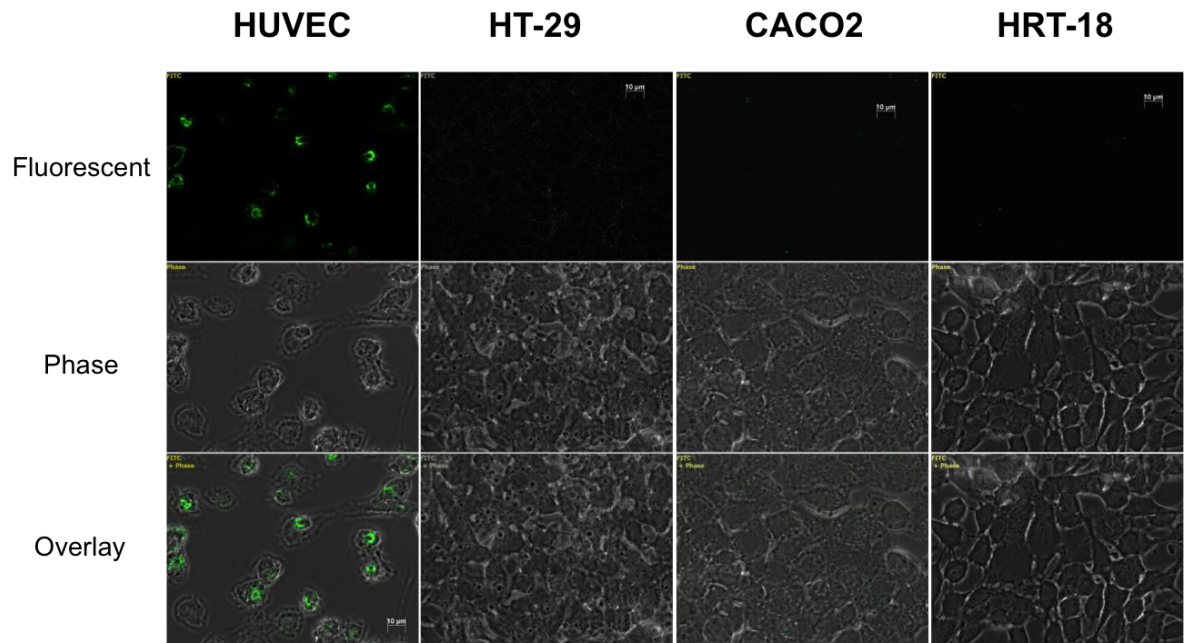


Figure 4.2. Anti-CD105 antibodies as a negative control.

Anti-CD105 antibodies act as a suitable negative control to demonstrate the specificity of anti-colorectal cell antigen/colorectal cancer cell binding. Four different cell types, as labelled, were seeded on glass coverslips and incubated in live culture with anti-CD105 antibodies (1h), before treatment to allow IF visualisation of antibody:antigen binding. Magnification = 63X.

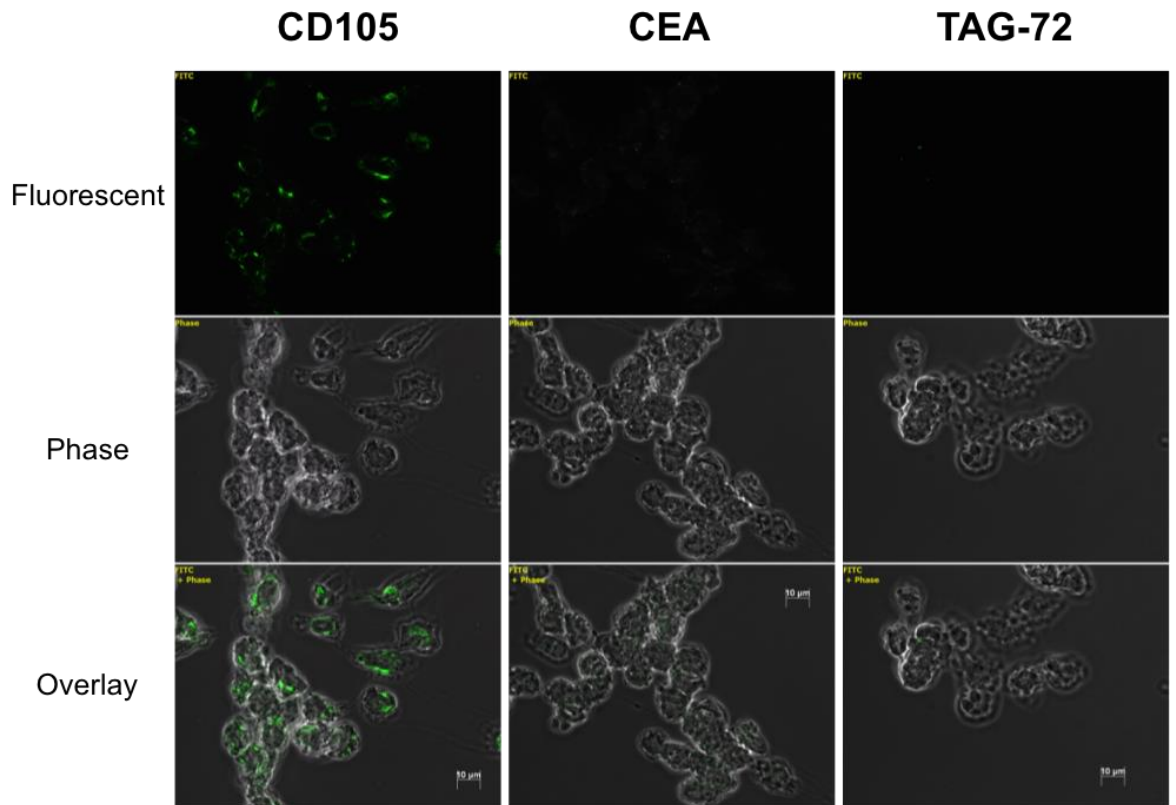


Figure 4.3. HUVECs as a negative control cell line.

HUVECs act as a suitable negative control cell line to demonstrate the specificity of anti-colorectal cell antigen/colorectal cancer cell binding. HUVEC cells were seeded on glass coverslips and incubated in live culture with anti-CD105, anti-CEA and anti-TAG-72 antibodies (1h), before treatment to allow IF visualisation of antibody:antigen binding. Magnification = 63X.

4.3.2.2 CEA and TAG-72 are available for immune-recognition in live colorectal cancer cells

Both CEA- and TAG-72-specific staining was demonstrated in live cells from all three colorectal cancer cell lines (Figure 4.4). When no primary antibody was used, no staining was apparent in any cell line.

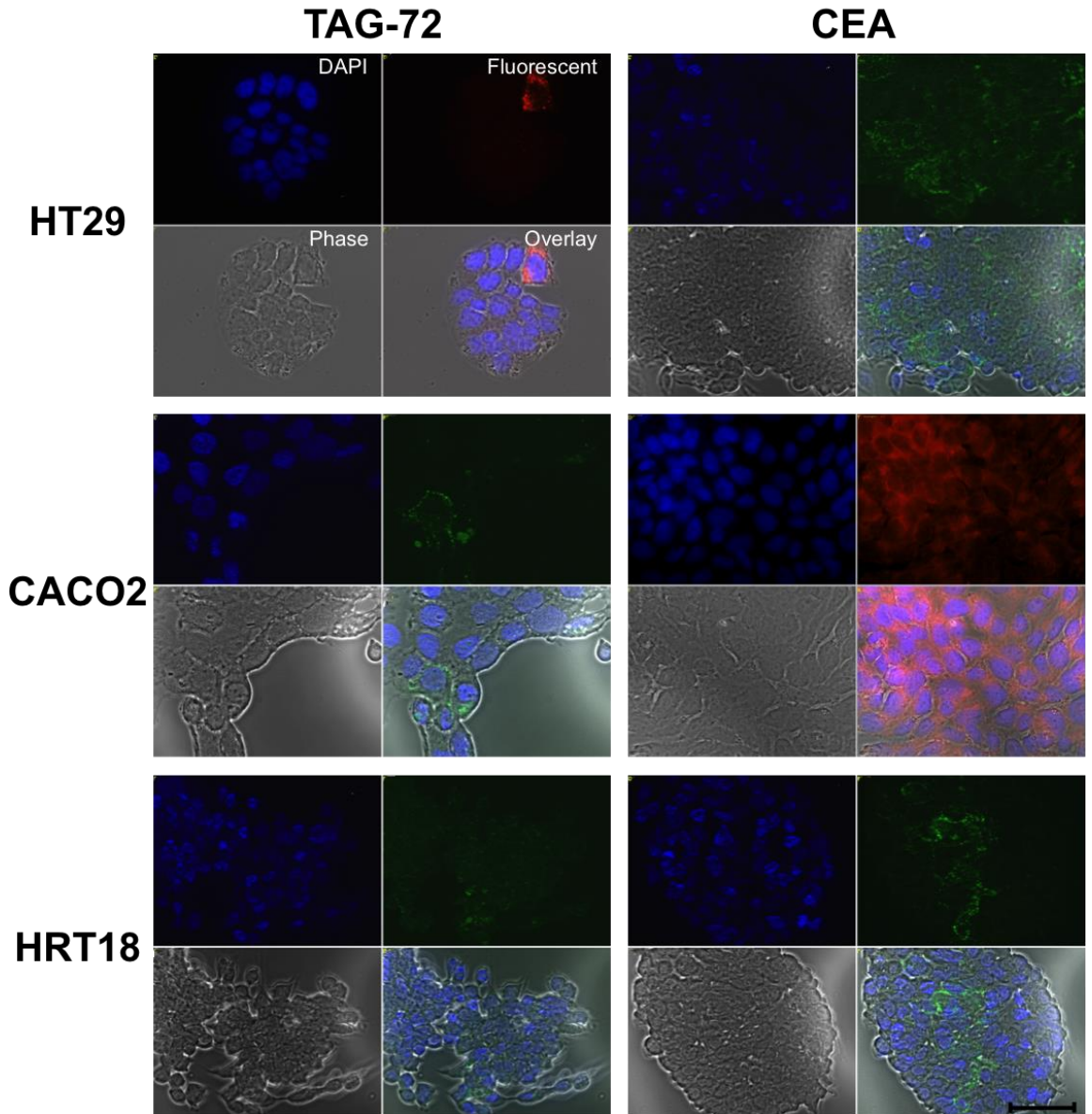


Figure 4.4. Immunostaining in live cells.

Live HT29, CACO2 and HRT18 cells show colorectal cancer cell specific immunostaining when incubated with anti-CEA and anti-TAG-72 antibodies and a suitable fluorescent antibody. Four images are shown for each: DAPI staining (top left), CEA/TAG-72 staining (top right), phase contrast (bottom left) and merged image (bottom right), X63 magnification. CEA-targeted staining appears to be stronger and more diffuse than TAG-72. Scale bar = 40 μ m.

Whilst staining was present in both fixed and live cells in all three cell lines when incubated with anti-CEA antibodies, staining was only present in live cells with anti-TAG-72 antibodies. The results are summarised in Table 4.1.

Cell line		No primary	CEA	TAG-72
HT-29	Fixed	No staining	Focal, strong	Nil
	Live	No staining	Diffuse, strong	Focal, moderate
CACO2	Fixed	No staining	Diffuse, mild	Nil
	Live	No staining	Diffuse, mild	Focal, mild
HRT-18	Fixed	No staining	Diffuse, moderate	Nil
	Live	No staining	Focal, moderate	Focal, mild

Table 4.1. Summary of immunostaining patterns.

Fluorescent immunostaining patterns of fixed and live cells from three colorectal cancer cell lines when incubated with anti-CEA and anti-TAG-72 antibodies.

Incubation with anti-CEA antibodies appears to produce a stronger and more diffuse staining pattern.

I concluded that both CEA and TAG-72 are available for antibody binding in a live cell culture *in vitro* system. Although the results are qualitative only, incubation with anti-CEA antibodies appears to produce a stronger and more diffuse staining pattern.

4.3.3 Assessment of the accessibility of CEA and TAG-72 for imaging in the context of tumour architecture

Having demonstrated the availability of CEA and TAG-72 for antigen-antibody binding in live colorectal cancer cell lines, I aimed to investigate accessibility in fresh frozen tissue, as this represents a model that is one step closer to live human tissue. Sections of archived fresh frozen colorectal tumour and matched normal colon tissue (five patients) were prepared and incubated with anti-CEA and anti-TAG-72 antibodies using the same immunofluorescence protocol as used previously. In each case, one slide was incubated with the secondary antibody only as a negative control and no staining was observed in any of these controls.

Although promising fluorescent images were obtained when fresh frozen colorectal cancer tissue was incubated with anti-CEA and anti-TAG-72 antibodies (Figure 4.5 and Figure 4.6), matched normal colonic tissue also yielded fluorescence. This was seen in all five matched patient samples. Extended TBS-Tween wash steps with gentle agitation were added to the method in an attempt to ensure unbound primary antibody was completely removed from the specimen but this had no effect (Figure 4.7).

I concluded that it was unclear if the fluorescent staining seen in fresh frozen tumour samples was the result of genuine antigen-specific antibody binding.

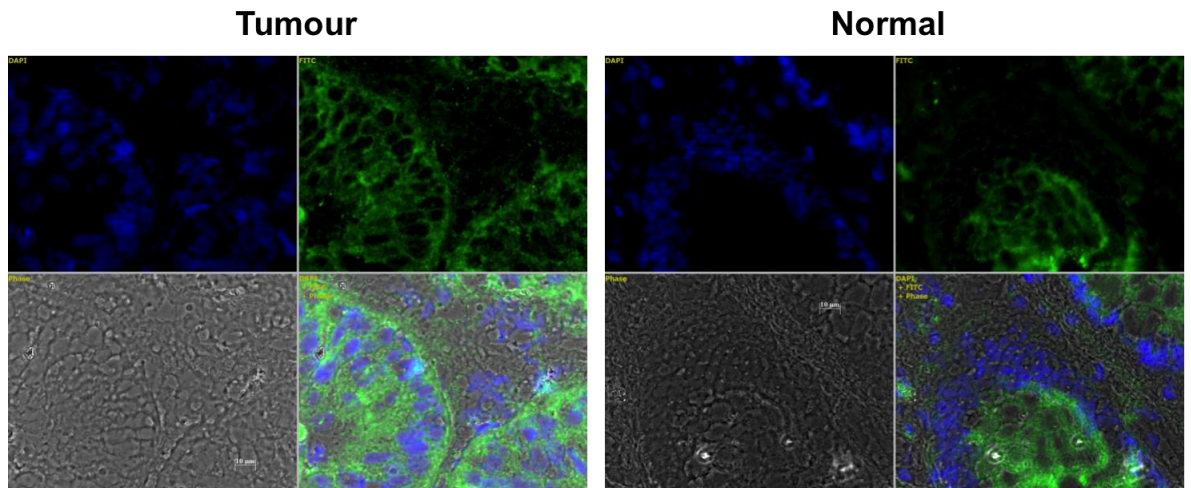


Figure 4.5. CEA immunostaining in fresh frozen tissue.

Fresh frozen colorectal cancer and matched normal tissue both exhibit fluorescent staining when incubated with anti-CEA antibodies. Tissue samples were sectioned and subjected to immunofluorescence with anti-CEA antibodies and an appropriate fluorescent secondary antibody. Four images are shown: DAPI staining (top left), CEA expression (top right), phase contrast (bottom left) and merged DAPI/CEA/phase, X63 magnification.

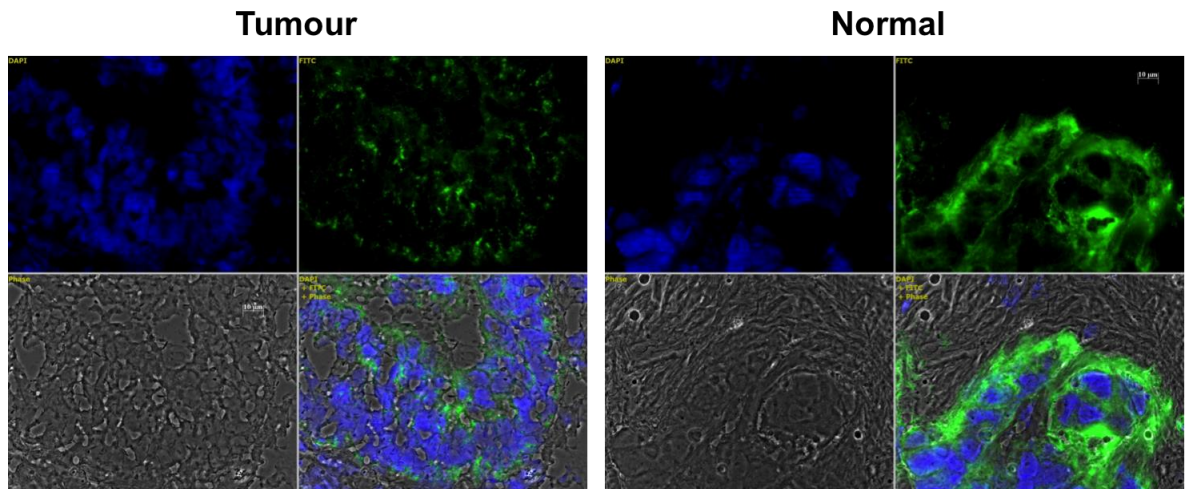


Figure 4.6. TAG-72 immunostaining in fresh frozen tissue.

Fresh frozen colorectal cancer and matched normal tissue both exhibit fluorescent staining when incubated with anti-TAG-72 antibodies. Tissue samples were sectioned and subjected to immunofluorescence with anti-TAG-72 antibodies and an appropriate fluorescent secondary antibody. Four images are shown: DAPI staining (top left), TAG-72 expression (top right), phase contrast (bottom left) and merged DAPI/TAG-72/phase, X63 magnification.

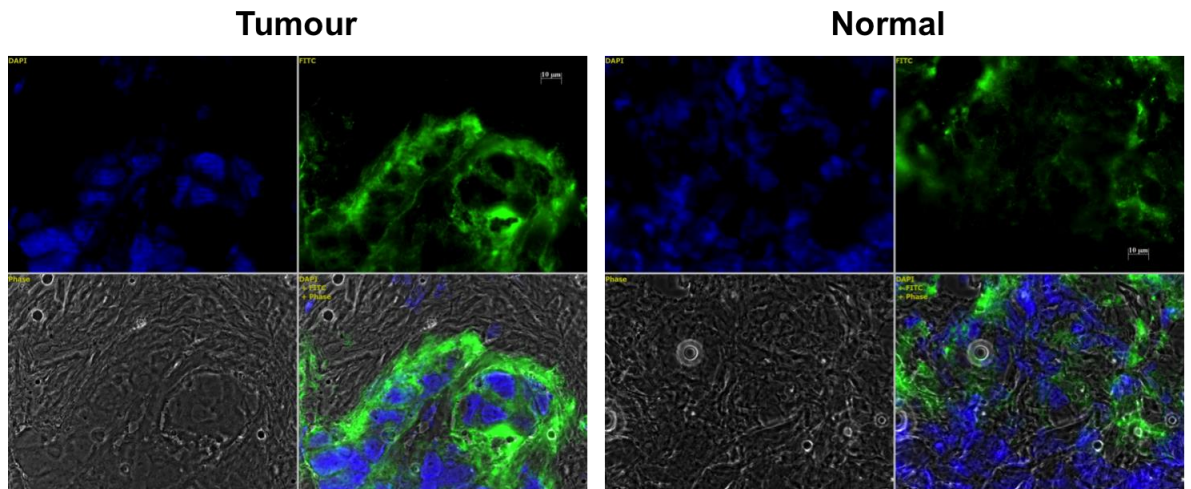


Figure 4.7. Immunostaining in fresh frozen tissue is not tumour-specific.

Fresh frozen colorectal cancer and matched normal tissue both exhibit fluorescent staining when incubated with anti-CEA antibodies despite extended wash and agitation steps prior to fluorescent secondary antibody incubation. Four images are shown: DAPI staining (top left), CEA expression (top right), phase contrast (bottom left) and merged DAPI/CEA/phase, X63 magnification.

4.3.4 Assessment of biomarker localisation in an *ex vivo* model of systemic antibody delivery

Having shown that CEA is available for antigen-antibody binding *in vitro* at least in cell lines, I sought to design a model to test whether antibodies could reach their antigens on the surface of tumour cells in the context of genuine tumour architecture and when delivered via the arterial vasculature. For this experiment I chose to focus on CEA as a target biomarker because it had performed best in FFPE human tissue samples and most consistently in cell lines. To do this I aimed to inject anti-CEA antibodies into the main supplying artery of freshly resected tumour specimens in the operating theatre, and then use immunohistochemistry to detect bound anti-CEA

antibodies. However, to prove that this model had the potential for success, I needed to show that routine histopathological examination, specifically fixation with formalin, would not prevent a secondary antibody binding to the primary anti-CEA antibody-antigen complex. I examined this by performing similar antibody-binding and subsequent fixation in HT-29 cells with A5B7 anti-CEA antibodies. Live HT-29 cells on coverslips were incubated with anti-CEA antibodies, and were then fixed with formalin, and subsequently incubated with fluorescent secondary antibodies. Figure 4.8 shows HT-29 cells treated in this way, along with cells that had undergone routine immunofluorescence with anti-CEA antibodies and a fluorescent secondary antibody (ie. live cells treated in turn with primary and secondary antibodies, and imaged unfixed). Successful localisation of the antibody-antigen complexes appeared to be unaffected by formalin fixation.

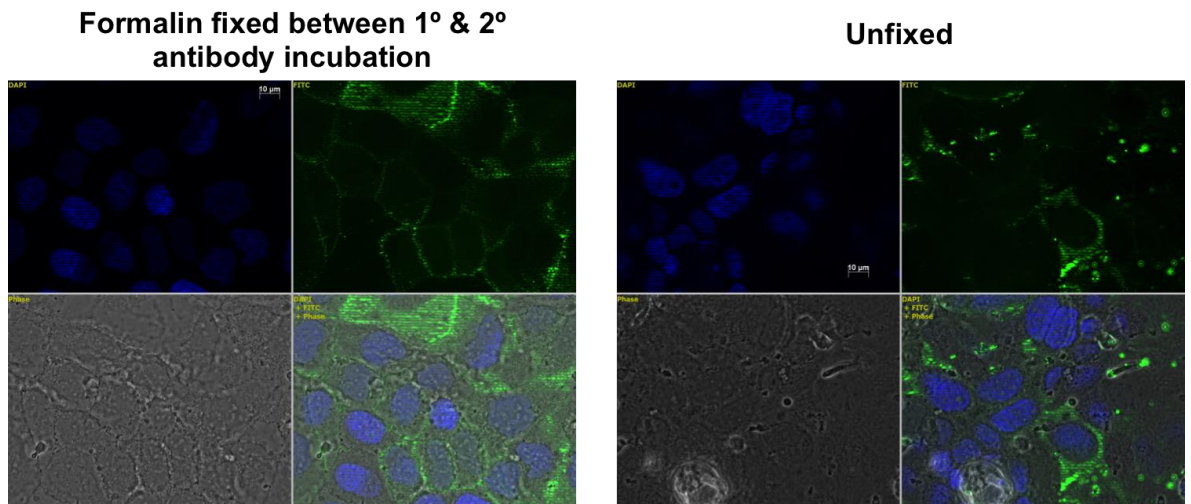


Figure 4.8. Formalin fixation did not prevent CEA immunostaining.

Formalin fixation of cells following incubation with anti-CEA antibodies but prior to incubation with fluorescent secondary antibodies does not affect staining. Left: live cells were incubated with anti-CEA antibodies and then fixed in formalin. Twenty-four hours later they were incubated with a suitable fluorescent secondary antibody. Right: live HT-29 cells were incubated with anti-CEA antibodies and a suitable fluorescent secondary antibody. Four images are shown: DAPI staining (top left), CEA expression (top right), phase contrast (bottom left) and merged DAPI/CEA/phase, X63 magnification.

Having successfully shown that recognition of anti-CEA antibodies by secondary antibodies was unaffected by formalin fixation, I proceeded to attempt to deliver the primary antibody to tumour cells by injection into the arteries of *ex vivo* tumours. I injected a solution of A5B7 antibody into the ileocolic artery of three freshly resected right-sided colonic cancer specimens in the operating theatre. Following routine histopathological staging, I subjected sections of paraffin embedded tumour tissue to immunohistochemistry to identify bound A5B7 antibody. As a control I incubated

slides with both the primary anti-CEA antibody and a suitable secondary antibody to show that the tumours expressed CEA. I then incubated a separate slide with the secondary antibody only: if primary anti-CEA antibodies had reached the tumour, I would expect immunostaining to be present. Unfortunately this was not detectable in any of the patients (Figure 4.9). I concluded that the antibodies may not reach the tumour cells in this *ex vivo* model.

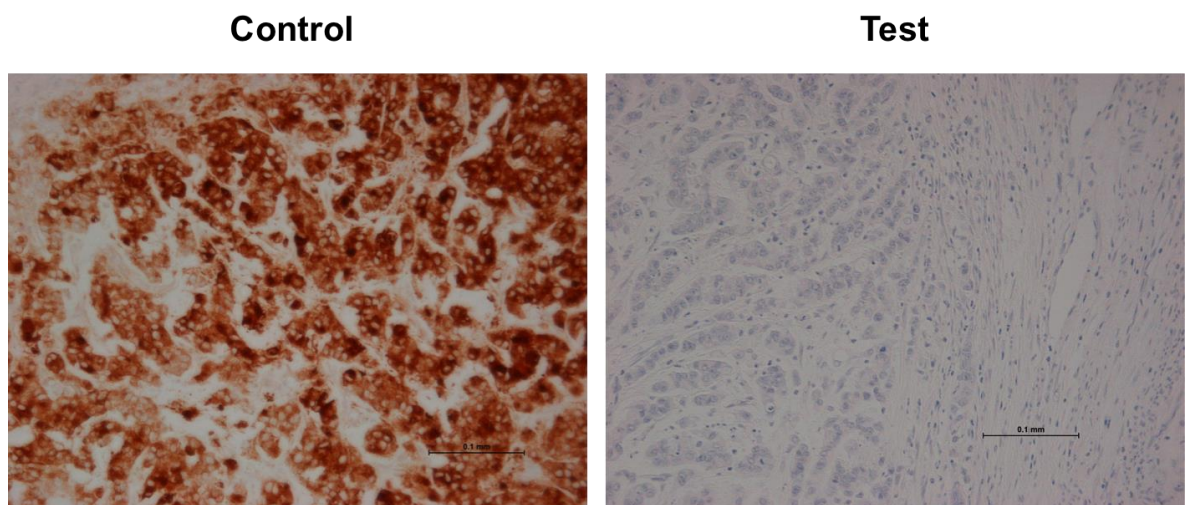


Figure 4.9. *Ex vivo* model immunohistochemical staining.

Anti-CEA antibodies injected into the main supplying artery of a freshly resected CEA-secreting tumour specimen prior to formalin fixation and paraffin embedding did not allow tumour specific immunohistochemical staining. Control: formalin fixed paraffin embedded tumour tissue was subjected to routine immunohistochemical analysis with further addition of anti-CEA antibodies. Test: Immunohistochemical analysis was undertaken using secondary antibodies only. Magnification 20X.

4.4 Discussion

Although my immunohistochemistry biomarker study (Chapter 3) showed a consistently high degree of CEA/TAG-72 expression and therefore antibody-antigen binding, it is difficult to draw conclusions about antigen availability; it may be that a colorectal tumour has high antigen expression but antibodies cannot access the binding sites in a live biological system, rather than in formalin-fixed, paraffin embedded tissue where the antigens are relatively accessible. Cultured cell lines provide a basic system in which to test whether the results seen in Chapter 3 can be reproduced in a less controlled and more realistic biological environment. Some of the recognised limitations of immunofluorescence - background noise, autofluorescence, non-specific binding and photobleaching (Swedlow et al., 2002, Wolf et al., 2007) - are all features that a systemically-delivered molecular imaging probe would need to overcome *in vivo*.

Initially I fixed the cells prior to antibody incubation, as is routinely done in immunofluorescence protocols, to confirm that specific antibody binding took place. This would be expected as the cells are in a similar state to those in the formalin-fixed paraffin-embedded tissue samples used in Chapter 3. Using the same conditions and antibody concentrations, I then incubated live cells with both antibodies. Although the results were non-quantitative, and therefore subjective in part, two apparent trends emerged: incubating colorectal cancer cells with anti-CEA antibodies produced a stronger and more diffuse staining pattern than anti-TAG-72; and incubating fixed cells with anti-TAG-72 antibodies produced no staining whereas live cells did. I would expect the first of these observations to be true, having already shown that CEA is more highly expressed than TAG-72 in a large cohort of colorectal tumours. The second observation was more surprising, but might be due to a

difference in the effect of fixation on live cells in media compared to human specimens where the cancer cells are within the tissue architecture comprising of the stroma and other cell types. Paraformaldehyde causes cross-linking, where covalent bonds form between proteins, and tends to damage cell membranes (Puchtler and Meloan, 1985); it may also reduce antigen availability or the cross-linking may reduce the number of available antigen-binding sites. From these experiments I was able to conclude that both CEA and TAG-72 are available for antibody binding in a live cell culture *in vitro* system, although potentially CEA appears to be more readily available for antibody binding than TAG-72.

Human fresh frozen tissue is frozen immediately after surgical resection, avoiding fixation. I aimed to assess whether I could reproduce the tumour-specific CEA and TAG-72 expression pattern seen in paraffin-embedded tumour samples and live cells by evaluating antibody binding in slices of fresh human tumour tissue and matched normal tissue. Although there appeared to be a high level of fluorescent staining in tumour samples, this was not tumour-specific; a similar pattern was observed in matched normal control tissue in all five patient samples. Non-specific background staining has been reported as being more common in frozen tissue than paraffin-embedded tissue (Elias, 1990). It is possible that the freezing process damages the cell membranes or the antigen binding sites and alters them in such a way as to enable non-specific binding. If this is the case, these findings do not threaten the eventual aim of my project. However, if these findings are due to a feature of human normal colonocytes that causes non-specific binding by these antibodies, this could prevent tumour-specific imaging of cancer cells *in vivo* by my proposed molecular probe. Given that both anti-CEA and anti-TAG-72 antibodies have been used for colorectal cancer targeting in human studies (Mayer et al., 2000, Povoski et al., 2012), I am optimistic that this is not the case.

Following the results of live cell incubation with anti-CEA and anti-TAG 72, together with the results from Chapter 3, I chose to focus on CEA as the biomarker target of choice as it had consistently out-performed TAG-72. I designed this experiment with the aim of showing whether systemically delivered antibodies could reach a tumour and bind in sufficient number to detect their presence using immunohistochemistry. First, I tested whether formalin fixation following primary antibody binding affected the detection of the primary with a secondary antibody; Figure 4.8 shows that this had no adverse effect on the immunofluorescent signal. I then injected an anti-CEA antibody solution into the ileocolic artery of three freshly resected right colonic cancer specimens and tested paraffin-embedded samples for CEA expression using immunohistochemistry. Unfortunately I was unable to demonstrate any tumour-specific binding. A likely reason for this is that pulsatile arterial blood flow is required to deliver molecules to the tumour cells; the act of injecting the solution will undoubtedly have forced antibodies along the artery to some extent but they may not have reached the small calibre arterioles supplying the tumour. Alternatively, the antibodies may have reached these vessels but require a hydrostatic pressure gradient to leave the vasculature and bind to cells; this is absent in my *ex vivo* system. Finally, there is an unavoidable delay between ligating the artery supplying blood and removing the tumour specimen prior to antibody injection, during which the blood within the vessel may have coagulated, obstructing antibody delivery. Despite these findings, there is evidence that systemically delivered antibodies are able to bind specifically and measurably to colorectal cancer cells. A5B7 anti-CEA antibodies bound to radioisotopes were used in radioimmunoguided surgery and radioimmunotherapy in UK clinical trials with success (Dawson et al., 1991, Meyer et al., 2009), suggesting that my model for systemic delivery may have been flawed. Were I to design the experiment again, I would have considered using an orthotopic mouse model of colorectal cancer where blood flow could be maintained to the tumour during and after antibody injection.

In conclusion, cell culture immunofluorescence shows that CEA and TAG-72 are available for antibody-antigen binding *in vitro*, and expression is similar to the patterns observed in Chapter 3, with CEA displaying the greatest binding. Although I was unable to demonstrate tumour-specific binding of anti-CEA antibodies using fresh frozen tissue samples or arterial delivery to fresh tumour specimens, there are a number of plausible reasons for this and I do not believe it prevents me from developing the project further.

Chapter Five

Indocyanine green conjugated anti-CEA antibodies allow fluorescent imaging of colorectal cancer cells

5 INDOCYANINE GREEN CONJUGATED ANTI-CEA ANTIBODIES ALLOW FLUORESCENT IMAGING OF COLORECTAL CANCER CELLS

5.1 Abstract

Background

Indocyanine green (ICG) is a near-infrared dye approved for use in humans in both the UK and USA. Its fluorescence is quenched when conjugated to an antibody, but reportedly this quenching is halted if the molecule is internalised by a cell, presumably by reversal of the conjugation and release of free dye. I aimed to assess whether ICG-conjugated anti-CEA antibodies would allow specific fluorescent labelling of colorectal cancer cells.

Methods

ICG-Sulfo-Osu was conjugated to A5B7 anti-CEA antibodies or control anti-digoxin antibodies. Conjugates were incubated with live LS174T, LoVo or HCT116 colorectal cancer cells and near-infrared fluorescence was imaged using confocal microscopy. Cellular fluorescence was quantified using ImageJ software.

Results

ICG-anti-CEA exhibited CEA-specific fluorescence in all three cell lines ($p < 0.01$) with fluorescence increasing until 24-36 hours, and reducing thereafter. The fold difference in fluorescence between ICG-anti-CEA and ICG-anti-digoxin treated cells at 36 hours was 5.2, 8.2 and 12.2 for LS174T, LoVo and HCT116 cells respectively.

When LS174T cells were incubated with only a 2 hour pulse of ICG-anti-CEA antibodies followed by subsequent incubation without the antibody, fluorescence accumulated with similar dynamics as before, peaking at 36 hours.

Conclusion

ICG conjugated to A5B7 anti-CEA antibodies allows CEA-specific imaging of colorectal cancer cells *in vitro*.

5.2 Introduction

A relatively simple fluorescent molecular probe for intra-operative cancer imaging is a fluorophore conjugated to a tumour-specific antibody and several groups have published small studies evaluating this, with moderate success (section 1.3.2). However, use of indocyanine green (ICG) as a simple antibody-fluorophore conjugate has demonstrated some promise. Importantly, ICG is a U.S. Food and Drug Standards Agency (FDA) and UK Medicines and Healthcare Products Regulatory Agency (MHRA) approved dye, so there is potential for rapid translation to clinical studies.

A slightly modified version of ICG (ICG-Sulfo-OSu, Figure 5.1) is quenched when bound to a protein such as an antibody (Ogawa et al., 2009) but has been shown to re-fluoresce when internalised by cells, a change that is thought to be due to cleavage of the bonds linking the dye to the antibody in lysosomes. Once internalised, the fluorescent signal from the ICG has been reported to remain detectable for up to 10 days (Nakajima et al., 2011), which in the clinical setting would allow a degree of flexibility in the timing an operation. As the fluorescence occurs in the cell cytoplasm rather than the cell membrane fluorescence seen in simple surface-bound fluorescent antibody systems, the signal density may be greater due to more target cell fluorophores.

I have already shown that CEA is the most suitable target for tumour-specific imaging of colorectal cancers (section 3.3), and that it is available to anti-CEA antibodies in live cells (section 4.3). Critically for my studies, Schmidt et al showed that anti-CEA antibodies are internalised by the colorectal cancer cell line LS174T (Schmidt et al., 2008), meaning that ICG-linked anti-CEA antibodies may well be induced to

fluoresce after internalisation. I therefore chose to evaluate the potential of ICG-anti-CEA antibodies for imaging of colorectal cancer cells *in vitro*.

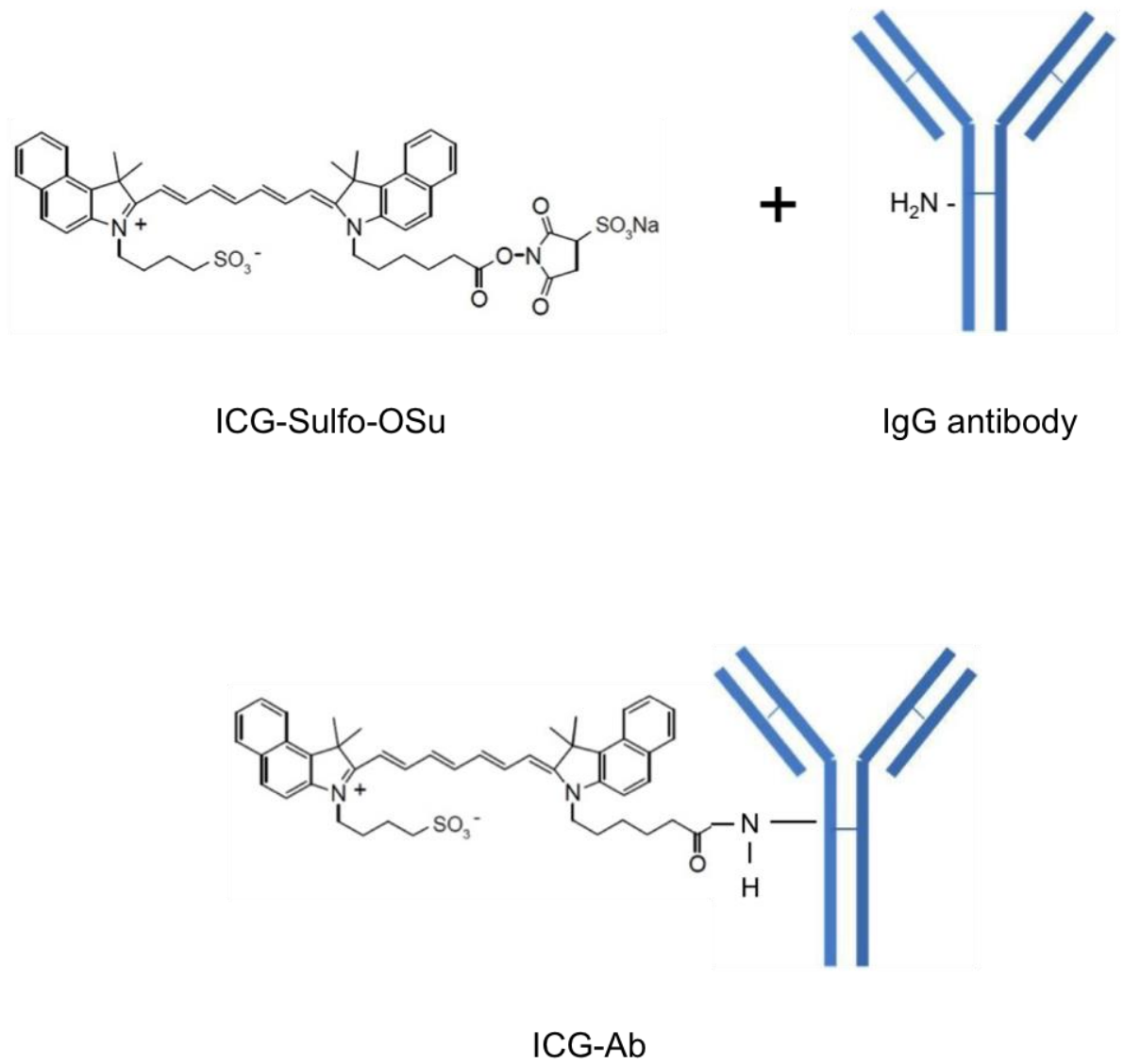


Figure 5.1. ICG-labelled IgG antibodies.

ICG-Sulfo-Osu is an amine-reactive derivative of ICG and can be conjugated to a free amine group on an IgG molecule.

5.3 Results

My first aim was to conjugate ICG to anti-CEA antibodies and to determine whether this conjugate would allow time-dependent and specific accumulation of fluorescence in colorectal cancer cells. I used three CEA-expressing colorectal cell lines for this work: LoVo cells have a high expression, LS174T cells a moderate/high expression and HCT116 cells a low expression (Ohannesian et al., 1995, Ashraf et al., 2009, da Paz et al., 2012, Fahlgren et al., 2003, Wang et al., 1999). I undertook a series of cell culture experiments to test whether cytoplasmic fluorescence was detectable (implying ICG-anti-CEA internalisation), whether this was CEA-specific and the relationship between signal intensity and time.

5.3.1 Qualitative assessment of ICG-anti-CEA fluorescence in LS174T cells

5.3.1.1 ICG-anti-CEA is CEA-specific and produces time-dependent cytoplasmic fluorescence

For my first experiment, I conjugated ICG-sulfo-OSu to A5B7 anti-CEA antibodies and incubated the conjugates with live LS174T cells. I used live cell confocal microscopy to assess cytoplasmic fluorescence at time points from 1 hour to 80 hours after the beginning of the incubation (Figure 5.2). As a negative control I saturated the surface of cells with unlabelled anti-CEA antibody to block the antigen binding sites, before washing away unbound antibody and treating as before.

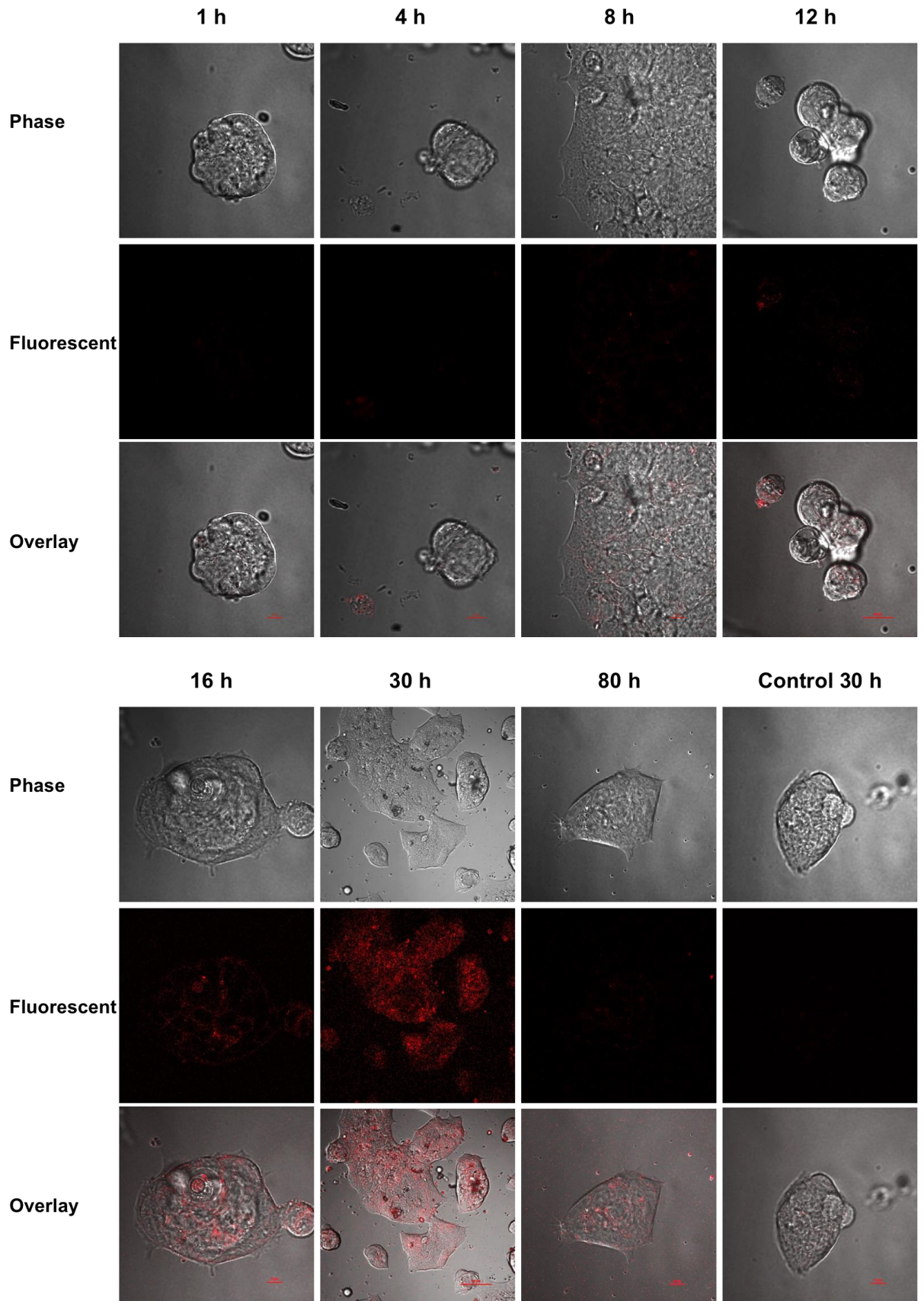


Figure 5.2. ICG-anti-CEA antibodies allow cytoplasmic fluorescence.

Anti-CEA antibodies conjugated to ICG-Sulfo-OSu are internalised by live LS184T colorectal cancer cells resulting in cytoplasmic fluorescence. Cells were incubated with 100 µg/ml ICG-anti-CEA and imaged at the times shown using confocal microscopy. Microscope settings were fixed throughout to allow the fluorescence at different time points to be directly comparable. As a control, cells were pre-incubated with 480 µg/ml of free anti-CEA antibody for one hour prior to incubation with the ICG-anti-CEA as above (image shown at 30 hours). (Magnification 100X, scale bar = 10 µm).

Cytoplasmic fluorescence was detectable from 4 hours and reached a peak at 30 hours. By 60 hours it had reduced considerably. Pre-incubation with unlabelled anti-CEA blocked accumulation of fluorescence at any time point tested. I concluded that ICG-anti-CEA binds specifically to CEA and is internalised leading to ICG fluorescence within the cytoplasm.

5.3.1.2 ICG-anti-CEA fluorescence is dose dependent

I also investigated whether the accumulation of fluorescence was dose-dependent. Three different dilutions of the conjugated antibody were used and fluorescence was assessed at 30 hours: 100 µg/ml, 10 µg/ml and 1 µg/ml. The highest of the three concentrations tested produced the greatest fluorescent signal (Figure 5.3).

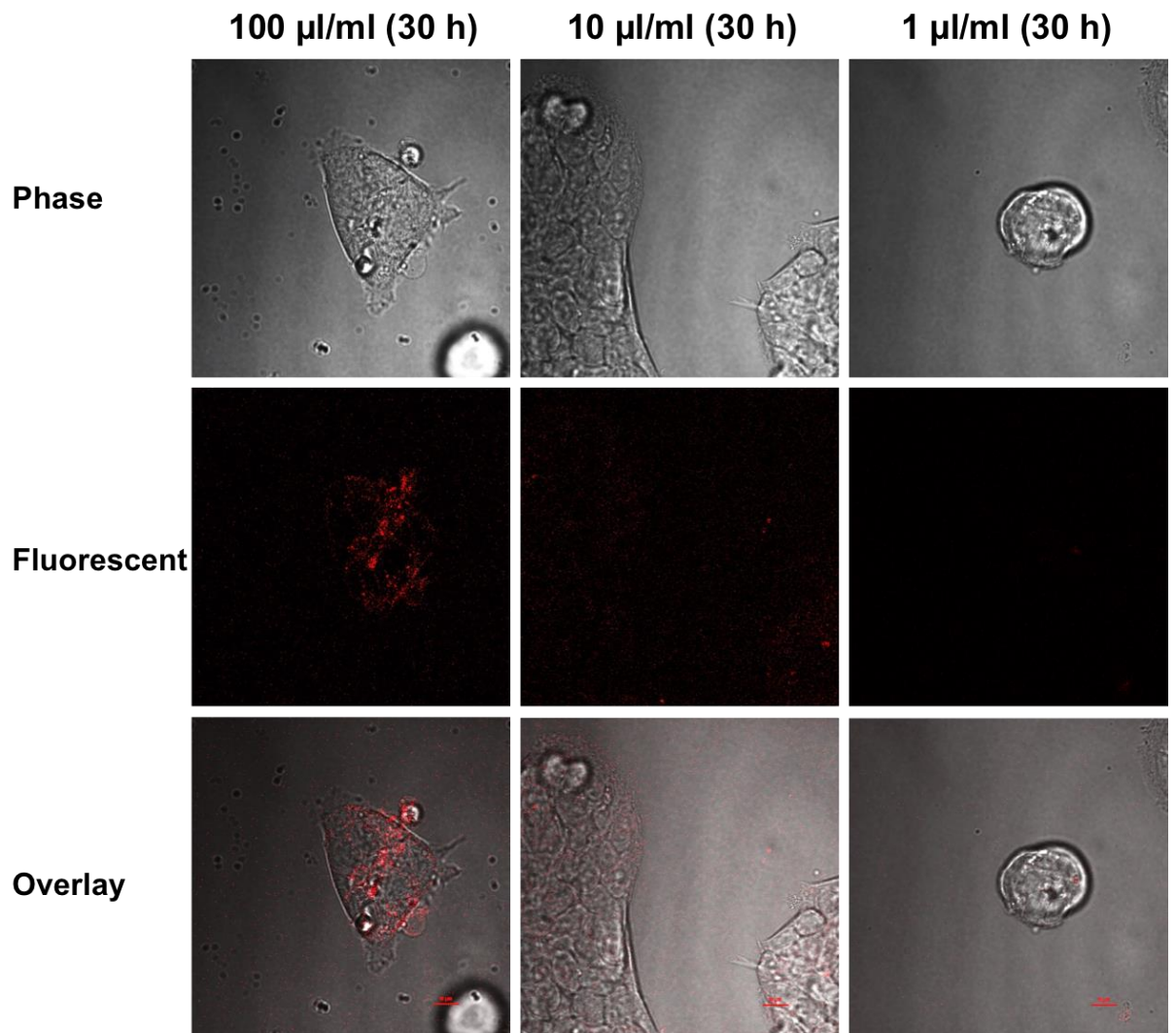


Figure 5.3. ICG-anti-CEA cytoplasmic fluorescence is dose-dependent.

Live LS174T cells in media were incubated with ICG-Ab suspended in PBS at concentrations of 1:10 (100 $\mu\text{g/ml}$), 1:100 (10 $\mu\text{g/ml}$) and 1:1000 (1 $\mu\text{g/ml}$). Confocal fluorescent microscope images were taken after 30 hours, representing peak fluorescence in earlier experiments. (Magnification 63X, scale bar = 10 μm).

5.3.2 Quantitative assessment of ICG-anti-CEA vs ICG-anti-digoxin fluorescence in colorectal cell lines

5.3.2.1 Anti-digoxin antibodies are a suitable control for immune-mediated colorectal cancer cell targeting experiments

I aimed to quantify the fluorescence produced by ICG-anti-CEA conjugates and compare this to that of ICG-labelled control antibodies. To do this I required a suitable control IgG antibody: I selected anti-digoxin, a mouse monoclonal IgG antibody for this purpose. Digoxin is a glycoside not expressed by colorectal cancer cells. To confirm that this negative control was suitable, I aimed to examine whether the cells I planned to use in my experiments not expressed digoxin. To do this I conjugated NHS-fluorescein, a commonly used label that retains its fluorescence when bound to proteins, to anti-CEA and anti-digoxin antibodies. To check that each antibody had a similar fluorescent signal, I used the molar extinction coefficient of NHS-fluorescein to calculate the number of fluorescein molecules conjugated to each IgG molecule: 9.23 for CEA and 10.03 for digoxin. I then incubated each with fixed cells from all three cell lines that I planned to use in my experiments. Whilst incubation with fluorescein-conjugated anti-CEA antibodies allowed fluorescent cell labelling, anti-digoxin antibodies produced no signal in any cell line (Figure 5.4). I concluded that anti-digoxin antibodies are an ideal control IgG antibody for immune-mediated colorectal cancer cell labelling experiments.

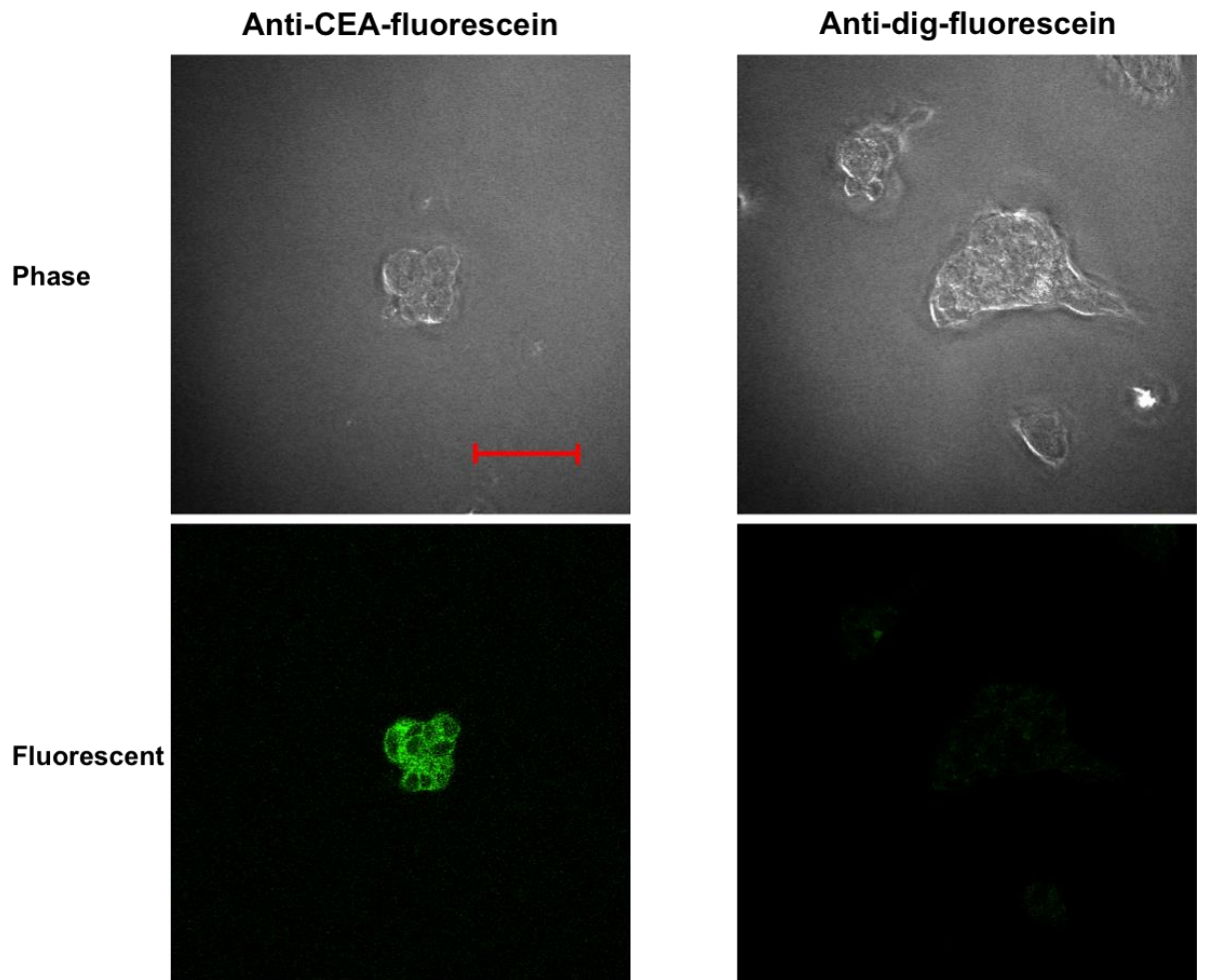


Figure 5.4. Anti-digoxin antibodies are a suitable negative control for colorectal cancer cell targeting experiments.

Fluorescein was conjugated to IgG antibodies and unbound fluorescein removed via filtration. Live LS174T cells were incubated with the conjugates for one hour, washed, mounted on slides and imaged with confocal microscopy. Scale bar = 50 μm . Magnification 63X.

5.3.2.2 ICG-anti-CEA allows tumour cell-specific imaging in a range of colorectal cancer cell lines.

For my next experiment, I aimed to use three CEA-expressing colorectal cancer cell lines: LS174T, LoVo and HCT116. Each cell line is known to express CEA at differing levels: LoVo cells have a high expression, LS174T cells a moderate/high expression and HCT116 cells a low expression (Ohannesian et al., 1995, Ashraf et al., 2009, da Paz et al., 2012, Fahlgren et al., 2003, Wang et al., 1999). I attempted to compare the expression levels of CEA for each cell line using Western Blot analysis. My results reflect the expression data in the literature, with LoVo cells exhibiting the strongest expression, LS174T moderate expression and HCT116 cells the lowest expression level (Figure 5.5).

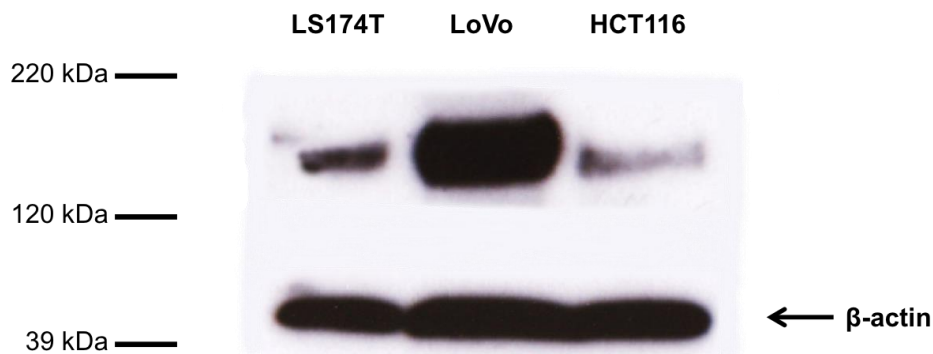


Figure 5.5. Expression of CEA by colorectal cancer cells was confirmed by Western Blot analysis.

LoVo cells showed the greatest CEA concentration, followed by LS174T cells and HCT116 cells.

I aimed to assess ICG-anti-CEA and ICG-anti-digoxin (control) binding in each cell line. I incubated the conjugates with live cells cultured in media in glass-

bottomed wells at a concentration of 100 µg/ml and I used confocal microscopy to capture comparable fluorescent images at 1, 6, 12, 24, 36 and 48 hours from the start of incubation. I quantified the fluorescence using ImageJ software by obtaining images of five cells of each cell line at each time point. I then calculated the mean fluorescent signal by measuring that of the cell and subtracting the mean background fluorescence. I plotted a graph for each cell line and compared the difference between test and control antibodies (Figure 5.6). Peak fluorescence occurred at 36 hours for LS174T and HCT116 cells and at 24 hours for LoVo cells. The fold difference in mean fluorescence between anti-CEA and control IgG conjugated ICG at 36 hours was 5.2, 8.2 and 12.2 for LS174T, LoVo and HCT117 respectively. The difference was significant at each time point from 6 to 36 hours for all cell lines. The fold increase in the fluorescent signal of the ICG anti-CEA antibodies at 1 hour and 36 hours was significant ($p < 0.05$) in LS174T cells (1.9) and HCT116 cells (3.5) but not in LoVo cells (1.5) (Figure 5.6). I concluded that continuous incubation with ICG-anti-CEA produced significantly greater cellular fluorescence than control ICG-anti-digoxin at each time point after 6 hours in all three cell lines.

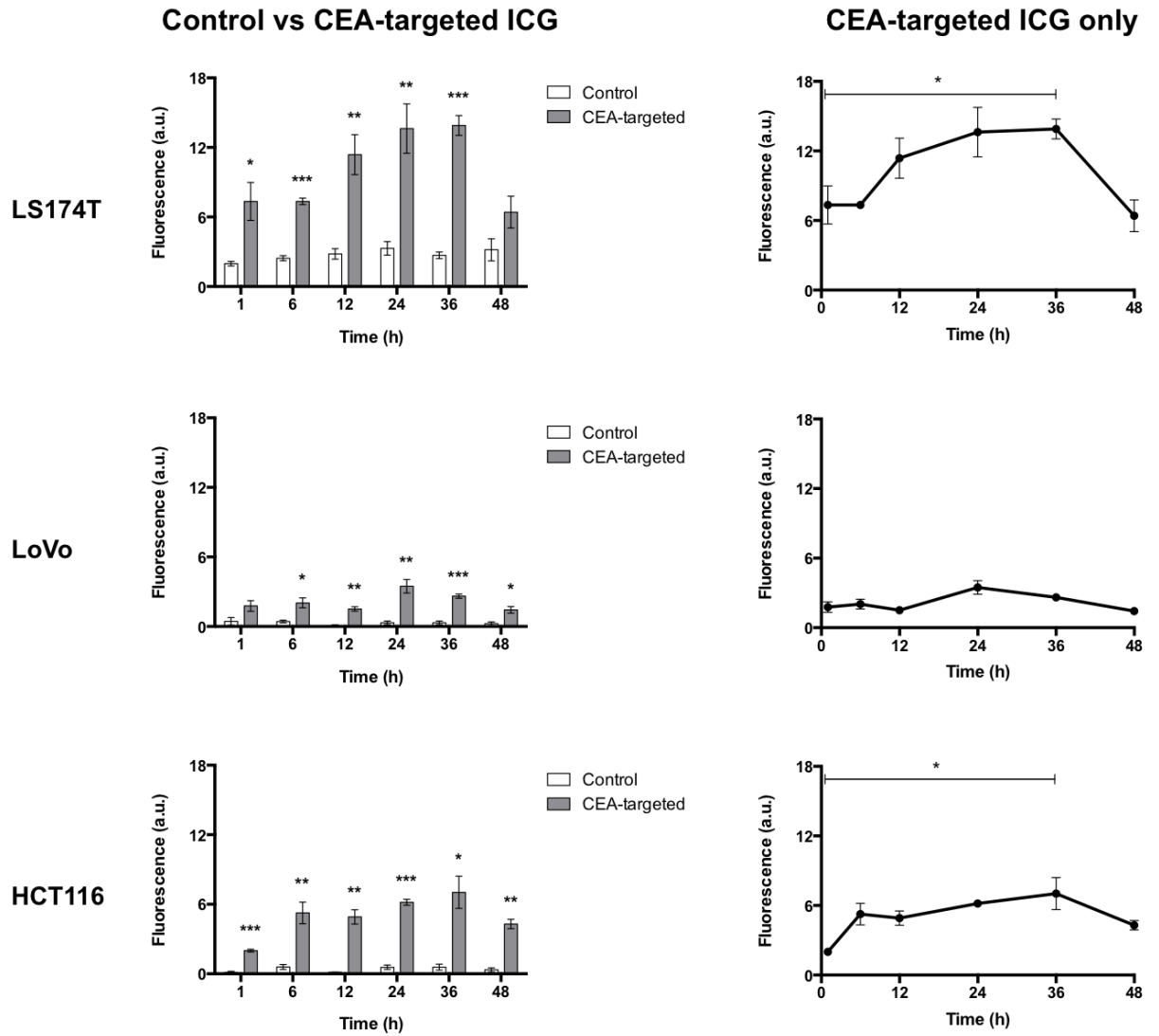


Figure 5.6. ICG-anti-CEA fluorescence in LS174T, LoVo and HCT116 cells.

*ICG-anti-CEA antibodies produce significantly more cellular fluorescence than control ICG-anti-digoxin antibodies when incubated with colorectal cancer cells, which peaks at 24-36 hours. Live LS174T, LoVo and HCT116 cells were seeded onto glass coverslips and continuously incubated with 100 μ g of ICG-antibody in 2 ml of media and images captured using confocal microscopy. Fluorescence was measured using ImageJ software. * p <0.05, ** p <0.01, *** p <0.001. Whiskers represent standard error of the mean. a.u. = arbitrary units.*

5.3.2.3 Cellular labelling is also achieved with only a short pulse of exposure to ICG-conjugated antibody

For my last experiment, I used LS174T cells only and conducted a pulse and chase experiment. This represents a more realistic model of systemically delivered fluorescent antibodies *in vivo*; they would reach a tumour via the arterial system but would be cleared from the bloodstream and excreted relatively quickly (Pedley et al., 1989). I incubated the cells with the same concentration of ICG-anti-CEA antibodies but removed unbound antibody after two hours, washed the cells, and replaced the media with media lacking anti-CEA antibodies. I then quantified the fluorescence at 6, 12, 24, 36, 48 and 72 hours after the limited incubation period (Figure 5.7). The fold change in mean fluorescence between the six hour and 36 hour (peak) time points was 4.1 ($p < 0.01$). The fluorescent signal had reduced significantly by 48 hours ($p < 0.01$). I concluded that, when exposed to ICG-anti-CEA for a limited time, LS174T cells demonstrate time-dependent fluorescence that peaks approximately 36 hours after incubation. This *in vitro* model suggests this mechanism of tumour-specific fluorescent imaging holds promise *in vivo*.

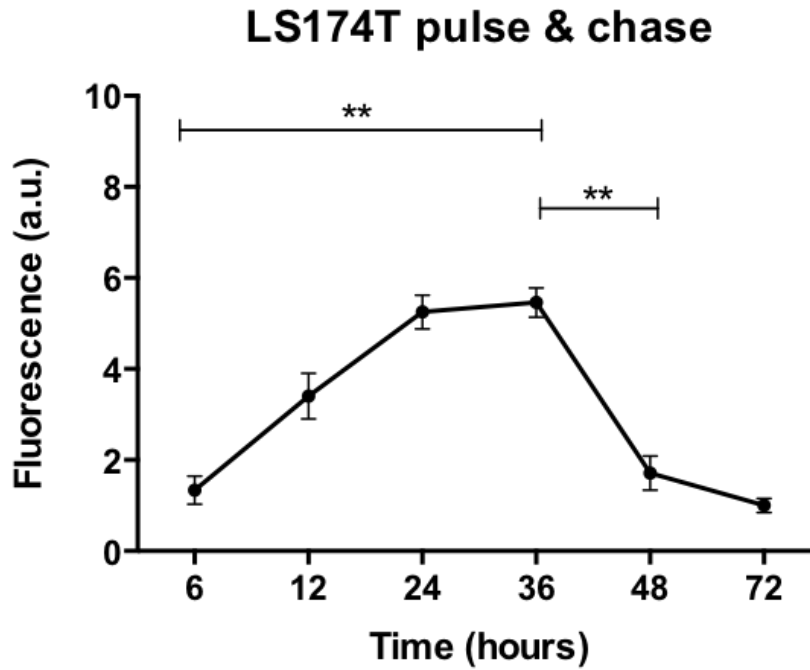


Figure 5.7. Pulse and chase incubation.

*LS174T cells demonstrate increasing cytoplasmic fluorescence with time when incubated with ICG-anti-CEA antibodies for two hours in a pulse and chase experiment. Incubation took place at 0-2 h. The peak signal occurred at 36 hours and then reduced significantly. Mean and standard error of the mean shown. ** $p < 0.01$. a.u. = arbitrary units.*

5.4 Discussion

I have shown that anti-CEA antibodies conjugated to ICG-Sulfo-OSu allow significant CEA-specific cellular fluorescence in a variety of colorectal cancer cell lines, which appears to be both time and dose dependent. Fluorescence at 36 hours was up to 12.2 fold greater than controls. When LS174T cells were exposed to ICG-anti-CEA for two hours only, cellular fluorescence peaked at 36 hours and then fell back to pre-six hour levels. These findings are the first of their kind in the field of colorectal cancer fluorescent imaging.

ICG fluorescence has been shown to quench when bound to IgG antibodies but re-fluoresce when internalised by the target cell (Ogawa et al., 2009), leading to target-cell specific cytoplasmic fluorescence. This is thought to be the result of cleavage of the covalent bond between the antibody and ICG molecule: the authors demonstrated re-fluorescence when sodium dodecyl sulphate (SDS) and 2-mercaptoethanol (2-MEA) were used to cleave the bonds. However, it has not been demonstrated conclusively that this occurs following internalisation by a cell membrane. It is conceivable that the antibody is degraded inside a lysosome, either leaving the ICG molecule intact, or the ICG degrading more slowly. For this technique to be used in colorectal cancer, bound anti-CEA antibodies must be internalised. This was thought not to be the case (Behr et al., 2000, Bryan et al., 2005) until Schmidt et al showed that all tested anti-CEA antibodies were internalised by LS174T cells with a half-life of 10-16 hours (Schmidt et al., 2008). I therefore tested the hypothesis that ICG-conjugated A5B7 anti-CEA antibodies allow tumour-specific imaging of colorectal cancer cells *in vitro*. Ogawa et al showed that when ICG-Sulfo-OSu was conjugated to IgG antibody the fluorescence intensity was low and unaffected by varying the antibody. Furthermore, when the antibody to ICG

molar ratio was increased, this 'quenching' effect also increased; at 1:1 conjugation the observed quenching capacity was 6-fold, whereas at 1:8 it was 58-fold. I similarly used a molar ratio of 1:8 when conjugating anti-CEA and antidigoxin antibodies with ICG-Sulfo-OSu. In all three cell lines that I tested, targeted ICG showed significantly greater fluorescence at each time point from six to 48 hours compared to non-targeted control ICG (Figure 5.6). The time dependent nature of the fluorescence and the fact that it appeared to be cytoplasmic, suggests the fluorophore had been internalised by the cells. Cellular fluorescence from control IgG-conjugated ICG was negligible in LoVo and HCT116 cells but greater in LS174T cells. LS174T cells are known to express mucin to a greater degree compared to other colorectal cancer cell lines (Bu et al., 2011), and this difference may explain the relatively high non-specific binding. Peak fluorescence occurred at 24 to 36 hours post incubation and decreased thereafter; in all three cell lines tested, the fluorescence at 48 hours was greater than at six hours. Ogawa et al used this technique to target HER2 expressing breast cancer cells and PASM-expressing prostate cancer cells, with peak fluorescence occurring at eight hours, but CEA is known to be internalised relatively slowly (Schmidt et al., 2008). The fold difference in mean fluorescence between anti-CEA and control IgG conjugated ICG at 36 hours was 5.2, 8.2 and 12.2 for LS174T, LoVo and HCT117 respectively ($p < 0.05$). Each cell line is known to express CEA but at differing concentrations: LoVo cells have a high expression, LS174T cells a moderate/high expression and HCT116 cells a low expression (Ohannesian et al., 1995, Ashraf et al., 2009, da Paz et al., 2012, Fahlgren et al., 2003, Wang et al., 1999). Interestingly, my results do not reflect these expression levels. This is the case even when non-specific control ICG binding is ignored (to take into account the higher levels in LS174T cells). This is likely to be due to differing steric hindrance, where the antigen density at the cell membrane can affect antibody binding (Kent et al., 1978), occurring between cell lines. Conjugating ICG-Sulfo-OSu to the IgG molecules may also alter the degree of steric hindrance by changing the surface

chemical properties of the heavy chains. Although my results demonstrate CEA-specific fluorescence, the relationship between cellular CEA concentration and fluorescence is not clear. The fate of the ICG dye is also unknown. In all three cell lines the cytoplasmic fluorescence reduced after 48 hours suggesting it was either excreted by the cell or degraded within it. This reduction in fluorescence also suggests that either the membrane-bound CEA molecules were recycled at a slower rate than they were bound and internalised, leading to a saturation effect, or the all the ICG-anti-CEA was processed by the cell membrane.

To model my proposed application for this imaging technique more closely, I conducted a pulse-chase experiment, where the cells were exposed to ICG-antibodies for a limited time only. This is analogous to pre-operative intravenous delivery, metabolism and excretion. A similar approach has been used in studies concerning imaging agents for PET (Kuang et al., 2014) and MRI (Mayer-Kuckuk et al., 2005) of hepatocellular cancer and bone precursor cells respectively, but not for intra-operative imaging. I chose LS174T cells for this experiment because although the fold difference between test and control antibodies at 36 hours was 5.2 compared to 12.2 for HCT116 cells, the overall mean peak fluorescent signal was greater (13.9 vs 4.35 vs 7.03 for LS174T, LoVo and HCT116 respectively) and showed the greatest difference in signal between one hour and peak (6.56 vs 2.57 vs 5.03). These data suggest that these cells would be most appropriate for future *in vivo* work. They have also been a popular choice by investigators using animal models of colorectal cancer, particularly in xenograft models (Ahlskog et al., 2009, Buchsbaum et al., 1988, Zou et al., 2009).

Following incubation, I removed the media, washed the cells to remove unbound antibodies, and replaced the media with an aliquot from an identical glass-bottomed well containing LS174T cells seeded at the same time and from the same cell

population. This was to ensure that the behaviour of the cells was not affected by removing the antibodies; the addition of fresh media could potentially increase internalisation and distort the results, precluding comparisons with the previous experiment where the antibodies were not removed. This is known as 'conditioned media', and contains metabolites, growth factors and extracellular matrix proteins secreted by the cancer cells (Michielsen et al., 2012). The fluorescent signal measurements followed the same pattern as the previous experiment, with a significant increase in fluorescence up to peak at 36 hours and then a significant decrease between 36 and 48 hours. Interestingly, the fold change between six and 36 hours was greater in this pulse and chase experiment than in the previous continuous incubation experiment (4.1 vs 1.9).

The potential of this imaging system for colorectal cancer is greatly enhanced by the nature of the reagents; ICG is approved for human use by both the FDA and MHRA, and A5B7 anti-CEA antibody has been used in a number clinical trials. If these *in vitro* results can be replicated *in vivo*, translation to the operating theatre will be rapid. My results suggest that peak fluorescence lasts for several hours, making it ideal for surgical resection.

In conclusion, A5B7 anti-CEA antibodies conjugated to ICG allow CEA-specific fluorescence *in vitro* in a variety of colorectal cancer cell lines. These data suggest clear potential for tumour-specific imaging in a range of tumour types. This warrants further investigation.

Chapter Six

CEA-targeted, dye-doped silica nanoparticles allow specific *in vivo* fluorescent imaging of colorectal cancer models

Some of the text and figures in this chapter have been published in the manuscript “CEA-targeted nanoparticles allow specific *in vivo* fluorescent imaging of colorectal cancer models” (Nanomedicine 2015; 10(8):1223-31) and reproduced here with permission.

6 CEA-TARGETED, DYE-DOPED SILICA NANOPARTICLES ALLOW SPECIFIC *IN VIVO* FLUORESCENT IMAGING OF COLORECTAL CANCER MODELS

6.1 Abstract

Background

Fluorescent laparoscopic imaging of primary colorectal tumours and lymph node metastases would improve localisation of early tumours and allow intra-operative staging, potentially facilitating intra-operative stratification of the extent of surgical resections thereby improving patient outcomes. I aimed to develop and test fluorescent nanoparticles capable of allowing localisation of tumours *in vivo*.

Methods

Dye-doped silica nanoparticles loaded with NIR664 dye were synthesised using a water-in-oil microemulsion technique. Anti-CEA IgGs or control IgGs were conjugated to nanoparticles using four different chemistries: sulfosuccinimidyl-4-(*N*-maleimidomethyl)cyclohexane-1-carboxylate (sulfo-SMCC); polyethylene glycol (PEG); 1-Ethyl-3-[3-dimethylaminopropyl]carbodiimide hydrochloride (EDC); or polyamidoamine dendrimers (PAMAM). Binding of CEA-targeted or control nanoparticles to colorectal cancer cells (LS174T, LOVO and HCT116) was quantified *in vitro* using confocal microscopy and ImageJ. A murine xenograft model and IVIS imaging were used to assess PAMAM-linked nanoparticles *in vivo*.

Results

CEA-targeted, PAMAM dendrimer-conjugated, nanoparticles allowed strong tumour-specific targeting, demonstrating 12.3-, 8.0- and 3.2-fold greater fluorescence than control IgG-targeted nanoparticles when incubated with LS174T, LoVo and HCT116 cells respectively ($p < 0.002$). EDC-linked nanoparticles showed 1.7 fold greater binding of CEA-targeted nanoparticles in LoVo cells only ($p = 0.016$). Use of sulfo-SMCC or PEG did not allow significant tumour-specific labelling. In LS174T xenografts, CEA-targeted nanoparticles demonstrated clear tumour-specific fluorescence from 6 to 72h after injection, as compared to only background fluorescence for control IgG-targeted nanoparticles at all time points (median radiant efficiency at 48h, $\eta_e = 16 \times 10^7$ v 0, $p < 0.0001$).

Conclusion

These findings are the first to demonstrate live tumour-specific fluorescent colorectal cancer imaging using an antibody-targeted nanoparticle *in vivo*. Dye-doped silica nanoparticles conjugated to anti-CEA antibodies via PAMAM dendrimers have potential to allow intra-operative fluorescent visualisation of tumour cells.

6.2 Introduction

In the previous chapter I exploited a unique feature of the near-infrared dye indocyanine green to improve the signal-to-background ratio of fluorescent anti-CEA antibodies. In an effort to further improve the required criteria for an *in vivo* molecular imaging probe (section 1.3.3), I aimed to develop a non-toxic, fluorescent nanoparticle capable of concentrating the fluorescent signal to allow sensitive and specific detection of colorectal cancer cells. Many types of nanoparticles have been described. The particular challenge in this application was to construct a particle that could simultaneously fluoresce and target tumour cells. Dye-doped silica nanoparticles (Santra et al., 2001) potentially meet the required criteria for *in vivo* imaging - a near-infrared fluorophore can be incorporated into their centre, there are multiple surface chemistry options for antibody conjugation and they are potentially small enough for *in vivo* systemic delivery.

6.2.1 Aims

The aims for this part of my project were to:

- i. Manufacture and characterise a dye-doped silica nanoparticle
- ii. Conjugate anti-CEA and control IgG antibodies to the surface of the particle using a variety of chemical linking strategies;
- iii. Assess the ability of the nanoparticles to bind to tumour cells *in vitro* and quantify the specificity and fluorescent signal magnitude for each linking strategy;
- iv. Test the best performing nanoparticle in a murine model of colorectal cancer *in vivo*.

I used two fluorescent dyes in this work to dope the silica particles: RuBpy and NIR664. RuBpy (Tris(bipyridine)ruthenium(II) chloride) has excitation and emission wavelengths of 452 nm and 640 nm respectively (Santra et al., 2001), is water-soluble and benefits from a long excited state lifetime (Rivarola et al., 2006), meaning the fluorescent signal persists for longer than other fluorophores. It has been used in the vast majority of published studies involving targeted dye-doped silica nanoparticles (Chen et al., 2012, He et al., 2013, He et al., 2008, He et al., 2012, Heitsch et al., 2008, Santra et al., 2001, Tan et al., 2010a, Tao et al., 2013, Wang et al., 2005, Wu et al., 2008, Hun and Zhang, 2007). NIR664 is an iodoacetamide dye with excitation and emission wavelengths of 672 nm and 694 nm respectively. It is stable across a wide range of pH values, has a quantum efficiency (ratio of light emitted to light absorbed) of 23%, a molar absorptivity (how well it absorbs light) of $187000 \text{ L mol}^{-1} \text{ cm}^{-1}$ and is relatively cheap (Mank and Yeung, 1995, Nooney et al., 2009). This compares to a quantum efficiency of 14% and molar absorptivity of $14600 \text{ L mol}^{-1} \text{ cm}^{-1}$ for RupBy (Kalyanasundaram, 1982, Reithmeier et al., 2012).

I aimed to target dye-doped silica nanoparticles to carcinoembryonic antigen (CEA) using the anti-CEA antibody from previous chapters. I also aimed to use robust controls, a feature absent in the majority of published studies, comprising of identical nanoparticles conjugated to IgG antibodies specific to an antigen not found on the surface of colorectal cancer cells. I aimed to assess four chemical linking strategies:

- i. sulfo-succinimidyl-4-(*N*-maleimidomethyl)cyclohexane-1-carboxylate (SMCC);
- ii. polyethylene glycol (PEG);
- iii. 1-Ethyl-3-[3-dimethylaminopropyl]carbodiimide hydrochloride (EDC);
- iv. polyamidoamine dendrimers (PAMAM).

SMCC is a heterobifunctional linker that can be used to conjugate a molecule with a free amine group to a molecule with a free sulfhydryl group. At the time of this work, SMCC was a very novel linker for conjugating nanoparticles to reduced antibodies for cell targeting. Only one published manuscript had described linking a reduced antibody to a fluorescent probe but in this case a quantum dot was used rather than a larger nanoparticle (Tiwari et al., 2009). The theoretical advantage of using reduced antibodies is that their orientation at the surface of the nanoparticle is controlled, as the location of the sulfhydryl group is known. In contrast, when amine groups on IgG antibodies are used, the location of the bond, and therefore the orientation of the antibody, are unknown and unpredictable (Xiao et al., 2014).

PEG is widely used in medicine, principally as a laxative (Dipalma et al., 1984). Incorporation of PEG, a hydrophilic co-polymer, to nanoparticle surfaces has been shown to effectively increase the circulating half-life by preventing opsonisation by the reticuloendothelial system (RES) (Owens Iii and Peppas, 2006). PEG molecules consist of repeating units and are therefore available in a range of lengths. I was therefore keen to test this as a potential linker for my application. I selected a short, bifunctional PEG linker capable of conjugating amine groups to sulfhydryl groups on reduced antibodies.

EDC is known as a zero-length crosslinker due to the 'leaving group' that is formed when it is used to conjugate carboxyl and amine groups. It has been used to conjugate whole IgG antibodies to silica nanoparticles (Zhao et al., 2004b, Wu et al., 2008) for tumour targeting *in vitro* but no *in vivo* studies have been published.

The use of dendrimers to conjugate antibodies to nanoparticles is novel, having been described by just one group (Gubala et al., 2010). Dendrimers are branched chains that can be synthesised to have a specific number of branches or 'generations'.

Whilst their structure inevitably increases the overall size of a nanoparticle, the surface density of available binding sites is increased and the inherent charge of the nanoparticle-antibody complex is potentially altered, which may increase bioreactivity.

6.3 Results

6.3.1 Dye-doped silica nanoparticles: manufacture and characterisation

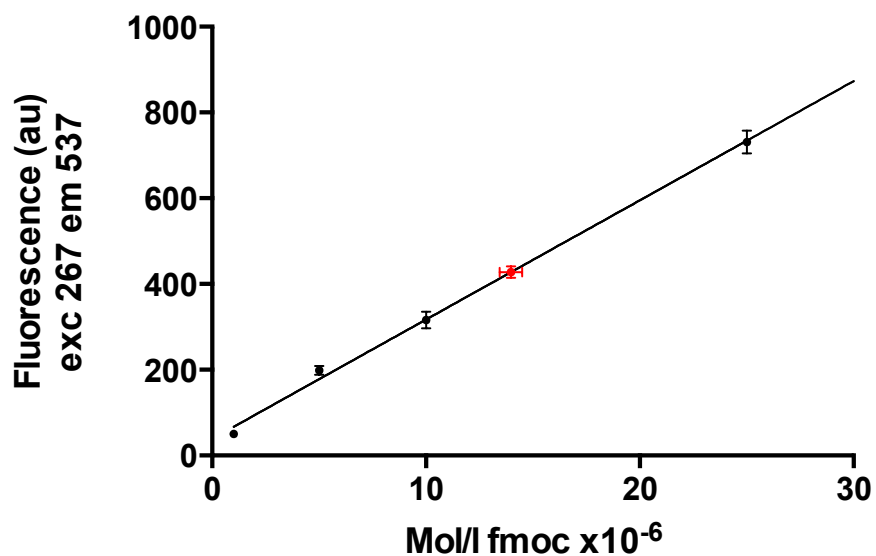
I manufactured basic dye-doped silica nanoparticles using a water-in-oil microemulsion technique. This produced particles with a fluorescent core and a silica shell surrounding it. I initially used the fluorescent dye Tris(2,2'-bipyridyl) dichlororuthenium (II) hexahydrate (RuBpy) as this had shown promise in the few studies that had successfully synthesised this type of nanoparticle. In later experiments I used NIR664, an iodo-acetamide dye, which has a longer wavelength, potentially reducing autofluorescence. I aimed to characterise these particles by measuring their size, the density of amine groups available for binding and their fluorescence spectra.

6.3.1.1 Physical characterisation of 'bare' nanoparticles

6.3.1.1.1 *Amine group quantification*

After manufacturing the basic dye-doped silica nanoparticle, I aminated the surface using 3-aminopropyltriethoxysilane (APTES). The amine groups allow conjugation of biofunctional linkers and their availability for binding is therefore essential for my proposed application. To determine the number of available groups I used fluorenylmethyloxycarbonyl chloride (Fmoc-Cl) in a method adapted from previously published work (Chen and Zhang, 2011). Following nanoparticle amination, I conjugated fluorescent Fmoc-Cl molecules to the free amine groups on the outer shell and then cleaved them using piperidine. I calculated how many amino groups were bound by measuring the absorbance of the solution containing the cleaved Fmoc-Cl molecules with reference to a standard curve for Fmoc-Cl absorbance

(Figure 6.1). My result of 3.41×10^{-7} mol/m is greater than the only other published study to quantify available amino groups in dye-doped silica nanoparticles (1.1×10^{-8} mol/mg), albeit using a slightly different method (Liu et al., 2007).



Sample	Fluorescence	Conc (mM)	Dilution	Sample mass (mg)	Mol Fmoc/mg	X Avagadro's constant (amine groups/mg)
1	453.0	14.9	1:30	3.3	1.51×10^{-7}	9.09×10^{15}
2	425.3	13.9	1:10	4	3.48×10^{-7}	20.96×10^{15}
3	404.5	13.1	1:10	2.5	5.24×10^{-7}	31.56×10^{15}
Mean					3.41×10^{-7}	2.054×10^{16}

Figure 6.1. The availability of amine groups on the surface of the bare nanoparticle quantified using Fmoc-Cl.

Dye-doped silica nanoparticles were manufactured using a water-in-oil microemulsion technique and aminated using APTES. Fmoc-Cl molecules were bound to the free amine groups on the particle surface before being cleaved and measured. A standard curve was plotted for Fmoc and readings taken for samples from three separate batches of bare nanoparticles.

6.3.1.1.2 Fluorescence analysis

To assess the fluorescence of the basic nanoparticles I used a fluorometer and recorded excitation and emission spectra at various concentrations. The peak excitation and emission wavelengths for particles loaded with RuBpy dye were 458 and 607 nm respectively (Figure 6.2) and 665 and 686 nm for NIR664-loaded particles. The fluorescent signal produced by particles suspended in phosphate buffered saline increased with increasing concentration up to approximately 1 mg/ml, after which the signal reduced (Figure 6.3). I used these data to plan later *in vitro* and *in vivo* experimental protocols.

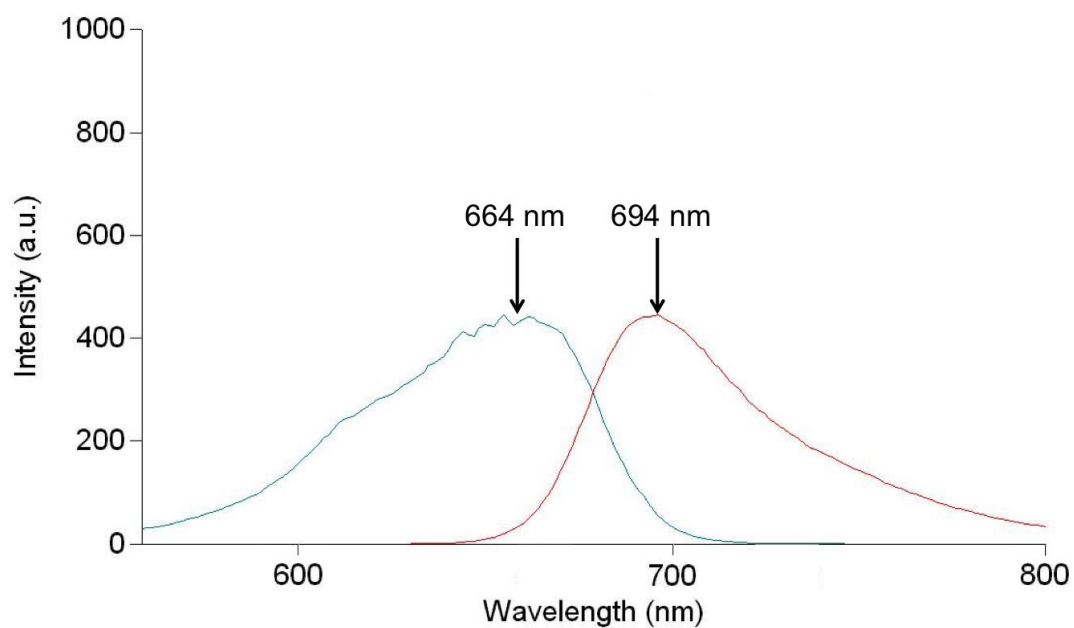
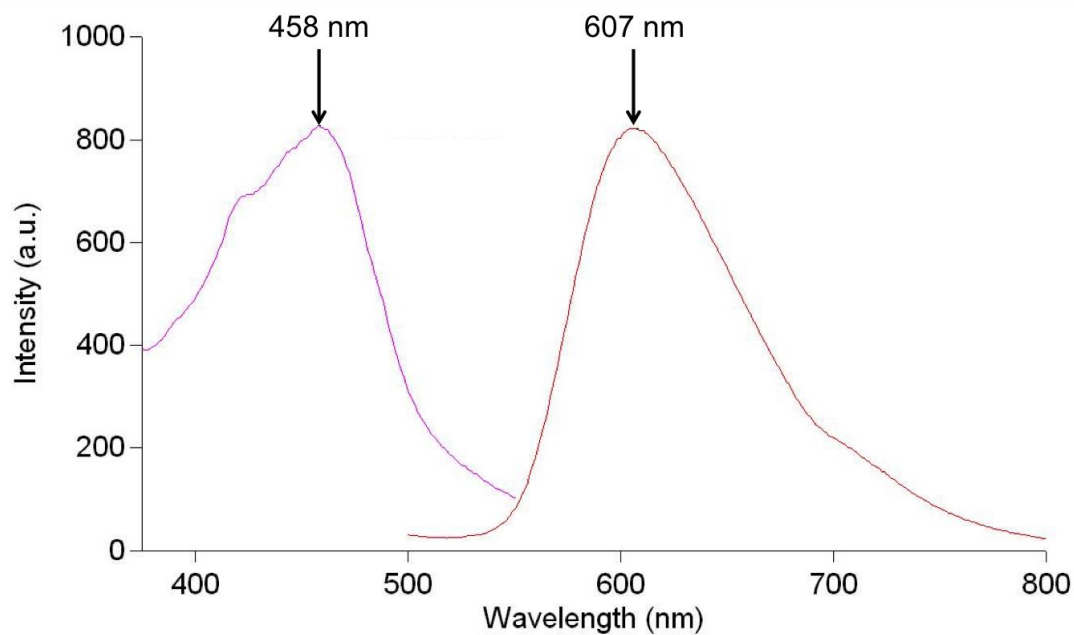


Figure 6.2. Fluorescence spectra of RupBy-doped and NIR664-doped silica nanoparticles.

Dye-doped silica nanoparticles were manufactured using a water-in-oil microemulsion technique and suspended in PBS. Peak absorption and emission wavelengths labelled for RupBy- and NIR664-doped particles. Relative intensities are not comparable due to setup differences.

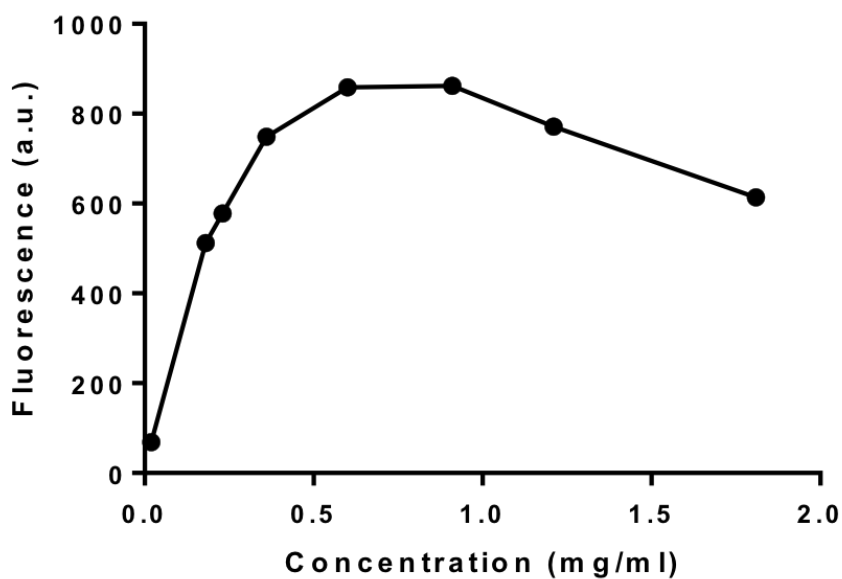


Figure 6.3. The relationship between RupBy-doped nanoparticle concentration and emission fluorescence.

Dye-doped silica nanoparticles were manufactured using a water-in-oil microemulsion technique and suspended in PBS at various concentrations. The fluorescent signal fell at concentrations in excess of 1 mg/ml.

6.3.1.1.3 Particle size

To measure particle size I used field emission gun scanning electron microscopy (FEG-SEM). I recorded images of a sample of the nanoparticles, randomly selected 50 and measured their diameter (Figure 6.4). The mean diameter was 56.57 nm (standard error of the mean = 0.99; standard deviation = 6.99).

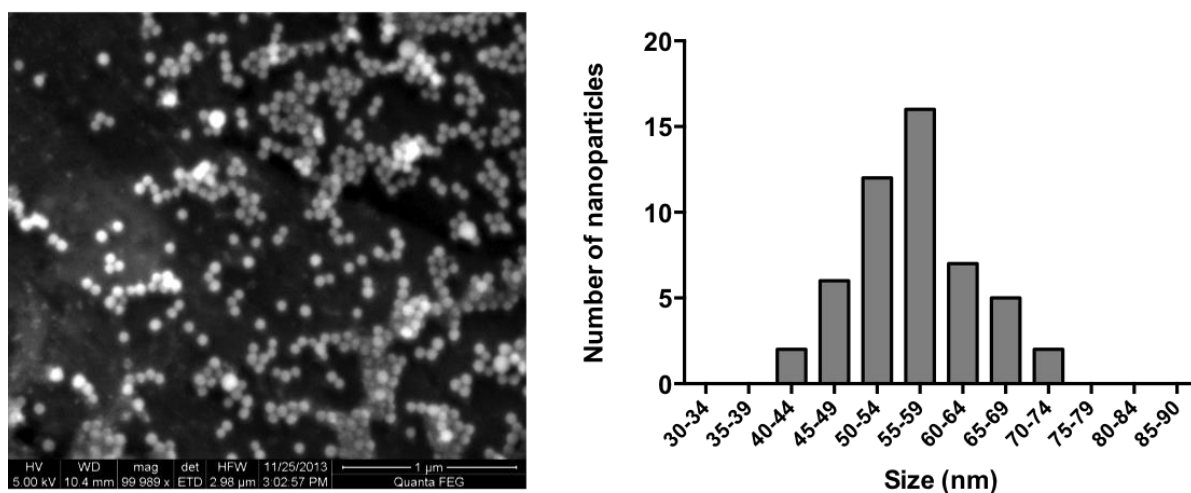


Figure 6.4. Size distribution of dye-doped silica nanoparticles.

NIR664-doped silica nanoparticles were manufactured using a water-in-oil microemulsion technique. The particles were imaged using FEG-SEM (left) and the diameter of 50 randomly-selected particles was measured using Photoshop. The size distribution is shown as a histogram (right). The mean diameter was 57 nm.

6.3.2 Chemical linkage strategies for antibody conjugation

I used a variety of chemical linkage strategies to attach antibodies to NPs. In each case, the chemistry is different and the assays used to assess successful conjugation are different. For example, SMCC required reduced “half” antibodies for conjugation as the chemistry is based on linking free amine groups to sulfhydryl groups, while EDC required whole antibodies conjugated via amine to carboxyl groups (Figure 6.5). Assays to assess conjugation include assessment of loss of sulfhydryl groups after conjugation, or measurement of the physical increase in size of the particles after conjugation. The conjugation strategies and their characterisation are described below in turn.

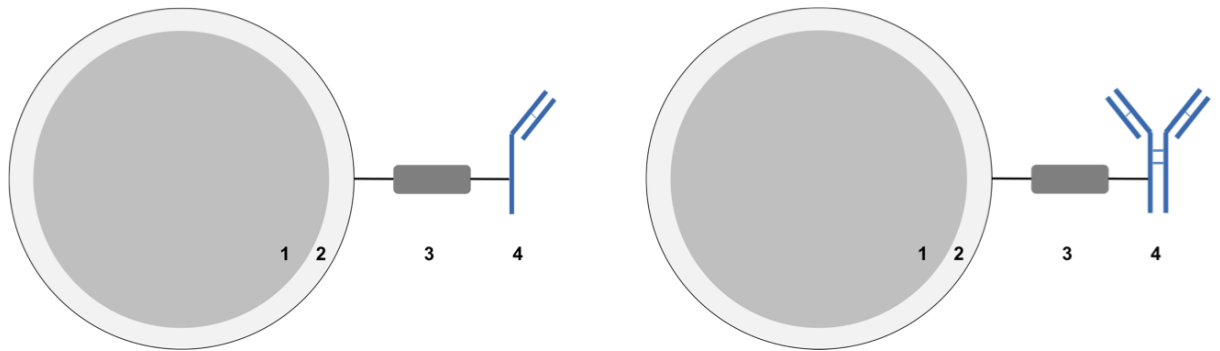


Figure 6.5. Nanoparticle-antibody conjugation.

Left: SMCC and bifunctional PEG were used to conjugate reduced antibodies to the nanoparticle. Right: EDC and PAMAM dendrimers were used to link whole IgG antibodies to the aminated surface of the dye-doped silica nanoparticle. 1 = fluorescent core; 2 = silica shell; 3 = biofunctional cross linker; 4 = antibody.

6.3.2.1 SMCC linkage to nanoparticles

I aimed to reduce anti-CEA antibodies and then link them via a free sulfhydryl group (Figure 6.6 and Figure 6.7) to the aminated nanoparticle surface using SMCC. I used 2-MEA to reduce the IgG antibodies, removed unreacted 2-MEA using spin centrifuge filters and examined the resultant protein species using high-pressure liquid chromatography (HPLC). I found that the 2-MEA had successfully reduced the antibody, producing two peaks, corresponding to non-reduced IgG molecules (the first peak, due to the larger molecular mass) and reduced IgG molecules.

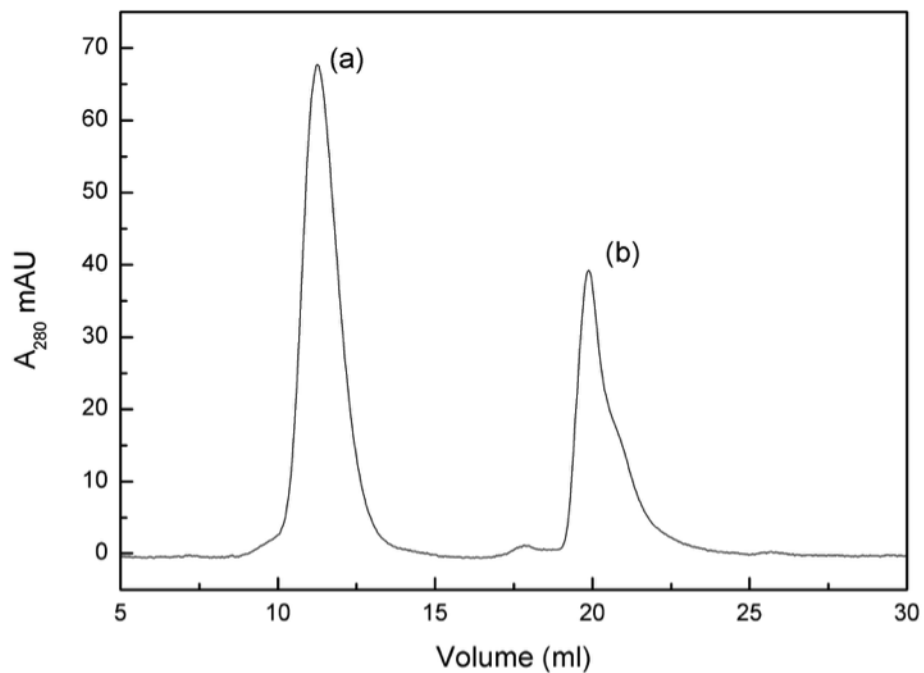
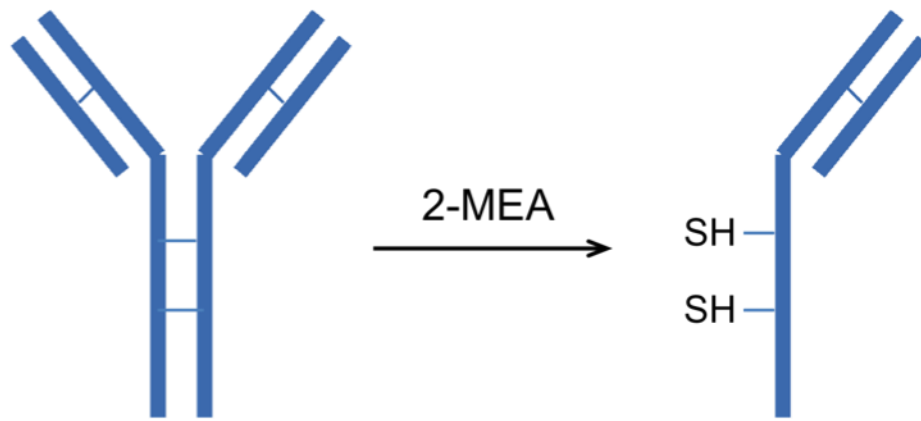


Figure 6.6. IgG antibody reduction.

IgG antibodies were successfully reduced using 2-MEA. The antibodies were incubated with 2-MEA at 37° Celsius for one hour to selectively reduce the disulphide bonds between heavy chains, providing free sulfhydryl groups for conjugation to SMCC. The solution was then subjected to HPLC. Peak (a) corresponds to whole, non-reduced IgG molecules (~150 kDa) and peak (b) to reduced IgG molecules (~75 kDa).

I incubated the aminated nanoparticles with SMCC and then washed them with ethanol to remove any unreacted biolinker. I then added the reduced antibody solution (containing both whole and reduced IgG molecules), incubated the mixture to allow conjugation and washed the particles with ethanol to remove unbound antibody. To confirm that the reduced antibodies had bound to the nanoparticles, I used Ellman's reagent to measure available sulfhydryl groups (Sedlak and Lindsay, 1968). Immediately after reduction with 2-MEA, 1.2 mg of A5B7 anti-CEA IgG antibody yielded 1.34×10^{-4} moles of sulfhydryl groups. Following incubation with the SMCC-conjugated nanoparticles, the reaction supernatant contained 4.21×10^{-7} moles of sulfhydryl groups. I concluded that the reduced antibodies appeared to have bound to the surface of the nanoparticles and, given that the residual sulfhydryl groups remained available despite prolonged incubation, that the available binding sites were likely to be saturated.

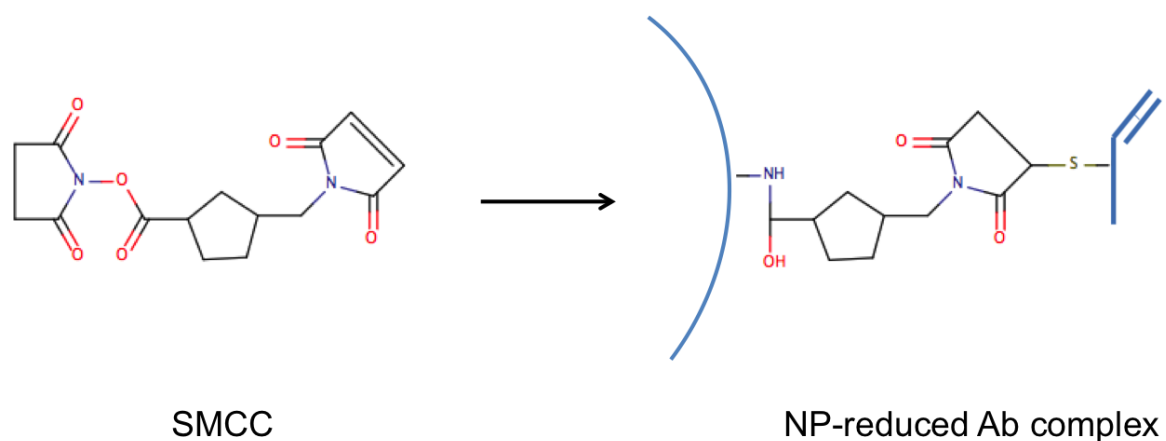


Figure 6.7. SMCC conjugation.

SMCC reacts with the aminated nanoparticle surface to form a stable amide bond with a maleimide group that can then be conjugated to the free sulfhydryl group on a reduced IgG fragment.

6.3.2.2 Bifunctional PEG linkage to nanoparticles

I used bifunctional PEG crosslinkers to conjugate reduced antibodies in a similar fashion, linking free amine groups on the surface of the nanoparticles to the free sulfhydryl groups on reduced antibodies (Figure 6.8). Ellman's reagent was again used to quantify available sulfhydryl groups before and after antibody and nanoparticles incubation and confirmed a reduction (1.97×10^{-4} moles versus 1.33×10^{-6} moles). I concluded that the reduced antibodies appeared to have bound to the surface of the nanoparticles and, given that the residual sulfhydryl groups remained available despite prolonged incubation, that the available binding sites were likely to be saturated.

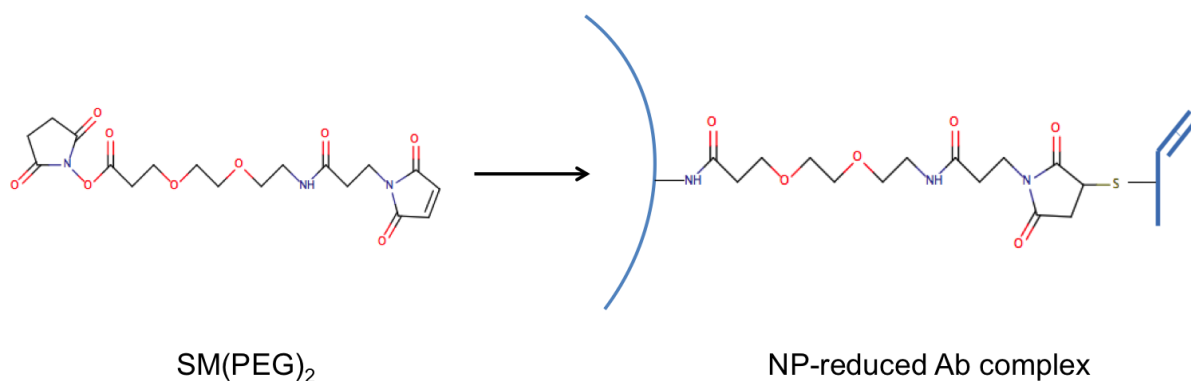


Figure 6.8. Bifunctional PEG conjugation.

Bifunctional PEG crosslinker was used to conjugate reduced IgG antibodies to aminated nanoparticles.

6.3.2.3 EDC linkage to nanoparticles

I carboxylated the nanoparticle surface and then used EDC (Figure 6.9) to link whole IgG antibodies. To confirm that the antibodies had bound and that no unbound antibodies remained in the nanoparticle suspension following wash steps, I measured the absorbance of the reaction mixture and each discarded supernatant following centrifugation. In each case, the absorbance at 280 nm, corresponding to protein, reduced following incubation and washing (Figure 6.10). From this assay I was able to confirm that: i) the antibodies were immobilised onto the nanoparticles; ii) the available binding sites were saturated; and iii) repeated washing via centrifugation successfully removed unbound antibodies.

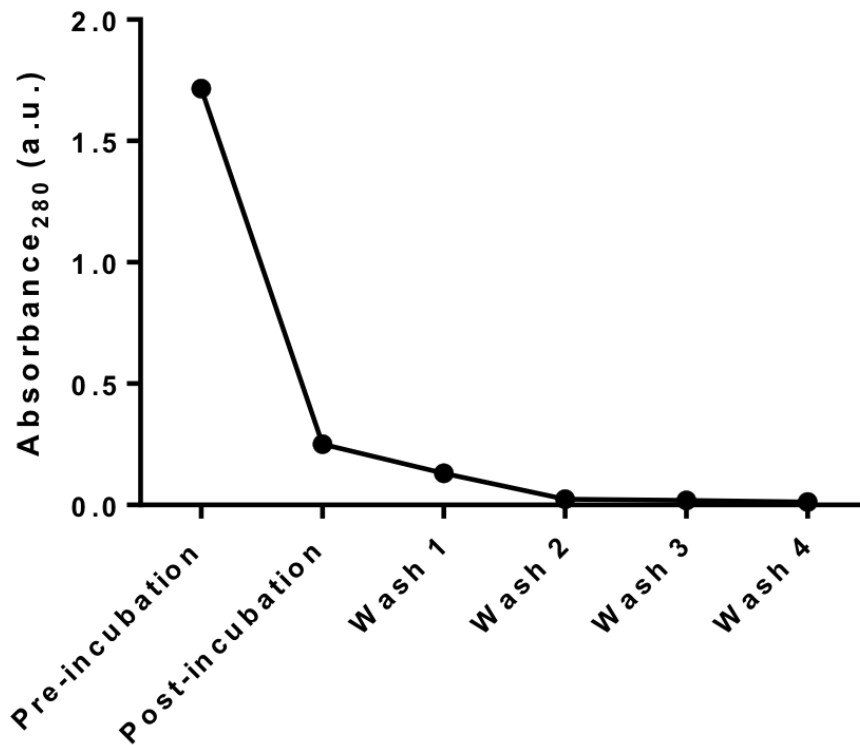


Figure 6.10. Absorbance assay to determine effectiveness of particle washing.

Absorbance at 280 nm of the reaction mixture (in this case sulfo-NHS, EDC and anti-CEA antibodies) prior to the nanoparticles being added (pre-incubation), following incubation but with the nanoparticles removed, and of the supernatant following washes in ethanol.

6.3.2.4 PAMAM linkage to nanoparticles

I also used PAMAM dendrimers to link whole IgG antibodies to the nanoparticle surface (Figure 6.11). I used EDC as a zero crosslinker between the dendrimer and nanoparticle and between the dendrimer and whole antibodies. I repeated the absorbance assay used to confirm antibody immobilisation on the nanoparticles. Of

the four linking strategies tested, PAMAM dendrimer conjugation leads to the greatest change in nanoparticle diameter due to its size (approximately 50 Angstroms). The next largest linker, PEG, is 17.6 Angstroms when conjugated. I therefore aimed to compare the size of 'bare' nanoparticles and CEA-targeted nanoparticles where PAMAM had been used as the linker. The mean diameter of PAMAM linked nanoparticles was 71 nm (standard error of the mean = 20.85, standard deviation 20.02 nm), compared to 57 nm (standard error of the mean = 0.99, standard deviation = 6.99 nm) for bare nanoparticles (Figure 6.12). I concluded that the targeted nanoparticles were still small enough to fulfil the requirements for my proposed application.

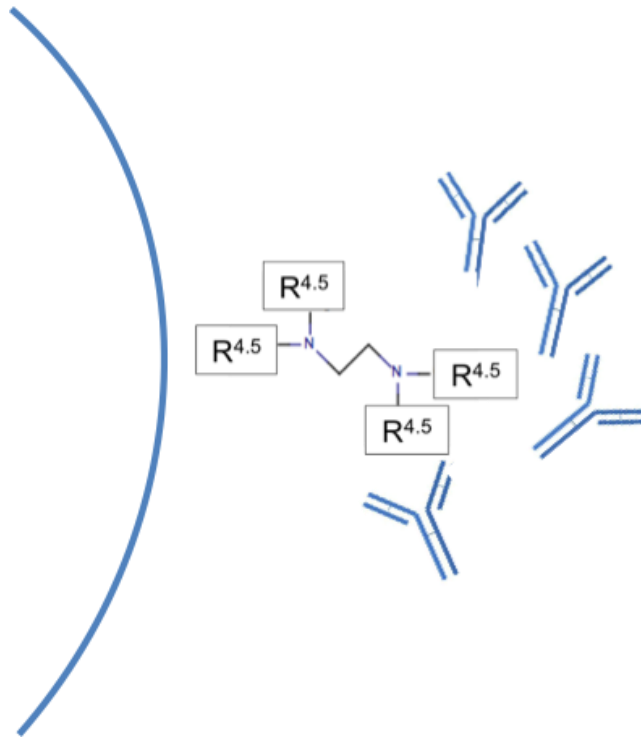
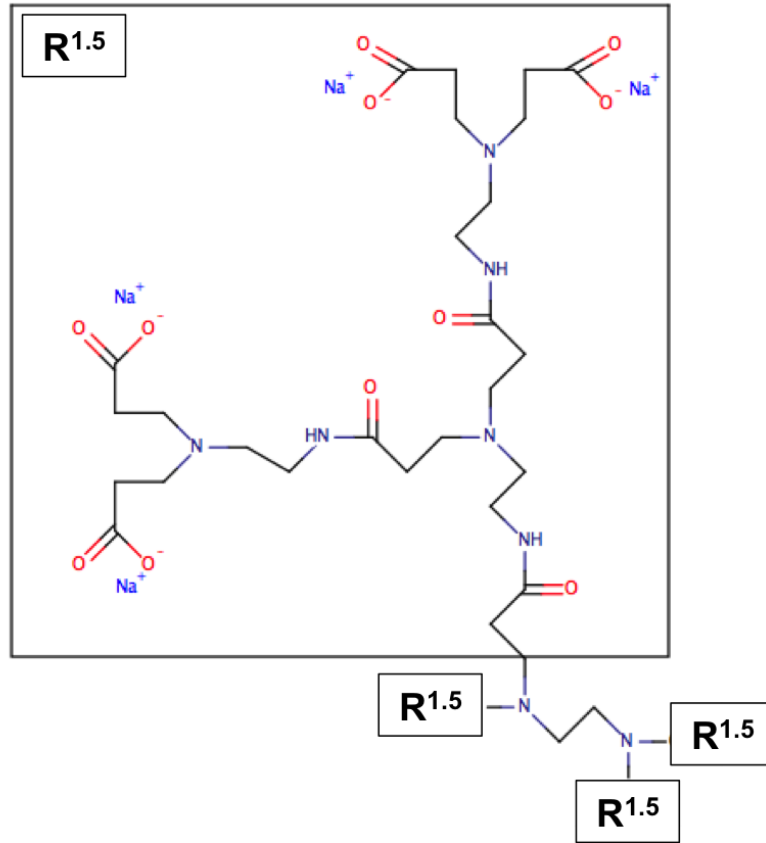


Figure 6.11. PAMAM dendrimer conjugation.

PAMAM dendrimers can be used to conjugate aminated nanoparticles to whole antibodies. PAMAM dendrimers are branched chain molecules that can be synthesised to contain a specified number of branches. Top: PAMAM generation 1.5 carboxylate sodium salt dendrimer. Half generations leave an outer carboxyl group available for binding to amines via EDC. Each of the four 'R' groups has four carboxyl groups available for binding amines. Bottom: I used PAMAM generation 4.5 carboxylate sodium salt dendrimers to conjugate aminated nanoparticles to whole IgG antibodies. Each 'R' group in this case has 16 available carboxyl groups, due to the increased number of branches (four versus one).

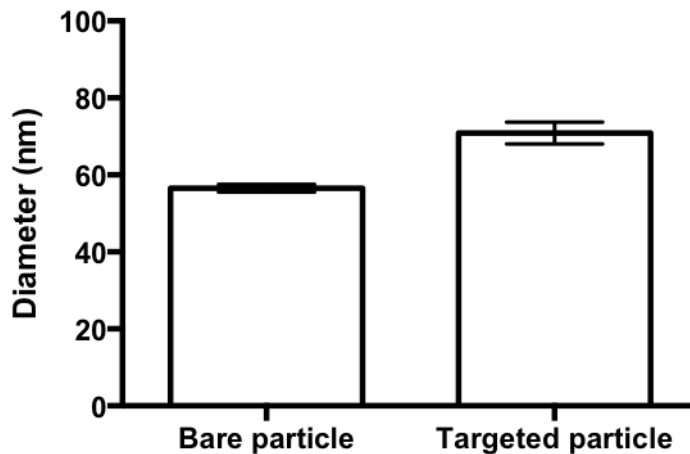


Figure 6.12. Bare particle versus targeted particle size.

Bare dye-doped silica nanoparticles had a mean diameter of 57 nm (standard error of the mean = 0.99, standard deviation = 6.99 nm) and nanoparticles conjugated to anti-CEA antibodies via PAMAM dendrimers had a mean diameter of 71 nm (standard error of the mean = 20.85, standard deviation = 20.02 nm, $p < 0.0001$, unpaired t-test).

6.3.3 *In vitro* analysis of binding of colorectal cancer cells by targeted nanoparticles

I aimed to assess the potential of each of the linking strategies for directing tumour-specific fluorescent imaging quantitatively. To do this I aimed to compare the ability of each conjugated NP type to direct binding of NPs to CEA-positive colorectal tumour cells *in vitro*. To assess the specificity of these interactions, in each case I compared binding directed by the anti-CEA antibody used previously, with a control IgG, specific for the glycoside digoxin. Using a control IgG antibody results in a control nanoparticle that is virtually identical in structure and chemical properties to the CEA-targeted nanoparticle. Digoxin is not expressed by colorectal cancer cells, as I have shown in chapter five and therefore anti-digoxin is a suitable control IgG molecule. The use of 'bare' nanoparticles as a control is inappropriate as the surface chemistry will be different from targeted particles, with inevitable differences in surface charge, size and potential for non-specific binding.

Three different colorectal cell lines were used, each of which expresses CEA at differing concentrations as demonstrated on Western blot analysis in section 5.3.2.2: LoVo cells have a high expression, LS174T cells a moderate/high expression and HCT116 cells a low expression. To assess nanoparticle binding, I used confocal microscopy to obtain fluorescent images and quantified fluorescence digitally in two ways: within a representative optical section through the cells, and within a 'maximum image projection image' (MIP), where the signals from multiple images taken throughout the depth of the cell are compressed and merged into a single image (see section 2.7.5.4 for further details). Data are expressed as the fold difference in fluorescent intensity between the cells incubated with control and CEA-directed particles.

PEG- and SMCC- linked nanoparticles failed to demonstrate any antibody-dependent tumour cell binding. A high degree of non-specific binding was observed with SMCC-linked particles whilst PEG-linked particles produced very little signal (Figure 6.13). Similarly, nanoparticles conjugated using EDC showed very poor antibody-dependent tumour cell binding, with only 1.7-fold greater binding of CEA-targeted nanoparticles as compared to control in only one cell line (LoVo, $p=0.017$).

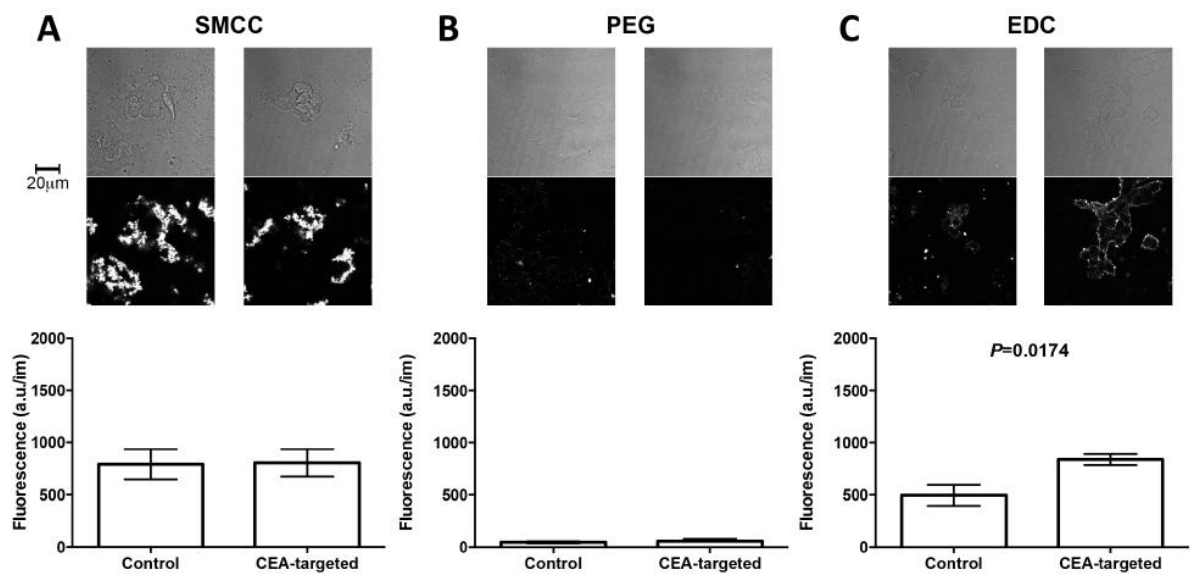


Figure 6.13. Fluorescence analysis: SMCC, PEG and EDC.

Antibody conjugation of dye-doped silica nanoparticles using SMC, PEG or EDC

failed to allow consistent specific fluorescent imaging in LoVo cells. LoVo cells were incubated with either nanoparticles conjugated to either anti-CEA, or control antibodies using conjugation chemistry based on SMC, PEG or EDC as shown.

Fluorescent images were collected using confocal microscopy and fluorescence was quantified. Representative phase contrast and fluorescent central optical section images are shown (magnification, x 63). Graphs representing mean fluorescence (with standard deviations) are shown; significance was tested using unpaired t-tests.

Conjugation via PAMAM dendrimers allowed strong tumour-specific targeting, with CEA-targeted nanoparticles demonstrating 12.3-, 8.0- and 3.2-fold greater fluorescence than control in LS174T, LoVo and HCT116 cells respectively ($p < 0.002$) for the single slice analysis (Figure 6.14). A similar pattern of successful CEA-targeted fluorescence was observed in the MIP analysis, with CEA-targeted nanoparticles demonstrating 4.5-, 3.7- and 2.6-fold greater fluorescence than control particles in LS174T, LoVo and HCT116 cells respectively ($p < 0.0002$). The results are summarised in Table 6.1. A three-dimensional fluorescent reconstruction image provided further confirmation that the nanoparticles were immobilised at the cell surface (Figure 6.15).

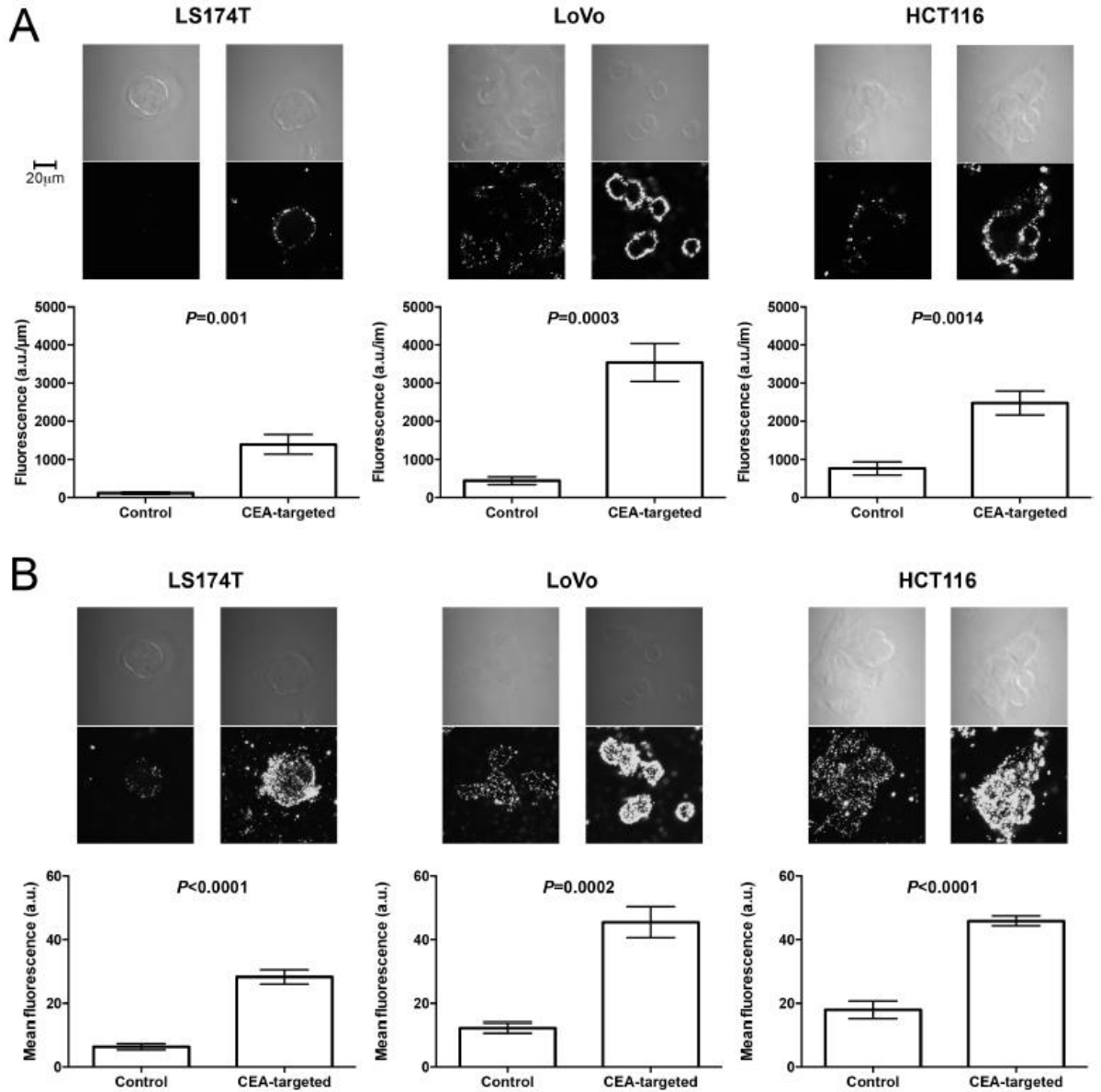


Figure 6.14. Fluorescence analysis: PAMAM dendrimers.

Dye-doped silica nanoparticles conjugated to anti-CEA antibodies via PAMAM dendrimers allow specific fluorescent imaging of colorectal cancer cell lines in vitro. Three different colorectal cancer cell lines were incubated with either nanoparticles conjugated to anti-CEA, or to control antibodies. Images were collected using confocal microscopy and fluorescence was quantified. Representative images are shown (magnification, x 63): A) phase contrast and fluorescent central optical sections; B) phase contrast and maximum image projection. Graphs representing

mean fluorescence (with standard deviations) are shown; significance was tested using unpaired t-tests.

			Unpaired t-test				Mann-Whitney			
			Mean CEA	Mean Dig	p value	Fold difference	Median CEA	Median Dig	p value	Fold difference
PAMAM	Single slice	LS174	1395.000	113.700	0.001	12.3	1302	123.100	0.0079	10.6
		LoVo	3544.000	442.500	0.0003	8.0	3914	424.600	0.0079	9.2
		HCT116	2478.000	765.900	0.0014	3.2	2657	506.3	0.0079	5.2
	MIP	LS174	28.230	6.330	0.0001	4.5	27.73	7.36	0.0079	3.8
		LoVo	45.510	12.170	0.0002	3.7	48.51	11.32	0.0079	4.3
		HCT116	45.860	17.910	0.0001	2.6	47.6	14.69	0.0079	3.2
SMCC	Single slice	LS174	943.600	1538.000	0.2602		908.8	1704	0.2222	
		LoVo	804.000	790.900	0.9475		674.9	805	0.8016	
		HCT116	371.300	546.900	0.6519		158.5	22.69	0.6667	
	MIP	LS174	11.010	14.250	0.3724		11.22	15.94	0.4127	
		LoVo	14.870	15.600	0.8121		13.35	16.94	0.8016	
		HCT116	14.690	9.412	0.4359		7.54	4.38	0.4127	
PEG	Single slice	LS174	60.640	116.500	0.336		42.78	69.25	0.3095	
		LoVo	57.660	47.030	0.6561		45.22	51.52	0.9444	
		HCT116	523.000	367.400	0.629		198.6	410.8	0.5317	
	MIP	LS174	2.682	2.702	0.9744		3.01	2.9	0.9444	
		LoVo	4.904	4.056	0.3751		4.82	4.29	0.4127	
		HCT116	8.296	12.380	0.3321		5.44	12.66	0.1508	
EDC	Single slice	LS174	903.300	545.700	0.3488		652.9	546.1	0.4127	
		LoVo	837.100	495.800	0.0174	1.7	794.2	470.5	0.0159	1.7
		HCT116	839.900	450.500	0.2986		413.9	407.5	0.4127	
	MIP	LS174	29.030	23.740	0.4259		24.83	22.37	0.5317	
		LoVo	30.080	21.850	0.0142	1.4	33.64	22.32	0.0317	1.5
		HCT116	26.010	5.855	0.1096		19.73	16.22	0.0159	1.2

Table 6.1. Summary of in vitro fluorescence quantification analysis.

Data from control and test experiments were compared using both parametric and non-parametric statistical analyses. MIP = maximum intensity projection. Statistically significant results in bold.

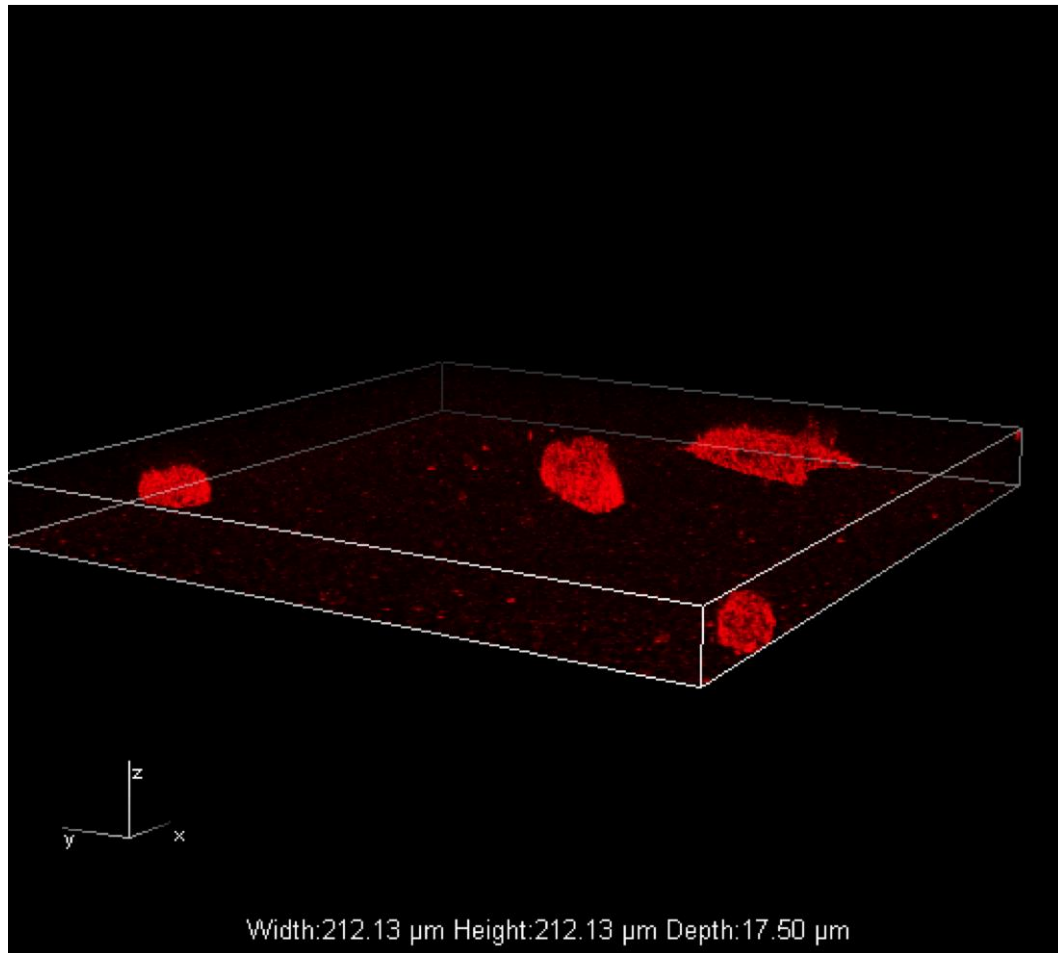


Figure 6.15. Three dimensional reconstruction of nanoparticle-coated cells.

Dye-doped silica nanoparticles conjugated to anti-CEA antibodies via PAMAM dendrimers bind to the cell membrane of LoVo cells. Nanoparticles were incubated with fixed cells and fluorescent images captured with confocal microscopy. A three-dimensional reconstruction was created using NHS-Elements software version 4.0 from z-stack images.

I concluded that dye-doped silica nanoparticles conjugated to anti-CEA antibodies via PAMAM dendrimers allowed tumour cell-specific fluorescent targeting *in vitro*, and had shown sufficient promise to justify testing in an animal model of colorectal cancer.

6.3.4 *In vivo* analysis of binding of colorectal cancer cells by targeted NPs

Having demonstrated specific targeting of colorectal cancer cells *in vitro* using PAMAM-conjugated nanoparticles, I aimed to test their potential for *in vivo* fluorescent targeting. To do this I designed a series of experiments involving systemic nanoparticle delivery to a murine xenograft model of colorectal cancer.

6.3.4.1 NIR664-doped silica nanoparticles are detectable *in vivo*.

First I confirmed that the IVIS small animal imaging system, which was to be used for all *in vivo* experimental imaging, was capable of detecting the fluorescent signal from the nanoparticles. I suspended the particles in PBS at 2 mg/ml, 200 µg/ml and 20 µg/ml and took fluorescent images with the appropriate wavelengths selected (Figure 6.16). I planned to use a dose of 50 mg/kg in the targeting experiments, in line with other silica nanoparticle mouse experiments (Meng et al., 2011, Tivnan et al., 2012), which equates to approximately 625 µg/ml (assuming a six week old BALB/c nu/nu female mouse has a weight of 25 g and circulating blood volume of 80 ml/kg (Doevendans et al., 1998) with uniform nanoparticle distribution throughout the vascular compartment). The strong fluorescent images I obtained with a 200 µg/ml suspension suggested that the IVIS system should be able to detect this concentration.



Figure 6.16. Fluorescent nanoparticles are detectable using an IVIS imaging system.

CEA-targeted nanoparticles suspended in PBS were detected using an IVIS small animal imaging system. Nanoparticles were in Eppendorf Tubes and blanked out with black card to allow comparison. Left: 2 mg/ml. Middle: 200 µg/ml. Right: 20 µg/ml.

Next I aimed to determine in a pilot experiment whether nanoparticles delivered systemically to mice were detectable, for how long, and their location. I injected CEA-targeted nanoparticles into the tail veins of three 6 week old BALB/c nu/nu female mice (without xenograft tumours) and took live IVIS images one minute, one hour, 24 hours, 48 hours and 72 hours after injection (Figure 6.17). At 24 hours post-injection, I sacrificed one of the mice, retrieved the liver, kidneys and spleen, and imaged the organs *ex vivo*. I did the same with a control mouse that had not been injected with nanoparticles.

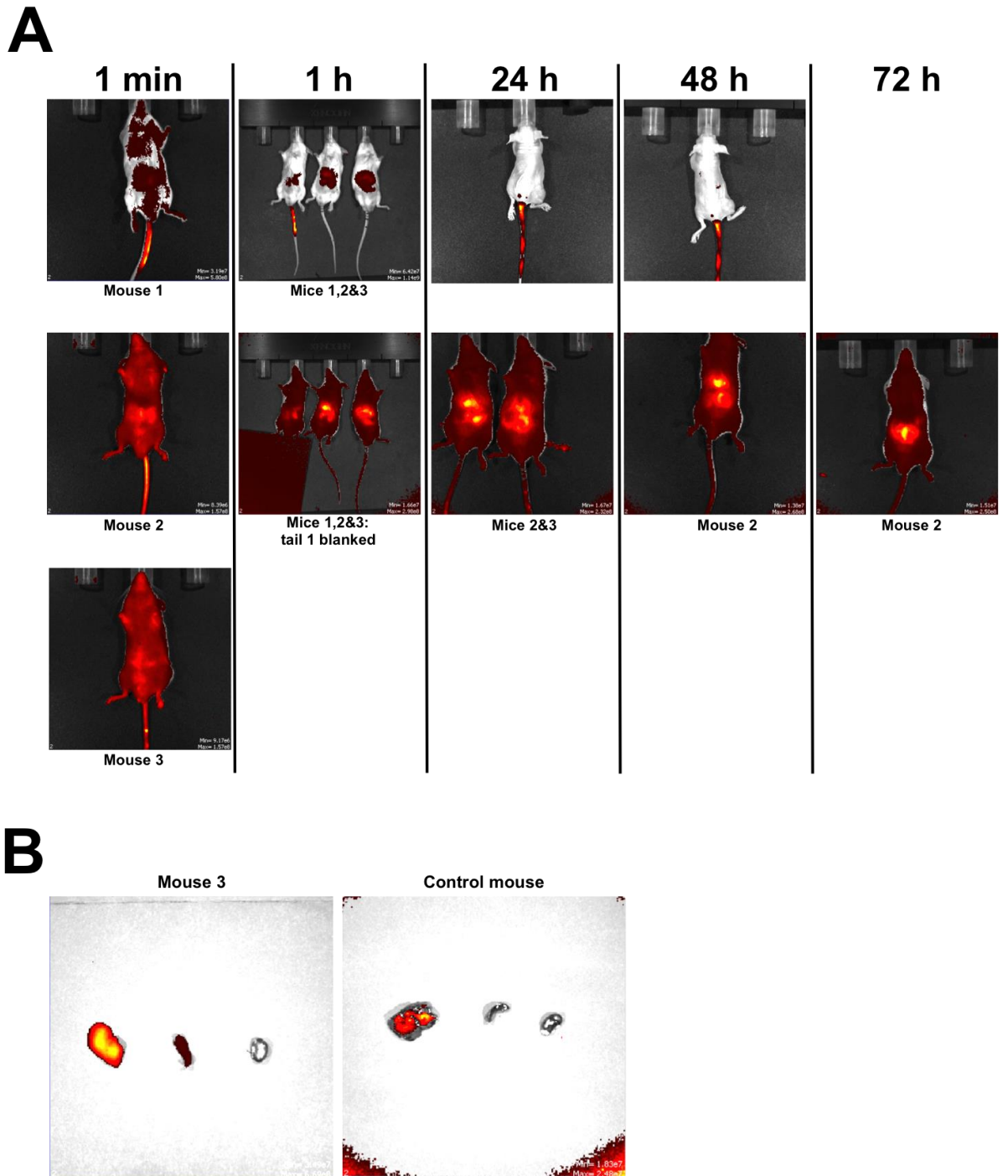


Figure 6.17. Systemically delivered nanoparticles are detectable *in vivo*.

Mice were injected with CEA-targeted nanoparticles and were imaged either individually or in groups using IVIS at various times as shown. Note that the injection in Mouse 1 failed to deliver successfully to the vein as evidenced by the fact that particles are visible in the subcutaneous tissues at one minute and one hour. At one hour post-injection, all three mice were imaged as normal (top picture) but also with

the tail fluorescence in Mouse 1 'blanked' with black card (bottom picture), allowing the IVIS system to auto-expose and detect more sensitively the fluorescence in the livers of Mouse 2 and Mouse 3. Mouse 1 was subsequently imaged separately. After 24 hours, organs were harvested from Mouse 3 and imaged ex vivo (panel B), along with the same organs from a mouse that had not received the nanoparticles. Only Mouse 2 was imaged at 48 and 72 hours.

The tail vein nanoparticle injection failed in Mouse 1, and the fluorescent signal remained in the subcutaneous tissues of the tail with no apparent decrease in signal even at 48h hours. The other mice demonstrate systemic delivery of particles within one minute and accumulation in the liver within one hour, consistent with hepatic excretion. At 24 hours post-injection there appeared to be biliary fluorescence in addition to hepatic fluorescence. By 72 hours, the hepatic fluorescence had decreased, leaving only biliary fluorescence. This was suggestive of hepatobiliary excretion, a feature observed previously in systemically delivered silica nanoparticles (Souris et al., 2010). The mean fluorescence of the *ex vivo* liver from Mouse 3 at 24 hours was 37.26×10^7 p/sec/cm²/sr/μW/cm², compared to a degree of natural fluorescence of 0.454×10^7 p/sec/cm²/sr/μW/cm² for the control mouse liver (a fold difference of 82). The control mouse spleen and kidney exhibited no natural fluorescence whilst the spleen and kidney from mouse three exhibited low level fluorescence (0.477 and 0.337×10^7 p/sec/cm²/sr/μW/cm² respectively).

I concluded that the nanoparticles were detectable *in vivo*, were deliverable systemically, and were metabolised and excreted predominately by the liver.

6.3.4.2 CEA-targeted fluorescent nanoparticles can be used for tumour-specific imaging in a murine xenograft model of colorectal cancer

For my final experiment, I aimed to test whether CEA-targeted nanoparticles were capable of tumour-specific labelling, as measured by fluorescence, *in vivo*. I injected seven mice bearing LS174T xenograft tumours with either CEA-targeted or control IgG-targeted nanoparticles and obtained fluorescent images at one minute, one hour, six hours, 24 hours, 48 hours and 72 hours post-injection (Figure 6.19). One of the tail vein injections failed, leaving three test and three control mice. Liver fluorescence was evident at six hours (mean 80.1×10^6 p/sec/cm²/sr/ μ W/cm²) and peaked at 24 hours (89.8×10^6 p/sec/cm²/sr/ μ W/cm²) before reducing (48 hours: 74.2×10^6 p/sec/cm²/sr/ μ W/cm² and 72 hours: 48.0×10^6 p/sec/cm²/sr/ μ W/cm²) (Figure 6.18).

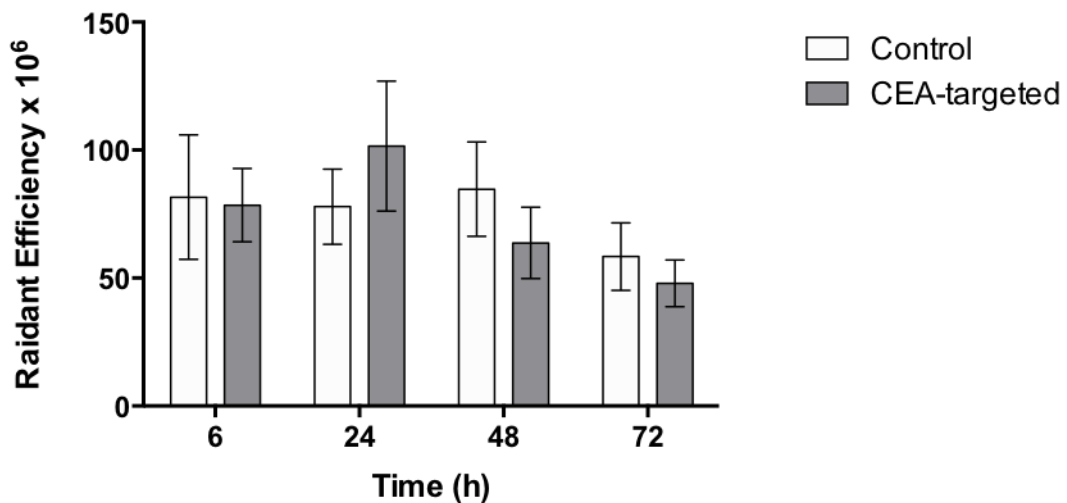


Figure 6.18. Hepatic fluorescence is similar for control and CEA-targeted nanoparticles.

Hepatic fluorescence following systemic delivery of control and CEA-targeted nanoparticles in vivo. Fluorescence peaked at 24 hours and reduced thereafter.

There was no significant difference in hepatic fluorescence between mice injected

with control particles and those injected with CEA-targeted particles at any time point (p ranging from 0.3 to 0.9).

Hepatic localisation was confirmed by *ex vivo* imaging of isolated organs. There was no significant difference in liver fluorescence between mice injected with control particles and those injected with CEA-targeted particles at any time point (p ranging from 0.3 to 0.9, Mann Whitney Test). Fluorescence in other mouse tissues was not seen for either control or CEA-targeted particles, demonstrating that the particles have negligible non-specific or antibody directed binding to host cells. Substantial tumour fluorescence was detected in all mice injected with CEA-targeted nanoparticles from six hours post-injection. Mean tumour fluorescence increased over the whole experiment from six hours (mean 0.62×10^7 p/sec/cm²/sr/ μ W/cm²) to 72 hours (mean 4.74×10^7 p/sec/cm²/sr/ μ W/cm²), although increases were only small after 48 hours. Mice injected with control IgG-targeted nanoparticles showed no tumour fluorescence above background at any point (Figure 6.20). Fluorescence in the CEA-targeted tumours was significantly greater than controls at every time point after and including 6 hours (p<0.0001, Wilcoxon Signed Rank Test). The continued accumulation of tumour fluorescence with the CEA-targeted nanoparticles for up to 72 hours suggests that at least a proportion of the conjugated particles are stable in the circulation for a minimum of 72 hours.

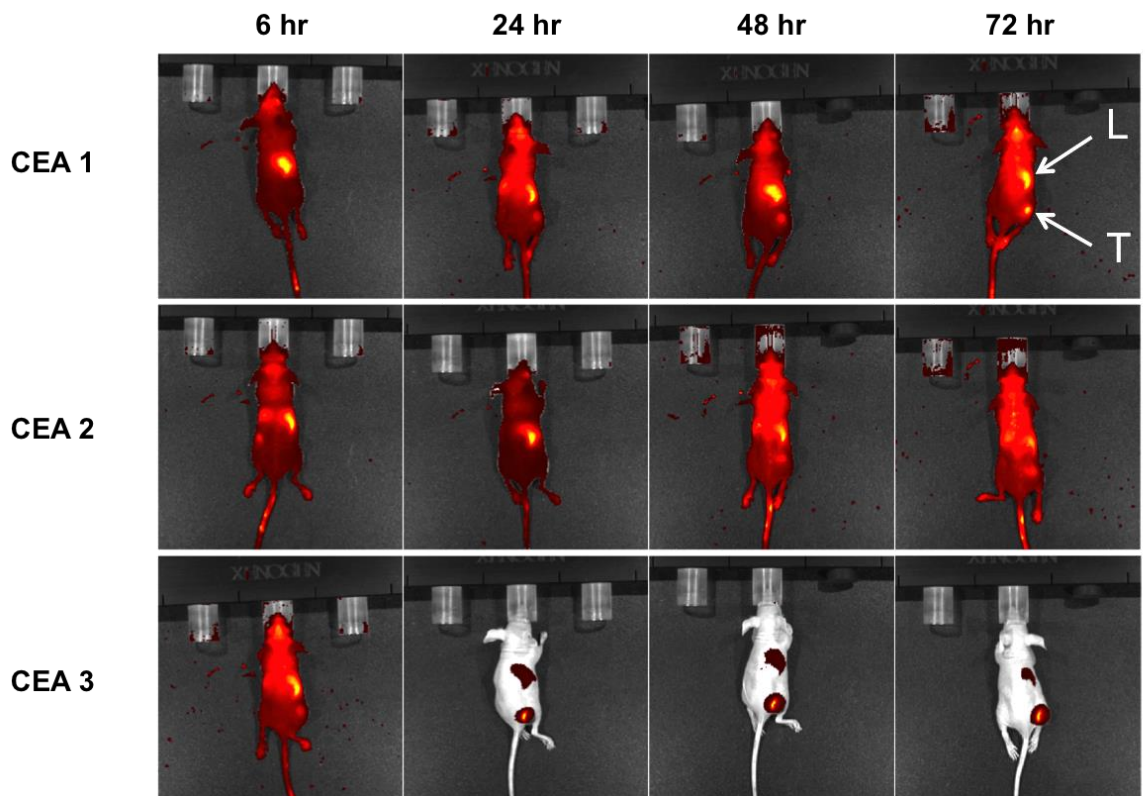
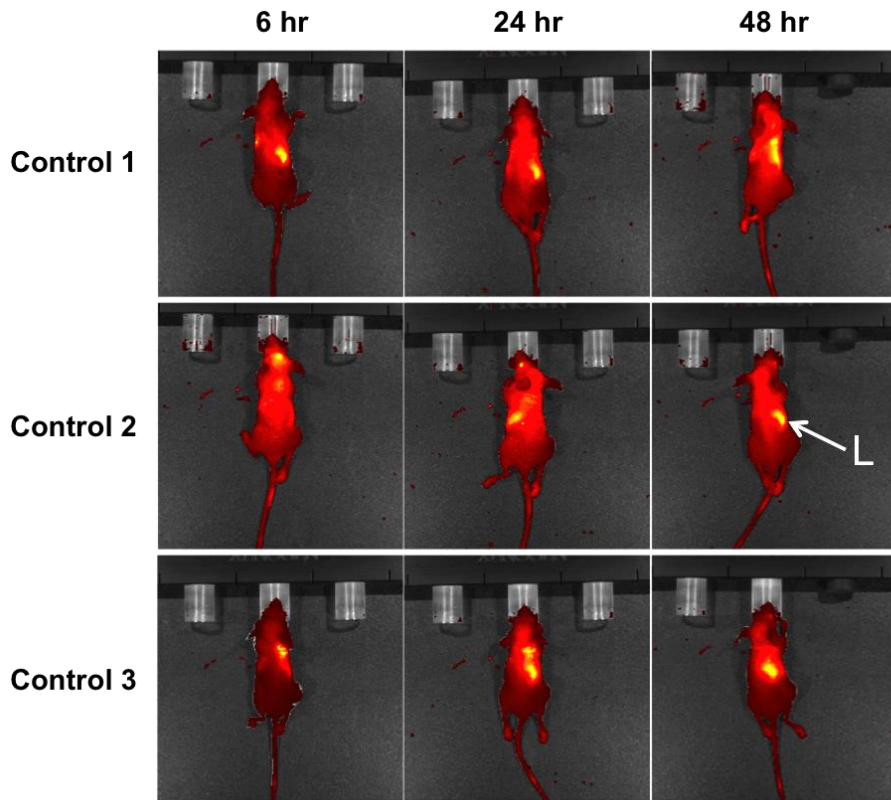


Figure 6.19. Systemic administration of CEA-targeted nanoparticles leads to tumour-specific fluorescence in a xenograft murine model of colorectal cancer.

No tumour cell fluorescence was observed in mice injected with control-IgG targeted nanoparticles whereas in all three mice injected with CEA-targeted nanoparticles tumour cell fluorescence was observed. Control images at 72 hours not available. L = liver, T = tumour.

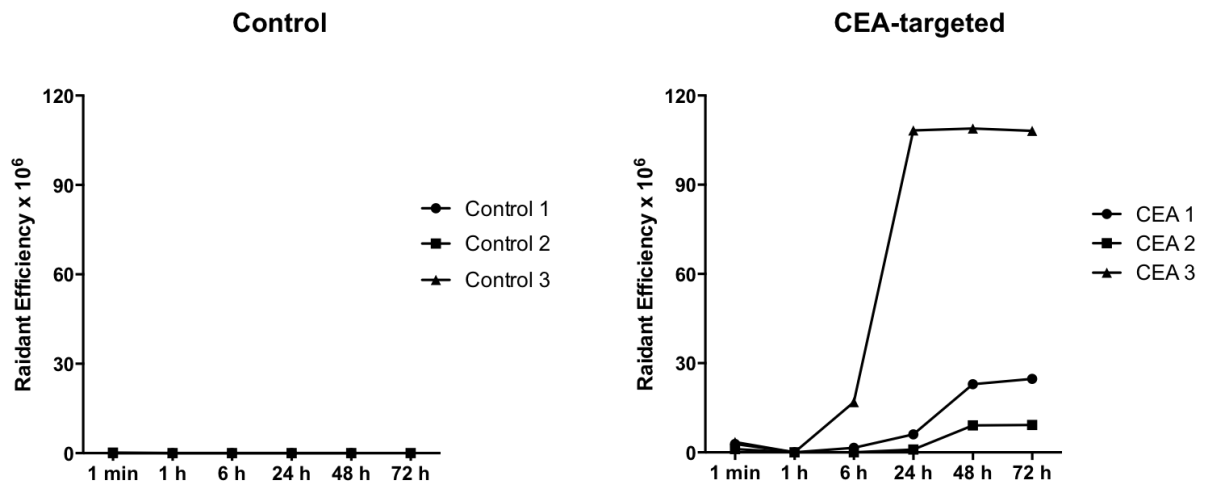


Figure 6.20. CEA-targeted nanoparticles allow fluorescent tumour detection in vivo.

Mean tumour fluorescence at 72 hours post-injection was 4.74×10^7

$p/\text{sec}/\text{cm}^2/\text{sr}/\mu\text{W}/\text{cm}^2$ for mice injected with CEA-targeted nanoparticles. No tumour fluorescence above background was detected in control mice ($p < 0.0001$).

6.4 Discussion

In this chapter I sought to use nanotechnology to provide a concentrated fluorescent signal in an antibody-mediated, tumour specific, *in vivo* imaging system.

Nanoparticles can be synthesised to be a large variety of sizes, shapes and chemical compositions. Polymeric microspheres, synthesised using an emulsion polymerisation process, have tended to be the most common type of particle used in biological applications (Soppimath et al., 2001). I initially focussed on polymeric nanoparticles as our laboratory had some prior experience with their synthesis (Vakurov et al., 2009). Their size can be readily controlled and their surface can be functionalised with a variety of groups for conjugation. However, both the fluorophore and antibody would need to be immobilised onto the surface using the same functional group: whilst theoretically possible this would require accurate and in-depth information about the reaction kinetics of each molecule for the appropriate ratio of antibody:fluorophore to be predicted and achieved. Dye-doped silica nanoparticles (Ow et al., 2005, Santra et al., 2001) represent a better solution: they have an inherent fluorescent core so the surface can be used solely for targeting; they are sufficiently small for my purposes; they are chemically inert and comparatively non-toxic; and they can be functionalised for conjugation to proteins relatively easily. They can be synthesised by two methods: the Stober method or the water-in-oil reverse microemulsion method. I chose to focus on the latter because, compared to the former, particles tend to be monodispersed and their diameter is easier to control, particularly below 100 nm (Bagwe and Khilar, 2000, Bagwe et al., 1999).

6.4.1 Manufacture and optimisation of dye-doped silica nanoparticles

The synthesis of the basic nanoparticle can be broadly divided into three parts:

- i. *Dye-doping a silica matrix.* This is where fluorescent molecules are embedded in silica and this forms the fluorescent core of the particle. The silica matrix is hydrophilic so the choice of dye is important - polar dye molecules are best as the electrostatic interaction with the negatively-charged silica molecules leads to a stable core. In addition, the dye molecules must be large enough to prevent dye leakage from the pores in the silica matrix (Zhao et al., 2004a). Initially I used RuBpy dye, most commonly used in published studies, but later switched to NIR664 due to its near-infrared wavelength (Malik et al., 2011).
- ii. *Formation of a water-in-oil microemulsion system.* This is formed by creating a stable, transparent solution of water, surfactant and co-surfactant. The molar ratio of these compounds and the choice of surfactant determine the size of the particles.
- iii. Creation of dye-doped particles with a silica shell. This occurs through hydrolysis of tetraorthosilicate (TEOS), catalysed by ammonium hydroxide, and 'nucleation' of the dye-doped silica into the water pools inside the reverse micelles of the water-in-oil microemulsion.

Having synthesised the basic dye-doped particle, the surface can be modified to make a functional group available for conjugation to another molecule. This group

determines the choice of linker for antibody conjugation. Within the remit of limiting the overall diameter of the particles as far as possible to allow them to pass out of the vasculature *in vivo*, three surface chemistries can be used. The basic particle has free -OH groups available and these were used for antibody conjugation in the original paper describing dye doped silica particles (Santra et al., 2001), in a study targeting human leukaemia cells *in vitro*. Cyanogen bromide was used to link the silica surface -OH groups to free amine groups on the leukaemia-specific cell-surface antibodies. The authors presented comparative images of leukaemia cells incubated with targeted and control nanoparticles, although fluorescence was not quantified. Cyanogen bromide appears not to have been repeated in any other relevant work, probably related to its toxicity and the associated practical implications. The surface free -OH groups can also be modified to make either amine or carboxyl groups available for conjugation. Amination occurs by the addition of 3-aminopropyl-(triethoxyl)silane (APS). The amine groups can then be used for conjugation to free amine groups on whole antibodies via glutaraldehyde (Huang et al., 2009). Alternatively, carboxyl groups can be introduced by adding trimethoxysilyl-propyldiethylenetriamine (DETA) (Zhao et al., 2004b, Lian et al., 2004). Carboxylation can also be achieved by reacting aminated particles with succinic anhydride and *N,N*-dimethylformamide (DMF) under an inert gas (Liu et al., 2007, Zhao et al., 2004b). Carboxyl-functionalised particles can then be conjugated to antibodies via streptavidin and biotin (Lian et al., 2004) or EDC (Liu et al., 2007, Wu et al., 2008, Zhao et al., 2004b). EDC is the most common linker used, and apparently the most successful conjugation method in published literature. SMCC has been used to conjugate whole antibodies to silica (Gubala et al., 2010) and iron oxide (Abdolahi et al., 2013) nanoparticles by converting free amine groups on the IgG antibody to sulfhydryl groups using Taut's Reagent (2-iminothiolane). Conjugation using heterobifunctional PEG is a further option that can increase the particle circulating half-life by preventing reticulo-endothelial opsonisation (Owens lii

and Peppas, 2006) and can link either a free amine or carboxyl group depending on the type polymer selected, all of which are available commercially. More recently dendrimers have also been used as novel linkers between nanoparticles and antibodies (Gubala et al., 2010).

There are two key and recurring issues in this field: experiments have tended to be either non-controlled or poorly controlled with 'bare' nanoparticles used as opposed to the more appropriate choice of non-targeting antibodies; and there has been a lack of a robust fluorescence quantification assay to enable statistically significant conclusions to be drawn. These issues are of particular importance since I have shown non-specific binding of antibody-conjugated nanoparticles is prevalent using some conjugation strategies, while antigen-specific targeting is more problematic.

I initially decided to focus on four linking chemistries. EDC has had the most promising results in published studies and was therefore a low risk strategy. Our laboratory has previously used reduced antibodies on nanoscale biosensor surfaces in an effort to control the orientation of the IgG molecule (Figure 6.6) and therefore increase the availability of antigen binding sites. I was keen to apply the same principle to my nanoparticles, using SMCC in the opposite manner to published studies by linking free amine groups on the nanoparticle surface to a sulfhydryl group made available by reducing an IgG antibody. I chose to use small length PEG linkers to conjugate reduced antibodies in the same way. Finally, I chose dendrimers to link whole antibodies. Although there was relatively little published literature relating to their use in this context, they potentially increase the number of available binding sites for the antibodies.

Steps ii. and iii. above were optimised by the group who pioneered this type of nanoparticle (Bagwe et al., 2004). However, there is a paucity of robust data

available regarding the modification of the surface chemistry and conjugation to bioactive molecules. I designed the methodology for each surface modification (amination or carboxylation) and subsequent conjugation process (SMCC, PEG, EDC and PAMAM) by studying published work in related fields and breaking down each methodology into individual reaction steps so that I could optimise the reaction conditions for each in terms of molar ratio, temperature, pH and equipment used. This was very much a pragmatic process; it would theoretically be possible to optimise each step in great detail by systematically controlling and varying all of the various conditions but this would not be feasible or practical in the development of my novel application, where combining nanoparticles with a cellular system yields a huge number of further unknown variables.

A major component of the manufacture process is the pelleting and re-suspending of the particles. This allows unreacted chemicals and/or reaction by-products to be removed, and for the suspension fluid to be changed so that the correct conditions can be achieved for the subsequent reaction step. Initially I used plastic tubes and relatively low centrifugation speeds, in line with the limited number of published studies (Liu et al., 2007), but found that this did not 'wash' the particles effectively. When I took SEM images of basic particles manufactured this way, surfactant was visible despite multiple wash steps. I therefore used higher centrifuge speeds but then found the nanoparticle pellet was difficult to re-suspend despite extensive sonication. I found that Corex glass centrifuge tubes overcame this problem, seemingly allowing much more efficient sonication of the pellet in comparison to plastic tubes, and allowing effective 'washes' (Figure 6.21). I also measured protein absorbance values for the supernatant produced in consecutive wash steps following antibody conjugation to check that the number of wash steps in my protocol was adequate for removing unbound IgG (Figure 6.10).



Figure 6.21. 'Bare' NIR664 doped silica nanoparticles.

Left: dried particles; middle: pelleted particles during ethanol wash steps; right: pellet re-suspended in ethanol via sonication.

Amination of the particles was required for all of my linking strategies. There are several established assays for quantifying the number of free amine groups in a substance (Habeeb, 1966) but they tend to rely on absorbance or fluorescence assays. This is a problem when the amine groups are located on a fluorescent particle as the results are distorted. A single paper has been published describing an optimised method for quantifying amine groups in fluorescent nanoparticles and I adapted this for use with my particles (Chen and Zhang, 2011), with similar results (approximately 2×10^{16} free amine groups per mg of particles, Figure 6.1). For conjugation using SMCC and bifunctional PEG, I used reduced antibodies. The antibodies were reduced using 2-MEA (Yoshitake et al., 1979). I was careful to use reaction conditions that resulted in cleavage of the disulphide bonds between the two heavy chains but preservation of the light chains and antigen binding capability. Typically this process produces a mixture of reduced and whole antibodies in a 2:3 ratio. To confirm that I had successfully reduced the IgG antibodies I subjected the mixture to HPLC (Figure 6.6), the two peaks representing reduced and whole antibodies. Following incubation with sulfhydryl-reactive nanoparticles, I confirmed a

reduction in the number of free sulfhydryl groups present in the reaction mixture, suggesting that the reduced antibody fragments had bound to the nanoparticle surface.

In order to maximise the fluorescent signal in my *in vitro* experiments, I measured the fluorescence of RuBpy-doped nanoparticles in suspension in PBS at various concentrations. A graph of the results increases to a plateau at 0.5 to 1 mg/ml with a decrease in fluorescence thereafter (Figure 6.3). This is probably due to self-quenching, which tends to occur at higher concentrations due to the formation of dimers or other quenching complexes in the dye solution (Penzkofer and Lu, 1986). I stored my particles at 2 mg/ml in the dark and then used them at 1 mg/ml in my *in vitro* experiments.

6.4.2 *In vitro* assays for specific antibody-directed binding

I carefully designed my *in vitro* experiments to be as robust as possible, with minimal potential for bias. I used anti-digoxin as a control IgG antibody and conjugated it to nanoparticles from the same batch, and at the same time as conjugating to anti-CEA. I used anti-digoxin IgG as a control in Chapter 5 and showed that digoxin is not present in colorectal cancer cells. I selected three cell lines known to express CEA at differing levels to reflect the heterogeneity in expression in human colorectal cancer. There are a number of sources of bias when assessing and comparing fluorescent images of cells:

- i. Cell selection
- ii. Image acquisition
- iii. Image selection
- iv. Fluorescence measurement

Most published studies that have quantified fluorescent nanoparticle cell binding have tended to use a single cell line and a simple fluorescent measurement of whole cells (Blechinger et al., 2013, Jonkman et al., 2014, Torrano and Brauchle, 2014, Jiwaji et al., 2014). They have not described robust protocols to minimise bias. One paper addressed differences in cell fluorescence measurements in the z plane but again this was in a single cell type (Prats-Mateu et al., 2014). I have compared membrane-specific fluorescence in three morphologically different cell lines between test and control nanoparticles, and have minimised all sources of bias as far as possible.

Cell selection: prevention of selection bias in the x-y plane

When capturing confocal images, I positioned the microscope over five pre-determined areas on each slide and selected cells using the phase white light image, blinding me to the fluorescent images and preventing selection bias in the x-y plane of the slide.

Image acquisition

To ensure that the confocal images for each cell line could be compared, I used the microscope software to select the optimum image settings (gain and intensity) for the first cell and then used these settings for all remaining measurements.

Image selection: prevention of selection bias in the z plane

I designed the fluorescence quantification assay taking into account that the nanoparticles were targeted to an antigen located at the cell membrane and cells from different cell lines have variable diameters. I took z-stack images for each image captured and then worked out the approximate diameter of cells from each cell line, so that I could consistently select optical slices through the cell centres for analysis, preventing selection bias in the z plane.

Fluorescence measurement

Simply measuring the fluorescence of a whole cell would prevent a comparison between cell lines as the non-fluorescing cytoplasm would have a greater impact on the measurements in some cell lines compared to others (for example, LS174T cells tend to grow in colonies whilst LoVo cells are small but tend to be separate). I therefore used ImageJ software to measure mean fluorescence per unit length of membrane, corrected for background fluorescence. To ensure consistency and prevent a further source of selection bias, I made the membrane trace using the phase image only and then transferred the trace to the fluorescent image. As a confirmatory analysis, I used a function in the confocal microscope software to construct Maximal Image Projection images, where the all the images taken in the z-stack are superimposed to give a single image. This leads to areas where the pixels in the images are saturated and potentially dampens any observed difference between positive and negative fluorescing cells. There are no published studies describing cell fluorescence measurements taking into account all sources of bias in this way.

When analysing the results, I used both parametric and non-parametric statistical tests (Table 6.1). If cellular fluorescence was measured for every single cell on each slide, there is nothing to suggest the results would not be normally distributed so I feel a parametric test to compare means is appropriate (unpaired t-test). However, for completeness I also treated the data as non-parametric and used the Mann-Whitney test to compare medians. The results of both statistical analyses and both types of image (single cell section and Maximal Image Projection) demonstrated a clear statistically significant difference in fluorescence between test and control antibodies in all three cell lines for nanoparticles conjugated to antibodies using

PAMAM dendrimers, suggesting that the type of statistical test used was not a key factor influencing the result.

6.4.3 The relative merits of the chemical linkage strategies tested

I evaluated four linking strategies, including established and novel techniques, which employed both whole and reduced anti-CEA antibodies. SMCC and PEG, both of which used reduced antibodies for targeting, failed to demonstrate any antibody-dependent cell binding. Control SMCC-linked particles produced high levels of non-specific fluorescence, whereas PEG-linked particles produced very little. I attempted to discover the cause of this by varying experimental conditions and using different control antibodies but this had no effect on the non-specific binding. I also hypothesised that a proportion of amine groups on the particle surface may not be bound to SMCC linkers and may be creating a positive surface charge leading to non-specificity. I used succinic anhydride, which converts free amine groups into negatively charged carboxylates (Singh, 1998) to test this but no difference in fluorescence was observed. I also used bovine serum albumin in excess instead of antibodies to ensure all maleimide groups on the SMCC linkers were bound but this also failed to reduce the non-specific binding. The lack of any fluorescent cell labelling with PEG-linked test or control nanoparticles suggests that either the SMCC linker itself or the inherent properties of the aminated basic nanoparticle may have been the cause of the non-specificity. However it also suggests that using reduced antibodies in this context may inhibit antibody-antigen binding. I selected these novel linking strategies in an effort to control the orientation of the antigen binding sites and therefore increase sensitivity while reducing steric hindrance. The selective reduction of the hinge region of IgG antibodies is well known (Yoshitake et al., 1979) and

investigators have experimented with Fab and fc antibody fragments for nanoparticle targeting to try to control binding site orientation (Cheng and Allen, 2008, Kumar et al., 2008) but not with silica nanoparticles. The results failed to show a significant sensitivity advantage.

EDC linking showed tumour-specific binding, although the effect was low (fold change 1.7) and observed in LoVo cells only. Of the limited work published exploring dye-doped silica nanoparticles for cell labelling applications, EDC seems to have been the most popular. However, none of the work used adequate controls. At the time of this work, only two papers described *in vitro* cancer cell targeting with this type of nanoparticle and neither described experiments that were adequately controlled - one used bare EDC-linked nanoparticles (Santra et al., 2001) and the other no controls at all (Huang et al., 2009). My data can be interpreted to suggest that the cell targeting potential of nanoparticles linked in this way has been overstated due to a lack of appreciation of the non-specific binding.

PAMAM dendrimer linking allowed strong tumour-specific imaging. The fluorescence fold change between test and control particles was 12.3, 8.0 and 3.2 for LS174T, LoVo and HCT116 cells respectively. Although these figures correlate with the relative expression of CEA by the cell lines, they are dependent on the level of non-specific fluorescence recorded for control nanoparticles, which varied considerably. It is difficult to draw any conclusions regarding the relationship between targeted-nanoparticle-induced fluorescence and cell surface antigen density. The relative size of the particles means there are likely to be unbound antigen sites between adjacent bound particles. Steric hindrance, where the size of the nanoparticle-antibody complex, the location and orientation of the antibodies on the surface, and the relative density of the antigen on the cell membrane can all reduce immunoreactivity (Lu et al., 1996, Jie et al., 2011).

The successful targeting seen with PAMAM-linked particles and, to a much lesser extent, with EDC-linked particles, may explain the failure of SMCC and PEG. Both PAMAM and EDC linking methodologies required the aminated surface of the particle to be carboxylated. This has the effect of producing an overall negative surface charge prior to attaching the linker and then antibody. Cells have a slight negative charge and positively-charged, non-targeted nanoparticles have been shown to be taken up by cells more rapidly than negatively charged controls (Chen et al., 2011a). Although I tried to eliminate any positive surface charge on SMCC-linked particles with succinic anhydride, this may not have been effective due to the antibodies having already been attached; attempting this prior to antibody incubation would prevent their conjugation. The difference in targeting between PEG-linked and EDC-linked particles might then be either due to the increase in available binding sites for the antibody molecules or the increase in distance between the antibody and nanoparticle surface. Having shown the difference in this pragmatic, proof-of-concept project, these questions now warrant future investigation.

6.4.4 *In vivo* potential for PAMAM-linked antibody-directed nanoparticles

Having developed a fluorescent nanoparticle with genuine specificity for a surface antigen that is over-expressed in colorectal cancer, I then examined the potential for this to be used to image tumours *in vivo*, using a murine xenograft model of colorectal cancer. The principle aim of this part of the project was to test whether the particles could reach the tumour cells following systemic delivery, and whether they showed tumour-specific binding. Only two other studies have investigated specific targeting of dye-doped silica nanoparticles to tumours via systemic delivery: Tivnan

et al (Tivnan et al., 2012) used dendrimer-conjugated particles targeted to neuroblastoma, whilst Soster et al (Soster et al., 2012) used PEG-conjugated particles targeted to colorectal cancer metastases, both in murine xenograft models. However, both studies used 'bare' nanoparticles as controls, which are potentially problematic in terms of demonstrating antigen-specific targeting, and both imaged fluorescence only on harvested organs *ex vivo*, which may relate to poor tissue penetration of fluorescence.

My *in vitro* results suggested that non-specific binding could be a potential problem and this might have been compounded by the fact that normal cells also express CEA. I therefore injected non-tumour bearing mice with CEA-targeted particles to evaluate non-specific binding to normal tissues. Reassuringly the only significant fluorescence observed was hepatobiliary, which peaked at 24 hours and reduced by 72 hours post-injection. This corroborates the only study to examine the biodistribution and excretion of mesoporous silica nanoparticles (Souris et al., 2010), which also found that a higher particle surface charge was associated with rapid excretion. I chose LS174T cells for my xenograft model because they showed the greatest fold difference between test and control (Table 6.1) and because they closely resemble colonic mucosal cells with numerous microvilli and intracytoplasmic mucin vacuoles (Tom et al., 1976). When the CEA-targeted and control-IgG targeted nanoparticles were injected into tumour-bearing mice, I observed significant time-dependent accumulation within tumours that was entirely absent for control IgG-targeted particles ($p < 0.0001$). A similar pattern of hepatic excretion was observed as in my first mouse experiment and there was no difference in liver fluorescence of control or test mice at any time point ($p = 0.3$ to 0.9). There was a wide variation in the tumour-specific fluorescence observed in the three test mice. This is probably due to two main factors: the quality of the tail vein injection and the blood supply to the xenograft tumour. The tail vein injections failed in a number of mice during the early

experiments in this work, despite appropriate needles and expertise. In Figure 6.19 a fluorescent signal persists in the tail of the second mouse injected with CEA-targeted particles throughout the experiment, suggesting that the entire dose was not effectively delivered. This mouse showed the least tumour-specific fluorescence of the three. On examining the tumours at the end of the experiment, the mouse with the greatest tumour-specific signal appeared to have a very vascularised, intra-muscular tumour (Figure 6.22), potentially enabling greater nanoparticle penetration. This could have been due to a deeper subcutaneous injection of tumour cells, where it is difficult to precisely control the depth of the flank injection. Therefore, although the fluorescence measurements had a wide range, more accurate and consistent tumour and nanoparticle injections would probably reduce this.



Figure 6.22. Dissection of xenograft tumour with the greatest tumour-specific signal.

The mouse with the greatest tumour-specific fluorescent signal had a highly vascularised, intra-muscular tumour. LS174T cell xenograft tumours were grown on the flank of six week old BALB/c nu/nu female mice and dye-doped silica nanoparticles were delivered systemically via the tail vein.

This work is, at the time of writing and to the best of my knowledge, the first to use nanoparticles successfully to provide tumour-specific, live, *in vivo* fluorescent imaging

in a murine model of colorectal cancer. Although the *in vivo* study utilised just three animals in each arm, the lack of any detectable signal in the xenograft tumours when injected with control particles makes the result highly significant. Throughout this section of the project I have maintained a pragmatic approach, aware that proof of concept was required and therefore a balance was struck between optimising each individual variable exhaustively and making relatively rapid progress. I believe it has paid off and there is now a great deal of further work that can be carried out, including chemical optimisation of the nanoparticle and larger *in vivo* experiments with orthotopic primary and metastatic colorectal cancer murine models. Critically my work shows great promise for clinical translation in the context of intra-operative imaging since fluorescence is bright, the antibody is humanised and has been used in clinical trials previously, and silica nanoparticles appear to have favourable toxicity profiles. Furthermore, the technology is applicable to imaging any tissue or pathology using antibodies targeting appropriate specific biomarkers.

Chapter Seven

Summary

7 SUMMARY

I aimed to develop a fluorescent, tumour-specific, molecular imaging probe for colorectal cancer that could potentially be used for laparoscopic intra-operative staging, locate impalpable tumours and allow stratification of resection radicality. To achieve this I divided the project into a number of distinct steps that followed a logical progression from the identification of an appropriate target for colorectal cancer to the development and *in vivo* testing of a tumour-specific, molecular probe for real-time fluorescent imaging.

7.1 Future perspectives

7.1.1 Biomarker targeting

The biomarker component of this work was crucial. The performance of the system is completely dependent upon the ability to discriminate between normal colorectal tissue and tumour tissue, meaning that even the perfect fluorescent molecular bio-imaging probe will fail if the biomarker is unable to achieve this. I showed that CEA has a high sensitivity and specificity as a biomarker for differentiating colorectal cancer. The large variation in treatment responses in targeted therapy for colorectal cancer has led to a greater appreciation of the heterogeneity of the disease, with specific epi-genetic and tumour micro-environment factors allowing a personalised approach to therapy (Linnekamp et al., 2015). The identification and classification of colorectal cancer subtypes could allow even more accurate tumour localisation - the

antibody component could be selected from a 'catalogue' of available options based on this information.

Although I chose antibodies as the targeting mechanism for my project, there are other novel methods of targeting membrane-bound molecules. I made this decision in the interest of time and progress, particularly as anti-CEA antibodies are readily available. Antibody fragments can be synthesised from the variable region of an IgG molecule and have a number of theoretical advantages over whole antibodies including small size, lower immunogenicity and potentially increased sensitivity over whole antibodies (Holliger and Hudson, 2005). They were used in radioimmunoguided surgery (section 1.2.1), an application closely related to mine in that antibodies were used for intra-operative tumour detection. Roselli et al (Roselli et al., 1996) and Percivale et al (Percivale et al., 1998) produced F(ab')₂ anti-CEA antibodies, where the constant and variable portions of the antibody are split, and their result suggested a possible improvement in sensitivity. Biparatropic antibodies (BpAbs) were prepared by cross-linking reduced Fab fragments of two different anti-CEA antibodies, so that they were able to bind to two different epitopes of CEA, in an attempt to further increase the sensitivity, with some success (Robert et al., 1999, Kim et al., 2002, Kim et al., 2005). These techniques could be applied to my chosen anti-CEA antibody. Other alternatives include various antibody mimetics, which target antigens but are structurally different and much smaller than antibodies (6-20 kDa versus 150 kDa) (Qiu et al., 2007), and aptamers (Farokhzad et al., 2006), which are less immunogenic and cheaper to produce for clinical applications than antibodies.

It is conceivable that one of the above alternative targeting mechanisms could be chemically substituted for the antibody on my final nanoparticle, although this may behave differently and require full characterisation with *in vitro* and *in vivo* studies.

An alternative, non-targeted approach to intra-operative fluorescent imaging exploits the endogenous fluorescent properties of protoporphyrin IX, which tend to be increased in certain cancers. 5-aminolevulinic acid can be used as a photosensitiser to enhance this natural fluorescence and its potential is currently under investigation in colorectal cancer.

7.1.2 Targeted indocyanine green

I exploited a unique feature of protein-bound ICG, which allows it to produce cytoplasmic fluorescence if internalised, to produce a simple system that allowed CEA-specific fluorescent imaging in live colorectal cancer cells. The major advantage of this strategy is that both ICG and the anti-CEA antibody I used in my experiments are approved by the MHRA so translation into clinical trials could potentially be rapid. I would anticipate the next steps in this process as being:

1. A small *in vivo* study to confirm my *in vitro* results. I would deliver the ICG-anti-CEA and ICG-control antibodies systemically to a murine xenograft model of colorectal cancer.
2. A proof of concept, first-in-human clinical trial. This would require ethical approval and manufacture of the conjugate to a satisfactory standard. Early correspondence with the appropriate regulatory bodies suggest that, based on our findings, authorisation for this would be granted.

7.1.3 Targeted fluorescent nanoparticles

I synthesised a fluorescent, CEA-targeted, silica nanoparticle that allowed tumour-specific fluorescent labelling in three different cell lines *in vitro* and in a xenograft

mouse model of colorectal cancer using one of these cell lines. Although my *in vivo* study consisted of just six mice, the following three observations make the results very powerful. Firstly, tumour-specific fluorescence was observed in *all* of the mice injected with CEA-targeted nanoparticles and *none* of the mice injected with control nanoparticles, producing a highly significant result and suggesting a high sensitivity and adequate signal strength. Secondly, the only fluorescence observed in non-tumour tissue was hepatic, consistent with nanoparticle excretion, meaning the particles are highly specific at least in a murine host. Thirdly, the nanoparticles and fluorescent signal persisted at 72 hours following delivery, suggesting stability *in vivo*. These three findings are perhaps the most important for translating this work into a clinical trial. Given my pragmatic approach to the synthesis of the nanoparticle, there is undoubtedly potential for further optimisation of the nanoparticle, with probable resultant improvements in *in vivo* diagnostic performance. Following this, a larger study using an orthotopic murine model of colorectal cancer, possibly with a metastatic model alongside, would provide the necessary information to inform a first-in-man study. However, rigorous toxicology studies would be required prior to this.

7.1.3.1 Targeted nanoparticles *versus* targeted ICG

The nanoparticles caused membranous fluorescence whereas the ICG caused cytoplasmic fluorescence. The fluorescence fold difference for CEA-targeted compared with control-targeted was similar for both strategies (3.2 - 12.3) but the intensity of the fluorescent signal was greater for the nanoparticles, which would be crucial for tissue penetration in laparoscopic surgery. The fold difference was similar for LoVo cells but for LS174T cells it was higher for the nanoparticles (12.3 vs 5.2) and for HCT116 cells it was higher for ICG (12.2 vs 3.2). The relationship between

fluorescent labelling and cellular CEA concentration is unclear: a number of factors may influence this, including steric hindrance, particle size and rate of internalisation.

7.2 Limitations

If I were to redesign the experiments in this project with the benefit of hindsight I would make a number of changes. If possible, I would test the sensitivity and specificity of my biomarkers in a large cohort of matched normal and malignant lymph nodes in addition to primary tumours, to confirm my findings in section 3.3. Whilst identifying the primary tumour is important for laparoscopic resection of small early tumours, the intra-operative lymph node status is arguably the single most important factor in determining the type of resection performed.

The ideal model for testing the delivery and fate of anti-CEA antibodies would be to inject them intravenously prior to a patient undergoing colorectal cancer resection and ascertain whether they were present in the specimen post-operatively. This would be a more realistic model than the *ex vivo* study I conducted in 4.3.4 and more likely to produce conclusive results, but would require a full Clinical Trial of a Medicinal Product study. This would be costly, time-consuming and probably unnecessary given the successful use of anti-CEA and anti-TAG-72 for *in vivo* tumour targeting in the past (section 0). A simple animal study would have been a better compromise: a murine orthotopic colorectal cancer model could be injected with the antibodies and immunohistochemical analysis performed on the resected tumour.

7.3 Potential impact

A strength of this work is that my findings can be applied to other scientific areas outside the remit of this project. I have identified CEA as the most appropriate biomarker for *in vivo* colorectal cancer targeting and this could be exploited for targeted non-invasive imaging and for targeted chemotherapeutics. Similarly, by substituting the conjugated antibody, my nanoparticle could be used for intra-operative imaging in other cancers that express membrane-bound, tumour-specific biomarkers.

It is my hope that the body of work presented will make a major contribution to the exciting and rapidly expanding field of intraoperative diagnostics and image-guided surgery. In particular, I hope that I have contributed to the clinical need for a platform to discriminate malignant and normal tissue *in vivo*, and therefore to the ambition to make stratified surgery for colorectal cancer a reality.

References

8 REFERENCES

- ABDOLAH, M., SHAHBAZI-GAHROUEI, D., LAURENT, S., SERMEUS, C., FIROZIAN, F., ALLEN, B. J., BOUTRY, S. & MULLER, R. N. 2013. Synthesis and in vitro evaluation of MR molecular imaging probes using J591 mAb-conjugated SPIONs for specific detection of prostate cancer. *Contrast Media Mol Imaging*, 8, 175-84.
- ABRAHAM, N. S., YOUNG, J. M. & SOLOMON, M. J. 2004. Meta-analysis of short-term outcomes after laparoscopic resection for colorectal cancer. *British Journal of Surgery*, 91, 1111-1124.
- ACPGBI 2007. *Guidelines for the management of colorectal cancer*, Association of Surgeons of Great Britain and Ireland.
- ADAM, R., LUCIDI, V. & BISMUTH, H. 2004. Hepatic colorectal metastases: methods of improving resectability. *Surg Clin North Am*, 84, 659-71.
- ADAMS, E. J., GREEN, J. A., CLARK, A. H. & YOUNGSON, J. H. 1999. Comparison of different scoring systems for immunohistochemical staining. *Journal of Clinical Pathology*, 52, 75-77.
- AHLSKOG, J. K. J., SCHLIEMANN, C., MARLIND, J., QURESHI, U., AMMAR, A., PEDLEY, R. B. & NERI, D. 2009. Human monoclonal antibodies targeting carbonic anhydrase IX for the molecular imaging of hypoxic regions in solid tumours. *Br J Cancer*, 101, 645-657.
- AITKEN, D. R., HINKLE, G. H., THURSTON, M. O., TUTTLE, S. E., MARTIN, D. T., OLSEN, J., HAAGENSEN, D. E., JR., HOUCHESS, D. & MARTIN, E. W., JR. 1984. A gamma-detecting probe for radioimmune detection of CEA-producing tumors. Successful experimental use and clinical case report. *Dis Colon Rectum*, 27, 279-82.
- AJCC 2002. *AJCC staging handbook*, New York, Springer.
- ALANDER, J. T., KAARTINEN, I., LAAKSO, A., PATILA, T., SPILLMANN, T., TUCHIN, V. V., VENERMO, M. & VALISUO, P. 2012. A review of indocyanine green fluorescent imaging in surgery. *International journal of biomedical imaging*, 2012, 940585-940585.
- ALEXIS, F., PRIDGEN, E., MOLNAR, L. K. & FAROKHZAD, O. C. 2008. Factors affecting the clearance and biodistribution of polymeric nanoparticles. *Molecular Pharmaceutics*, 5, 505-515.
- ALLRED, D. C., CLARK, G. M., ELLEDGE, R., FUQUA, S. A. W., BROWN, R. W., CHAMNESS, G. C., OSBORNE, C. K. & MCGUIRE, W. L. 1993. ASSOCIATION OF P53 PROTEIN EXPRESSION WITH TUMOR-CELL PROLIFERATION RATE AND CLINICAL OUTCOME IN NODE-NEGATIVE BREAST-CANCER. *Journal of the National Cancer Institute*, 85, 200-206.
- AMAYA, H., TANIGAWA, N., LU, C., MATSUMURA, M., SHIMOMATSUYA, T., HORIUCHI, T. & MURAOKA, R. 1997. Association of vascular endothelial growth factor expression with tumor angiogenesis, survival and thymidine

phosphorylase/platelet-derived endothelial cell growth factor expression in human colorectal cancer. *Cancer Lett*, 119, 227-35.

ANDRE, T., BONI, C., NAVARRO, M., TABERNERO, J., HICKISH, T., TOPHAM, C., BONETTI, A., CLINGAN, P., BRIDGEWATER, J., RIVERA, F. & DE GRAMONT, A. 2009. Improved Overall Survival With Oxaliplatin, Fluorouracil, and Leucovorin As Adjuvant Treatment in Stage II or III Colon Cancer in the MOSAIC Trial. *Journal of Clinical Oncology*, 27, 3109-3116.

ANDRESEN, T. L., THOMPSON, D. H. & KAASGAARD, T. 2010. Enzyme-triggered nanomedicine: Drug release strategies in cancer therapy (Invited Review). *Molecular Membrane Biology*, 27, 353-363.

ARNOLD, M. W., SCHNEEBAUM, S., BERENS, A., PETTY, L., MOJZISIK, C., HINKLE, G. & MARTIN, E. W., JR. 1992. Intraoperative detection of colorectal cancer with radioimmunoguided surgery and CC49, a second-generation monoclonal antibody. *Ann Surg*, 216, 627-32.

ASHITATE, Y., STOCKDALE, A., CHOI, H. S., LAURENCE, R. G. & FRANGIONI, J. V. 2012. Real-Time Simultaneous Near-Infrared Fluorescence Imaging of Bile Duct and Arterial Anatomy. *Journal of Surgical Research*, In Press, Corrected Proof.

ASHRAF, S. Q., UMANA, P., MOESSNER, E., NTOUROUPI, T., BRUENKER, P., SCHMIDT, C., WILDING, J. L., MORTENSEN, N. J. & BODMER, W. F. 2009. Humanised IgG1 antibody variants targeting membrane-bound carcinoembryonic antigen by antibody-dependent cellular cytotoxicity and phagocytosis. *British Journal of Cancer*, 101, 1758-1768.

ASSOCIATION OF BREAST SURGERY AT BASO 2009. Surgical guidelines for the management of breast cancer. *Ejso*, 35, S1-S22.

ASTM 2012. E2456-06 Standard terminology relating to nanotechnology.

BAGWE, R. P. & KHILAR, K. C. 2000. Effects of intermicellar exchange rate on the formation of silver nanoparticles in reverse microemulsions of AOT. *Langmuir*, 16, 905-910.

BAGWE, R. P., MISHRA, B. K. & KHILAR, K. C. 1999. Effect of chain length of oxyethylene group on particle size and absorption spectra of silver nanoparticles prepared in non-ionic water-in-oil microemulsions. *Journal of Dispersion Science and Technology*, 20, 1569-1579.

BAGWE, R. P., YANG, C., HILLIARD, L. R. & TAN, W. 2004. Optimization of dye-doped silica nanoparticles prepared using a reverse microemulsion method. *Langmuir*, 20, 8336-42.

BALLOU, B., LAGERHOLM, B. C., ERNST, L. A., BRUCHEZ, M. P. & WAGGONER, A. S. 2003. Noninvasive Imaging of Quantum Dots in Mice. *Bioconjugate Chemistry*, 15, 79-86.

BARBET, J., BARDIES, M., BOURGEOIS, M., CHATAL, J.-F., CHEREL, M., DAVODEAU, F., FAIVRE-CHAUVET, A., GESTIN, J.-F. & KRAEBER-BODERE, F. 2012. Radiolabeled antibodies for cancer imaging and therapy. *Methods in molecular biology (Clifton, N.J.)*, 907, 681-97.

BEHR, T. M., BEHE, M., LOHR, M., SGOUROS, G., ANGERSTEIN, C., WEHRMANN, E., NEBENDAHL, K. & BECKER, W. 2000. Therapeutic advantages of

Auger electron- over beta-emitting radiometals or radioiodine when conjugated to internalizing antibodies. *European Journal of Nuclear Medicine*, 27, 753-765.

BELLONE, G., GRAMIGNI, C., VIZIO, B., MAURI, F. A., PRATI, A., SOLERIO, D., DUGHERA, L., RUFFINI, E., GASPARRI, G. & CAMANDONA, M. 2010. Abnormal expression of Endoglin and its receptor complex (TGF-beta 1 and TGF-beta receptor II) as early angiogenic switch indicator in premalignant lesions of the colon mucosa. *International Journal of Oncology*, 37, 1153-1165.

BEMBENEK, A., SCHNEIDER, U., GRETSCHER, S., FISCHER, J. & SCHLAG, P. M. 2005. Detection of lymph node micrometastases and isolated tumor cells in sentinel and nonsentinel lymph nodes of colon cancer patients. *World Journal of Surgery*, 29, 1172-1175.

BEMBENEK, A., STRING, A., GRETSCHER, S. & SCHLAG, P. M. 2008. Technique and clinical consequences of sentinel lymph node biopsy in colorectal cancer. *Surg Oncol*, 17, 183-93.

BERTELSEN, C. A., BOLS, B., INGEHOLM, P., JANSEN, J. E., NEUENSCHWANDER, A. U. & VILANDT, J. 2011. Can the quality of colonic surgery be improved by standardization of surgical technique with complete mesocolic excision? *Colorectal Disease*, 13, 1123-1129.

BHARGAVA, R., CHEN, B., KLIMSTRA, D. S., SALTZ, L. B., HEDVAT, C., TANG, L. H., GERALD, W., TERUYA-FELDSTEIN, J., PATY, P. B., QIN, J. & SHIA, J. 2006. Comparison of two antibodies for immunohistochemical evaluation of epidermal growth factor receptor expression in colorectal carcinomas, adenomas, and normal mucosa. *Cancer*, 106, 1857-1862.

BILCHIK, A., NISSAN, A., WAINBERG, Z., SHEN, P., MCCARTER, M., PROTIC, M., HOWARD, R., ELASHOFF, D., TYLER, J., PEOPLES, G. E. & STOJADINOVIC, A. 2010. Surgical Quality and Nodal Ultrastaging Is Associated With Long-Term Disease-Free Survival in Early Colorectal Cancer An Analysis of 2 International Multicenter Prospective Trials. *Annals of Surgery*, 252, 467-476.

BILCHIK, A. J., HOON, D. S. B., SAHA, S., TURNER, R. R., WIESE, D., DINOME, M., KOYANAGI, K., MCCARTER, M., SHEN, P., IDINGS, D., CHEN, S. L., GONZALEZ, M., ELASHOFF, D. & MORTON, D. L. 2007. Prognostic impact of micrometastases in colon cancer - Interim results of a prospective multicenter trial. *Annals of Surgery*, 246, 568-577.

BILCHIK, A. J., NORA, D., TOLLENAAR, R. A. E. M., VAN DE VELDE, C. J. H., WOOD, T., TURNER, R., MORTON, D. L. & HOON, D. S. B. 2002. Ultrastaging of early colon cancer using lymphatic mapping and molecular analysis. *European Journal of Cancer*, 38, 977-985.

BIPAT, S., GLAS, A. S., SLORS, F. J. M., ZWINDERMAN, A. H., BOSSUYT, P. M. M. & STOKER, J. 2004. Rectal cancer: Local staging and assessment of lymph node involvement with endoluminal US, CT, and MR imaging - A meta-analysis. *Radiology*, 232, 773-783.

BLECHINGER, J., BAUER, A. T., TORRANO, A. A., GORZELANNY, C., BRÄUCHLE, C. & SCHNEIDER, S. W. 2013. Uptake Kinetics and Nanotoxicity of Silica Nanoparticles Are Cell Type Dependent. *Small*, 9, 3970-3980.

- BOERMAN, O. C. & OYEN, W. J. G. 2011. Immuno-PET of Cancer: A Revival of Antibody Imaging. *Journal of Nuclear Medicine*, 52, 1171-1172.
- BOPPART, S. A., BOUMA, B. E., PITRIS, C., SOUTHERN, J. F., BREZINSKI, M. E. & FUJIMOTO, J. G. 1998. In vivo cellular optical coherence tomography imaging. *Nature Medicine*, 4, 861-865.
- BOPPART, S. A., DEUTSCH, T. F. & RATTNER, D. W. 1999. Optical imaging technology in minimally invasive surgery - Current status and future directions. *Surgical Endoscopy-Ultrasound and Interventional Techniques*, 13, 718-722.
- BOPPART, S. A., LUO, W., MARKS, D. L. & SINGLETARY, K. W. 2004. Optical coherence tomography: feasibility for basic research and image-guided surgery of breast cancer. *Breast Cancer Research and Treatment*, 84, 85-97.
- BRENNAN, D. J., O'CONNOR, D. P., REXHEPAJ, E., PONTEN, F. & GALLAGHER, W. M. 2010. Antibody-based proteomics: fast-tracking molecular diagnostics in oncology. *Nat Rev Cancer*, 10, 605-617.
- BROWN, G., RICHARDS, C. J., BOURNE, M. W., NEWCOMBE, R. G., RADCLIFFE, A. G., DALLIMORE, N. S. & WILLIAMS, G. T. 2003. Morphologic Predictors of Lymph Node Status in Rectal Cancer with Use of High-Spatial-Resolution MR Imaging with Histopathologic Comparison¹. *Radiology*, 227, 371-377.
- BRYAN, J. N., JIA, F., MOHSIN, H., SIVAGUMA, G., MILLER, W. H., ANDERSON, C. J., HENRY, C. J. & LEWIS, M. R. 2005. Comparative uptakes and biodistributions of internalizing vs. noninternalizing copper-64 radioimmunoconjugates in cell and animal models of colon cancer. *Nuclear Medicine and Biology*, 32, 851-858.
- BU, X. D., LI, N., TIAN, X. Q. & HUANG, P. L. 2011. Caco-2 and LS174T cell lines provide different models for studying mucin expression in colon cancer. *Tissue Cell*, 43, 201-6.
- BUCHSBAUM, D., LLOYD, R., JUNI, J., WOLLNER, I., BRUBAKER, P., HANNA, D., SPICKER, J., BURNS, F., STEPLEWSKI, Z., COLCHER, D. & ET AL. 1988. Localization and imaging of radiolabeled monoclonal antibodies against colorectal carcinoma in tumor-bearing nude mice. *Cancer Res*, 48, 4324-33.
- BUCKLEY, A. F. & KAKAR, S. 2007. Comparison of the dako EGFR pharmDx kit and zymed EGFR antibody for assessment of EGFR status in colorectal adenocarcinoma. *Applied Immunohistochemistry & Molecular Morphology*, 15, 305-309.
- BURNS, A., OW, H. & WIESNER, U. 2006. Fluorescent core-shell silica nanoparticles: towards "Lab on a Particle" architectures for nanobiotechnology. *Chemical Society Reviews*, 35, 1028-1042.
- BURROWS, F. J., DERBYSHIRE, E. J., TAZZARI, P. L., AMLOT, P., GAZDAR, A. F., KING, S. W., LETARTE, M., VITETTA, E. S. & THORPE, P. E. 1995. Up-regulation of endoglin on vascular endothelial cells in human solid tumors: implications for diagnosis and therapy. *Clinical Cancer Research*, 1, 1623-1634.
- CAHILL, R., ANDERSON, M., WANG, L., LINDSEY, I., CUNNINGHAM, C. & MORTENSEN, N. 2012. Near-infrared (NIR) laparoscopy for intraoperative lymphatic

road-mapping and sentinel node identification during definitive surgical resection of early-stage colorectal neoplasia. *Surgical Endoscopy*, 1-8.

CAHILL, R. A. 2010. Natural orifice transluminal endoscopic surgery--here and now. *Surgeon*, 8, 44-50.

CAHILL, R. A., ASAKUMA, M., TRUNZO, J., SCHOMISCH, S., WIESE, D., SAHA, S., DALLEMAGNE, B., MARKS, J. & MARESCAUX, J. 2010. Intraperitoneal virtual biopsy by fibered optical coherence tomography (OCT) at natural orifice transluminal endoscopic surgery (NOTES). *J Gastrointest Surg*, 14, 732-8.

CAHILL, R. A., LEROY, J. & MARESCAUX, J. 2009. Localized resection for colon cancer. *Surgical Oncology-Oxford*, 18, 334-342.

CAHILL, R. A., RIS, F. & MORTENSEN, N. J. 2011. Near-infrared laparoscopy for real-time intra-operative arterial and lymphatic perfusion imaging. *Colorectal Dis*, 13 Suppl 7, 12-7.

CAMP, R. L., CHARETTE, L. A. & RIMM, D. L. 2000. Validation of tissue microarray technology in breast carcinoma. *Laboratory Investigation*, 80, 1943-1949.

CARRASQUILLO, J. A., PANDIT-TASKAR, N., O'DONOGHUE, J. A., HUMM, J. L., ZANZONICO, P., SMITH-JONES, P. M., DIVGI, C. R., PRYMA, D. A., RUAN, S., KEMENY, N. E., FONG, Y., WONG, D., JAGGI, J. S., SCHEINBERG, D. A., GONEN, M., PANAGEAS, K. S., RITTER, G., JUNGBLUTH, A. A., OLD, L. J. & LARSON, S. M. 2011. 124I-huA33 Antibody PET of Colorectal Cancer. *Journal of Nuclear Medicine*, 52, 1173-1180.

CHEN, L., MCCRATE, J. M., LEE, J. C. & LI, H. 2011a. The role of surface charge on the uptake and biocompatibility of hydroxyapatite nanoparticles with osteoblast cells. *Nanotechnology*, 22, 105708.

CHEN, L., WANG, Y., CHENG, D., DOU, S., LIU, X., LIU, G., HNATOWICH, D. J. & RUSCKOWSKI, M. 2011b. Comparing two TAG-72 binding peptides previously identified by phage display as potential imaging agents. *Nuclear Medicine Communications*, 32, 920-924.

CHEN, L., WANG, Y., LIU, X., DOU, S., LIU, G., HNATOWICH, D. J. & RUSCKOWSKI, M. 2008. A new TAG-72 cancer marker peptide identified by phage display. *Cancer Letters*, 272, 122-132.

CHEN, S. L. & BILCHIK, A. J. 2006. More extensive nodal dissection improves survival for stages I to III of colon cancer - A population-based study. *Annals of Surgery*, 244, 602-610.

CHEN, W.-T., KHAZAIE, K., ZHANG, G., WEISSLEDER, R. & TUNG, C.-H. 2005. Detection of dysplastic intestinal adenomas using a fluorescent folate imaging probe. *Molecular imaging*, 4, 67-74.

CHEN, Y. & ZHANG, Y. 2011. Fluorescent quantification of amino groups on silica nanoparticle surfaces. *Analytical and Bioanalytical Chemistry*, 399, 2503-2509.

CHEN, Z. Z., CAI, L., DONG, X. M., TANG, H. W. & PANG, D. W. 2012. Covalent conjugation of avidin with dye-doped silica nanoparticles and preparation of high

density avidin nanoparticles as photostable bioprobes. *Biosens Bioelectron*, 37, 75-81.

CHENG, W. W. K. & ALLEN, T. M. 2008. Targeted delivery of anti-CD19 liposomal doxorubicin in B-cell lymphoma: A comparison of whole monoclonal antibody, Fab' fragments and single chain Fv. *Journal of Controlled Release*, 126, 50-58.

CHERUKURI, P. & CURLEY, S. A. 2010. Use of Nanoparticles for Targeted, Noninvasive Thermal Destruction of Malignant Cells. In: GROBMYER, S. R. & MOUDGIL, B. M. (eds.) *Cancer Nanotechnology: Methods and Protocols*.

CHESTER, K., PEDLEY, B., TOLNER, B., VIOLET, J., MAYER, A., SHARMA, S., BOXER, G., GREEN, A., NAGL, S. & BEGENT, R. 2004. Engineering antibodies for clinical applications in cancer. *Tumor Biology*, 25, 91-98.

CHO, M., LIM, K. & WOO, K. 2010. Facile synthesis and optical properties of colloidal silica microspheres encapsulating a quantum dot layer. *Chemical Communications*, 46, 5584-5586.

CHUNG, K. Y., SHIA, J., KEMENY, N. E., SHAH, M., SCHWARTZ, G. K., TSE, A., HAMILTON, A., PAN, D., SCHRAG, D., SCHWARTZ, L., KLIMSTRA, D. S., FRIDMAN, D., KELSEN, D. P. & SALTZ, L. B. 2005. Cetuximab shows activity in colorectal cancer patients with tumors that do not express the epidermal growth factor receptor by immunohistochemistry. *J Clin Oncol*, 23, 1803-10.

CLASPER, S., ROYSTON, D., BABAN, D., CAO, Y., EWERS, S., BUTZ, S., VESTWEBER, D. & JACKSON, D. G. 2008. A Novel Gene Expression Profile in Lymphatics Associated with Tumor Growth and Nodal Metastasis. *Cancer Research*, 68, 7293-7303.

COHEN, A. M., MARTIN, E. W., JR., LAVERY, I., DALY, J., SARDI, A., AITKEN, D., BLAND, K., MOJZISIK, C. & HINKLE, G. 1991. Radioimmunoguided surgery using iodine 125 B72.3 in patients with colorectal cancer. *Arch Surg*, 126, 349-52.

COLCHER, D., MILENIC, D., ROSELLI, M., RAUBITSCHKE, A., YARRANTON, G., KING, D., ADAIR, J., WHITTLE, N., BODMER, M. & SCHLOM, J. 1989. Characterization and Biodistribution of Recombinant and Recombinant/Chimeric Constructs of Monoclonal Antibody B72.3. *Cancer Research*, 49, 1738-1745.

COLOR STUDY GROUP 2005. Laparoscopic surgery versus open surgery for colon cancer: short-term outcomes of a randomised trial. *The Lancet Oncology*, 6, 477-484.

CONAGHAN, P. J., ASHRAF, S. Q., TYTHERLEIGH, M. G., WILDING, J. L., TCHILIAN, E., BICKNELL, D., MORTENSEN, N. J. & BODMER, W. F. 2008. Targeted killing of colorectal cancer cell lines by a humanised IgG1 monoclonal antibody that binds to membrane-bound carcinoembryonic antigen. *British Journal of Cancer*, 98, 1217-1225.

CONAGHAN, P. J., MAXWELL-ARMSTRONG, C. A., GARRIOCH, M. V., HONG, L. & ACHESON, A. G. 2010. Leaving a mark: the frequency and accuracy of tattooing prior to laparoscopic colorectal surgery. *Colorectal Disease*, no-no.

CRUK. 2007. *Bowel Cancer Statistics - Key Facts* [Online]. Available: <http://info.cancerresearchuk.org/cancerstats/types/bowel/>.

CRUK. 2010. *Bowel Cancer Statistics - Key Facts* [Online]. Available: <http://info.cancerresearchuk.org/cancerstats/types/bowel/incidence>.

CUNNINGHAM, D., HUMBLET, Y., SIENA, S., KHAYAT, D., BLEIBERG, H., SANTORO, A., BETS, D., MUESER, M., HARSTRICK, A., VERSLYPE, C., CHAU, I. & VAN CUTSEM, E. 2004. Cetuximab monotherapy and cetuximab plus irinotecan in irinotecan-refractory metastatic colorectal cancer. *N Engl J Med*, 351, 337-45.

DA PAZ, M. C., ALMEIDA SANTOS, M. D. F. M., SANTOS, C. M. B., DA SILVA, S. W., DE SOUZA, L. B., LIMA, E. C. D., SILVA, R. C., LUCCI, C. M., MORAIS, P. C., AZEVEDO, R. B. & LACAVALA, Z. G. M. 2012. Anti-CEA loaded maghemite nanoparticles as a theragnostic device for colorectal cancer. *International Journal of Nanomedicine*, 7, 5271-5282.

DARBANDI, M., URBAN, G. & KRÜGER, M. 2010. A facile synthesis method to silica coated CdSe/ZnS nanocomposites with tuneable size and optical properties. *Journal of Colloid and Interface Science*, 351, 30-34.

DAVIDSON, E. M., BARENHOLZ, Y., COHEN, R., HAROUTIUNIAN, S., KAGAN, L. & GINOSAR, Y. 2010. High-Dose Bupivacaine Remotely Loaded into Multivesicular Liposomes Demonstrates Slow Drug Release Without Systemic Toxic Plasma Concentrations After Subcutaneous Administration in Humans. *Anesthesia & Analgesia*, 110, 1018-1023.

DAWSON, P. M., BLAIR, S. D., BEGENT, R. H. J., KELLY, A. M. B., BOXER, G. M. & THEODOROU, N. A. 1991. THE VALUE OF RADIOIMMUNOGUIDED SURGERY IN 1ST AND 2ND LOOK LAPAROTOMY FOR COLORECTAL-CANCER. *Diseases of the Colon & Rectum*, 34, 217-222.

DE HAAS, R. J., ADAM, R., WICHERTS, D. A., AZOULAY, D., BISMUTH, H., VIBERT, E., SALLOUM, C., PERDIGAO, F., BENKABBOU, A. & CASTAING, D. 2010. Comparison of simultaneous or delayed liver surgery for limited synchronous colorectal metastases. *Br J Surg*, 97, 1279-89.

DE JONG, G. M., BLEICHRODT, R. P., EEK, A., OYEN, W. J. G., BOERMAN, O. C. & HENDRIKS, T. 2011. Experimental study of radioimmunotherapy versus chemotherapy for colorectal cancer. *British Journal of Surgery*, 98, 436-441.

DEARLING, J. L. J., FLYNN, A. A., QURESHI, U., WHITING, S., BOXER, G. M., GREEN, A., BEGENT, R. H. J. & PEDLEY, R. B. 2009. Localization of radiolabeled anti-CEA antibody in subcutaneous and intrahepatic colorectal xenografts: influence of tumor size and location within host organ on antibody uptake. *Nuclear Medicine and Biology*, 36, 883-894.

DES GUETZ, G., UZZAN, B., NICOLAS, P., CUCHERAT, M., DE MESTIER, P., MORERE, J. F., BREAU, J. L. & PERRET, G. 2007. Is sentinel lymph node mapping in colorectal cancer a future prognostic factor? A meta-analysis. *World Journal of Surgery*, 31, 1304-1312.

DIGHE, S., PURKAYASTHA, S., SWIFT, I., TEKKIS, P. P., DARZI, A., A'HERN, R. & BROWN, G. 2010. Diagnostic precision of CT in local staging of colon cancers: a meta-analysis. *Clinical Radiology*, 65, 708-719.

DIPALMA, J. A., BRADY, C. E., STEWART, D. L., KARLIN, D. A., MCKINNEY, M. K., CLEMENT, D. J., COLEMAN, T. W. & PIERSON, W. P. 1984. COMPARISON OF

COLON CLEANSING METHODS IN PREPARATION FOR COLONOSCOPY. *Gastroenterology*, 86, 856-860.

DOEVENDANS, P. A., DAEMEN, M. J., DE MUINCK, E. D. & SMITS, J. F. 1998. Cardiovascular phenotyping in mice. *Cardiovasc Res*, 39, 34-49.

DOORNEBOSCH, P. G., GOSSELINK, M. P., NEIJENHUIS, P. A., SCHOUTEN, W. R., TOLLENAAR, R. & DE GRAAF, E. J. R. 2008. Impact of transanal endoscopic microsurgery on functional outcome and quality of life. *International Journal of Colorectal Disease*, 23, 709-713.

DOORNEBOSCH, P. G., TOLLENAAR, R., GOSSELINK, M. P., STASSEN, L. P., DIJKHUIS, C. M., SCHOUTEN, W. R., DE VELDE, C. J. V. & DE GRAAF, E. J. R. 2007. Quality of life after transanal endoscopic microsurgery and total mesorectal excision in early rectal cancer. *Colorectal Disease*, 9, 553-558.

DUFF, S. E., JEZIOBSKA, M., ROSA, D. D., KUMAR, S., HABOUBI, N., SHERLOCK, D., O'DWYER, S. T. & JAYSON, G. C. 2006. Vascular endothelial growth factors and receptors in colorectal cancer: implications for anti-angiogenic therapy. *Eur J Cancer*, 42, 112-7.

DUKES, C. 1932. The classification of cancer of the rectum. *Journal of Pathological Bacteriology*, 35, 323.

ELIAS, J., MAUAD, F. M., MUGLIA, V. F., CAETANO, E., DOS SANTOS, J. S., KEMP, R., PAVAN, T. Z. & CARNEIRO, A. A. O. Intraoperative application of real-time tissue elastography for the diagnosis and staging of pancreatic tumours. Health Care Exchanges (PAHCE), 2011 Pan American, March 28 2011-April 1 2011 2011. 179-181.

ELIAS, J. M. 1990. Immunohistochemical methods. *Immunohistopathology: A Practical Approach to Diagnosis*. Chicago: ASCP Press.

FAHLGREN, A., BARANOV, V., FRANGSMYR, L., ZOUBIR, F., HAMMARSTROM, M. L. & HAMMARSTROM, S. 2003. Interferon-gamma tempers the expression of carcinoembryonic antigen family molecules in human colon cells: A possible role in innate mucosal defence. *Scandinavian Journal of Immunology*, 58, 628-641.

FAROKHZAD, O. C., KARP, J. M. & LANGER, R. 2006. Nanoparticle-aptamer bioconjugates for cancer targeting. *Expert Opinion on Drug Delivery*, 3, 311-324.

FAWCETT, T. 2006. An introduction to ROC analysis. *Pattern Recognition Letters*, 27, 861-874.

FENG, Q. Y., WEI, Y., ZHU, D. X., YE, L. C., LIN, Q., LI, W. X., QIN, X. Y., LYU, M. Z. & XU, J. M. 2014. Timing of Hepatectomy for Resectable Synchronous Colorectal Liver Metastases: For Whom Simultaneous Resection Is More Suitable - A Meta-Analysis. *Plos One*, 9.

FOERSCH, S., KIESSLICH, R., WALDNER, M. J., DELANEY, P., GALLE, P. R., NEURATH, M. F. & GOETZ, M. 2010. Molecular imaging of VEGF in gastrointestinal cancer in vivo using confocal laser endomicroscopy. *Gut*, 59, 1046-1055.

FOGH J, T. G. 1975. *Human Tumour Cells In Vivo*, New York, Plenum.

FOX, I. J., BROOKER, L. G. S., HESELTINE, D. W. & ESSEX, H. E. 1957. A TRICARBOCYANINE DYE FOR CONTINUOUS RECORDING OF DILUTION CURVES IN WHOLE BLOOD INDEPENDENT OF VARIATIONS IN BLOOD OXYGEN SATURATION. *Federation Proceedings*, 16, 39-39.

FU, C., LIU, T., LI, L., LIU, H., CHEN, D. & TANG, F. 2013. The absorption, distribution, excretion and toxicity of mesoporous silica nanoparticles in mice following different exposure routes. *Biomaterials*, 34, 2565-2575.

GABIZON, A., SHMEEDA, H. & BARENHOLZ, Y. 2003. Pharmacokinetics of pegylated liposomal doxorubicin - Review of animal and human studies. *Clinical Pharmacokinetics*, 42, 419-436.

GAO, X. H., CUI, Y. Y., LEVENSON, R. M., CHUNG, L. W. K. & NIE, S. M. 2004. In vivo cancer targeting and imaging with semiconductor quantum dots. *Nature Biotechnology*, 22, 969-976.

GAUR, U., SAHOO, S. K., DE, T. K., GHOSH, P. C., MAITRA, A. & GHOSH, P. K. 2000. Biodistribution of fluoresceinated dextran using novel nanoparticles evading reticuloendothelial system. *International Journal of Pharmaceutics*, 202, 1-10.

GEORGE, S., PRIMROSE, J., TALBOT, R., SMITH, J., MULLEE, M., BAILEY, D., DU BOULAY, C., JORDAN, H. & WESSEX COLORECTAL CANC, A. 2006. Will Rogers revisited: prospective observational study of survival of 3592 patients with colorectal cancer according to number of nodes examined by pathologists. *British Journal of Cancer*, 95, 841-847.

GIANTONIO, B. J., CATALANO, P. J., MEROPOL, N. J., O'DWYER, P. J., MITCHELL, E. P., ALBERTS, S. R., SCHWARTZ, M. A. & BENSON, A. B., 3RD 2007. Bevacizumab in combination with oxaliplatin, fluorouracil, and leucovorin (FOLFOX4) for previously treated metastatic colorectal cancer: results from the Eastern Cooperative Oncology Group Study E3200. *J Clin Oncol*, 25, 1539-44.

GOETZ, M., ZIEBART, A., FOERSCH, S., VIETH, M., WALDNER, M. J., DELANEY, P., GALLE, P. R., NEURATH, M. F. & KIESSLICH, R. 2010. In Vivo Molecular Imaging of Colorectal Cancer With Confocal Endomicroscopy by Targeting Epidermal Growth Factor Receptor. *Gastroenterology*, 138, 435-446.

GOODWIN, J. F. & CHOI, S.-Y. 1970. Quantification of Protein Solutions with Trinitrobenzenesulfonic Acid. *Clinical Chemistry*, 16, 24-31.

GRONE, J., DOEBLER, O., LODDENKEMPER, C., HOTZ, B., BUHR, H. J. & BHARGAVA, S. 2006. Robo1/Robo4: Differential expression of angiogenic markers in colorectal cancer. *Oncology Reports*, 15, 1437-1443.

GUBALA, V., LE GUEVEL, X., NOONEY, R., WILLIAMS, D. E. & MACCRAITH, B. 2010. A comparison of mono and multivalent linkers and their effect on the colloidal stability of nanoparticle and immunoassays performance. *Talanta*, 81, 1833-1839.

GUILLOU, P. J., QUIRKE, P., THORPE, H., WALKER, J., JAYNE, D. G., SMITH, A. M. H., HEATH, R. M. & BROWN, J. M. 2005. Short-term endpoints of conventional versus laparoscopic-assisted surgery in patients with colorectal cancer (MRC CLASICC trial): multicentre, randomised controlled trial. *The Lancet*, 365, 1718-1726.

- HABEEB, A. F. 1966. Determination of free amino groups in proteins by trinitrobenzenesulfonic acid. *Anal Biochem*, 14, 328-36.
- HAMMARSTRÖM, S. 1999. The carcinoembryonic antigen (CEA) family: structures, suggested functions and expression in normal and malignant tissues. *Seminars in Cancer Biology*, 9, 67-81.
- HAMY, A., CURTET, C., PAINEAU, J., CHATAL, J. F. & VISSET, J. 1995. Feasibility of radioimmunoguided surgery of colorectal carcinoma using indium 111 CEA specific antibody and simulation with a phantom using 2 steps targeting with bispecific antibody. *Tumori*, 81, 103-6.
- HANRAHAN, V., CURRIE, M. J., GUNNINGHAM, S. P., MORRIN, H. R., SCOTT, P. A., ROBINSON, B. A. & FOX, S. B. 2003. The angiogenic switch for vascular endothelial growth factor (VEGF)-A, VEGF-B, VEGF-C, and VEGF-D in the adenoma-carcinoma sequence during colorectal cancer progression. *J Pathol*, 200, 183-94.
- HARITOGLOU, C., GANDORFER, A., SCHAUMBERGER, M., TADAYONI, R. & KAMPIK, A. 2003. Light-absorbing properties and osmolarity of indocyanine-green depending on concentration and solvent medium. *Investigative Ophthalmology & Visual Science*, 44, 2722-2729.
- HASHIGUCHI, Y., HASE, K., UENO, H., MOCHIZUKI, H., SHINTO, E. & YAMAMOTO, J. 2011. Optimal margins and lymphadenectomy in colonic cancer surgery. *British Journal of Surgery*, 98, 1171-1178.
- HE, X., HU, C., GUO, Q., WANG, K., LI, Y. & SHANGGUAN, J. 2013. Rapid and ultrasensitive Salmonella Typhimurium quantification using positive dielectrophoresis driven on-line enrichment and fluorescent nanoparticles label. *Biosens Bioelectron*, 42, 460-6.
- HE, X., NIE, H., WANG, K., TAN, W., WU, X. & ZHANG, P. 2008. In vivo study of biodistribution and urinary excretion of surface-modified silica nanoparticles. *Anal Chem*, 80, 9597-603.
- HE, X., WANG, Y., WANG, K., CHEN, M. & CHEN, S. 2012. Fluorescence resonance energy transfer mediated large Stokes shifting near-infrared fluorescent silica nanoparticles for in vivo small-animal imaging. *Anal Chem*, 84, 9056-64.
- HEATH, C. H., DEEP, N. L., SWEENEY, L., ZINN, K. R. & ROSENTHAL, E. L. 2012. Use of Panitumumab-IRDye800 to Image Microscopic Head and Neck Cancer in an Orthotopic Surgical Model. *Annals of Surgical Oncology*, 19, 3879-3887.
- HEINE, M., NOLLAU, P., MASSLO, C., NIELSEN, P., FREUND, B., BRUNS, O. T., REIMER, R., HOHENBERG, H., PELDSCHUS, K., ITTRICH, H. & SCHUMACHER, U. 2011. Investigations on the Usefulness of CEACAMs as Potential Imaging Targets for Molecular Imaging Purposes. *PLoS ONE*, 6, e28030.
- HEITSCH, A. T., SMITH, D. K., PATEL, R. E., RESS, D. & KORGEL, B. A. 2008. Multifunctional Particles: Magnetic Nanocrystals and Gold Nanorods Coated with Fluorescent Dye-Doped Silica Shells. *J Solid State Chem*, 181, 1590-1599.
- HERMANEK, P., HUTTER, R. V. P., SOBIN, L. H. & WITTEKIND, C. 1999. Classification of isolated tumor cells and micrometastasis. *Cancer*, 86, 2668-2673.

HILDERBRAND, S. A. & WEISSLEDER, R. 2010. Near-infrared fluorescence: application to in vivo molecular imaging. *Current Opinion in Chemical Biology*, 14, 71-79.

HOGAN, A. M. & WINTER, D. C. 2009. Complete mesocolic excision (CME): A "novel" concept? *Journal of Surgical Oncology*, 100, 182-183.

HOHENBERGER, W., WEBER, K., MATZEL, K., PAPADOPOULOS, T. & MERKEL, S. 2009. Standardized surgery for colonic cancer: complete mesocolic excision and central ligation - technical notes and outcome. *Colorectal Disease*, 11, 354-364.

HOLLIGER, P. & HUDSON, P. J. 2005. Engineered antibody fragments and the rise of single domains. *Nature Biotechnology*, 23, 1126-1136.

HOLZ, F. G., BELLMANN, C., ROHRSCHEIDER, K., BURK, R. O. W. & VOLCKER, H. E. 1998. Simultaneous confocal scanning laser fluorescein and indocyanine green angiography. *American Journal of Ophthalmology*, 125, 227-236.

HUANG, D., SWANSON, E. A., LIN, C. P., SCHUMAN, J. S., STINSON, W. G., CHANG, W., HEE, M. R., FLOTTE, T., GREGORY, K., PULIAFITO, C. A. & FUJIMOTO, J. G. 1991. OPTICAL COHERENCE TOMOGRAPHY. *Science*, 254, 1178-1181.

HUANG, S., LI, R., QU, Y., SHEN, J. & LIU, J. 2009. Fluorescent Biological Label for Recognizing Human Ovarian Tumor Cells Based on Fluorescent Nanoparticles. *Journal of Fluorescence*, 19, 1095-1101.

HUN, X. & ZHANG, Z. 2007. Fluoroimmunoassay for tumor necrosis factor-alpha in human serum using Ru(bpy)(3)Cl(2)-doped fluorescent silica nanoparticles as labels. *Talanta*, 73, 366-71.

HUTTEMAN, M., CHOI, H. S., MIEOG, J. S., VAN DER VORST, J. R., ASHITATE, Y., KUPPEN, P. J., VAN GRONINGEN, M. C., LOWIK, C. W., SMIT, V. T., VAN DE VELDE, C. J., FRANGIONI, J. V. & VAHRMEIJER, A. L. 2010. Clinical Translation of Ex Vivo Sentinel Lymph Node Mapping for Colorectal Cancer Using Invisible Near-Infrared Fluorescence Light. *Ann Surg Oncol*.

HUTTEMAN, M., CHOI, H. S., MIEOG, J. S. D., VAN DER VORST, J. R., ASHITATE, Y., KUPPEN, P. J. K., VAN GRONINGEN, M. C., LOWIK, C. W. G. M., SMIT, V. T. H. B. M., VAN DE VELDE, C. J. H., FRANGIONI, J. V. & VAHRMEIJER, A. L. 2011. Clinical Translation of Ex Vivo Sentinel Lymph Node Mapping for Colorectal Cancer Using Invisible Near-Infrared Fluorescence Light. *Annals of Surgical Oncology*, 18, 1006-1014.

IDDINGS, D., AHMAD, A., ELASHOFF, D. & BILCHIK, A. 2006. The prognostic effect of micrometastases in previously staged lymph node negative (N0) colorectal carcinoma: A meta-analysis. *Annals of Surgical Oncology*, 13, 1386-1392.

ILIUM, L., HUNNEYBALL, I. M. & DAVIS, S. S. 1986. The effect of hydrophilic coatings on the uptake of colloidal particles by the liver and by peritoneal macrophages. *International Journal of Pharmaceutics*, 29, 53-65.

INOUE, Y., TAKAHASHI, M., ARITA, J., AOKI, T., HASEGAWA, K., BECK, Y., MAKUUCHI, M. & KOKUDO, N. 2010. Intra-operative freehand real-time

elastography for small focal liver lesions: "Visual palpation" for non-palpable tumors. *Surgery*, 148, 1000-1011.

ISHIZAWA, T., TAMURA, S., MASUDA, K., AOKI, T., HASEGAWA, K., IMAMURA, H., BECK, Y. & KOKUDO, N. 2009. Intraoperative fluorescent cholangiography using indocyanine green: a biliary road map for safe surgery. *Journal of the American College of Surgeons*, 208, e1-4.

ISO. 2008. *ISO/TS 27687:2008 Nanotechnologies - Terminology and definitions for nano objects - nanoparticle, nanofibre and nanoplate*. [Online]. Available: http://www.iso.org/iso/iso_catalogue.htm.

ITO, S., MUGURUMA, N., KAKEHASHI, Y., HAYASHI, S., OKAMURA, S., SHIBATA, H., OKAHISA, T., KANAMORI, M., SHIBAMURA, S., TAKESAKO, K., NOZAWA, M., ISHIDA, K. & SHIGA, M. 1995. DEVELOPMENT OF FLUORESCENCE-EMITTING ANTIBODY LABELING SUBSTANCE BY NEAR-INFRARED RAY EXCITATION. *Bioorganic & Medicinal Chemistry Letters*, 5, 2689-2694.

ITOH, A., UENO, E., TOHNO, E., KAMMA, H., TAKAHASHI, H., SHIINA, T., YAMAKAWA, M. & MATSUMURA, T. 2006. Breast disease: Clinical application of US elastography for diagnosis. *Radiology*, 239, 341-350.

JACOBS, M., VERDEJA, J. C. & GOLDSTEIN, H. S. 1991. Minimally invasive colon resection (laparoscopic colectomy). *Surgical laparoscopy & endoscopy*, 1, 144-50.

JAMIESON, J. K. & DOBSON, J. F. 1909. The lymphatics of the colon - With special reference to the operative treatment of cancer of the colon. *Annals of Surgery*, 50, 1077-1090.

JANTSCHKEFF, P., TERRACCIANO, L., LOWY, A., GLATZ-KRIEGER, K., GRUNERT, F., MICHEEL, B., BRÜMMER, J., LAFFER, U., METZGER, U., HERRMANN, R. & ROCHLITZ, C. 2003. Expression of CEACAM6 in Resectable Colorectal Cancer: A Factor of Independent Prognostic Significance. *Journal of Clinical Oncology*, 21, 3638-3646.

JAYNE, D. G., THORPE, H. C., COPELAND, J., QUIRKE, P., BROWN, J. M. & GUILLOU, P. J. 2010. Five-year follow-up of the Medical Research Council CLASICC trial of laparoscopically assisted versus open surgery for colorectal cancer. *British Journal of Surgery*, 97, 1638-1645.

JEONG, M.-H., KIM, K., KIM, E.-M., CHEONG, S.-J., LEE, C.-M., JEONG, H.-J., KIM, D. W., LIM, S. T., SOHN, M.-H. & CHUNG, J. 2012. In vivo and in vitro evaluation of Cy5.5 conjugated epidermal growth factor receptor binding peptide. *Nuclear Medicine and Biology*, 39, 805-812.

JIE, G. F., WANG, L. & ZHANG, S. S. 2011. Magnetic Electrochemiluminescent Fe₃O₄/CdSe-CdS Nanoparticle/Polyelectrolyte Nanocomposite for Highly Efficient Immunosensing of a Cancer Biomarker. *Chemistry-a European Journal*, 17, 641-648.

JIWAJI, M., SANDISON, M. E., REBOUD, J., STEVENSON, R., DALY, R.,

BARKESS, G., FAULDS, K., KOLCH, W., GRAHAM, D., GIROLAMI, M. A., COOPER, J. M. & PITT, A. R. 2014. Quantification of functionalised gold nanoparticle-targeted knockdown of gene expression in HeLa cells. *PLoS One*, 9, e99458.

JOHNSON, V. G., SCHLOM, J., PATERSON, A. J., BENNETT, J., MAGNANI, J. L. & COLCHER, D. 1986. Analysis of a Human Tumor-associated Glycoprotein (TAG-72) Identified by Monoclonal Antibody B72.3. *Cancer Research*, 46, 850-857.

JONKER, D. J., O'CALLAGHAN, C. J., KARAPETIS, C. S., ZALCBERG, J. R., TU, D., AU, H.-J., BERRY, S. R., KRAHN, M., PRICE, T., SIMES, R. J., TEBBUTT, N. C., VAN HAZEL, G., WIERZBICKI, R., LANGER, C. & MOORE, M. J. 2007. Cetuximab for the treatment of colorectal cancer. *New England Journal of Medicine*, 357, 2040-2048.

JONKMAN, J., BROWN, C. M. & COLE, R. W. 2014. Quantitative confocal microscopy: beyond a pretty picture. *Methods Cell Biol*, 123, 113-34.

JOOSTEN, J. J. A., STROBBE, L. J. A., WAUTERS, C. A. P., PRUSZCZYNSKI, M., WOBBS, T. & RUERS, T. J. M. 1999. Intraoperative lymphatic mapping and the sentinel node concept in colorectal carcinoma. *British Journal of Surgery*, 86, 482-486.

KAASGAARD, T. & ANDRESEN, T. L. 2010. Liposomal cancer therapy: exploiting tumor characteristics. *Expert Opinion on Drug Delivery*, 7, 225-243.

KALYANASUNDARAM, K. 1982. Photophysics, photochemistry and solar energy conversion with tris(bipyridyl)ruthenium(II) and its analogues. *Coordination Chemistry Reviews*, 46, 159-244.

KAMPHUIS, M. M. J., JOHNSTON, A. P. R., SUCH, G. K., DAM, H. H., EVANS, R. A., SCOTT, A. M., NICE, E. C., HEATH, J. K. & CARUSO, F. 2010. Targeting of Cancer Cells Using Click-Functionalized Polymer Capsules. *Journal of the American Chemical Society*, 132, 15881-15883.

KATO, K., SUGIMOTO, H., KANAZUMI, N., NOMOTO, S., TAKEDA, S. & NAKAO, A. 2008. Intra-operative application of real-time tissue elastography for the diagnosis of liver tumours. *Liver International*, 28, 1264-1271.

KAUSHAL, S., MCELROY, M. K., LUIKEN, G. A., TALAMINI, M. A., MOOSSA, A. R., HOFFMAN, R. M. & BOUVET, M. 2008. Fluorophore-conjugated anti-CEA Antibody for the Intraoperative Imaging of Pancreatic and Colorectal Cancer. *Journal of Gastrointestinal Surgery*, 12, 1938-1950.

KENT, S. P., RYAN, K. H. & SIEGEL, A. L. 1978. STERIC HINDRANCE AS A FACTOR IN REACTION OF LABELED ANTIBODY WITH CELL-SURFACE ANTIGENIC DETERMINANTS. *Journal of Histochemistry & Cytochemistry*, 26, 618-621.

KIM, J. C., ROH, S. A., KOO, K. H., CHO, Y. K., KIM, H. C., YU, C. S., OH, S. J., RYU, J. S., BICKNELL, D. C. & BODMER, W. F. 2005. Preclinical application of radioimmunoguided surgery using anti-carcinoembryonic antigen biparatopic antibody in the colon cancer. *Eur Surg Res*, 37, 36-44.

KIM, J. C., ROH, S. A., KOO, K. H., RYU, J. H., HONG, H. K., OH, S. J., RYU, J. S., KIM, H. J. & BODMER, W. F. 2002. Enhancement of colorectal tumor targeting using a novel biparatopic monoclonal antibody against carcinoembryonic antigen in experimental radioimmunoguided surgery. *Int J Cancer*, 97, 542-7.

- KIM, N. K., KIM, M. J., PARK, J. K., PARK, S. I. & MIN, J. S. 2000. Preoperative staging of rectal cancer with MRI: Accuracy and clinical usefulness. *Annals of Surgical Oncology*, 7, 732-737.
- KING, D. S., FIELDS, C. G. & FIELDS, G. B. 1990. A CLEAVAGE METHOD WHICH MINIMIZES SIDE REACTIONS FOLLOWING FMOC SOLID-PHASE PEPTIDE-SYNTHESIS. *International Journal of Peptide and Protein Research*, 36, 255-266.
- KOIVISTO, T. & SALASPURO, M. 1997. Effects of Acetaldehyde on Brush Border Enzyme Activities in Human Colon Adenocarcinoma Cell Line Caco-2. *Alcoholism: Clinical and Experimental Research*, 21, 1599-1605.
- KONIG, K., SCHEIPERS, U., PESAVENTO, A., LORENZ, A., ERMERT, H. & SENGE, T. 2005. Initial experiences with real-time elastography guided biopsies of the prostate. *Journal of Urology*, 174, 115-117.
- KOPANSKY, E., SHAMAY, Y. & DAVID, A. 2011. Peptide-directed HPMAC copolymer-doxorubicin conjugates as targeted therapeutics for colorectal cancer. *Journal of Drug Targeting*, 19, 933-943.
- KOPPE, M. J., BLEICHRODT, R. P., OYEN, W. J. G. & BOERMAN, O. C. 2005. Radioimmunotherapy and colorectal cancer. *British Journal of Surgery*, 92, 264-276.
- KORETZ, K., SCHLAG, P. & MOLLER, P. 1990. EXPRESSION OF EPIDERMAL GROWTH-FACTOR RECEPTOR IN NORMAL COLORECTAL MUCOSA, ADENOMA, AND CARCINOMA. *Virchows Archiv a-Pathological Anatomy and Histopathology*, 416, 343-349.
- KUANG, Y., WANG, F., CORN, D. J., TIAN, H. & LEE, Z. 2014. In vitro characterization of uptake mechanism of L-[methyl-(3)H]-methionine in hepatocellular carcinoma. *Mol Imaging Biol*, 16, 459-68.
- KUMAR, S., AARON, J. & SOKOLOV, K. 2008. Directional conjugation of antibodies to nanoparticles for synthesis of multiplexed optical contrast agents with both delivery and targeting moieties. *Nature Protocols*, 3, 314-320.
- KUSANO, M., TAJIMA, Y., YAMAZAKI, K., KATO, M., WATANABE, M. & MIWA, M. 2008. Sentinel node mapping guided by indocyanine green fluorescence imaging: A new method for sentinel node navigation surgery in gastrointestinal cancer. *Digestive Surgery*, 25, 103-108.
- LANDSMAN, M. L. J., KWANT, G., MOOK, G. A. & ZIJLSTRA, W. G. 1976. LIGHT-ABSORBING PROPERTIES, STABILITY, AND SPECTRAL STABILIZATION OF INDOCYANINE GREEN. *Journal of Applied Physiology*, 40, 575-583.
- LANE, D. M., EAGLE, K. F., BEGENT, R. H. J., HOPESTONE, L. D., GREEN, A. J., CASEY, J. L., KEEP, P. A., KELLY, A. M. B., LEDERMANN, J. A., GLASER, M. G. & HILSON, A. J. W. 1994. RADIOIMMUNOTHERAPY OF METASTATIC COLORECTAL TUMORS WITH IODINE-131-LABELED ANTIBODY TO CARCINOEMBRYONIC ANTIGEN - PHASE I/II STUDY WITH COMPARATIVE BIODISTRIBUTION OF INTACT AND F(AB')(2) ANTIBODIES. *British Journal of Cancer*, 70, 521-525.
- LEE, J. C., WANG, S. T., CHOW, N. H. & YANG, H. B. 2002. Investigation of the prognostic value of coexpressed erbB family members for the survival of colorectal cancer patients after curative surgery. *European Journal of Cancer*, 38, 1065-1071.

- LEEMAN, M. F., MCKAY, J. A. & MURRAY, G. I. 2002. Matrix metalloproteinase 13 activity is associated with poor prognosis in colorectal cancer. *Journal of Clinical Pathology*, 55, 758-762.
- LEWINSKI, N., COLVIN, V. & DREZEK, R. 2008. Cytotoxicity of nanoparticles. *Small*, 4, 26-49.
- LI, C. G., HAMPSON, I. N., HAMPSON, L., KUMAR, P., BERNABEU, C. & KUMAR, S. 2000. CD105 antagonizes the inhibitory signaling of transforming growth factor beta 1 on human vascular endothelial cells. *Faseb Journal*, 14, 55-64.
- LI, J. J. E., MURALIKRISHNAN, S., NG, C.-T., YUNG, L.-Y. L. & BAY, B.-H. 2010. Nanoparticle-induced pulmonary toxicity. *Experimental Biology and Medicine*, 235, 1025-1033.
- LI, Z., BARNES, J. C., BOSOY, A., STODDART, J. F. & ZINK, J. I. 2012. Mesoporous silica nanoparticles in biomedical applications. *Chemical Society Reviews*, 41, 2590-2605.
- LIAN, T. & HO, R. J. Y. 2001. Trends and developments in liposome drug delivery systems. *Journal of Pharmaceutical Sciences*, 90, 667-680.
- LIAN, W., LITHERLAND, S. A., BADRANE, H., TAN, W. H., WU, D. H., BAKER, H. V., GULIG, P. A., LIM, D. V. & JIN, S. G. 2004. Ultrasensitive detection of biomolecules with fluorescent dye-doped nanoparticles. *Analytical Biochemistry*, 334, 135-144.
- LINNEKAMP, J. F., WANG, X., MEDEMA, J. P. & VERMEULEN, L. 2015. Colorectal cancer heterogeneity and targeted therapy: a case for molecular disease subtypes. *Cancer Res*, 75, 245-9.
- LIU, S., ZHANG, H.-L., LIU, T.-C., LIU, B., CAO, Y.-C., HUANG, Z.-L., ZHAO, Y.-D. & LUO, Q.-M. 2007. Optimization of the methods for introduction of amine groups onto the silica nanoparticle surface. *Journal of Biomedical Materials Research Part A*, 80A, 752-757.
- LOGAN, R. F. A., PATNICK, J., NICKERSON, C., COLEMAN, L., RUTTER, M. D. & VON WAGNER, C. 2011. Outcomes of the Bowel Cancer Screening Programme (BCSP) in England after the first 1 million tests. *Gut*.
- LOMBARDI, D. P., GERADTS, J., FOLEY, J. F., CHIAO, C., LAMB, P. W. & BARRETT, J. C. 1999. Loss of KAI1 Expression in the Progression of Colorectal Cancer. *Cancer Research*, 59, 5724-5731.
- LOWRY, O. H., ROSEBROUGH, N. J., FARR, A. L. & RANDALL, R. J. 1951. PROTEIN MEASUREMENT WITH THE FOLIN PHENOL REAGENT. *Journal of Biological Chemistry*, 193, 265-275.
- LU, B., SMYTH, M. R. & OKENNEDY, R. 1996. Oriented immobilization of antibodies and its applications in immunoassays and immunosensors. *Analyst*, 121, R29-R32.
- LYALL, M. S., DUNDAS, S. R., CURRAN, S. & MURRAY, G. I. 2006. Profiling markers of prognosis in colorectal cancer. *Clinical Cancer Research*, 12, 1184-1191.

LYSHCHIK, A., HIGASHI, T., ASATO, R., TANAKA, S., ITO, J., MAI, J. J., PELLOT-BARAKAT, C., INSANA, M. F., BRILL, A. B., SAGA, T., HIRAOKA, M. & TOGASHI, K. 2005. Thyroid gland tumor diagnosis at US elastography. *Radiology*, 237, 202-211.

MALIK, R., QIAN, S. & LAW, B. 2011. Design and synthesis of a near-infrared fluorescent nanofiber precursor for detecting cell-secreted urokinase activity. *Anal Biochem*, 412, 26-33.

MANK, A. J. G. & YEUNG, E. S. 1995. DIODE LASER-INDUCED FLUORESCENCE DETECTION IN CAPILLARY ELECTROPHORESIS AFTER PRECOLUMN DERIVATIZATION OF AMINO-ACIDS AND SMALL PEPTIDES. *Journal of Chromatography A*, 708, 309-321.

MARAQA, L., CUMMINGS, M., PETER, M. B., SHAABAN, A. M., HORGAN, K., HANBY, A. M. & SPEIRS, V. 2008. Carcinoembryonic Antigen Cell Adhesion Molecule 6 Predicts Breast Cancer Recurrence following Adjuvant Tamoxifen. *Clinical Cancer Research*, 14, 405-411.

MARIANICOSTANTINI, R., MURARO, R., FICARI, F., VALLI, C., BEI, R., TONELLI, F., CARAMIA, F. & FRATI, L. 1991. IMMUNOHISTOCHEMICAL EVIDENCE OF IMMUNE-RESPONSES TO TUMOR-ASSOCIATED ANTIGENS IN LYMPH-NODES OF COLON-CARCINOMA PATIENTS. *Cancer*, 67, 2880-2886.

MARQUIS, B. J., LOVE, S. A., BRAUN, K. L. & HAYNES, C. L. 2009. Analytical methods to assess nanoparticle toxicity. *Analyst*, 134, 425-439.

MARSDEN, J. R., NEWTON-BISHOP, J. A., BURROWS, L., COOK, M., CORRIE, P. G., COX, N. H., GORE, M. E., LORIGAN, P., MACKIE, R., NATHAN, P., PEACH, H., POWELL, B. & WALKER, C. 2010. Revised UK guidelines for the management of cutaneous melanoma 2010. *British Journal of Dermatology*, 163, 238-256.

MATSUI, A., WINER, J. H., LAURENCE, R. G. & FRANGIONI, J. V. 2011. Predicting the survival of experimental ischaemic small bowel using intraoperative near-infrared fluorescence angiography. *British Journal of Surgery*, 98, 1725-1734.

MATSUMURA, Y. & MAEDA, H. 1986. A New Concept for Macromolecular Therapeutics in Cancer Chemotherapy: Mechanism of Tumor-tropic Accumulation of Proteins and the Antitumor Agent Smancs. *Cancer Research*, 46, 6387-6392.

MAYER, A., TSIOMPANOU, E., O'MALLEY, D., BOXER, G. M., BHATIA, J., FLYNN, A. A., CHESTER, K. A., DAVIDSON, B. R., LEWIS, A. A. M., WINSLET, M. C., DHILLON, A. P., HILSON, A. J. W. & BEGENT, R. H. J. 2000. Radioimmunoguided Surgery in Colorectal Cancer Using a Genetically Engineered Anti-CEA Single-Chain Fv Antibody. *Clinical Cancer Research*, 6, 1711-1719.

MAYER-KUCKUK, P., GADE, T. P. F., BUCHANAN, I. M., DOUBROVIN, M., AGEYEVA, L., BERTINO, J. R., BOSKEY, A. L., BLASBERG, R. G., KOUTCHER, J. A. & BANERJEE, D. 2005. High-Resolution Imaging of Bone Precursor Cells Within the Intact Bone Marrow Cavity of Living Mice. *Mol Ther*, 12, 33-41.

MCCARTY, K. S. J., SZABO, E., FLOWERS, J. L., COX, E. B., LEIGHT, G. S., MILLER, L., KONRATH, J., SOPER, J. T., BUDWIT, D. A. & ET AL. 1986. USE OF A MONOCLONAL ANTI-ESTROGEN RECEPTOR ANTIBODY IN THE

IMMUNOHISTOCHEMICAL EVALUATION OF HUMAN TUMORS. *Cancer Research*, 46, 4244S-4248S.

MCCORMACK, D., AL-SHAER, M., GOLDSCHMIDT, B. S., DALE, P. S., HENRY, C., PAPAGEORGIO, C., BHATTACHARYYA, K. & VIATOR, J. A. 2009. Photoacoustic detection of melanoma micrometastasis in sentinel lymph nodes. *Journal of biomechanical engineering*, 131, 074519.

MCLAUGHLIN, R. A., SCOLARO, L., ROBBINS, P., HAMZA, S., SAUNDERS, C. & SAMPSON, D. D. 2010. Imaging of human lymph nodes using optical coherence tomography: potential for staging cancer. *Cancer Res*, 70, 2579-84.

MELLA, J., BIFFIN, A., RADCLIFFE, A. G., STAMATAKIS, J. D. & STEELE, R. J. C. 1997. Population-based audit of colorectal cancer management in two UK health regions. *British Journal of Surgery*, 84, 1731-1736.

MELLER, B., RAVE-FRAENCK, M., BREUNIG, C., SCHIRMER, M., BAEHRE, M., NADROWITZ, R., LIERSCH, T. & MELLER, J. 2011. Novel Carcinoembryonic-Antigen-(CEA)-Specific Pretargeting System to Assess Tumor Cell Viability after Irradiation of Colorectal Cancer Cells. *Strahlentherapie Und Onkologie*, 187, 120-126.

MENG, H., XUE, M., XIA, T., JI, Z., TARN, D. Y., ZINK, J. I. & NEL, A. E. 2011. Use of size and a copolymer design feature to improve the biodistribution and the enhanced permeability and retention effect of doxorubicin-loaded mesoporous silica nanoparticles in a murine xenograft tumor model. *ACS Nano*, 5, 4131-44.

MEREDITH, R. F., KHAZAELI, M. B., PLOTT, W. E., GRIZZLE, W. E., LIU, T., SCHLOM, J., RUSSELL, C. D., WHEELER, R. H. & LOBUGLIO, A. F. 1996. Phase II study of dual ¹³¹I-labeled monoclonal antibody therapy with interferon in patients with metastatic colorectal cancer. *Clinical Cancer Research*, 2, 1811-1818.

MEYER, T., GAYA, A. M., DANCEY, G., STRATFORD, M. R. L., OTHMAN, S., SHARMA, S. K., WELLSTED, D., TAYLOR, N. J., STIRLING, J. J., POUPARD, L., FOLKES, L. K., CHAN, P.-S., PEDLEY, R. B., CHESTER, K. A., OWEN, K., VIOLET, J. A., MALARODA, A., GREEN, A. J., BUSCOMBE, J., PADHANI, A. R., RUSTIN, G. J. & BEGENT, R. H. 2009. A Phase I Trial of Radioimmunotherapy with ¹³¹I-A5B7 Anti-CEA Antibody in Combination with Combretastatin-A4-Phosphate in Advanced Gastrointestinal Carcinomas. *Clinical Cancer Research*, 15, 4484-4492.

MICHALET, X., PINAUD, F. F., BENTOLILA, L. A., TSAY, J. M., DOOSE, S., LI, J. J., SUNDARESAN, G., WU, A. M., GAMBHIR, S. S. & WEISS, S. 2005. Quantum dots for live cells, in vivo imaging, and diagnostics. *Science*, 307, 538-544.

MICHELSEN, A. J., O'SULLIVAN, J. N. & RYAN, E. J. 2012. Tumor conditioned media from colorectal cancer patients inhibits dendritic cell maturation. *Oncoimmunology*, 1, 751-753.

MILLER, C. R., BONDURANT, B., MCLEAN, S. D., MCGOVERN, K. A. & O'BRIEN, D. F. 1998. Liposome-cell interactions in vitro: Effect of liposome surface charge on the binding and endocytosis of conventional and sterically stabilized liposomes. *Biochemistry*, 37, 12875-12883.

- MOGHIMI, S. M., HUNTER, A. C. & ANDRESEN, T. L. 2012. Factors Controlling Nanoparticle Pharmacokinetics: An Integrated Analysis and Perspective. *Annual Review of Pharmacology and Toxicology*, Vol 52, 52, 481-503.
- MONICI, M. 2005. Cell and tissue autofluorescence research and diagnostic applications. In: EL-GEWELY, M. R. (ed.) *Biotechnology Annual Review*. Elsevier.
- MUGURUMA, N., ITO, S., BANDO, T., TAOKA, S., KUSAKA, Y., HAYASHI, S., ICHIKAWA, S., MATSUNAGA, Y., TADA, Y., OKAMURA, S., II, K., IMAIZUMI, K., NAKAMURA, K., TAKESAKO, K. & SHIBAMURA, S. 1999. Labeled carcinoembryonic antigen antibodies excitable by infrared rays: A novel diagnostic method for micro cancers in the digestive tract. *Internal Medicine*, 38, 537-542.
- MUGURUMA, N., ITO, S., HAYASHI, S., TAOKA, S., KAKEHASHI, H., II, K., SHIBAMURA, S. & TAKESAKO, K. 1998. Antibodies labeled with fluorescence-agent excitable by infrared rays. *Journal of Gastroenterology*, 33, 467-471.
- MULLER, M. G., GEORGAKOUDI, I., ZHANG, Q. G., WU, J. & FELD, M. S. 2001. Intrinsic fluorescence spectroscopy in turbid media: disentangling effects of scattering and absorption. *Applied Optics*, 40, 4633-4646.
- MULSOW, J., WINTER, D. C., O'KEANE, J. C. & O'CONNELL, P. R. 2003. Sentinel lymph node mapping in colorectal cancer. *British Journal of Surgery*, 90, 659-667.
- NAGATA, K., ENDO, S., HIDAKA, E., TANAKA, J., KUDO, S. & SHIOKAWA, A. 2006. Laparoscopic sentinel node mapping for colorectal cancer using infrared ray laparoscopy. *Anticancer Research*, 26, 2307-2311.
- NAKAJIMA, T., MITSUNAGA, M., BANDER, N. H., HESTON, W. D., CHOYKE, P. L. & KOBAYASHI, H. 2011. Targeted, Activatable, In Vivo Fluorescence Imaging of Prostate-Specific Membrane Antigen (PSMA) Positive Tumors Using the Quenched Humanized J591 Antibody-Indocyanine Green (ICG) Conjugate. *Bioconjugate Chemistry*, 22, 1700-1705.
- NATIONAL CANCER INTELLIGENCE NETWORK (NCIN) 2009. Colorectal Cancer Survival by Stage. London: ONS.
- NOONEY, R. I., MCCAHEY, C. M. N., STRANIK, O., GUEVEL, X. L., MCDONAGH, C. & MACCRAITH, B. D. 2009. Experimental and theoretical studies of the optimisation of fluorescence from near-infrared dye-doped silica nanoparticles. *Analytical and Bioanalytical Chemistry*, 393, 1143-1149.
- O'DONOGHUE, J. A., SMITH-JONES, P. M., HUMM, J. L., RUAN, S., PRYMA, D. A., JUNGBLUTH, A. A., DIVGI, C. R., CARRASQUILLO, J. A., PANDIT-TASKAR, N., FONG, Y., STRONG, V. E., KEMENY, N. E., OLD, L. J. & LARSON, S. M. 2011. ¹²⁴I-huA33 Antibody Uptake Is Driven by A33 Antigen Concentration in Tissues from Colorectal Cancer Patients Imaged by Immuno-PET. *Journal of Nuclear Medicine*, 52, 1878-1885.
- OFFICE FOR NATIONAL STATISTICS 2010. Colorectal incidence and mortality, 1972 - 2007. Office for National Statistics.
- OGAWA, M., KOSAKA, N., CHOYKE, P. L. & KOBAYASHI, H. 2009. In vivo Molecular Imaging of Cancer with a Quenching Near-Infrared Fluorescent Probe

Using Conjugates of Monoclonal Antibodies and Indocyanine Green. *Cancer Research*, 69, 1268-1272.

OHANNESIAN, D. W., LOTAN, D., THOMAS, P., JESSUP, J. M., FUKUDA, M., GABIUS, H. J. & LOTAN, R. 1995. CARCINOEMBRYONIC ANTIGEN AND OTHER GLYCOCONJUGATES ACT AS LIGANDS FOR GALECTIN-3 IN HUMAN COLON-CARCINOMA CELLS. *Cancer Research*, 55, 2191-2199.

OSIAC, E., SAFTOIU, A., GHEONEA, D. I., MANDRILA, I. & ANGELESCU, R. 2011. Optical coherence tomography and Doppler optical coherence tomography in the gastrointestinal tract. *World Journal of Gastroenterology*, 17, 15-20.

OW, H., LARSON, D. R., SRIVASTAVA, M., BAIRD, B. A., WEBB, W. W. & WIESNER, U. 2005. Bright and stable core-shell fluorescent silica nanoparticles. *Nano Lett*, 5, 113-7.

OWENS III, D. E. & PEPPAS, N. A. 2006. Opsonization, biodistribution, and pharmacokinetics of polymeric nanoparticles. *International Journal of Pharmaceutics*, 307, 93-102.

PARK, I. J., CHOI, G. S., KANG, B. M., LIM, K. H. & JUN, S. H. 2009. Lymph node metastasis patterns in right-sided colon cancers: is segmental resection of these tumors oncologically safe? *Ann Surg Oncol*, 16, 1501-6.

PEDLEY, R. B., BODEN, J. A., BODEN, R. W., GREEN, A., BOXER, G. M. & BAGSHAW, K. D. 1989. THE EFFECT OF SERUM CEA ON THE DISTRIBUTION AND CLEARANCE OF ANTI-CEA ANTIBODY IN A PANCREATIC TUMOR XENOGRAFT MODEL. *British Journal of Cancer*, 60, 549-554.

PEER, D., KARP, J. M., HONG, S., FAROKHZAD, O. C., MARGALIT, R. & LANGER, R. 2007. Nanocarriers as an emerging platform for cancer therapy. *Nat Nano*, 2, 751-760.

PELLEY, J. L., DAAR, A. S. & SANER, M. A. 2009. State of Academic Knowledge on Toxicity and Biological Fate of Quantum Dots. *Toxicological Sciences*, 112, 276-296.
PENZKOFER, A. & LU, Y. 1986. FLUORESCENCE QUENCHING OF RHODAMINE 6G IN METHANOL AT HIGH-CONCENTRATION. *Chemical Physics*, 103, 399-405.

PERACCHIA, M. T., FATTAL, E., DESMAËLE, D., BESNARD, M., NOËL, J. P., GOMIS, J. M., APPEL, M., D'ANGELO, J. & COUVREUR, P. 1999. Stealth® PEGylated polycyanoacrylate nanoparticles for intravenous administration and splenic targeting. *Journal of Controlled Release*, 60, 121-128.

PERCIVALE, P., BERTOGLIO, S., MESZAROS, P., SCHENONE, F., GIPPONI, M., MORESCO, L., COSSO, M. & BADELLINO, F. 1998. Radioimmunoguided surgery with different iodine-125 radiolabeled monoclonal antibodies in recurrent colorectal cancer. *Semin Surg Oncol*, 15, 231-4.

PERRAULT, S. D., WALKEY, C., JENNINGS, T., FISCHER, H. C. & CHAN, W. C. W. 2009. Mediating Tumor Targeting Efficiency of Nanoparticles Through Design. *Nano Letters*, 9, 1909-1915.

PETROS, R. A. & DESIMONE, J. M. 2010. Strategies in the design of nanoparticles for therapeutic applications. *Nature Reviews Drug Discovery*, 9, 615-627.

- POTOMSKI, J., HARLOZINSKA, A., STARZYK, H., RICHTER, R. & WOZNIEWSKI, A. 1979. CORRELATION BETWEEN IMMUNOHISTOCHEMICAL LOCALIZATION OF CARCINOEMBRYONIC ANTIGEN (CEA) AND HISTOLOGICAL ESTIMATION OF CARCINOMAS, NORMAL MUCOSAE AND LYMPH-NODES OF THE DIGESTIVE-TRACT IN HUMANS. *Archivum Immunologiae Et Therapiae Experimentalis*, 27, 177-186.
- POVOSKI, S., HATZARAS, I., MOJZISIK, C., ARNOLD, M., HINKLE, G., HITCHCOCK, C., YOUNG, D. & MARTIN, E. 2012. Antigen-Directed Cancer Surgery for Primary Colorectal Cancer: 15-Year Survival Analysis. *Annals of Surgical Oncology*, 19, 131-138.
- PRATS-MATEU, B., ERTL, P. & TOCA-HERRERA, J. L. 2014. Influence of HepG2 cell shape on nanoparticle uptake. *Microsc Res Tech*, 77, 560-5.
- PUCHTLER, H. & MELOAN, S. N. 1985. ON THE CHEMISTRY OF FORMALDEHYDE FIXATION AND ITS EFFECTS ON IMMUNOHISTOCHEMICAL REACTIONS. *Histochemistry*, 82, 201-204.
- QHOBOSHEANE, M., SANTRA, S., ZHANG, P. & TAN, W. 2001. Biochemically functionalized silica nanoparticles. *Analyst*, 126, 1274-8.
- QI, S., MIAO, Z., LIU, H., XU, Y., FENG, Y. & CHENG, Z. 2012. Evaluation of Four Affibody based Near-infrared Fluorescent Probes for Optical Imaging of Epidermal Growth Factor Receptor Positive Tumors. *Bioconjugate Chemistry*.
- QIU, X.-Q., WANG, H., CAI, B., WANG, L.-L. & YUE, S.-T. 2007. Small antibody mimetics comprising two complementarity-determining regions and a framework region for tumor targeting. *Nature Biotechnology*, 25, 921-929.
- RAHBARI, N. N., BORK, U., MOTSCHALL, E., THORLUND, K., BÜCHLER, M. W., KOCH, M. & WEITZ, J. 2012. Molecular Detection of Tumor Cells in Regional Lymph Nodes Is Associated With Disease Recurrence and Poor Survival in Node-Negative Colorectal Cancer: A Systematic Review and Meta-Analysis. *Journal of Clinical Oncology*, 30, 60-70.
- RAJKUMAR, V., BOXER, G., ROBSON, M., MUDDLE, J., PAPASTAVROU, Y. & PEDLEY, R. B. 2012. A comparative study of PDGFR inhibition with imatinib on radiolabeled antibody targeting and clearance in two pathologically distinct models of colon adenocarcinoma. *Tumor Biology*, 33, 2019-2029.
- REDDY, J. A. & LOW, P. S. 1998. Folate-mediated targeting of therapeutic and imaging agents to cancers. *Critical Reviews in Therapeutic Drug Carrier Systems*, 15, 587-627.
- REITHMEIER, R., BRUCKMEIER, C. & RIEGER, B. 2012. Conversion of CO₂ via Visible Light Promoted Homogeneous Redox Catalysis. *Catalysts*, 2, 544-571.
- RIS, F., HOMPES, R., CUNNINGHAM, C., LINDSEY, I., GUY, R., JONES, O., GEORGE, B., CAHILL, R. & MORTENSEN, N. 2014. Near-infrared (NIR) perfusion angiography in minimally invasive colorectal surgery. *Surgical Endoscopy*, 1-6.
- RIVAROLA, C. R., BERTOLOTTI, S. G. & PREVITALI, C. M. 2006. Photoreduction of Ru(bpy)₃(3)²⁺ by amines in aqueous solution. Kinetics characterization of a long-lived nonemitting excited state. *Photochem Photobiol*, 82, 213-8.

RIZZARDI, A. E., JOHNSON, A. T., VOGEL, R. I., PAMBUCCIAN, S. E., HENRIKSEN, J., SKUBITZ, A. P. N., METZGER, G. J. & SCHMECHEL, S. C. 2012. Quantitative comparison of immunohistochemical staining measured by digital image analysis versus pathologist visual scoring. *Diagnostic Pathology*, 7.

ROBERT, B., DORVILLIUS, M., BUCHEGGER, F., GARAMBOIS, V., MANI, J. C., PUGNIERES, M., MACH, J. P. & PELEGRIN, A. 1999. Tumor targeting with newly designed biparatopic antibodies directed against two different epitopes of the carcinoembryonic antigen (CEA). *International Journal of Cancer*, 81, 285-291.

ROSELLI, M., GUADAGNI, F., BUONOMO, O., BELARDI, A., VITTORINI, V., CAVAZZANA, A., SPAGNOLI, L. G., CIPRIANI, C. & CASCIANI, C. U. 1996. Intraoperative radioimmunolocalization of an anti-CEA MAb F(Ab')(2) (F023C5) in CEA serum-negative colorectal cancer patients. *Anticancer Research*, 16, 883-889.

SĂFTOIU, A., VILMANN, P., CIUREA, T., POPESCU, G. L., IORDACHE, A., HASSAN, H., GORUNESCU, F. & IORDACHE, S. 2007. Dynamic analysis of EUS used for the differentiation of benign and malignant lymph nodes. *Gastrointestinal Endoscopy*, 66, 291-300.

SÁNCHEZ-ELSNER, T., BOTELLA, L. M., VELASCO, B., LANGA, C. & BERNABÉU, C. 2002. Endoglin Expression Is Regulated by Transcriptional Cooperation between the Hypoxia and Transforming Growth Factor- β Pathways. *Journal of Biological Chemistry*, 277, 43799-43808.

SANTRA, S., ZHANG, P., WANG, K. M., TAPEC, R. & TAN, W. H. 2001. Conjugation of biomolecules with luminophore-doped silica nanoparticles for photostable biomarkers. *Analytical Chemistry*, 73, 4988-4993.

SCARTOZZI, M., BEARZI, I., BERARDI, R., MANDOLESI, A., FABRIS, G. & CASCINU, S. 2004. Epidermal Growth Factor Receptor (EGFR) Status in Primary Colorectal Tumors Does Not Correlate With EGFR Expression in Related Metastatic Sites: Implications for Treatment With EGFR-Targeted Monoclonal Antibodies. *Journal of Clinical Oncology*, 22, 4772-4778.

SCHIMANSKI, C., ZIMMERMANN, T., SCHMIDTMANN, I., GOCKEL, I., LANG, H., GALLE, P., MOEHLER, M. & BERGER, M. 2010a. K-ras mutation status correlates with the expression of VEGFR1, VEGFR2, and PDGFR α in colorectal cancer. *International Journal of Colorectal Disease*, 25, 181-186.

SCHIMANSKI, C., ZIMMERMANN, T., SCHMIDTMANN, I., GOCKEL, I., LANG, H., GALLE, P., MOEHLER, M. & BERGER, M. 2010b. K-ras mutation status correlates with the expression of VEGFR1, VEGFR2, and PDGFR α in colorectal cancer. *International Journal of Colorectal Disease*, 25, 181-186.

SCHMIDT, M. M., THURBER, G. M. & WITTRUP, K. D. 2008. Kinetics of anti-carcinoembryonic antigen antibody internalization: effects of affinity, bivalency, and stability. *Cancer Immunology Immunotherapy*, 57, 1879-1890.

SCHOFFELEN, R., SHARKEY, R. M., GOLDENBERG, D. M., FRANSSEN, G., MCBRIDE, W. J., ROSSI, E. A., CHANG, C.-H., LAVERMAN, P., DISSELHORST, J. A., EEK, A., VAN DER GRAAF, W. T. A., OYEN, W. J. G. & BOERMAN, O. C. 2010. Pretargeted Immuno-Positron Emission Tomography Imaging of Carcinoembryonic Antigen-Expressing Tumors with a Bispecific Antibody and a Ga-68- and F-18-

Labeled Hapten Peptide in Mice with Human Tumor Xenografts. *Molecular Cancer Therapeutics*, 9, 1019-1027.

SCHOFFELEN, R., VAN DER GRAAF, W. T., SHARKEY, R. M., FRANSSSEN, G. M., MCBRIDE, W. J., CHANG, C.-H., LAVERMAN, P., GOLDENBERG, D. M., OYEN, W. J. & BOERMAN, O. C. 2012. Pretargeted immuno-PET of CEA-expressing intraperitoneal human colonic tumor xenografts: a new sensitive detection method. *EJNMMI research*, 2, 5-5.

SCHWENK, W., BOHM, B., WITT, C., JUNGHANS, T., GRUNDEL, K. & MULLER, J. M. 1999. Pulmonary function following laparoscopic or conventional colorectal resection: a randomized controlled evaluation. *Arch Surg*, 134, 6-12; discussion 13.

SEDLAK, J. & LINDSAY, R. H. 1968. ESTIMATION OF TOTAL PROTEIN-BOUND AND NONPROTEIN SULFHYDRYL GROUPS IN TISSUE WITH ELLMANS REAGENT. *Analytical Biochemistry*, 25, 192-&.

SHARKEY, R. M., CARDILLO, T. M., ROSSI, E. A., CHANG, C. H., KARACAY, H., MCBRIDE, W. J., HANSEN, H. J., HORAK, I. D. & GOLDENBERG, D. M. 2005. Signal amplification in molecular imaging by pretargeting a multivalent, bispecific antibody. *Nature Medicine*, 11, 1250-1255.

SHIA, J., KLIMSTRA, D. S., NITZKORSKI, J. R., LOW, P. S., GONEN, M., LANDMANN, R., WEISER, M. R., FRANKLIN, W. A., PRENDERGAST, F. G., MURPHY, L., TANG, L. H., TEMPLE, L., GUILLEM, J. G., WONG, W. D. & PATY, P. B. 2008. Immunohistochemical expression of folate receptor [alpha] in colorectal carcinoma: patterns and biological significance. *Human Pathology*, 39, 498-505.

SINGH, P. 1998. Terminal groups in Starburst dendrimers: activation and reactions with proteins. *Bioconjug Chem*, 9, 54-63.

SIRIWARDENA, A. K., MASON, J. M., MULLAMITHA, S., HANCOCK, H. C. & JEGATHEESWARAN, S. 2014. Management of colorectal cancer presenting with synchronous liver metastases. *Nature Reviews Clinical Oncology*, 11, 446-459.

SLOWING, I. I., VIVERO-ESCOTO, J. L., WU, C.-W. & LIN, V. S. Y. 2008. Mesoporous silica nanoparticles as controlled release drug delivery and gene transfection carriers. *Advanced Drug Delivery Reviews*, 60, 1278-1288.

SMITH, A. E., PINKNEY, M., PIGGOTT, N. H., CALVERT, H., MILTON, I. D. & LUNEC, J. 2007. Novel monoclonal antibody for detection of folate receptor alpha in paraffin-embedded tissues. *Hybridoma*, 26, 281-288.

SOENEN, S. J. H. & DE CUYPER, M. 2010. Assessing iron oxide nanoparticle toxicity in vitro: current status and future prospects. *Nanomedicine*, 5, 1261-1275.

SOLTESZ, E. G., KIM, S., KIM, S. W., LAURENCE, R. G., DE GRAND, A. M., PARUNGO, C. P., COHN, L. H., BAWENDI, M. G. & FRANGIONI, J. V. 2006. Sentinel lymph node mapping of the gastrointestinal tract by using invisible light. *Annals of Surgical Oncology*, 13, 386-396.

SOPPIMATH, K. S., AMINABHAVI, T. M., KULKARNI, A. R. & RUDZINSKI, W. E. 2001. Biodegradable polymeric nanoparticles as drug delivery devices. *Journal of Controlled Release*, 70, 1-20.

- SOSLOW, R. A., DANNENBERG, A. J., RUSH, D., WOERNER, B. M., KHAN, K. N., MASFERRER, J. & KOKI, A. T. 2000. COX-2 is expressed in human pulmonary, colonic, and mammary tumors. *Cancer*, 89, 2637-2645.
- SOSTER, M., JURIS, R., BONACCHI, S., GENOVESE, D., MONTALTI, M., RAMPAZZO, E., ZACCHERONI, N., GARAGNANI, P., BUSSOLINO, F., PRODI, L. & MARCHIO, S. 2012. Targeted dual-color silica nanoparticles provide univocal identification of micrometastases in preclinical models of colorectal cancer. *International Journal of Nanomedicine*, 7, 4797-4807.
- SOURIS, J. S., LEE, C.-H., CHENG, S.-H., CHEN, C.-T., YANG, C.-S., HO, J.-A. A., MOU, C.-Y. & LO, L.-W. 2010. Surface charge-mediated rapid hepatobiliary excretion of mesoporous silica nanoparticles. *Biomaterials*, 31, 5564-5574.
- SPANO, J.-P., LAGORCE, C., ATLAN, D., MILANO, G., DOMONT, J., BENAMOUGIZ, R., ATTAR, A., BENICHO, J., MARTIN, A., MORERE, J.-F., RAPHAEL, M., PENAULT-LLORCA, F., BREAU, J.-L., FAGARD, R., KHAYAT, D. & WIND, P. 2005. Impact of EGFR expression on colorectal cancer patient prognosis and survival. *Annals of Oncology*, 16, 102-108.
- STEAD, M. L., BROWN, J. M., BOSANQUET, N., FRANKS, P. J., GUILLOU, P. J., QUIRKE, P., JAYNE, D., MONSON, J. R. T. & WEBB, A. V. 2000. Assessing the relative costs of standard open surgery and laparoscopic surgery in colorectal cancer in a randomised controlled trial in the United Kingdom. *Critical Reviews in Oncology Hematology*, 33, 99-103.
- SUN, D., BLOOMSTON, M., HINKLE, G., AL-SAIF, O. H., HALL, N. C., POVOSKI, S. P., ARNOLD, M. W. & MARTIN, E. W. 2007. Radioimmunoguided surgery (RIGS), PET/CT image-guided surgery, and fluorescence image-guided surgery: Past, present, and future. *Journal of Surgical Oncology*, 96, 297-308.
- SUN, L., WU, H. & GUAN, Y. S. 2008. Colonography by CT, MRI and PET/CT combined with conventional colonoscopy in colorectal cancer screening and staging. *World Journal of Gastroenterology*, 14, 853-863.
- SUPPIAH, A., MASLEKAR, S., ALABI, A., HARTLEY, J. E. & MONSON, J. R. T. 2008. Transanal endoscopic microsurgery in early rectal cancer: time for a trial? *Colorectal Disease*, 10, 314-327.
- SWEDLOW, J. R., HU, K., ANDREWS, P. D., ROOS, D. S. & MURRAY, J. M. 2002. Measuring tubulin content in *Toxoplasma gondii*: a comparison of laser-scanning confocal and wide-field fluorescence microscopy. *Proc Natl Acad Sci U S A*, 99, 2014-9.
- TAN, C., XIE, Y., HE, X., WANG, K. & JIANG, Y. 2010a. Hyper-efficient quenching of a conjugated polyelectrolyte by dye-doped silica nanoparticles: better quenching in the nonaggregated state. *Langmuir*, 26, 1528-32.
- TAN, K. Y., KAWAMURA, Y. J., MIZOKAMI, K., SASAKI, J., TSUJINAKA, S., MAEDA, T., NOBUKI, M. & KONISHI, F. 2010b. Distribution of the first metastatic lymph node in colon cancer and its clinical significance. *Colorectal Disease*, 12, 44-47.
- TANG, F., LI, L. & CHEN, D. 2012. Mesoporous Silica Nanoparticles: Synthesis, Biocompatibility and Drug Delivery. *Advanced Materials*, 24, 1504-1534.

TANG, Y., YANG, S., GARIÉPY, J., SCOLLARD, D. A. & REILLY, R. M. 2007. Construction and Evaluation of the Tumor Imaging Properties of ¹²³I-Labeled Recombinant and Enzymatically Generated Fab Fragments of the TAG-72 Monoclonal Antibody CC49. *Bioconjugate Chemistry*, 18, 677-684.

TAO, L., SONG, C., SUN, Y., LI, X., LI, Y., JIN, B., ZHANG, Z. & YANG, K. 2013. A fluorescent and chemiluminescent difunctional mesoporous silica nanoparticle as a label for the ultrasensitive detection of cancer cells. *Anal Chim Acta*, 761, 194-200.

TAYLOR, E. F., THOMAS, J. D., WHITEHOUSE, L. E., QUIRKE, P., JAYNE, D., FINAN, P. J., FORMAN, D., WILKINSON, J. R. & MORRIS, E. J. A. 2013. Population-based study of laparoscopic colorectal cancer surgery 2006-2008. *British Journal of Surgery*, 100, 553-560.

TEEGUARDEN, J. G., HINDERLITER, P. M., ORR, G., THRALL, B. D. & POUNDS, J. G. 2007. Particokinetics in vitro: Dosimetry considerations for in vitro nanoparticle toxicity assessments. *Toxicological Sciences*, 95, 300-312.

TIVNAN, A., ORR, W. S., GUBALA, V., NOONEY, R., WILLIAMS, D. E., MCDONAGH, C., PRENTER, S., HARVEY, H., DOMINGO-FERNANDEZ, R., BRAY, I. M., PISKAREVA, O., NG, C. Y., LODE, H. N., DAVIDOFF, A. M. & STALLINGS, R. L. 2012. Inhibition of Neuroblastoma Tumor Growth by Targeted Delivery of MicroRNA-34a Using Anti-Disialoganglioside GD(2) Coated Nanoparticles. *Plos One*, 7.

TIWARI, D. K., TANAKA, S., INOUE, Y., YOSHIZAWA, K., WATANABE, T. M. & JIN, T. 2009. Synthesis and Characterization of Anti-HER2 Antibody Conjugated CdSe/CdZnS Quantum Dots for Fluorescence Imaging of Breast Cancer Cells. *Sensors (Basel)*, 9, 9332-64.

TOM, B. H., RUTZKY, L. P., JAKSTYS, M. M., OYASU, R., KAYE, C. I. & KAHAN, B. D. 1976. HUMAN COLONIC ADENOCARCINOMA CELLS .1. ESTABLISHMENT AND DESCRIPTION OF A NEW LINE. *In Vitro-Journal of the Tissue Culture Association*, 12, 180-191.

TOMPKINS, W. A., WATRACH, A. M., SCHMALE, J. D., SCHULTZ, R. M. & HARRIS, J. A. 1974. CULTURAL AND ANTIGENIC PROPERTIES OF NEWLY ESTABLISHED CELL STRAINS DERIVED FROM ADENOCARCINOMAS OF HUMAN COLON AND RECTUM. *Journal of the National Cancer Institute*, 52, 1101-1110.

TONRA, J. R., DEEVI, D. S., CORCORAN, E., LI, H. L., WANG, S., CARRICK, F. E. & HICKLIN, D. J. 2006. Synergistic antitumor effects of combined epidermal growth factor receptor and vascular endothelial growth factor receptor-2 targeted therapy. *Clinical Cancer Research*, 12, 2197-2207.

TORHORST, J., BUCHER, C., KONONEN, J., HAAS, P., ZUBER, M., KOCHLI, O. R., MROSS, F., DIETERICH, H., MOCH, H., MIHATSCH, M., KALLIONIEMI, O. P. & SAUTER, G. 2001. Tissue microarrays for rapid linking of molecular changes to clinical endpoints. *American Journal of Pathology*, 159, 2249-2256.

TORRANO, A. A. & BRAUCHLE, C. 2014. Precise quantification of silica and ceria nanoparticle uptake revealed by 3D fluorescence microscopy. *Beilstein J Nanotechnol*, 5, 1616-24.

UUSARO, A., RUOKONEN, E. & TAKALA, J. 1995. ESTIMATION OF SPLANCHNIC BLOOD-FLOW BY THE FICK PRINCIPLE IN MAN AND PROBLEMS IN THE USE OF INDOCYANINE GREEN. *Cardiovascular Research*, 30, 106-112.

VAHRMEIJER, A. L., HUTTEMAN, M., VAN DER VORST, J. R., VAN DE VELDE, C. J. H. & FRANGIONI, J. V. 2013. Image-guided cancer surgery using near-infrared fluorescence. *Nature Reviews Clinical Oncology*, 10, 507-518.

VAKUROV, A., PCHELINTSEV, N. A., FORDE, J., FAGAIN, C. O., GIBSON, T. & MILLNER, P. 2009. The preparation of size-controlled functionalized polymeric nanoparticles in micelles. *Nanotechnology*, 20.

VAN CUTSEM, E., KOHNE, C. H., HITRE, E., ZALUSKI, J., CHIEN, C. R. C., MAKHSON, A., D'HAENS, G., PINTER, T., LIM, R., BODOKY, G., ROH, J. K., FOLPRECHT, G., RUFF, P., STROH, C., TEJPAR, S., SCHLICHTING, M., NIPPGEN, J. & ROUGIER, P. 2009. Cetuximab and Chemotherapy as Initial Treatment for Metastatic Colorectal Cancer. *New England Journal of Medicine*, 360, 1408-1417.

VAN DER PAS, M. H. G. M., HAGLIND, E., CUESTA, M. A., FÜRST, A., LACY, A. M., HOP, W. C. J. & BONJER, H. J. 2013. Laparoscopic versus open surgery for rectal cancer (COLOR II): short-term outcomes of a randomised, phase 3 trial. *The Lancet Oncology*, 14, 210-218.

VAN DER PAS, M. H. G. M., MEIJER, S., HOEKSTRA, O. S., RIPHAGEN, I. I., DE VET, H. C. W., KNOL, D. L., VAN GRIEKEN, N. C. T. & MEIJERINK, W. J. H. J. 2011. Sentinel lymph node procedure in colon and rectal cancer: a systematic review and meta-analysis. *Lancet Oncology*, 12, 540-550.

VAN DIEST, P. J., VAN DAM, P., HENZEN-LOGMANS, S. C., BERNS, E., VAN DER BURG, M. E., GREEN, J. & VERGOTE, I. 1997. A scoring system for immunohistochemical staining: consensus report of the task force for basic research of the EORTC-GCCG. European Organization for Research and Treatment of Cancer-Gynaecological Cancer Cooperative Group. *J Clin Pathol*, 50, 801-4.

VAN SCHELTINGA, A. G. T. T., VAN DAM, G. M., NAGENGAST, W. B., NTZIACHRISTOS, V., HOLLEMA, H., HEREK, J. L., SCHRODER, C. P., KOSTERINK, J. G. W., LUB-DE HOOG, M. N. & DE VRIES, E. G. E. 2011. Intraoperative Near-Infrared Fluorescence Tumor Imaging with Vascular Endothelial Growth Factor and Human Epidermal Growth Factor Receptor 2 Targeting Antibodies. *Journal of Nuclear Medicine*, 52, 1778-1785.

VEIT-HAIBACH, P., KUEHLE, C. A., BEYER, T., STERGAR, H., KUEHL, H., SCHMIDT, J., BORSCH, G., DAHMEN, G., BARKHAUSEN, J., BOCKISCH, A. & ANTOCH, G. 2006. Diagnostic accuracy of colorectal cancer staging with whole-body PET/CT colonography. *Jama-Journal of the American Medical Association*, 296, 2590-2600.

VIGOR, K. L., KYRTATOS, P. G., MINOGUE, S., AL-JAMAL, K. T., KOGELBERG, H., TOLNER, B., KOSTARELOS, K., BEGENT, R. H., PANKHURST, Q. A., LYTHGOE, M. F. & CHESTER, K. A. 2010. Nanoparticles functionalised with recombinant single chain Fv antibody fragments (scFv) for the magnetic resonance imaging of cancer cells. *Biomaterials*, 31, 1307-1315.

WANG, B., XIAO, Y., DING, B.-B., ZHANG, N., YUAN, X.-B., GUI, L., QIAN, K.-X., DUAN, S., CHEN, Z., RAO, Y. & GENG, J.-G. 2003. Induction of tumor angiogenesis by Slit-Robo signaling and inhibition of cancer growth by blocking Robo activity. *Cancer Cell*, 4, 19-29.

WANG, H., RAJAGOPAL, S., REYNOLDS, S., CEDERBERG, H. & CHAKRABARTY, S. 1999. Differentiation-promoting effect of 1-O (2 methoxy) hexadecyl glycerol in human colon cancer cells. *Journal of Cellular Physiology*, 178, 173-178.

WANG, L., YANG, C. Y. & TAN, W. H. 2005. Dual-luminophore-doped silica nanoparticles for multiplexed signaling. *Nano Letters*, 5, 37-43.

WATSON, A., WU, X. Y. & BRUCHEZ, M. 2003. Lighting up cells with quantum dots. *Biotechniques*, 34, 296-+.

WEEKS, J. C., NELSON, H., GELBER, S., SARGENT, D., SCHROEDER, G. & GRP, C. S. 2002. Short-term quality-of-life outcomes following laparoscopic-assisted colectomy vs open colectomy for colon cancer - A randomized trial. *Jama-Journal of the American Medical Association*, 287, 321-328.

WEISSLEDER, R. & NTZIACHRISTOS, V. 2003. Shedding light onto live molecular targets. *Nat Med*, 9, 123-128.

WEITZ, J., KOCH, M., DEBUS, J., HÖHLER, T., GALLE, P. R. & BÜCHLER, M. W. 2005. Colorectal cancer. *The Lancet*, 365, 153-165.

WEST, N. P., MORRIS, E. J. A., ROTIMI, O., CAIRNS, A., FINAN, P. J. & QUIRKE, P. 2008. Pathology grading of colon cancer surgical resection and its association with survival: a retrospective observational study. *Lancet Oncology*, 9, 857-865.

WEST, N. P., SUTTON, K. M., INGEHOLM, P., HAGEMANN-MADSEN, R. H., HOHENBERGER, W. & QUIRKE, P. 2010. Improving the Quality of Colon Cancer Surgery Through a Surgical Education Program. *Diseases of the Colon & Rectum*, 53, 1594-1603.

WIESE, D., SIROP, S., YESTREPSKY, B., GHANEM, M., BASSILY, N., NG, P., LIU, W. M., QUIACHON, E., AHSAN, A., BADIN, J. & SAHA, S. 2010. Ultrastaging of sentinel lymph nodes (SLNs) vs. non-SLNs in colorectal cancer-do we need both? *American Journal of Surgery*, 199, 354-358.

WINDER, T. & LENZ, H.-J. 2010. Vascular Endothelial Growth Factor and Epidermal Growth Factor Signaling Pathways as Therapeutic Targets for Colorectal Cancer. *Gastroenterology*, 138, 2163-2176.

WOLF, D. E., SAMARASEKERA, C. & SWEDLOW, J. R. 2007. Quantitative analysis of digital microscope images. *Methods Cell Biol*, 81, 365-96.

WU, H., HUO, Q., VARNUM, S., WANG, J., LIU, G., NIE, Z., LIU, J. & LIN, Y. 2008. Dye-doped silica nanoparticle labels/protein microarray for detection of protein biomarkers. *Analyst*, 133, 1550-1555.

WU, J., MA, R., CAO, H., WANG, Z., JING, C., SUN, Y., ZHANG, Y., YANG, Z., HOFFMAN, R. M. & TANG, J. 2013. Intraoperative Imaging of Metastatic Lymph Nodes Using a Fluorophore-conjugated Antibody in a HER2/neu-expressing Orthotopic Breast Cancer Mouse Model. *Anticancer Research*, 33, 419-424.

- WU, X. Y., LIU, H. J., LIU, J. Q., HALEY, K. N., TREADWAY, J. A., LARSON, J. P., GE, N. F., PEALE, F. & BRUCHEZ, M. P. 2003. Immunofluorescent labeling of cancer marker Her2 and other cellular targets with semiconductor quantum dots. *Nature Biotechnology*, 21, 41-46.
- XIAO, B., LAROUÏ, H., VIENNOIS, E., AYYADURAI, S., CHARANIA, M. A., ZHANG, Y., ZHANG, Z., BAKER, M. T., ZHANG, B., GEWIRTZ, A. T. & MERLIN, D. 2014. Nanoparticles with surface antibody against CD98 and carrying CD98 small interfering RNA reduce colitis in mice. *Gastroenterology*, 146, 1289-300 e1-19.
- YANG, L., MAO, H., WANG, Y. A., CAO, Z., PENG, X., WANG, X., DUAN, H., NI, C., YUAN, Q., ADAMS, G., SMITH, M. Q., WOOD, W. C., GAO, X. & NIE, S. 2009. Single Chain Epidermal Growth Factor Receptor Antibody Conjugated Nanoparticles for in vivo Tumor Targeting and Imaging. *Small*, 5, 235-243.
- YANG, S.-J., LIN, F.-H., TSAI, K.-C., WEI, M.-F., TSAI, H.-M., WONG, J.-M. & SHIEH, M.-J. 2010a. Folic Acid-Conjugated Chitosan Nanoparticles Enhanced Protoporphyrin IX Accumulation in Colorectal Cancer Cells. *Bioconjugate Chemistry*, 21, 679-689.
- YANG, Z., LIU, Z. W., ALLAKER, R. P., REIP, P., OXFORD, J., AHMAD, Z. & REN, G. 2010b. A review of nanoparticle functionality and toxicity on the central nervous system. *Journal of the Royal Society Interface*, 7, S411-S422.
- YAZAKI, P. J., KASSA, T., CHEUNG, C.-W., CROW, D. M., SHERMAN, M. A., BADING, J. R., ANDERSON, A.-L. J., COLCHER, D. & RAUBITSCHKEK, A. 2008. Biodistribution and tumor imaging of an anti-CEA single-chain antibody–albumin fusion protein. *Nuclear Medicine and Biology*, 35, 151-158.
- YOSHITAKE, S., YAMADA, Y., ISHIKAWA, E. & MASSEYEFF, R. 1979. Conjugation of glucose oxidase from *Aspergillus niger* and rabbit antibodies using N-hydroxysuccinimide ester of N-(4-carboxycyclohexylmethyl)-maleimide. *Eur J Biochem*, 101, 395-9.
- ZHANG, L., ZHU, W., YANG, C., GUO, H., YU, A., JI, J., GAO, Y., SUN, M. & ZHAI, G. 2012. A novel folate-modified self-microemulsifying drug delivery system of curcumin for colon targeting. *International Journal of Nanomedicine*, 7, 151-162.
- ZHAO, X. J., BAGWE, R. P. & TAN, W. H. 2004a. Development of organic-dye-doped silica nanoparticles in a reverse microemulsion. *Advanced Materials*, 16, 173-+.
- ZHAO, X. J., HILLIARD, L. R., MECHERY, S. J., WANG, Y. P., BAGWE, R. P., JIN, S. G. & TAN, W. H. 2004b. A rapid bioassay for single bacterial cell quantitation using bioconjugated nanoparticles. *Proceedings of the National Academy of Sciences of the United States of America*, 101, 15027-15032.
- ZOU, P., XU, S., POVOSKI, S. P., WANG, A., JOHNSON, M. A., MARTIN, E. W., SUBRAMANIAM, V., XU, R. & SUN, D. 2009. Near-Infrared Fluorescence Labeled Anti-TAG-72 Monoclonal Antibodies for Tumor Imaging in Colorectal Cancer Xenograft Mice. *Molecular Pharmaceutics*, 6, 428-440.
- ZOUBIR, F., ZEROMSKI, J., SIKORA, J., SZMEJA, J., HEDIN, A. & HAMMARSTROM, S. 1990. TUMOR SPECIFICITY OF MONOCLONAL-

ANTIBODIES TO CARCINOEMBRYONIC ANTIGEN - IMMUNOHISTOCHEMICAL ANALYSIS. *Tumor Biology*, 11, 5-19.

ZWEIG, M. H. & CAMPBELL, G. 1993. RECEIVER-OPERATING CHARACTERISTIC (ROC) PLOTS - A FUNDAMENTAL EVALUATION TOOL IN CLINICAL MEDICINE. *Clinical Chemistry*, 39, 561-577.

ZYSK, A. M., NGUYEN, F. T., OLDENBURG, A. L., MARKS, D. L. & BOPPART, S. A. 2007. Optical coherence tomography: a review of clinical development from bench to bedside. *Journal of Biomedical Optics*, 12.